Thermodynamic based modelling of biohydrogen production by anaerobic fermentation

Juan Rodrigo Bastidas Oyanedel

UNIVERSITE MONTPELLIER II
SCIENCES ET TECHNIQUES DU LANGUEDOC

T H E S E

pour obtenir le grade de
DOCTEUR DE L'UNIVERSITE MONTPELLIER II

Discipline : Génie des Procédés
Ecole Doctorale : Sciences des Procédés – Sciences des Aliments

Soutenue publiquement
par
Juan-Rodrigo BASTIDAS-OYANEDEL

le 24 février 2011

Titre :

THERMODYNAMIC BASED MODELLING OF BIOHYDROGEN PRODUCTION BY ANAEROBIC FERMENTATION

JURY

P. BUFFIERE,	Rapporteur
A. GRASMICK,	Examinateur
E. LATRILLE,	Examinateur
C. MOLINA-JOUVE,	Examinateur
M.N. PONS,	Rapporteur
J.P. STEYER,	Directeur de Thèse

ABSTRACT

This thesis deals with thermodynamic based modelling of metabolic shifts during acidogenic fermentation. Acidogenic fermentation is an anaerobic process of double purpose: while treating organic residues, it produces chemical compounds, such as hydrogen, ethanol and organic acids. Therefore, acidogenic fermentation arises as an attractive biotechnology process towards the biorefinery concept. Moreover, this process does not need sterile operating conditions and works under a wide range of pH.

Changes of operating conditions produce metabolic shifts, inducing variability on acidogenic product yields. In order to study these metabolic shifts, an experiment design was based on reactor headspace N_2-flushing (gas phase) and pH step changes (liquid phase). A major result was the hydrogen yield increase from 1 to 3.2 ($mol_{H2} \cdot mol_{glucose}^{-1}$) at pH 4.5 and N_2-flushing of 58.4 ($L \cdot d^{-1}$). This yield is close to the theoretical acidogenic value (4 $mol_{H2} \cdot mol_{glucose}^{-1}$).

The thermodynamic model, based on the assumption that acidogenic fermentation is characterised by limited energy available for biological process, allowed to explain the mechanisms that govern hydrogen metabolic shifts, showing that the synthesis of extra hydrogen, *i.e.* yield of 3.2 ($mol_{H2} \cdot mol_{glucose}^{-1}$), was due to reverse H_2/NAD^+ redox reaction, which is thermodynamically feasible at low hydrogen partial pressures (*e.g.* 0.02 bar). Moreover, low hydrogen yields were explained by the action of homoacetogenesis hydrogen consuming reaction. However, the model was not capable to explain the metabolic shifts of acetate, butyrate and ethanol on acidogenic glucose fermentation.

Modélisation de la digestion anaérobie par une approche basée sur la thermodynamique

RESUMÉ

Ce travail de thèse a eu pour objectif principal l'étude thermodynamique des changements métaboliques dans l'acidogénèse. L'acidogénèse est un procédé anaérobie à double intérêt qui en traitant des résidus organiques, permet de produire des composés chimiques comme l'hydrogène, l'éthanol et les acides organiques. Par conséquent, l'acidogénèse se place comme un procédé biotechnologique dans le concept de bioraffinerie. En outre, ce processus n'a pas besoin de conditions stériles d'opération et fonctionne sur une large gamme de pH.

Ces changements métaboliques sont dépendants des modifications dans les conditions opératoires. Afin d'étudier ces changements métaboliques, des expériences basées sur des modifications du ciel gazeux du réacteur par introduction d'azote et sur des changements du pH, ont été menées. Un des résultats les plus intéressants a été l'augmentation du rendement de production d'hydrogène de 1 à 3,2 $mol_{H2} \cdot mol_{glucose}^{-1}$ à pH 4,5 et débit de N_2 de 58,4 ($L \cdot d^{-1}$). Ce rendement est proche de la valeur théorique (4 $mol_{H2} \cdot mol_{glucose}^{-1}$).

L'étude thermodynamique a permis d'expliquer les mécanismes métaboliques concernant l'hydrogène, dont la production importante, représentée par le rendement de 3,2 $mol_{H2} \cdot mol_{glucose}^{-1}$, est due à la réaction inverse H_2/NAD^+, qui est thermodynamiquement faisable à faibles pressions partielles d'hydrogène (par exemple 0,02 bar). En outre, les bas rendements en hydrogène ont été expliqués par l'action consommatrice d'hydrogène par la réaction d'homoacetogénèse. Cependant, le modèle n'a pas été capable d'expliquer les changements métaboliques de l'acétate, du butyrate et de l'éthanol lors de la fermentation acidogénique du glucose.

DISCIPLINE : Génie des Procédés, Biotechnologie de l'Environnement

MOTS-CLES : Thermodynamics, acidogenesis, anaerobic digestion, hydrogen, ethanol, volatile fatty acids (VFA), Membrane inlet mass spectrometry (MIMS).

INTITULE ET ADRESSE DU LABORATOIRE : Laboratoire de Biotechnologie de l'Environnement. UR0050, Avenue des Etangs, Narbonne F-11100, France

RESUMÉ ÉTENDU

Cette thèse, intitulée « Modélisation de la digestion anaérobie par une approche basée sur la thermodynamique », a cherché à mieux comprendre la digestion anaérobie et à la regarder du point de vue de la Bioraffinerie.

Ce travail s'est centré sur l'étude fondamentale, notamment thermodynamique, d'une étape du procédé de digestion anaérobie : l'« acidogénèse ». Cette étape a gagné en intérêt scientifique ces dernières années car elle permet de produire de l'hydrogène à partir de résidus organiques et des molécules d'intérêt industriel comme l'éthanol ou l'acide acétique (*e.g.* afin de produire par la suite des bioplastiques).

Malgré ces avantages, nos connaissances des mécanismes qui gouvernent l'acidogénèse sont encore limitées. En particulier, divers facteurs environnementaux, comme la composition du ciel gazeux ou le pH, produisent des changements dans la composition des produits mais ceci ne sont pas totalement maitrisés ni optimisés.

La thèse a donc tenté d'obtenir une meilleure compréhension de ces mécanismes et de contribuer à répondre à la question scientifique suivante: comment et pourquoi des conditions environnementales affectent la gamme et la composition de produits issus de l'acidogénèse ?

Plus spécifiquement, l'objectif de ce travail de thèse s'est basé sur l'identification et la modélisation par une approche thermodynamique des phénomènes fondamentaux qui permettent de manipuler la gamme et la composition des produits de l'acidogénèse. Pour aboutir à cet objectif, des fermentations acidogènes de glucose ont été effectuées et des perturbations environnementales, telles que la composition du ciel gazeux et le pH, ont été imposées. Des objectifs secondaires ont été définis :

1. Définir et piloter des fermentations pour évaluer les perturbations environnementales précédemment citées.

2. Implémenter la méthodologie analytique de spectrométrie de masse d'introduction par membrane (MIMS) sur des réacteurs d'acidogénèse, appliquée au suivi quantitatif des cinétiques de fermentation dans les phases liquides et gazeuses.

3. Développer un modèle simplifié et modulaire des voies métaboliques de l'acidogénèse.

4. Développer et implémenter un modèle thermodynamique du métabolisme acidogène.

5. Analyser les résultats expérimentaux en utilisant le modèle thermodynamique, pour expliquer les changements des voies métaboliques sous les perturbations environnementales imposées.

Les résultats obtenus lors de ce travail de thèse sont résumés ci-dessous:

1. La conception d'un modèle mathématique, basé sur la thermodynamique et les principales voies métaboliques de l'acidogénèse, a été achevée. Ce modèle permet d'analyser les mécanismes métaboliques qui produisent des changements de la composition de produits à partir des résultats expérimentaux.

2. L'implémentation d'un système MIMS pour la mesure en ligne et simultanée des cinétiques de production de l'hydrogène et du dioxyde de carbone en phases gazeuse et liquide, et de l'éthanol en phase liquide.

3. La rédaction d'un protocole pour la calibration des signaux issus du MIMS en mesures quantifiables.

4. Quatorze fermentations continues en état stationnaire ont été achevées, dont 9 correspondent aux perturbations de la composition du ciel gazeux et 5 aux changements du pH.

5. Un total de 10 cinétiques, issues des états transitoires entre états stationnaires, a été suivi, dont 6 correspondent aux changements de la composition du ciel gazeux et 4 aux perturbations du pH.

6. Les cinétiques issues du changement du pH ont montré que la composition du ciel gazeux atteint le nouvel état stationnaire plus vite que le milieu liquide.

7. Le point précédent et les expériences de perturbation de la composition de la phase gazeuse ont servi pour démontrer que ces dernières perturbations sont suffisantes pour contrôler la composition de produits issus de la fermentation acidogène de glucose.

8. Ces expériences de changements de la composition du ciel gazeux on montré leur pertinence pour mieux étudier les mécanismes métaboliques qui gouvernent la production d'hydrogène.

9. L'analyse des résultats expérimentaux par le modèle thermodynamique a montré que l'augmentation du rendement de production d'hydrogène, issue d'une diminution de sa pression partielle, est gouvernée par des changements du ratio NAD+/NADH.

Une partie des ces résultats a été déjà publiée ou est en cours de rédaction comme indiqué ci-dessous :

1. Bastidas-Oyanedel J.R., Aceves-Lara C.A., Ruiz-Filipi G., Steyer J.P. 2008. Thermodynamic analysis of energy transfer in acidogenic cultures. Engineering in Life Science 8(5):487-498.

2. Bastidas-Oyanedel J.R., Mohd-Zaki Z., Pratt S., Steyer J.P., Batstone D.J. 2010. Development of membrane inlet mass spectrometry for examination of fermentation processes. Talanta 83(2):482-492.

3. Bastidas-Oyanedel J.R., Mohd-Zaki Z., Zeng R., Pratt S., Steyer J.P., Bernet N., Batstone D.J. Manipulating mixed culture fermentation product spectrum by head-space gas composition changes: continuous bio-hydrogen production. En préparation.

4. Mohd-Zaki Z., Bastidas-Oyanedel J.R., Batstone D.J., Pratt S., Zeng R. Diversity of product spectrum in mixed culture fermentation. En préparation

Ces résultats nous conduisent à envisager des perspectives intéressantes comme l'étude de la récupération des produits volatils par stripping du gaz, notamment l'éthanol et les acides gras volatils. Cela pourra être également applicable à des bioprocédés comme la production de bioéthanol. En outre, le stripping du gaz pourra se combiner à des technologies de biofilm pour augmenter simultanément le rendement de production d'hydrogène et la capacité de traitement de rejets organiques liquides.

ACKNOWLEDGMENTS

I acknowledge the support received by the PhD scholarship from the Chilean Commission for Science and Technology (CONICYT) that allowed the achievement of this work.

I would like to express my gratitude to my supervisor, Dr Jean-Philippe Steyer, who made this thesis possible, and all the people I met at the LBE.

It is a pleasure to thank all the scientific support received from Dr Damien Batstone and his team from the Advanced Wastewater Management Centre of the University of Queensland, Brisbane, Australia. This cooperation was possible thanks to the international project Anamix IRSES EU Project Contract Grant No. GA-2008-230829.

Also, I would like to thank the Jury Members, professors Pierre Buffiere, Alain Grasmick, Carole Molina-Jouve, Marie-Noëlle Pons and Dr. Théodore Bouchez for their commitment, and valuable scientific discussion.

TABLE OF CONTENTS

LIST OF FIGURES

LIST OF TABLES

LIST OF NOMENCLATURE

Latin notation

Notation	Name	Value	Units
A^-	Dissociated acid		
ACOA	Acetyl Coenzyme A		
ACT	Acetate		
ACTH	Acetic acid		
ADP	Adenosine diphosphate		
AH	Undissociated acid		
ATP	Adenosine triphosphate		
BTR	Butyrate		
BTRH	Butyric acid		
c	Compound composition, *i.e.* concentration or partial pressure		[M] or [bar]
C	Compound carbon composition		$[mol_C \cdot mol^{-1}]$
c_0	Compound initial composition		[M] or [bar]
CG	composition gain		[M] or [bar]
CO2	Carbon dioxide		
$CO_{2(dissolved)}$	Dissolved CO_2 concentration		[M]
$CO_{2(total)}$	Total dissolved CO_2 concentration		[M]

COA	Coenzyme A	
d	Displacement	[m]
D	Time delay	[d]
$D(c)$	Concentration dependent diffusion coefficient	$[cm^2 \cdot s^{-1}]$
d_m	Membrane depth	[cm]
e	Electron exchanges in reaction	[eeq]
e_{EA}	Accepted electrons	[eeq]
e_{ED}	Donated electrons	[eeq]
eeq	Electron equivalent unit	
EOH	Ethanol	
F	Force applied	[N]
fa	Fraction of dissociated acid	$[mol \cdot mol^{-1}]$
fah	Fraction of undissociated acid	$[mol \cdot mol^{-1}]$
FDO	Ferredoxine oxidized	
FDR	Ferredoxine reduced	
f_e	Electron fraction used for energy released	
$fGLC$	Fraction of catabolic glucose participating in reaction	$[mol_{catGLC} \cdot mol_{GLC}^{-1}]$
FRM	Formate	
FRMH	Formic acid	
f_s	Electron fraction used for biomass synthesis	

G	Gibbs free energy		[J]
GFR	Gas flow rate		[$L \cdot d^{-1}$]
GLC	Glucose		
GLC	Glucose		
H	Enthapy		[J]
H	Proton		
[H^+]	Proton concentration		[M]
H2	Hydrogen		
H2O	Water		
H_2t	Hydrogen evolution (Gompertz equation)		
Hc	Compound hydrogen composition		[$mol_H \cdot mol^{-1}$]
H_{max}	Hydrogen production (Gompertz equation)		[mL]
HRT	Hydraulic retention time		[d]
i	Subscript denoting compound "i"		
j	Subscript denoting reaction "j"		
$J(x,t)$	Molecular flux		[$mol \cdot s^{-1} \cdot cm^{-2}$]
k	First order rate constant		d^{-1}
K_a	Acid-base equilibrium constant		
Ka_1	Bicarbonate equilibrium constant at 37°C	$5 \cdot 10^{-7}$	
Ka_2	Carbonate equilibrium constant at 37°C	$5.8 \cdot 10^{-11}$	

K_s	Monod saturation constant		$[g \cdot L^{-1}]$
LCT	Lactate		
LCTH	Lactic acid		
MIMS	Membrane inlet mass spectrometry		
NAD	Nicotinamide adenine dinucleotide		
NADH	Nicotinamide adenine dinucleotide reduced		
N_i	Compound nitrogen composition		$[mol_N \cdot mol^{-1}]$
O_i	Compound oxygen composition		$[mol_O \cdot mol^{-1}]$
p	Kinetic parameter vector		
P	Pressure		[Pa]
PI	Phosphate		
PRN	Propionate		
PYR	Pyruvic acid		
Q	Heat		[J]
q_s^{max}	Maximum specific substrate convertion rate		$[g_S \cdot (g_X \cdot h)^{-1}]$
R	Ideal gas constant	8.31447	$[J \cdot K^{-1} \cdot mol^{-1}]$ or $[m^3 \cdot Pa \cdot K^{-1} \cdot mol^{-1}]$
r1	Glycolysis pathway		
r2	Lactic fermentation pathway		
r3	Pyruvate-formic liase pathway		
r4	Formate hydrogenase pathway		

r5	Acetate fermentation pathway	
r6	Butyric fermentation pathway	
r7	Ethanol fermentaion pathway	
r8	NAD-hydrogen redox pathway	
r9	Homoacetogenesis pathway	
rA	Global lactate synthesis reaction	
rB	Global formate synthesis reaction	
rC	Global hydrogen synthesis reaction	
rD	Global acetate synthesis reaction	
rE	Global butyrate synthesis reaction	
rF	Global ethanol synthesis reaction	
rH_2	Hydrogen production rate (Gompertz equation)	$[mL \cdot h^{-1}]$
r^{max}	Maximum reaction rates vector	$[h^{-1}]$
s	Limiting substrate concentration	$[g \cdot L^{-1}]$
S	Entropy	$[J \cdot K^{-1}]$
SCN	Succinate	
t	Time	[s]
t	Time	[h]
t	Time	[d]
T	Actual temperature of reaction	[K]

T°	Standard temperature	298.15	[K]
U	Internal energy		[J]
V	Volume		[m^3]
W	Work		[J]
W_{max}	Maximum work		[J]
W_{net}	Net work		[J]
x	Biomass concentration		[$g \cdot L^{-1}$]
Y	Yield of compounds on glucose		[$mol_i \cdot mol_{GLC}^{-1}$]
Y_GLC_{cat}	Catabolic glucose yield		[$mol_{catGLC} \cdot mol_{GLC}^{-1}$]
Y_GLC_{tot}	Total yield of glucose	1	[$mol_{GLC} \cdot mol_{GLC}^{-1}$]
Y_{sx}	Biomass yield on substrate		[$g_X \cdot g_S^{-1}$]
Y_X	Biomass yield on glucose		[$mol \cdot mol_{GLC}^{-1}$]

Greek notation

Notation	Name	Value	Units
γ	Reduction degree of compounds		[eqq·mol^{-1}]
γ_C	Carbon reduction degree	4	[eqq·mol^{-1}]
γ_d	degree of reduction of electron donor		[eqq·mol^{-1}]
γ_H	Hydrogen reduction degree	1	[eqq·mol^{-1}]
γ_N	Nitrogen reduction degree	-3	[eqq·mol^{-1}]
γ_O	Oxygen reduction degree	-2	[eqq·mol^{-1}]
γ_X	Degree of reduction of biomass	20	[eqq·mol^{-1}]
$\Delta G°$	Standard Gibbs energy change of reactions		[kJ·mol^{-1}]
$\Delta G'$	Actual Gibbs energy of reaction		[kJ·mol^{-1}]
$\Delta G'_{ab}$	Actual Gibbs energy of global acid-base reactions		[kJ·mol$_{GLC}^{-1}$]
$\Delta G'_G$	Global Gibbs energy		[kJ·mol$_{GLC}^{-1}$]
$\Delta G'_{Gp}$	Actual Gibbs energy of global reaction		[kJ·mol$_{GLC}^{-1}$]
$\Delta G'_S$	Actual Gibbs energy of the system		[kJ·mol$_{GLC}^{-1}$]
ΔG_a	Gibbs energy of the half electron acceptor		[kJ·mol$_{GLC}^{-1}$]
ΔG_d	Gibbs energy of the half electron donor		[kJ·mol$_{GLC}^{-1}$]
ΔG_e	Gibbs energy released from the energy source		[kJ·mol$_{GLC}^{-1}$]
$\Delta Gf°$	Standard Gibbs energy of compound formation		[kJ·mol^{-1}]
ΔG_{ic}	Gibbs energy of the conversion of the electron donor to acetyl-CoA		[kJ·mol$_{GLC}^{-1}$]

ΔG_{in}	Gibbs energy of acetyl-CoA reduction	30.9	[kJ·eeq^{-1}]
ΔG_{intra}	Gibbs energy of metabolic reactions		[kJ·mol$_{GLC}^{-1}$]
ΔG_o	The Gibbs energy dissipation		[kJ·mol$_X^{-1}$]
ΔG_{pc}	Gibbs energy of the conversion of acetyl-CoA to biomass	18.8	[kJ·eeq^{-1}]
ΔG_S	Gibbs energy for biomass synthesis		[kJ·mol$_{GLC}^{-1}$]
$\Delta G_T°$	Standard Gibbs energy chage of reaction at actual temperature		[kJ·mol^{-1}]
$\Delta H°$	Standard enthalpy of reaction		[kJ·mol^{-1}]
$\Delta Hf°$	Standard enthalpy of compound formation		[kJ·mol^{-1}]
ε	Energy tranfer efficiency		
λ	Lag phase (Gompertz equation)		[h]
μ	Specific biomass growth rate		[h^{-1}]
μ_{max}	Maximum specific biomass growth rate		[h^{-1}]
v	Compound stoichiometric coefficient of reaction		
v_{GLC}	Glucose stoichiometric coefficient of reaction		

OBJECTIVES OF THIS WORK

In the past decades we, as society, have been concerned by a global environmental context. Decrease of fossil resources, air, soil and water pollution, deforestation, ozone layer depletion, greenhouse gases and global warming have become part of the 20th century's common vocabulary together with decontamination, recycling, conservation, renewable resources and alternatives energies.

In this new millennium, we have inherited the challenge of creating a sustainable society based on renewable resources industry and economy, in order to stop using our non-renewable petrochemical resources and therefore being able to produce carbon neutral emissions.

Hence, scientific efforts have been addressed to develop innovative concepts to replace petrochemical refinery industry. This is the case of the biomass based technologies, a vast renewable concept in which photosynthetic organisms play the main role, transforming solar energy and CO_2 into a wide range of carbon based chemical products, such as fuels, and polymers.

However, biomass based technologies produce several organic residue streams, which have to be treated for health-and-environmental safe considerations. In this context, **acidogenic mixed culture fermentation** (from here referred as "acidogenic fermentation") appears as an interesting process of double purpose: while treating organic residues, it can produce chemical compounds that are, in the present days, mainly produced by petrochemical reforming. In such a way, we are in the presence of a more efficient biomass based technology.

Flexibility is the main feature of acidogenic fermentation, since it is capable of consuming a wide range of organic substrates (residues), it does not need sterile operational conditions, it works on a wide range of operational pH, and it is capable of producing a wide spectrum of products that are basically composed by hydrogen, ethanol and organic acids. Therefore,

acidogenic fermentation arises as an attractive biotechnology process towards the "biorefinery" concept [1,2].

Acidogenic fermentation has been subject of several experimental studies, mostly in the area of biohydrogen production by dark fermentation. The main issues that arose are related to limited understanding of the mechanisms involved during metabolic shifts, *i.e.* changes on product spectra. Product spectra changes depend on operational conditions, such as gas phase composition, pH, substrate nature and concentration, among others [3].

It was observed that these environmental disturbances, *i.e.*, changes on operational conditions, produce changes in the metabolic network fluxes of the acidogenic microorganisms, which are responsible of the intrinsic variable product yield of acidogenic fermentation process. However, the question of "how and why those changes are produced?" has been partly answered [4].

Mathematical modelling appears crucial for seeking the mechanisms that answer the previous question. Several models have been developed to simulate acidogenic fermentation. They are based on empirical and mechanistic approaches and are capable, to some extent, to simulate the process. However, as stated before, the main question is still partially answered.

In the last years, a new approach based on thermodynamics has arisen. In acidogenic systems, the energy available for biological process is limited. Hence, acidogenic fermentation occurs close to thermodynamic equilibrium. This issue makes it possible to consider thermodynamics of metabolic networks into mathematical models, in order to clarify the understanding of the factors that determine changes on metabolic fluxes, and might contribute to answer "how and why environmental conditions affects the product yield spectra".

The aforementioned considerations set the main objective of this work, *i.e.* **to find the foundations for manipulating acidogenic product spectrum through a thermodynamic approach**. To this aim, our experimental set-up was based on continuous acidogenic glucose fermentation by a mixed culture ecosystem. The studied environmental disturbances were operational gas-phase composition and pH. Secondary objectives were defined as listed below:

1) To define and run a set of experiments in order to evaluate the above mentioned environmental disturbances that produce changes on acidogenic yield product.
2) To implement the "membrane inlet mass spectrometry" analytical methodology to acidogenic fermentation, in order to quantitatively monitor the gas and liquid phases of acidogenic fermentation in transient and steady states.
3) To build a simplified and flexible acidogenic metabolic network model of acidogenic fermentation, considering the ecosystem as a whole.
4) To develop and implement a thermodynamic model of the simplified acidogenic metabolic network capable of analysing the metabolic changes at steady state.
5) To analyse the acidogenic experimental results using the thermodynamic model in order to explain the metabolic changes in product yield under environmental disturbances.

Part of the results obtained in this work have been published or are in preparation, as listed below:

Bastidas-Oyanedel J.R., Aceves-Lara C.A., Ruiz-Filipi G., Steyer J.P. 2008. Thermodynamic analysis of energy transfer in acidogenic cultures. Engineering in Life Science 8(5):487-498.

Bastidas-Oyanedel J.R., Mohd-Zaki Z., Pratt S., Steyer J.P., Batstone D.J. 2010. Development of membrane inlet mass spectrometry for examination of fermentation processes. Talanta 83(2):482-492.

Bastidas-Oyanedel J.R., Mohd-Zaki Z., Zeng R., Pratt S., Steyer J.P., Bernet N., Batstone D.J. Manipulating mixed culture fermentation product spectrum by head-space gas composition changes: continuous bio-hydrogen production. In preparation

Mohd-Zaki Z., Bastidas-Oyanedel J.R., Batstone D.J., Pratt S., Zeng R. Diversity of product spectrum in mixed culture fermentation. In preparation

This thesis is organised as follow:

Chapter 1 reviews the scientific literature available on acidogenic fermentation, modelling of anaerobic digestion process and membrane inlet mass spectrometry methodology.

Chapter 2 presents the materials and methods, while chapter 3 describes the results obtained in terms of MIMS calibration, products spectra obtained during the experiments, and thermodynamic model. These results are then discussed in chapter 4 before concluding and drawing some perspectives.

The two published papers are given in appendix. They present with detail, some of the results discussed in the thesis, but for the sake of clarity, not all the results described in the papers are presented in the manuscript.

1 STATE OF THE ART

Crude-oil crisis and environmental concerns have triggered research on bio-based fuel-energy alternatives [5] among which hydrogen and ethanol [6,7] are very promising. Fermentative production of energy and chemicals from renewable sources indeed offers unlimited generation of these compounds highlighting the importance of bioprocesses as an alternative to petrochemical processes [8,9].

Hydrogen production by acidogenic fermentation, also known as dark fermentation [10], is an attractive bioprocess since, simultaneously to hydrogen, it produces solvents and other chemical compounds of industrial interest, allowing the production of liquid fuels and bioplastics, among others. Hence acidogenic fermentation has an important role among biorefinery processes [11] and is becoming an alternative to petrochemical refinery that is increasingly studied.

Several studies on acidogenic fermentation, mostly on hydrogen production, have been performed since 90s decade [12-54]. They observed that changes on product yield spectra are dependent of environmental parameters, such as reactor gas-phase composition or pH. Nevertheless, there is currently only a limited understanding of the mechanisms involved on those changes in product yield spectra. One approach to clarify those mechanisms is mathematical modelling, that is proven as a very useful tool in describing complex systems.

In the last decade, scientific effort has been indeed addressed in order to mathematically model the hydrogen producing acidogenic fermentation [3,4,55-68]. Nevertheless, most of the existing mathematical models, which were originally conceived for aerobic systems, are not adequate for describe acidogenic ecosystems that are in general energy limited.

Acidogenic fermentative reactions occur close to thermodynamic equilibrium [69]. Hence thermodynamics considerations of metabolic reactions are crucial in order to study in detail these ecosystems [4]. The analysis of metabolic thermodynamics will clarify the understanding of the factors that determine reaction fluxes and might contribute to answer

"how environmental parameters, such as pH or gas phase composition, affect the products yield spectra".

In that way, the present work proposes a thermodynamic model of a simplified and flexible representation of acidogenic fermentation ecosystem as a single metabolic network leading to the main acidogenic products, *e.g.* hydrogen, carbon dioxide, solvents and organic acids.

Figure 1 illustrates the topics treated in this work, that are detailed as follow: 1) induction of changes in acidogenic product yield spectra by environmental disturbances in mixed culture acidogenic glucose fermentation; 2) elaboration of a metabolic model based on thermodynamics; and 3) analysis of the experimental results by the thermodynamic model.

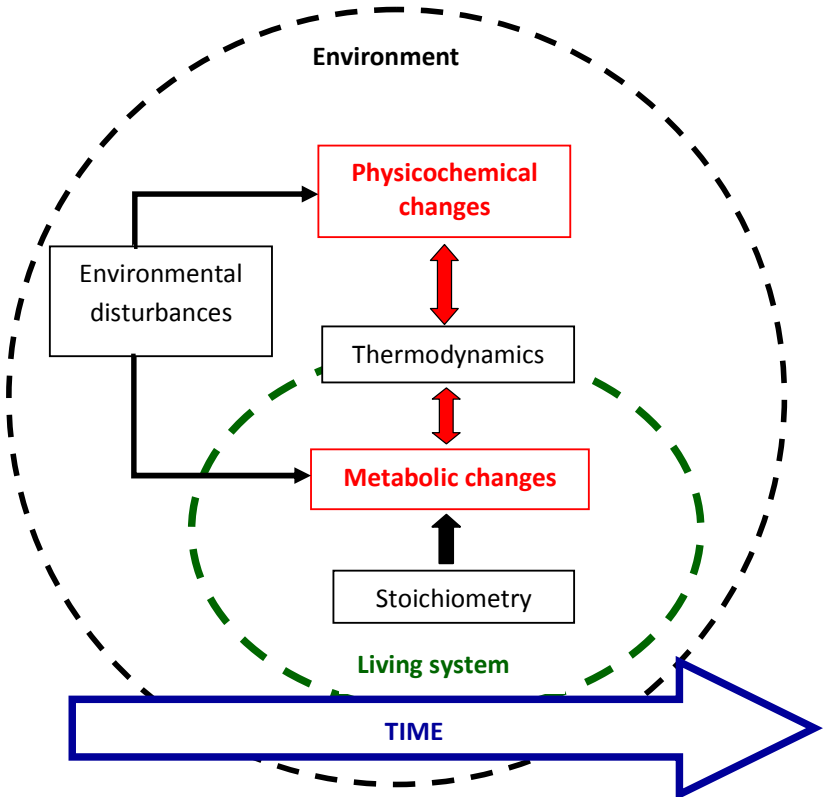

Figure 1: Simplified diagram of topics treated in this thesis

1.1 Acidogenic Fermentation as a Biorefinery Concept

The preservation and management of the diverse natural resources are fundamental political tasks in order to accomplish a sustainable development in this new millennium. An economy based on sustainable processes requires safe and sustainable resources for industrial production, investment and finance system, ecological and health safety, and sustainable life and work perspectives for the population [70,71].

Fossil resources are not regarded as sustainable anymore and their availability is more than questionable in the long-term. Therefore, it is essential to establish solutions that will reduce the rapid consumption of fossil resources, petroleum, natural gas, coal, minerals, which are not renewable. An approach is the stepwise conversion of large parts of the global economy into a sustainable biobased economy with bioenergy, biofuels, and biobased products as its main foundations [72].

For energy generation, there is a variety of alternative renewable processes that can be established, *e.g.* solar, wind, tide, hydroelectric, biomass incineration, nuclear fission, etc. However, products derived from petrochemical processes are ubiquitous in our present day society. Transport fuels, adhesives, plastics, among other, are the most used and known by the public. Research has to be addressed towards new technologies capable of replacing both petrochemical technology and products [72], in order to transform our society into a sustainable one. Therefore, industry based on conversion of sustainable material, for example the chemical industry, industrial biotechnology and the fuel production, will depend on biomass technologies.

Biomass technologies are a vast and interdisciplinary renewable concept in which the main role is played by solar energy recovery and CO_2 transformation into biomass, *i.e.* photosynthesis. Under any sustainable scenario of biomass based bioprocesses, organic residues will be produced. In this context, acidogenic mixed culture fermentation appears as an attractive solution that will reduce those residues, and increasing the global efficiency of biomass based production of energy and valuable chemicals.

As stated above, the acidogenic fermentation of those organic residues yields energy carrier and fuels, such as hydrogen and ethanol, and chemicals like acetic acid, lactic acid and formic acid among others. In present days, hydrogen, acetic acid and formic acid are mostly produced by petrochemical reforming. The production of those compounds by acidogenic fermentation makes it attractive as a petrochemical refinery alternative.

Even though ethanol and lactic acid are mainly produced by very specific design bioprocess, their production by acidogenic fermentation from biomass technologies residues increased their global efficiency production, avoiding the competition of those bioprocesses.

The technological importance of acidogenic fermentation products in the present and future chemical industry is reviewed below.

1.1.1 Hydrogen

Hydrogen is an invisible, tasteless and colourless gas. It is the most abundant element in the universe; it is believed to make up about 75 percent of the mass of the universe and to account for more than 90 percent of its molecules. Hydrogen is a non-polluting and renewable form of energy being the fuel of stars and galaxies. And it is essential in innumerable chemical and biological processes [73].

One of the hydrogen uses is as energy storage. Electricity can indeed be produced in a renewable way by solar, wind or tide processes. But electricity has to be consumed the instant it is produced. It is difficult to store it in large quantities. Hydrogen, even if its storage posses some difficulties, would solve that problem [74]. Hydrogen can be stored as a high-pressure gas or as an integral component in certain alloys known as hydrides, but also on microscopic carbon fibres.

Moreover, the combustion of hydrogen with oxygen produces only water, unlike to hydrocarbon internal-combustion engines that produce carbon monoxide, carbon dioxide, unburned hydrocarbons, stench and smoke [75].

As a cryogenic liquid, hydrogen in combination with liquid oxygen is also a powerful fuel for space shuttles and other rockets, and it promises to lead better, faster and more efficient, environmentally clean airplane designs [74].

However, hydrogen performs even better in fuel cells, which are electrochemical engines that produce electricity combining hydrogen and oxygen in an electrochemically flameless process. By-products of this process are heat and pure distilled water. Fuel cells have no moving parts. Nearly silent, they can be as much as 2.5 times as efficient as internal-combustion engines [76].

Furthermore to their fuel applications, hydrogen is widely used in many industries as a chemical raw material, especially in the production of fertilisers, dyes, drugs, and plastics. Also, it is used in the treatment of oils and fats, to make gasoline from coal, and to produce methanol.

Hydrogen is commercially produced in an almost a dozen processes. Most of them involve its extraction from hydrocarbons. The most widely used and least costly process is steam reforming, in which natural gas is made to react with steam, releasing hydrogen. The production of hydrogen by water electrolysis, in which water is broken down into hydrogen and oxygen by running an electrical current through it, is used where electricity is cheap and where high purity is required [73].

1.1.2 Acetic acid

This molecule has been a useful chemical since antiquity. Its availability probably precedes the first written language. The first recorded report of acetic acid as vinegar from alcohol is reported to be dated at earlier than 3000 B.C. Until late in the 19th century, all acetic acid was derived by the same process of sugar fermentation to ethyl alcohol and subsequent oxidation to acetic acid to produce vinegar. For most of human history, this was the sole source of acetic acid. Late in the 19th century, this process was replaced by wood distillation, which provided and additional source of acetic acid [77].

In 1916, the first dedicated plant for the production of acetic acid by chemical rather than biological means became a commercial process. This petrochemical method based on acetylene-derived acetaldehyde marks the beginning of inexpensive commercial acetic acid and hence the birth of a viable industry based on its use [77].

Acetic acid uses cover the production of several derived molecules covering day to day uses in our society. Among them, vinyl acetate represents the single largest use of acetic acid. Several processes have been used to generate this material on commercial scales. Vinyl acetate derived polymers are ubiquitous in modern society, which are found as part of wood-panels, paper bags, cardboard boxes, labels adhesives (stamps), white glue, latex paints, high-quality paper coating, textiles, cement additive, etc [77,78].

Vinyl acetate is expected to continue to grow as a significant derivative of acetic acid. The technology is well established, and new technologies will guarantee that vinyl acetate continue to be an important chemical commodity in the future, even if the petrochemical industry suffers severe setbacks due to petroleum shortages [79].

Acetic acid also serves as precursor of several products like cellulose acetate, alcohol acetates, halogenated acetic acid, acetic anhydride, citrate esters, diketene, methyl acetoacetate, acetoacetamides, acetoacetylated polymers, which serve as precursor molecules with vast applications on the production of pharmaceuticals (such as aspiring, vitamin E, beta-lactam and oxacillin antibiotics, antiepilectic drugs), agrochemicals (insecticides, fungicides), and dye, colorant and polymers industries. Furthermore, acetic acid chemistry still offers ample opportunity for providing new discoveries in the future [77].

1.1.3 Ethanol

Ethanol has a long and diverse history, certainly as a beverage, but equally so as a fuel, which only came into sharp focus toward the middle of the 19th century when it was used for lighting [80]. Nowadays it is also used in the chemical industry [81].

Ethyl alcohol is produced by chemical synthesis and by fermentation or biosynthetic processes. For well over one hundred years, researchers around the world have pursued ways

to make ethanol from biomass such as wood, grasses, and waste materials. In general, ethanol made through fermentation is referred to as bioethanol.

Ethanol is produced in largest volume by industrial fermentation. Most of the ethanol in the United States is produced of corn. Expanding fuel ethanol production will require developing lower-cost feedstocks, and only lignocellulosic feedstocks are available in sufficient quantities to substitute for corn starch [81].

Brazil is an example of sustainable transportation fuel production. With significant domestic oil resources but limited infrastructure to develop it, Brazil relied heavily on petroleum imports and was hard-hit by the 1973 embargo. With a serious trade deficit at hand and the threat of monumental inflation, the government launched its "Programa Nacional do Alcool". Its goal was the phase-out of all transportation fuel derived from fossil sources, to be replaced with domestically produced ethanol [80]. The notorious air quality of cities such as Sao Paulo has improved with the introduction of ethanol-fuelled vehicles, and the reduction of greenhouse gases nationwide credited to the use of ethanol is estimated at 86 percent.

In chemical industry, ethanol is used as solvent, antifreeze and as fuel supplement. The major use of ethanol is as an intermediate feedstock in the synthesis of innumerable organic chemicals. Biomolecular dehydration of ethanol gives diethyl ether, which is employed as a solvent, extractant, and anesthetic. Dehydrogenation of ethanol yields acetaldehyde, which is the raw material for production of a large number of organic chemicals such as acetic acid, acetic anhydride, chloral, butanol, crotonaldehyde, and ethylhexanol. Reaction with carboxylic acids or anhydrides yields esters which are useful in many applications. The hydroxyl group of ethanol may be replaced by halogen to give ethyl halides. Treatment with sulphuric acid gives ethyl hydrogen sulphate and diethyl sulphate, a useful ethylating agent. Reaction of ethanol with aldehydes yields the respective diethyl acetals, and reaction with acetylene produces the acetals, as well as ethyl vinyl ether. These and other ethanol-derived chemicals are used in dyes, drugs, synthetic rubber, solvents, detergents, plasticisers, surface coatings, adhesives, mouldings, cosmetics, explosives, pesticides, and synthetic fibre resins [81].

1.1.4 Lactic acid

In 1985 industrial lactic acid fermentation has been developed by the pharmaceutical entrepreneur A. Boehringer. The Swedish pharmacist C.W. Scheele had already discovered lactic acid in 1780 and the conversion of carbohydrates into lactic acid had been known for ages in food preservation (*e.g.* Sauerkraut) or agriculture (silage fermentation). Because of the activity of Boehringer, the German company Boerhinger-Ingelheim can be regarded as the pioneer of industrial biotechnology. Both the process and the demand for lactic acid by dyeing factories, and the leather, textile, and food industries made the company leading supplier. In 1932, W.H. Carothers, who was also the inventor of polyamide-6.6, developed, together with van Natta, a polyester made from lactic acid, poly(lactic acid). In the late 1990s this poly(lactic acid) was commercialised by the company NatureWorks [72].

1.1.5 Formic acid

The simplest carboxylic acid, is an important organic chemical and widely used in industries. Recently, it got more and more attention to be used as environmental storage and transportation medium for hydrogen, the clean energy in future [82], which can be generated by the catabolic decomposition of formic acid. Also some researchers have demonstrated that formic acid has the potential to direct power fuel cells for electricity generation and transportation [83,84].

1.2 Acidogenic Fermentation Process

In this section, acidogenic fermentation process is first covered from an historical point of view. Then are presented the most common metabolic pathways that have been described for this system, and finally the environmental factors that influence acidogenic fermentation are described.

Acidogenic fermentation is a part of an old bioprocess known as anaerobic digestion (AD). As a general definition, anaerobic digestion is a biologically mediated process in which microorganisms degrade organic compounds, in the absence of oxygen, to methane and carbon dioxide. AD is present in nature, *e.g.*, aquatic sediments, animal guts, including human

being [85]. Through scientific research, AD gained academic recognition in the 1930s. This research led to the discovery of anaerobic bacteria and methanogenic archaea.

In the last decade, scientific and technological research on AD has conceived new alternative processes to classical anaerobic digestion. Innovative AD processes have been used for the production of methane-alternative energy carriers, as hydrogen and ethanol, and valuable organic acids for the chemical industry, *e.g.* acetic acid among other organic acids [72]. Also, it is possible now to produce electricity directly from waste streams by microbial fuel cell process [8,11].

1.2.1 Anaerobic digestion – a brief history

Scientific records of gas produced by natural decomposition of organic matter was first reported in the 16th century by Robert Boyle and Stephen Hale, who noted that an inflammable gas was released by disturbing the sediment of streams and lakes and associated this "inflammable air" with decomposing organic material in the sediments [86].

However, it was Alessandro Volta who first discovered methane by collecting the gas from marshes in 1776-1777 [85]. One century later (1859), an anaerobic digester was built in Bombay, India, becoming the first record of AD technological use [87]. Then in 1895, a septic tank was used to generate methane for street lighting in Exeter, England, [88].

The classical AD process is widely used to treat organic waste streams as wastewater and organic solids. However, more interest has been placed in the capability of AD to produce renewable energy in the form of biogas rich in methane and CO_2, providing an alternative to fossil fuels, and allowing the recovery of nutrients as phosphate fertiliser [89].

Furthermore, since 1997 classical AD has been recognised by the United Nations as one of the most useful decentralised sources of energy supply, as they are less capital intensive than large power plants [70], and in a recent report, AD is considered crucial to fighting against poverty and energy isolation in developing countries [71].

1.2.2 Classic anaerobic digestion process

Anaerobic digestion involves the transformation of organic compounds to various inorganic and organic products. During AD, a portion of an organic compound may be oxidised while another portion is reduced. It is from this oxidation-reduction of organic compounds that anaerobic microorganisms obtain their energy and produce numerous simplistic and soluble organic compounds [90].

The digestion process begins with bacterial hydrolysis of the fed organic materials in order to break down insoluble polymers, making them available for microorganism consumption. Acidogenic bacteria then convert the products of hydrolysis into carbon dioxide, hydrogen, ammonia, alcohols and organic acids. Acetogenic bacteria convert these resulting alcohols and organic acids into acetic acid, along with additional ammonia, hydrogen and carbon dioxide. Finally, methanogenic archaea converts these products to methane and carbon dioxide [90-92]. Figure 2 illustrates this AD structure, which is detailed as follow.

Hydrolysis is the first step required for anaerobic microbial utilisation of complex polymers, which cannot be hydrolysed by methanogenic archaea themselves. Hydrolytic fermentative bacteria facilitate the extracellular enzymatic hydrolysis of the initial complex organic matter formed by polymers such as polysaccharides, proteins and fats. The hydrolases (enzymes) that catalyses these reactions are cellulase, amylase, protease, and lipase, among others. Hydrolases may be secreted to the extracellular environment or be bound to the cell surface [93,94].

Polysaccharides are generally converted into simple monomeric or dimeric sugars as glucose. Hydrolysis of starch and cellulose yields glucose as monomeric sugar, while hemicellulose is degraded to galactose, arabinose, xylose, mannose and glucose. Proteins are broken down into amino acids, small peptide, ammonia and carbon dioxide by proteases. Lipids are hydrolysed into long and short chain fatty acids and glycerol by lipases [90,93,95]. The hydrolysis products then become substrates for the fermentation processes that follow.

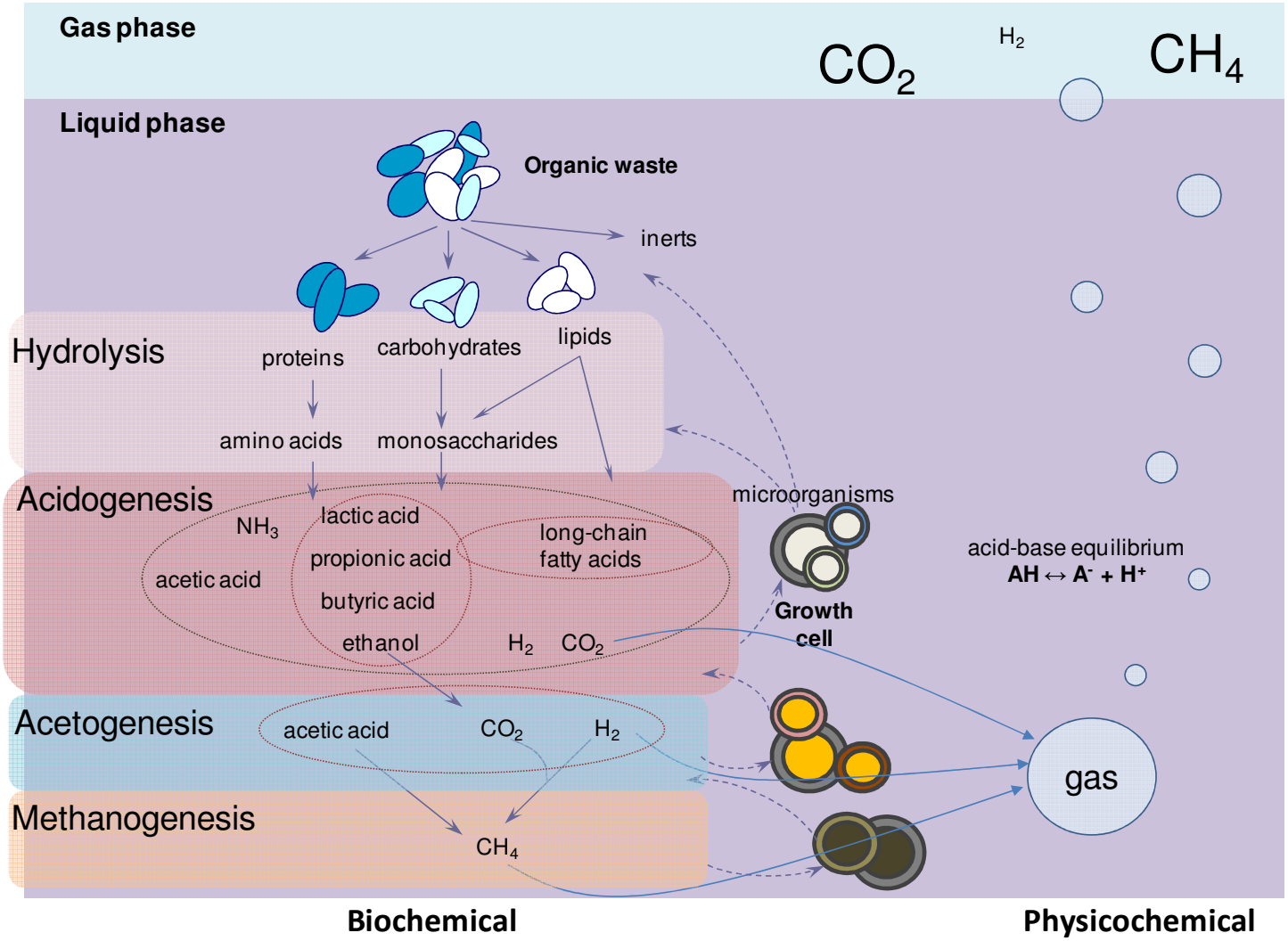

Figure 2: Anaerobic digestion scheme describing the main biochemical degradation pathways. From top to bottom: Hydrolysis of complex organic polymers yielding amino acids, monosaccharides and fatty acids; Acidogenesis consuming the sugars and amino acids to produce CO_2, H_2, volatile organic acids and alcohols. Acetogenesis from acidogenesis products and long-chain fatty acids. Methanogenesis from acetic acid and H_2.

Acidogenesis. Monosaccharides and amino acids, released after the hydrolysis of their respective polymers, serve as substrates to the acidogenic fermentation [95]. Groups of facultative and anaerobic fermentative or anaerobic oxidising organisms utilise these substrates yielding compounds such as ethanol, acetate, propionate, H_2 and CO_2 as intermediary products. Acidogenesis is a process in which intracellular reduced co-factors such as NADH are being oxidised. The regeneration of co-factors is vital to the process as a whole, as these co-factors serve as intermediary electron acceptors in the catabolic reactions that proceed continuously within the digestion system. The regeneration of these co-factors is done by the production of the alcohols and organic acids yielded in this process [69,90,92].

Acetogenesis. Acetogenic organisms use the intermediary products resulting from acidogenesis and long-chain fatty acids resulting from fats hydrolysis to produce acetate, H_2 and CO_2. This process is dependent upon a low partial pressure of hydrogen in order to yield energy from degradation of the substrates to acetate [90]. The organisms that perform this conversion are very slow-growing and do not easily adapt to changes in the organic loading rate (OLR). They are sensitive organisms that require long periods to adapt to given conditions. If these organisms do not adapt to environmental conditions, methane production will decrease as the acetogens may limit the digestion of the organic material that is utilised by methanogenic species [90,92].

Methanogenesis. The products from acetogenesis are utilised by methanogenic archaea producing the final products CH_4 and CO_2 [90,92]. Over 2/3 of the methane produced from AD is the result of decarboxylation of acetate to methane, while the remainder results mainly from the consumption of H_2. The acetoclastic reaction that converts acetate into methane is not dependent upon H_2 partial pressure and proceeds regardless. However, H_2 producing acetogenic organisms and H_2 consuming archaea benefits from a low H_2 partial pressure, since high H_2 partial pressure inhibits the acetogenic process, which stops the production of acetic acid then stopping the production of methane [96], *i.e.* only if the methanogenic bacteria keep the H_2 partial pressure low, then the acetogenesis is exergonic and the reaction can be pulled to the product side. Because of their mutual dependence, these mixed cultures are referred to as syntrophic cultures [97].

1.2.3 Acidogenesis fermentation metabolism

As exposed above, acidogenic fermentation is a step of the classical anaerobic digestion process in which, the last step of methanogenesis is suppressed to produce hydrogen instead of methane. Methanogens are strict anaerobic and very sensitive to many chemicals. Thus, activity of hydrogen-consuming methanogens can be inhibited by simple aeration or by the addition of toxic chemicals as 2-bromoethanesulfonate, acetylene and chloroform [12]. Other methanogenesis suppression techniques include heat pre-treatment of inocula, decreasing hydraulic retention time (HRT), and decreasing reactor pH (~5.0).

However, acidogenic fermentation has been mainly used for hydrogen production [12-14], where main efforts have been addressed to maximise the hydrogen yield. However, a group of organic acids and alcohols is simultaneously produced even when the maximum yield of hydrogen is achieved.

As stated above, this makes acidogenic fermentation an attractive and flexible biorefinery process. Mixed culture acidogenic fermentation includes some advantages, such as: 1) broad substrate range, where acidogenic fermentation can consume residues from other processes like farming, food and beverage processing, or municipal solid waste, industrial waste water, etc; and 2) no sterile conditions are needed, since anaerobic environment acts as a selection pressure where only adapted organisms can growth [9].

In a mixed culture acidogenic fermentation, where many microbial species are present, most of the fermentative conversions explained below are possible. The fermentation patterns observed are the result of the combined effect and interaction among the microbial consortium present. Therefore, main metabolic pathways are described in classical biochemistry books.

Acidogenic bacteria are capable of performing a variety of oxidation-reduction reactions involving organic compounds, carbon dioxide, molecular hydrogen, etc. Acidogenic bacteria include facultative anaerobes, aerotolerant anaerobes, and strict anaerobes. Some fermentative bacteria such as the *Clostridia* produce a large variety of products, whereas others such as *Acetobacterium* produce a very small number of products.

In such an ecosystem, the microorganism consortia activity depends on environmental condition changes, *e.g.* changes in gas phase composition or pH for instance. Environmental changes will conduct changes on the consortia metabolism and/or physiology, affecting the types and quantities of compounds that are produced through fermentation [90].

Metabolism is the sum of all biochemical reactions performed by a living organism. The reactions have two main purposes, 1) to generate energy for the organism, and 2) to build new cell material. Reactions related to generating energy are called catabolism, and all reactions leading to formation of cell material are called anabolism.

In the organisms that carry out mixed product fermentation, microbial growth is based on balanced changes (metabolic fluxes) between catabolic reactions in response to anabolic needs. Metabolic fluxes are highly variable and change with both environmental conditions and the growth rate of the organism; faster-growing cells require a higher rate of metabolism. Catabolic redox processes of many anaerobic bacteria are branched, and both the extent and thermodynamic efficiencies of ATP synthesis are variable [4]. The fluxes in different metabolic pathways are adjusted so that the ATP gain and the thermodynamic efficiency are optimal for the specific growth condition [98]. The acidogenic fermentation product composition is influenced by the operational-environmental conditions [55,99], showing a clear variable product yield.

Metabolism starts consuming biodegradable substrates. The most common substrate found in organic residues is glucose. The acidogenic fermentation of glucose extracts energy in the form of ATP by substrate-level phosphorylation during oxidative substrate breakdown [100]. The resulting reducing equivalents (in the form of NADH) are transferred into metabolic intermediates, leading to the formation of a variety of reduced products such as H_2, ethanol, and organic acids (lactic, propionic, formic, acetic, butyric acids), depending on the fermentation pathways utilised [99]. Acidogenic bacteria generally possess alternative pathways leading to the formation of these products, and the relative proportions of the different products formed depend on the environmental conditions. Thus, the level of ATP production and maintenance of redox balance can be modulated through shifts between alternative pathways in response to carbon source availability and gas phase composition [4,55].

Table 1 and Figure 3 illustrate the main catabolic pathways in acidogenic glucose fermentation. Glycolysis (or Embden-Meyerhof-Parnas pathway) is thought to be the archetype of a universal metabolic pathway [101]. It occurs, with variations, in nearly all organisms, both aerobic and anaerobic. The wide occurrence of glycolysis indicates that it is one of the most ancient known metabolic pathways [102]. Glycolysis is a sequence of ten reactions. Here, it is lumped into one reaction starting from glucose giving pyruvate. The resulting lumped reaction is presented as reaction (1). In this process, the consumption of one mole of glucose produces 2 moles of ATP, which is then use as energy source for biomass growth and maintenance processes.

The NADH resulting from glycolysis should be reconverted to NAD^+ to allow glycolysis to continue. In anaerobic conditions, organisms are able to oxidase NADH back to NAD^+ in several ways. One method is lactic acid fermentation, where pyruvate is converted into lactate, reaction (2). Propionic acid is formed also as a reduced product of glucose fermentation. Propionic acid can be produced through the so called acrylate pathway [103] or via the succinate pathway [104]. Acrylate pathway, reaction (3), reconverts and extra NADH to NAD^+ and also produces 1 ATP. Succinate pathway, reactions (4) and (5), allows the reconvertion of 2 NADH and the production of 1 ATP, this pathway also consumes CO_2 for succinate synthesis.

Production of acetyl-coenzyme-A through pyruvate decarboxilation is a different way to regulate glucose metabolism. Two different pathways exist in anaerobic bacteria, the pyruvate formate lyase pathway and the pyruvate dehydrogenase pathway [98], reactions (6) and (7), respectively. Simultaneous presence and expression of genes encoding pyruvate formate lyase and pyruvate ferredoxin oxidoreductase is not uncommon in members of the genus *Clostridium* [98].

The synthesis of acetic acid proceeds from acetyl-CoA, reaction (11). Part or all the acetyl-CoA is therefore available for the synthesis of ATP, which proceeds via the phosphotransacetylase and the acetate kinase reactions, both enzymes been founded in all anaerobic bacteria that form acetyl-CoA in their energy metabolism and use the acetyl-CoA to synthesise ATP [100]. The detection of acetate kinase activity in *C. thermolacticum*

confirmed the presence of the acetate branch from acetyl-CoA and the supplementary ATP formation associated to this pathway [105].

Table 1: Condensed metabolic pathways in acidogenic fermentation

See abbreviations in Table 2

	Reaction name	Reaction
(1)	Glycolysis	GLC + 2 NAD + 2 ADP + 2 PI → 2 PYR + 2 NADH + 2 H + 2 ATP + 2 H2O
(2)	LTC fermentation	PYR + NADH + H → LCT + NAD
(3)	Acrylic pathway	LCT + NADH + H + ADP + PI → PRN + NAD + ATP + 2 H2O
(4)	SCN pathway	PYR + CO2 + 2 NADH + 2 H + ADP + PI → SCN + 2 NAD + ATP + 2 H2O
(5)	PRN fermentation	SCN → PRN + CO2
(6)	PYR FRM lyase	PYR + COA → ACOA + FRM
(7)	PYR dehydrogenase	PYR + COA + FDO → ACOA + CO2 + FDR
(8)	FRM hydrogenase	FRM → H2 + CO2
(9)	Ferredoxin hydrogenase	FDR → H2 + FDO
(10)	Ferredoxin oxidation	FDR + NAD → FDO + NADH + H
(11)	ACT fermentation	ACOA + ADP + PI → ACT + COA + ATP
(12)	BTR fermentation	ACOA + ACT + 2 NADH + 2 H + ADP + PI → BTR + COA + 2 NAD + ATP + 2 H2O
(13)	EOH fermentation	ACOA + 2 NADH + 2 H → EOH + COA + 2 NAD
(14)	Homoacetogenesis	4 H2 + 2 CO2 → ACT + 2 H2O

Butyric acid synthesis, reaction (12), takes place in a cycle starting with the condensation of molecules of acetyl-CoA. This cycle goes on until the formation of butyril-CoA, wich reacts with a molecule of acetic acid to yield one molecule of butyric acid and one of acetyl-CoA, which is the starting point for a new cycle. The simplification of this cycle starts with the condensation of acetyl-CoA and acetic acid to produce butyric acid. Butyrate fermentation has been proposed to not only regenerate NAD^+ from NADH produced in the glycolysis, but that it might also lead to further energy gains. During the conversion of acetyl-CoA to butyric acid, one of the enzymatic complex, the butyryl-CoA dehydrogenase electron-transferring flavoprotein, may generate a proton motive force with a membrane-associated NADH:ferredoxin oxidoreductase [99].

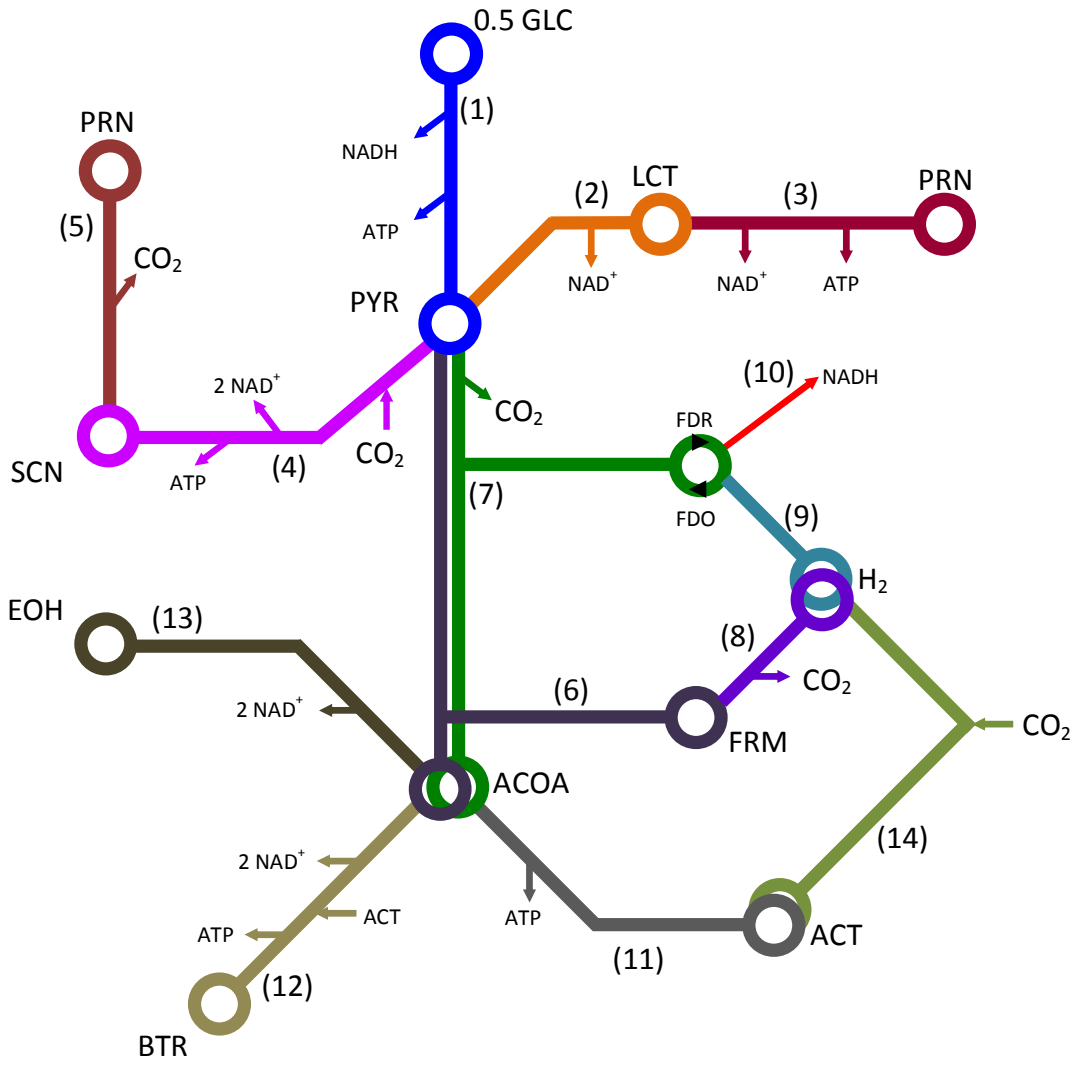

Figure 3: Simplified diagram of acidogenic metabolic pathways

The formation of ethanol from acetyl-CoA, reaction (13), involves two enzyme, aldehyde dehydrogenase and ethanol dehydrogenase. The first one catalyses the reaction of acetyl-CoA to acetaldehyde [100], while the second enzyme catalyses the dehydrogenation of acetaldehyde to ethanol [105].

Table 2: Abbreviation of acidogenic fermentation metabolites

Abbr	Name
ACOA	Acetyl Coenzyme A
ACT	Acetate
ADP	Adenosin diphosphate
ATP	Adenosin triphosphate
BTR	Butyrate
CO2	Carbon dioxide
COA	Coenzyme A
EOH	Ethanol
FDO	Ferredoxine oxidized
FDR	Ferredoxine reduced
FRM	Formate
GLC	Glucose
H	Proton
H2	Hydrogen
H2O	Water
LCT	Lactate
NAD	Nicotinamide adenine dinucleotide
NADH	Nicotinamide adenine dinucleotide reduced
PI	Phosphate
PRN	Propionate
PYR	Pyruvate
SCN	Succinate

1.2.4 Influence of gas-phase composition and pH on acidogenic fermentation

As stated before, the distribution of acidogenic fermentation products is affected by environmental conditions. This is technologically advantageous since it allows controlling and optimising the production of certain compounds giving flexibility to this process. Here, the influence of gas phase composition and pH on acidogenic fermentation product yields is described.

Gas phase composition effects

Previous works have observed head-space gas composition as an important environmental variable to regulate product spectrum in anaerobic fermentation. Hillman *et al.* [106] working on anaerobic protozoa batch cultures showed how different initial gas phase compositions resulted in considerable differences in the distribution of produced volatile fatty acids (VFAs)

at the end of fermentations. Their main results showed that with an initial 100% N_2 gas-phase, the proportion of VFAs produced was 40% acetic, 50% butyric and 10% propionic acid. When the initial gas-phase was composed by a mixture of N_2 and H_2, the proportion of acetic acid increased, butyric acid decreased and no propionic acid was produced. A mixture of CO_2 and N_2 in the gas phase resulted in propionic acid increase, butyric acid decrease and acetic acid remaining unchanged.

Similar conclusions were reached for acidogenic fermentations by Tanisho *et al.* [52] and Karlsson *et al.* [15]. However, mixed culture fermentation (MCF) experiments with N_2 sparging performed by Kim *et al.* [16] and Mizuno *et al.* [53], indicated that even when H_2 yield was increased, no significant change in liquid end products was observed.

Further research employing hydrogen extraction performed by Karlsson *et al.* [15] related the increased H_2 yield to acetic acid production increase. Experiments on nitrogen-sparged acidogenic reactors by Kraemer and Bagley [17] resulted in both H_2 and butyric acid yields increase. Similar observation was found by Kim *et al.* [16] on their sparging CO_2 experiment, where butyric acid yield was increased, acetic and lactic acids were decreased, and propionic acid and ethanol yields not significantly affected by CO_2 sparging.

As a consequence, the control of gas-phase composition arose as an attractive method to increase acidogenic produced hydrogen yield close to its theoretical maximum, *i.e.* 4 $molH_2 \cdot (mol_{hexose})^{-1}$ [107].

High H_2 partial pressures limit the H_2 production by end product inhibition, *i.e.* making the re-oxidation of reduced ferredoxin and H_2-carrying coenzymes less favourable [3,18]. Therefore, a decrease in H_2 partial pressure should increase H_2 yields [18].

Different techniques have been applied in decreasing the H_2 partial pressure in acidogenic bioreactors including gas sparging [16,19,52,53], membrane separation [20,21], and direct suction from reactor headspace [22].

pH effects

The effect of pH has been the most environmental variable studied on acidogenic fermentation [12,23,51,108,109]. Ruggeri *et al.* [24] suggested that pH has a crucial role in the regulation of the enzymes pool involved in H_2 evolution, while Fang and Liu [51] observed that microbial diversity increased with pH.

However, the pH modifies the acidogenic metabolism in mixed culture fermentation. Li and Fang review [12] on acidogenic hydrogen production have reported 22 "optimal pHs". But many of these values came from fermentation experiments in batch reactors without pH control. For the pH controlled studies reported, the observed optimal pH range was between 5.2 and 7.0 for cultures consuming synthetic media. The use of complex substrates, such as industrial effluents or solid waste narrowed the pH range to 5.2 and 5.6.

Shifts from butyric to acetic acid when pH is increased have been described in literature [51,108,109]. Fang and Liu [51] observed that acetate production was favoured at pH 6.5, whilst butyrate was at pHs lower than 6.0. They have also showed that propionic acid was suppressed at low pH, but increased dramatically at pHs higher than 6.5. Temudo *et al.* [108] noted H_2 presence at low pH range (4-6.5), whilst acetic acid, ethanol and formic acid were present at high pH range (6.5-8.5).

1.3 Mathematical Modelling of Acidogenic Fermentation

Mathematical models are crucial tools in the difficult tasks of integrate, analyse and investigate the large quantity of flow-information coming from microbial, chemical and physical phenomena that are taking place within microbiologic mediated processes. Mathematical models can also be used to test scientific hypotheses, to design experiments or to control and optimise an already existing bioprocess.

The key role of mathematical models in biotechnology has become clear and well established over the previous decades. Nowadays, mathematical models are indispensable at every stage of bioprocess development, from the earliest research phase to large-scale industrial implementation.

Mathematical models have different levels of complexity that depend on the objective to attain. Model elaboration can be based on a mechanistic approach, empirical knowledge, or a mixture of both. Mechanistic modelling approach accounts for actual mechanisms occurring in the system, while empirical models attempt to fit the observed behaviour using mathematical correlations [4].

In the particular case of acidogenic fermentation, mathematical modelling efforts have been driven by the necessity of process simulation, control and optimisation. Because the natural link between acidogenic fermentation and anaerobic digestion, these modelling efforts were mostly based on previous models designed to simulate anaerobic digestion process. Those models assumed that the systems are kinetically controlled, *i.e.* without energy limitations as in the aerobic fermentations case.

In this decade, the fact that acidogenic fermentation is an energy-limited process, *i.e.* being thermodynamically controlled rather than kinetically, has turned the attention to a mechanistic modelling approach based on thermodynamics. With this approach, it is expected to understand and clarify the mechanisms that control acidogenic fermentation.

The next sections present a brief history of anaerobic digestion modelling, followed by the efforts made to modelling acidogenic fermentation processes, and the thermo-kinetic considerations that have been took in this challenge.

1.3.1 Anaerobic digestion modelling – a brief historical review

Anaerobic digestion modelling has been an active research area during the last decades. As stated before, its main driving force was the simulation, control and optimisation of AD bioprocess, which resulted on the elaboration of several dynamic models [110], which have mostly been applied to anaerobic wastewater treatment systems [60,62,111].

Mathematical models for AD have several degrees of complexity. These differences are essentially from the hypothesis used for the model structure assumptions, such as metabolic regulation and inhibitions. Simplest models considered organic matter as a global

homogeneous whole, enclosing the total substrate composition in the chemical oxygen demand (COD) rather than a detailed specific substrate composition [25]. Therefore, their applications are reduced to substrates with low variability in composition, such as residues from oil, diary [112] and winery industries [110].

The first attempts of AD modelling began in 1974 with Graef and Andrews [113]. Then, based on the previous authors, Hill and Barth [114], Kleinstreuer et Poweigha [115] and Moletta *et al.* [116] developed new models with Monod-type kinetic equations for simulate process dynamics. Those models describe the last AD step, *i.e.* methanogenesis, and represent the total volatile fatty acids (VFA) composition as acetic acid equivalent. These models also explain the accumulation of VFAs phenomena by VFA inhibition of methanogenesis, considering Haldane type kinetics equations [117]. The complexity level of these models started to increase. Models proposed by Kalyuzhnyi and Davlyatshina [118] and Kalyuzhnyi [119] consider five steps and five pH dependent microorganism groups.

Angelidaki *et al.* model [120] was structured into four steps: hydrolysis, acidogenesis, acetogenesis and methanogenesis. The main model hypotheses are: 1) methanogenesis inhibition by ammonia; 2) acetogenesis inhibition by acetic acid; and 3) acidogenesis inhibition by total VFA. Non-competitive inhibition functions were used, where ammonium ionisation is dependent of pH and temperature. Siegriest *et al.* [121] also considered ammonia into the sludge anaerobic digestion process, predicting the system pH.

Other research groups considered the H_2 gas-phase composition into the modelling process, since it was thought to participate in the AD inhibition. In 1983, Mosey [122] considered four microorganism groups based on growth rate differences in his model: acidogenic bacteria and methanogenic hydrogenotrophes were considered as high growth rate microorganisms, whilst the acetate producers and consumers were considered as low growth rate. In this model, hydrogen regulates the redox cell potential. The main model hypotheses are: 1) constant intracellular pH equal to 7.0; 2) instantaneous hydrogen diffusion trough the cellular membrane; 3) identical partial pressure between intracellular and extracellular compartments; and 4) identical redox potential between intracellular and extracellular compartments. The main limitation is that this model cannot be applied to low pH anaerobic processes.

In 1991, Costello [123,124] has integrated lactic acid production to the Mosey model. Costello considered that lactic acid is consumed to produce propionic acid and finally acetic acid. This model has limitations, it predicts less propionic and butyric acid concentrations and more biogas flow rate [125]. Romli *et al.* [126] have adapted and applied this model to two-stage reactor processes, *i.e.* an acidogenic reactor followed by a methanogenic. The physico-chemical expressions have been modified in order to calculate the pH. This gives better predictions of pH, base consumption, and gas composition. But this model fails when considering recirculation from the methanogenic reactor to the acidogenic. In 2000, Batstone *et al.* [127,128], based on Romli *et al.* [126], have structured their model into nine microorganism groups and three different extracellular hydrolysis processes for lipids, proteins and carbohydrates, being able to simulate anaerobic digestion of complex substrates, such as slaughterhouse effluent.

In 1997, the International Water Association (IWA) has created an interdisciplinary group for modelling the AD, and to develop a generic model. This model was publish in 2002 [111] under the name of Anaerobic Digestion Model No 1 (ADM1). ADM1 considers two extracellular steps, *i.e.* disintegration and hydrolysis, and three intracellular steps, *i.e.* acidogenesis, acetogenesis and methanogenesis. These three steps are catalysed by seven microorganism groups. The model hypotheses are: 1) constant product yields; and 2) VFA degradation inhibition by hydrogen. ADM1 biomass inhibition by pH expressions were based on those empiric functions developed by Angelidaki *et al.* [120]. The inhibition of acetic acid consuming methanogenesis by hydrogen and ammonia was modelled by non-competitive inhibition expressions.

ADM1 does not consider lactic acid. It takes into account the ionic equilibrium phenomena and the gas-liquid equilibrium for CO_2, H_2 and methane. The physicochemical equilibria are represented either by algebraic equations or differential equations. ADM1 also considers the cellular death and their recycle into as complex organic matter. This model has been validated with different experimental data, such as two-stage anaerobic digestion process [129], or a UASB reactor [130]. The agglomeration structure of flocks has been also simulated based in ADM1 [131].

Generalities among the existing AD dynamic models typically consist of several mass-balanced based differential equations, one for each chemical compound and microorganism group considered. Each microbial activity is described by an overall growth reaction with constant biomass and product yield values, as well as with Monod-type kinetic equations describing metabolic reaction rates. Microbial and other chemical reactions occur simultaneously, and all their contributions are added in the net reaction term. The dynamics of each species and the global system is obtained by solving the entire set of mass-balance based differential equations [4].

1.3.2 Acidogenic fermentation modelling

As seen above, AD models have been considerably improved over the previous decades. These models are capable to describe the dynamic performance of anaerobic processes, with broad application in control and optimum operation of wastewater treatment industry.

However, they fail when describing acidogenic fermentations in a satisfactory manner and are not able to determine the dependence of product formation on the environmental conditions imposed in the microbial community [4]. In this context different approaches have been addressed, such as purely empirical models, ADM1-type based models, and thermo-kinetic models [63]. Most of these models were design to simulate acidogenic hydrogen production.

Empirical models

Among the empirical approaches, most studies used the Gompertz equation [62]. This equation fits the hydrogen evolution composition, H_2t, at time t (h) by adjusting three parameters: hydrogen production, H_{max} (mL), H_2 production rate, rH_2 (mL·h^{-1}) and the lag phase, λ (h).

$$H_2t = H_{max} \cdot exp\left\{-exp\left[\frac{rH_2}{H_{max}}(\lambda - t) + 1\right]\right\} \quad (1)$$

Even though this curve-fitting approach yields high correlation coefficients between the observed and fitted hydrogen evolution data, the three model parameters determined by curve-fitting are restricted to specific experimental conditions and cannot be used in a predictive mode [62]. Also, it cannot account for relevant process variables such as substrate and VFA concentration evolution, temperature, pH, substrate types, etc [62]. However, in some studies, the Gompertz equation has been modified to accommodate typical kinetics of substrate degradation, biomass growth, and hydrogen production [26,56,64].

Another empirical approach by Nikhil *et al.* [67] consisted on a computational clustering hybrid regression, which does not required detailed *a priori* knowledge of the bioprocess. This computational approach can detect and visualise prevailing metabolic patterns in the bioprocess dataset using self organising maps [132] which are a powerful data exploration tool for the analysis and visualisation of nonlinear and multidimensional dataset. Self organising maps are generally used in the data-understanding phase of the model development, and to detect statistically significant features, inherent in the nonlinear and multidimensional dataset, which are not easily understood using normal plots.

The model was constructed to predict H_2 production rate based on the process performance, *i.e.* CO_2 production rate, concentrations of organic acids and ethanol and operational conditions (pH and HRT). This model has been applied to two substrates, glucose and xylose, in acidogenic H_2 production fermentations [68].

ADM1-type based models

Dynamic modelling of acidogenic fermentation has been mostly based on the ADM1 model. However, direct utilisation of ADM1 on acidogenic fermentation does not well simulate the process. Therefore, modifications are needed. These modifications account for a restructuration of model parameters, or by considering product yield variability, as previously discussed by Mosey [122] and Batstone [127,128].

Restructuration of parameters. Aceves-Lara *et al.* [65] have developed a model based on experimental data to estimate pseudo-stoichiometric coefficients with a constrained nonlinear optimisation. Their results show that two reactions, one being associated with hydrogen

production and the other one with acetate production, could explain 89% of the total variance of the experimental data. This accurately predicts the dynamic evolution of H_2 production, biomass and VFAs. This model takes into account physicochemical processes kinetics: acid-base reactions and liquid-gas mass transfer. The model has been validated using data from literature and using a second set of dynamic experimental data different from that used for parameter identification.

Arudchelvam *et al.* [133] have developed a model to predict VFA formation. The model was constructed upon experimental data from cattle manure fermentation. The model is based on the assumption that biodegradable components of cattle manure are composed of particulate forms of cellulose and hemicelluloses that are first hydrolysed to their respective forms and then consumed by acidogenesis to produce H_2, CO_2 and VFAs. Biomass growth was modelled as a single biomass consuming two substrates with different kinetic consumption constants. The acidogenic products are modelled following the ADM1 model, with the exclusion of the methane formation step. Their results conclude that the assumptions used are valid since the model achieved a goodness of fit between the experimentally measured and predicted profiles of COD, acetic acid and butyric acid, and to a lesser extent in the case of propionic acid.

Hafez *et al.* [57] modelled a CSTR that decouples the SRT from the HRT, incorporating this in the software BioWin (EnviroSim Associates Ltd., Flamborough, Ontario, Canada), which is widely used for modelling wastewater treatment plants. This model was based on two populations: acidogenic and acetogenic microorganisms. The biomass recirculated undergoes decay. The products of decay include unbiodegradable organic, nitrogen and phosphorous components. Hydrolysis is mediated by acidogenic microorganisms. The acidogenic fermentation produces acetic acid, propionic acid, hydrogen and carbon dioxide. Propionic acid is converted to acetic acid by acetogenic bacteria. Hydrogen is switched off at high levels of propionate, using a propionate inhibition expression. The stoichiometry of each of these processes is previously calibrated to achieve the appropriate product mix. The calibration can be done by trial and error to achieve the best match between modelled and measured data.

Variability of product yields. Rodriguez *et al.* [55] have modified the ADM1 using variable yield coefficients, and assuming that the product transport from the intracellular to extracellular compartments was ATP-dependent. This model considers a variable acetate and butyrate yields dependent on the hydrogen dissolved concentration and reactor pH. The main change predicted is a shift from acetate to butyrate as the main fermentation product at decreasing pH (7-5.5) and/or increasing hydrogen dissolved concentration. A mechanistic explanation of this prediction is related to energetic issues. Lower pH values required higher energy costs for the cells to transport acid molecules outwards the membrane and on the other hand, the maximum concentration of a product is limited by the thermodynamic feasibility of its production where hydrogen plays a key role especially in the acetate production. Based on their simulations, they concluded that acidogenic fermentation is thermodynamic rather than kinetic controlled. Also, their dynamic results assume that the yield changes occur instantaneously because the stoichiometry functions do not incorporate any time related issue. This is not realistic but was used as a starting point to test the effect of such a dynamic yield change would be in the most extreme situations of instantaneous changes of yields. Slow yield changes may occur in reality but similar results are expected maybe with minor time delays or small variations. However, this model badly predict the effect of pH on ethanol production

Penumathasa *et al.* [66] have used the variable stoichiometric approach of Rodriguez [55]. They assumed that the biomass and product yields from glucose degradation are dynamically dependent on the total concentration of undissociated acids in the reactor. At each time instant of the modified ADM1 simulation, the total concentration of undissociated acids is calculated from the current acid concentrations and pH. From this value the biomass yield and the acetate, butyrate and hydrogen yields are computed by linear interpolation from values that were obtained from pseudo steady state at total undissociated concentrations. The remaining COD is allocated to lactate to maintain a closed COD balance all times during simulations. The model was validated with mesophilic sucrose fermenting biohydrogen producing reactor. This model achieved good predictions with the implementation of the variable stoichiometry, without any parameter fitting, *i.e.* using the standard ADM1 parameters values. The model predicts the stationary and dynamic behaviour of hydrogen, acetate and butyrate concentrations.

1.3.3 Acidogenic fermentation modelling – thermokinetics considerations

Existing kinetic models often neglect energetic and thermodynamic limitations because they have been based on aerobic processes that entail large Gibbs free energy values. In anaerobic systems, this might lead to unrealistic predictions, such as the catalysis of endergonic reactions that are impossible according to the second law of thermodynamics [4].

These unrealistic predictions might occur because reactions in these systems proceed close to thermodynamic equilibrium, and accumulation of products can easily result in positive Gibbs energy values and might even reverse the reaction fluxes [4]. Thermodynamic limitations could, in theory, be easily incorporated into the existing acidogenic kinetic-based models.

Microbiological kinetics models can be expressed as follows: a biological system consisted of a set of processes (biological mediated reactions and transport processes) that transform substrates into metabolic precursors and energy metabolites. The rate at which these processes take place depends on the concentration of reactants and products, and the amount of inhibitors or activators [134].

For a metabolic system of *m* reactions, *n* metabolites, and *k* kinetic parameters, the reaction rates are related through the mass balance of the metabolites [134]. These mass balances can be described by a set of ordinary differential equations:

$$\frac{dc}{dt} = v \cdot r^{max} \cdot f(c,p) \tag{2}$$

where *c* is the *n*-dimensional vector of metabolite concentrations, *v* is the *n*x*m* stoichiometric matrix, r^{max} is the *m*-dimensional vector of maximum reaction rates, *f*(c,p) is a non linear function of *c* and the *k*-dimensional vector of kinetic parameters, *p*, that affects the reactions. Typical example for *f*(c,p) is Monod equation:

$$\mu = \mu_{max} \frac{s}{s + K_s} \tag{3}$$

Monod equation, Eq. (3), shows a functional relationship between the microbiological specific growth rate (μ) and a limiting substrate concentration (s), in which μ_{max} is the maximum specific growth rate and K_s is the half saturation parameter also known as the Monod coefficient. Monod equation has no mechanistic basis and can be regarded as a empirical equation derived from the Michaelis-Menten equation [135,136].

However, the Monod equation [137] has been widely applied to describe microbial growth, and forms the basis for the kinetic description of microbial metabolism. Monod-based description of substrate conversion, s ($g \cdot L^{-1}$), and biomass growth, x ($g \cdot L^{-1}$), has been mostly modelled using constant biomass yields, Y_{sx} ($g_X \cdot g_S^{-1}$), for growth of biomass on substrate, and a maximum specific substrate conversion rate, q_s^{max},($g\text{-}s \cdot (g\text{-}x \cdot h)^{-1}$). In a batch culture, these expressions become:

$$\frac{ds}{dt} = -q_S^{max} \cdot \frac{s}{K_S + s} \cdot x \tag{4}$$

$$\frac{dx}{dt} = Y_{sx} \cdot q_S^{max} \cdot \frac{s}{K_S + s} \cdot x \tag{5}$$

These equations form the basis for the kinetic description of microbial metabolism. Introduction of additional terms for substrate consumption for maintenance purposes, bacterial decay, substrate competition, and product inhibition have been used for description of a large variety of kinetic data. In anaerobic fermentations, product inhibition has repeatedly been recognised [135]. In analogy with the inhibitory effect of product on enzyme-catalysed reactions, competitive, noncompetitive and uncompetitive inhibition relationships have been used for description of product inhibition in anaerobic fermentation [135].

These equations can be applied without significant error in systems where energy is available in abundance in order to drive the metabolic reaction, *e.g.* aerobic systems. However, these equations are unsuitable in limited energy systems [138], and hence are inconsistent with the requirements of thermodynamics.

In such systems, the Monod equation predicts that microorganisms will continue to metabolise substrates until their concentration asymptotically approaches zero. But when a substrate concentration decreases, the energy that it can offer also decreases, and eventually metabolic reactions may become energetically unfavourable [138]. This is especially true for acidogenic fermentation, where the substrate-energy available is limited [97,100,135]. This inconsistence could be eliminated by incorporating thermodynamic terms into the kinetic expressions [4].

Vlyssides *et al.* [139] have taken thermodynamics into account, where overall biological reactions were determined by evaluating catabolic and anabolic reactions separately and then adding them together. For each differential time interval, the biomass produced was estimated from the stoichiometry of these reactions, in contrast to the conventional anaerobic models where a constant yield is used. The feasibility of each reaction was determined by thermodynamic calculations, according to the relative percentage of their free energies. Nevertheless, their expressions are kinetically controlled using Monod equations with inhibition terms rather than thermodynamically.

In this aim, Hoh and Cord-Ruwish [140] derived a microbial kinetic expression based on reversible enzyme kinetics, considering the actual Gibbs energy of reaction, $\Delta G'$ (kJ·mol^{-1}):

$$q_S = q_S^{max} \cdot \frac{s \cdot \left(1 - e^{\left(\frac{\Delta G'}{RT}\right)}\right)}{K_S + s \cdot \left(1 + e^{\left(\frac{\Delta G'}{RT}\right)}\right)} \tag{6}$$

where R is the ideal gas constant and T (K) the actual temperature of reaction. Significant advantages over classical Monod-based equations are obtained. Substrate consumption proceeds only when the free energy change for the chemical conversion reaction is exergonic, obeying thermodynamic laws. Threshold substrate concentration, as frequently encountered in anaerobic conversion reactions, is predicted by this expression as a result of the free energy change becoming endergonic at low substrate and high product concentrations. In a same

way, Jin and Bethke [138] used a thermodynamic potential factor to correct the kinetic equations. However, these expressions should be regarded as empirical.

Hoh and Cord-Ruwisch [140] assumed that the free energy change of the catabolic reaction is fully used as the driving force of the reaction and lost as heat. However, microbial metabolism can be described as a balance of catabolic and anabolic reactions coupled by ATP/ADP. Metabolic energy is partly conserved through ATP formation from ADP and Pi and partly lost in the form of heat. Biomass is formed at expense of ATP, and again, part of the energy is lost as heat. Part of the formed ATP is furthermore consumed for maintenance purposes [135].

In such a thermodynamic approach, Kleerebezem and Stams [135] assumed that the energy generated in the catabolic reaction has to be conserved in the form of ATP to enable growth of the bacteria. For the various anabolic reactions, it was assumed that a fixed stoichiometry between ATP consumption and biomass formation exist [135]. Furthermore, they stated a non-fixed stoichiometry of cytoplasmatic ATP-driven proton pump, but considering that the H^+/ATP stoichiometry as a variable, depending on the ADP/ATP ratio in the cell.

Even though thermokinetic approaches have address some of the thermodynamic inconsistencies of the classic traditional AD models, the question of "how and why metabolic changes are produced" has been partly answered. Thence, more-profound thermodynamic considerations based on fundamental cell processes, *e.g.* metabolism, are necessary to accurately describe the activity of anaerobic microbial ecosystems.

1.4 Biothermodynamics Based Modelling of Acidogenic Fermentation

As already exposed in the previous sections, metabolic variability and difficulties obtaining the same products spectrum is often observed in acidogenic fermentation under similar operational conditions. The mechanisms where environmental factors, such as pH, temperature and concentration affect the product fluxes are not yet fully understood in this system.

There is a general consensus that the laws of physics are well understood today and it is time to apply them to systems and processes with high degrees of complexity such as living systems [101]. Living systems are extremely complex and organised hierarchically. This is clearly a result of the process of evolution.

Biology was the first branch of science that attempted to reconstruct past events from today's knowledge of the biosphere. This quest started with the discovery of fossils of long-extinct species, such as living creatures with calcium carbonate or silica based skeleton (540 million years ago). Contemporary techniques allow uncovering fossils of much simpler organisms that do not possess a skeleton. The first well preserved petrified micro-stamps of organised living organisms, similar to present cyanobacteria, emerged about 3.5 billion years ago [141].

In 1859, Charles Darwin [142] proposed a method that has had great potential to reconstruct the history of life based on differences in selected features of living animal species and not extinct ones. In modern applications of this methodology, the most fundamental characteristics are the genomes of species. Based on the mathematically well defined distance between genomes, it is possible to reconstruct the history of the species, *e.g.* human evolution [143].

Contemporary biochemistry and molecular biology provide numerous examples of 'living fossils'. These are archaic metabolic pathways and more or less conserved domains in enzymes [101,102]. The organisation of existing animate matter reflects the history of its evolution and, conversely, the living structures that we encounter on the Earth today are products of the evolution of life.

The three most important characteristics of life that distinguish it from other physical systems were expressed by Darwin in his theory of evolution. Taking into account the achievements of contemporary genetics and biochemistry, these three characteristics can be defined as: life is a process characterised by continuous (1) reproduction, (2) variability and (3) selection (survival of the fittest) [101].

However, living organisms are physical systems, and irrespective of form, complexity, time or place, all known organisms are alike in that they must capture transducer, store and use

energy in order to live. This is a fundamental statement, where the concept of energy is the most basic one of all science and technology [144].

Living organisms conserve energy by coupling its production to the synthesis of ATP, the common chemical energy storing currency in all living organisms [138]. Then, ATP can be expended for cellular purposes such as maintenance, biomass synthesis and/or reproduction, and chemical species transport across its membrane as depicted in Figure 4.

Regarding acidogenic microorganisms, they couple this ATP synthesis to the breakdown of complex substrate molecules found in their environment as explained in previous sections. The breakdown produces simpler species, one more oxidised and the other more reduced than the substrate.

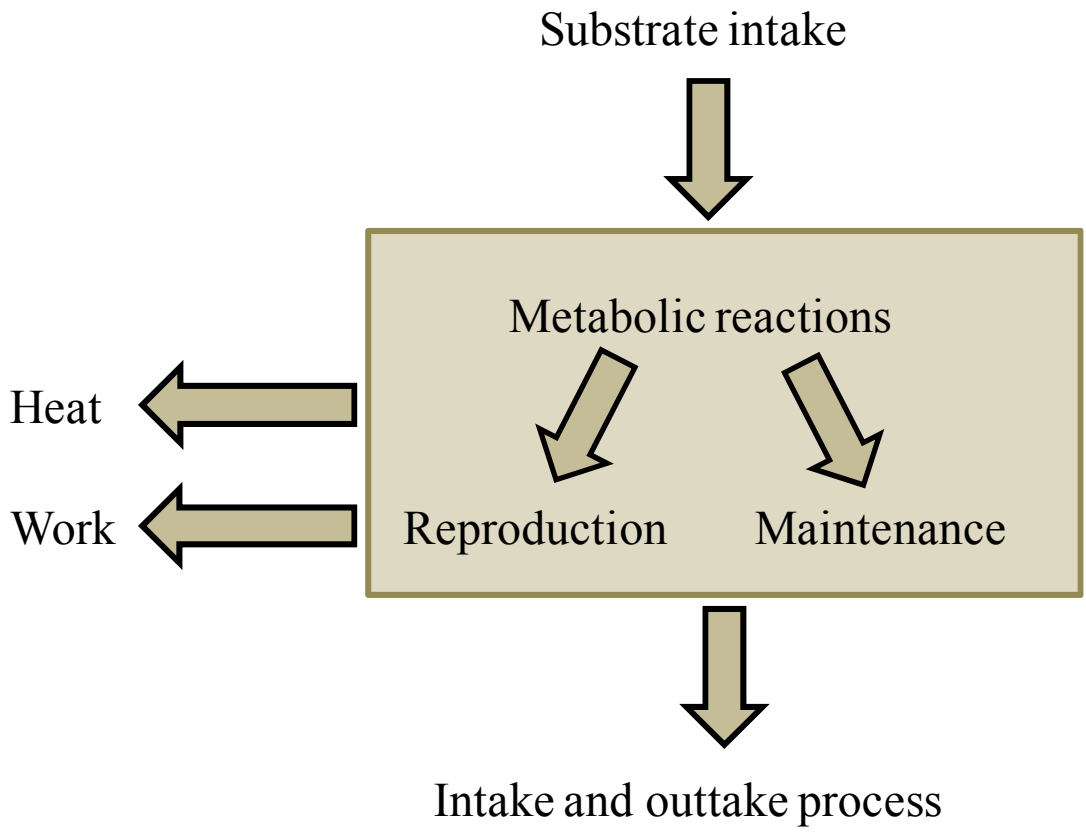

Figure 4: Schematic representation of energy transformations in biological systems.

Thus, acidogenic microorganisms affect the chemistry of their environment by catalysing chemical reactions. The environment, on the other hand, controls the activities of

microorganisms by providing habitats, nutrients and energy resources and in this way the community structures of microbial populations [138].

This allows to regard acidogenic fermentation (as any other physical structure) as an organised structure or, in other words, as a system with imposed boundaries and constraints [101]. Thermodynamics based modelling provides additional boundary conditions to systems in addition to mass conservation laws considerations of classic AD modelling. These additional thermodynamic boundaries must be obeyed by any reaction that is described by a realistic model. However, contemporary biophysics, partially explains the structures of the elements of living systems, since it treats certain other components as given [101]. So a multidisciplinary approach, which includes thermodynamics, is desired.

This section describes the fundamental laws of thermodynamics, followed by the two different approaches to model microorganism systems, *i.e.* biomass yield and metabolic networks. This section concluded by a description of literature thermodynamics analysis performed on acidogenic fermentation systems.

1.4.1 Fundamental laws of thermodynamic

The word thermodynamics was coined around 1840 from two Greek roots: *therme*, heat, and *dynamis*, power. This branch of physics is concerned with energy storage, transformation and dissipation. Thermodynamics aims to describe and relate, in relative simple mathematical terms, the physical properties of energy and matter of a given system [144]. Any system, physical, chemical or even biological, can be considered as a thermodynamical system and the laws of thermodynamics can be applied to it, if it utilises energy in any form [145]. Energy as well as thermodynamics, has a Greek root: *en*, in, and *ergon*, work.

Thermodynamics requires a measurement of energy. The units of energy are Joules, in the International System of Units. One Joules is equal to the energy expended (or work done) in applying a force of one Newton through a distance of one metre, or in passing a current of one

ampere through a resistance of one ohm for one second [146]. Furthermore, thermodynamics is constituted by three laws, which are the most important and fundamental laws in physics.

The first law of thermodynamics

The first law of thermodynamics can be stated as: "The total energy of the Universe is constant". Here it is stated the conservation of energy; *i.e.* it can be changed from one form to another; energy can neither be created nor destroyed. The energy of a system plus surroundings is constant in time. This law resembles the law of conservation of matter, according to which the total amount of matter is constant in the course of a chemical reaction. The first law of thermodynamics is empirical in nature; it cannot be derived mathematically from more basic principles [144].

The more basic forms of energy are work, heat and internal energy. Work, W, is defined as:

$$W = F \cdot d \tag{7}$$

where F is the force applied in the body and d is its displacement under the application of this force. The work done by a system is taken to be positive, while the work done on a system is negative.

Heat, Q, is described as an energy transfer between physical entities in any other way than due to work performed on the system. It is also defined as the energy transfer due to thermal contact when the physical entities are at different temperatures.

Work and heat are inter-convertible, and unlike pressure, volume, and mass, they are not intrinsic properties of a system. A system can go from one state to another through an infinite number of different processes or paths. The values of W and Q for each one of these paths are different. However, the difference, Q-W remains the same and is independent of the path taken. Thus

$$dU = dQ - dW \tag{8}$$

where *dU* is the change in the internal energy, an intrinsic property of the system. Eq.(8) is the first law of thermodynamics. It can be paraphrased as 'energy can neither be created nor destroyed' [145].

Second law of thermodynamics

The second law of thermodynamics is concerned with the direction in which the energy transfer proceeds. This law is stated in many different ways. One of the conventional statements is "it is not possible to convert heat completely to work with no other change taking place". It is also stated in terms of heat flow, as follows: "It is impossible for heat to flow from one body to another which is at a higher temperature, with no other change taking place" [145]. The second law of thermodynamics, as it was worded by Clausius, states that "any arbitrary adiabatic process entropy of the final state is larger than or equal to entropy of the initial state [147]".

Third law of thermodynamics

This law states that the entropy of a pure solid or liquid is zero at the absolute zero temperature. It is sometimes stated as follows: "It is impossible to attain absolute zero temperature through a finite number of operations" [145].

In second and third laws of thermodynamics appears the entropy concept, which is explained below.

Entropy

Entropy, *S*, is defined as a thermodynamic function where change is independent of the path of transformation of the system, *i.e.* the change in *S* is measured as the ratio of the change in heat to the temperature, *T*, at which the change takes place in a reversible process. It is given by:

$$\mathrm{d}S = \frac{\mathrm{d}Q}{T} \tag{9}$$

Like temperature and internal energy, entropy is an intrinsic property of the system, and like *T* and *U*, it is called a state function describing the state of the system [145]. In the case of irreversible processes, the change in entropy between two equilibrium states is calculated by finding a reversible path between the two states and calculating the entropy change for that path. The second law of thermodynamics can be restated to say that the entropy of an irreversible process in an isolated system always increases, *i.e.*

$$\Delta S > 0 \tag{10}$$

Thus, naturally occurring spontaneous irreversible processes, such as biological processes, always result in an increase in entropy [145]. The difference between the chemically useful energy and the wasted energy can be quantified using the concept of entropy.

When an amount of heat is transferred at temperature *T*, the system gaining the heat has its entropy increased by *ΔQ/T*. For example, sunlight (which has roughly speaking a radiation temperature of 6000 K) is a radiation with low entropy. A joule of thermal radiation from the surface of an organism at 300 K (20 times cooler) transmits 20 times as much entropy as a joule of solar radiation. This theme is a common one in biology: energy is acquired from low-entropy sources, and is used in a variety of different biochemical, physiological and ecological mechanisms. Ultimately, the energy is lost to a sink for energy at low temperature and correspondingly high entropy [148].

Traditional thermodynamics discusses heat engines (such as the steam turbines at thermal power stations) taking heat from the high-temperature source, converting part of it into work, rejecting the rest as heat into the low-temperature sink (the cooling tower) and generating entropy in so doing.

The biology of (most of) the biosphere depends thus not only upon the energy from the sun (a source at T ~ 6000 K) but also upon the ultimate sink of energy, the night sky (at ~ 3 K) [148].

In non equilibrium systems, living systems as part of them, entropy is maximised. The so-called maximum entropy production principle states that a nonequilibrium system develops so as to maximise its entropy production under present constraints [147].

However, in chemical and biochemical processes, where energy systems could do work on the environment and/or receive heat form the environment, the energy is measured as enthalpy and Gibbs free energy [148]. Both are explained in detail below.

Enthalpy

Enthalpy, *H*, of a system is defined as:

$$H = U + PV \tag{11}$$

where *U* is the internal energy, *P* the pressure and *V* the volume. *P* and *V* are intrinsic properties and hence thermodynamic parameters. Their product is expressed in units of energy. Therefore, enthalpy is also expressed in units of energy and is known as the heat content of a system. Since *H* is a combination of state functions and parameters that are independent of the path of transformation of the system, enthalpy is independent of the path. The change in enthalpy is obtained by considering the differential form of Eq. (11), which is:

$$dH = dU + PdV + VdP \tag{12}$$

At constant pressure $VdP = 0$, therefore:

$$dH = dU + PdV \tag{13}$$

But from the first law of thermodynamics we know that:

$$dQ = dU + PdV \tag{14}$$

where W, the work done, equals PdV (at constant pressure), therefore:

$$dQ = dH \tag{15}$$

Thus enthalpy is an intrinsic property of the system. Its increase is equal to the amount of heat absorbed from the environment at constant pressure. A reaction is exothermic when heat is let out to the surroundings and the enthalpy change is then negative. On the other hand, in an endothermic reaction, heat is absorbed from the surroundings, and the enthalpy change is positive [145].

The Gibbs free energy of a system

Gibbs free energy is used to describe biological process, and is defined as:

$$G = U - TS + PV \tag{16}$$

Under constant pressure and temperature, the change in this potential is given by the appropriate differential form of the equation:

$$dG = dU - TdS + PdV = dH - TdS \tag{17}$$

For reversible process using Eq. (9) we have

$$-dW_{max} = dU - TdS \tag{18}$$

Since the maximum work is done in such processes. Thus

$$dG = -dW_{max} + PdV \tag{19}$$

Therefore

$$-dG = dW_{max} - PdV = dW_{net} \tag{20}$$

At equilibrium *dG*, and *dS* are both zero. Once again the decrease in free energy is a measurement of the useful work done under conditions of constant pressure and temperature [145].

Equilibrium

By definition, equilibrium is achieved when the relevant parameters cease to vary with time. Global chemical equilibrium is rarely of direct interest to biologists. However, in many cases, local equilibria are achieved, *e.g.* thermal and hydraulic equilibrium [148]. Equilibrium is differentiated from steady state which is defined below.

Steady state

In a system in steady state, energy and/or matter enter the system and leave the system at the same rate. The energy may leave in a different form or at a different temperature. In steady state, most of the parameters of the system do not change with time. The maintenance of a steady state requires a continuous throughput of energy, which has been previously schematised in Figure 4. Removing the sources or the sink of energy has as a consequence the living system coming to equilibrium, *i.e.* it dies [148].

1.4.2 Modelling of biomass yield

Biomass yield is a critical parameter in order to understand the behaviour of microorganisms, predict biodegration of organic anthropogenic compounds, or develop stoichiometries for biochemical processes.

Biomass yield represents the amount of biomass formed for a unit of substrate consumed. The first reference of biomass yield thermodynamic based prediction was in 1965 by McCarty [149]. Since then, different models have been developed [150-156].

The common axis of these models was the flow of carbon, electron and energy from substrates to biomass at a given energy transfer efficiency. They describe how the electrons coming from a donor substrate is divided into two fractions: 1) energy uptake, and 2) biomass synthesis.

Energy uptake is due to the flow of electrons from donor to acceptors. In literature [150,155], the assumed efficiency of capture of energy available has been considered to vary in a range of 0.2 to 0.8. But often, this parameter is taken as a constant.

Furthermore, these models do not focus on the prediction of product formation as a function of the environmental condition. Nevertheless, they provide an excellent basis for a bioenergetic approach to this problem.

1.4.3 Modelling of metabolic networks

Other efforts have been addressed to define and detect thermodynamic bottlenecks in biochemical pathways [157], in order to determine if a reaction is feasible or not. This is achieved introducing new equations based on the three laws of thermodynamics [158] (see section 2.5). Though, constraints are based on physical laws, and do not make use of unknown parameters.

In a metabolic network, its stoichiometric matrix provides constraints on the fluxes in a biochemical network which are feasible according to mass balance and the laws of thermodynamics [159].

1.4.4 Thermodynamic analysis of acidogenic fermentation

As seen above, a well known application of the thermodynamic principles for biotechnological processes is the observed correlation between the microbial yield and Gibbs free energy changes of microbial conversions. Furthermore, the mechanisms of formation of intermediate compounds can be analysed using thermodynamic considerations [97].

The application of thermodynamic laws to biochemical processes provides a theoretical basis for analysis of experimental results and an important tool in understanding bacterial growth and energy metabolism [97].

In literature, thermodynamic analysis of acidogenic fermentations is scarce. It has first been proposed by Yu *et al.* [97] that have studied the thermodynamics on batch acidogenesis of lactose.

Yu *et al.* [97] experiments produced H_2 and CO_2 in the gas phase, while in the liquid phase organic acids: acetic, propionic and butyric acids, and in smaller quantities lactic, i-butyric, valeric, i-valeric and caproic acids; and alcohols: ethanol, propanol, butanol and traces of methanol.

The kinetics of lactose and products fermentation indicated that valeric, i-valeric, i-butyric, caproic acids, butanol and propenol where produced from primary acidogenic products, *i.e.* H_2, CO_2 acetic, butyric, propionic acids.

The thermodynamic analysis gives an idea of which metabolic reactions would be more likely feasible for the production of these secondary products. Thermodynamics suggest that valeric acid production requires H_2 as electron donor, consuming propionic acid and carbon dioxide. More feasible synthesis reaction for caproic acid consumed H_2, butyric acid and CO_2.

Propanol was most likely produced by H_2, CO_2 and acetic acid, while i-butyric and i-valeric were produced directly from their corresponding straight-chain isomers.

However, this analysis was only based on thermodynamics. To find the presence of the enzyme systems catalysing those reactions, enzymatic assays are needed in order to validate the thermodynamic hypotheses. Anyway, there are also examples of microbial reactions that were first predicted thermodynamically and subsequently confirmed experimentally in natural and man-made ecosystems, such as anaerobic ammonium oxidation [160], and methane oxidation with sulphate [161] or nitrate [162]. In addition, this analysis did not answer the question of which mechanisms are operating to generate different patterns in acidogenic fermentations.

In any case, thermodynamic analysis of acidogenic fermentation relies on quantitative measurements of fermentation products. Methods allowing the online measurement of these products are crucial for monitoring kinetics on transient states produced by environmental disturbances. The next section introduces the online analytical method: membrane inlet mass spectrometry, which was used in this work.

1.5 Membrane Inlet Mass Spectrometry

Membrane inlet mass spectrometry (or membrane introduction mass spectrometry, MIMS) is an analytical method in which a semipermeable membrane is the only interface between a liquid or a gaseous sample at experimental pressure and the vacuum of a mass spectrometer (Figure 5). The membrane creates a tight seal between the two sides, allowing the pass to volatile compounds. Key features of MIMS are its simplicity, speed and sensitivity for monitoring dynamic chemical systems, allowing on-line data gathering from complex matrices such as fermentations [163,164].

MIMS was introduced for the first time in 1963 by Hoch and Kok [165], who used it for monitoring the kinetics of dissolved O_2 and CO_2 during photosynthesis. Fermentation kinetics monitoring by MIMS was first reported by Reuss *et al.* [166] in 1975. Over the years, MIMS has gained more interest and recognition among scientist because of the following MIMS

advantages over other on-line analytical methods: 1) minimally invasive technique, 2) rapid response of seconds to minutes, 3) measures volatile compounds up to 200 molecular weight, 4) high sample frequency, 5) high sensitivity (*e.g.* 0.25 µM O_2), 6) measurements can be made in gas and/or liquid phase, 7) and low analytical costs [167].

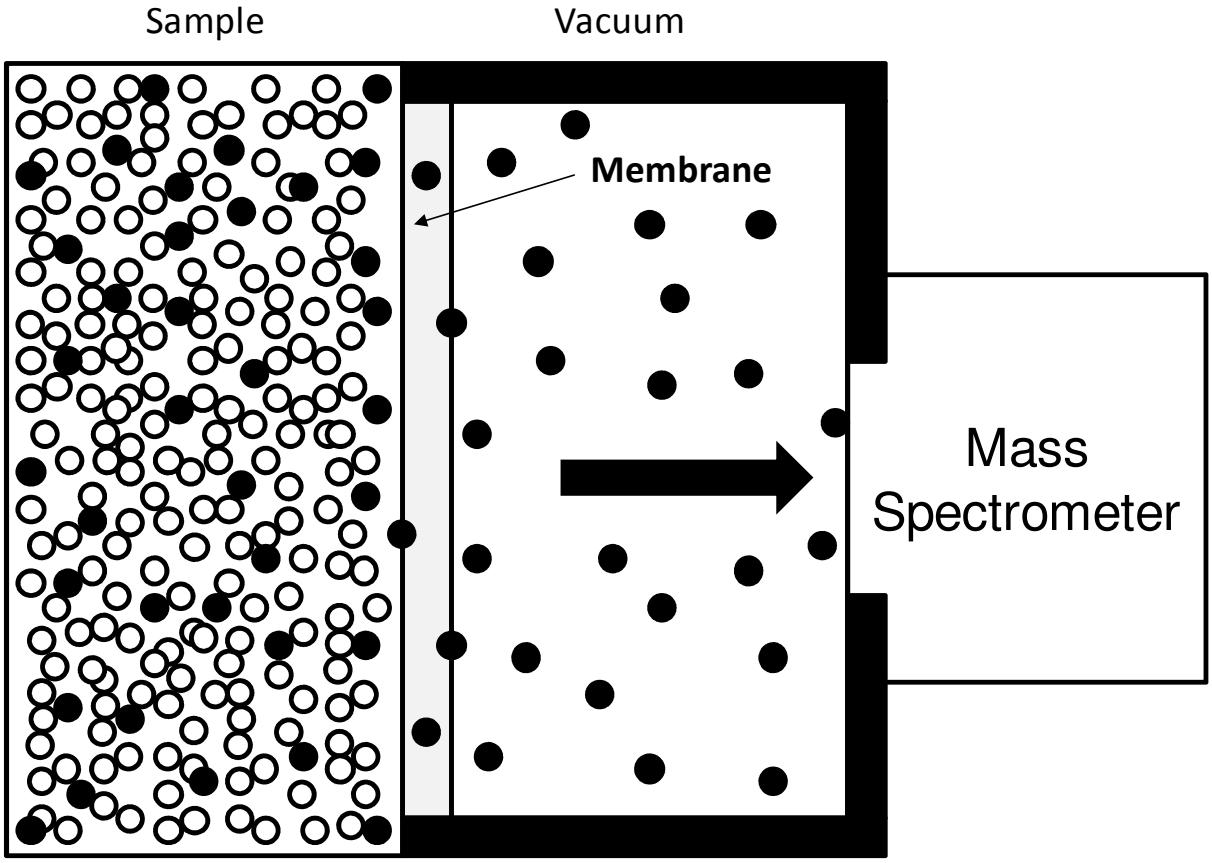

Figure 5: Schematic representation of MIMS. Volatile compounds (black circles) pass through the membrane towards the mass spectrometer aided by the vacuum pressure, while non-volatile compounds (white circles) are impeded to pass by the membrane.

1.5.1 Membrane - the interface of MIMS

Membrane allows achieving a rapid and selective transport of analytes into the mass spectrometer. Most common membranes are silicone polymers (non-porous). They are either sheet or tubular, used for chemical and biological reactor monitoring as well as environmental monitoring. Other non-porous polymers used are polyesters and polyethylene. These membranes are hydrophobic and therefore strongly favour the transport of hydrophobic organic compounds as compared to water. Microporous membranes are used for monitoring

specific chemical systems such as aqueous solutions with glow discharge. These membranes give no chemical selectivity. Microporous polymers are polypropylene and Teflon.

Non-porous membranes allow the permeation of typical fermentation compounds such as gases (CO_2, CH_4, H_2 and O_2) and volatile organic compounds such as ethanol, undissociated volatile fatty acids (acetic acid, butyric acid), etc.
Transport of compounds through non-porous membrane is a process called pervaporation which involves three steps: 1) selective adsorption of analytes onto the membrane surface; 2) analyte diffusion through the membrane, and; 3) desorption/evaporation of analytes into the vacuum [168]. This process can be described by Fick's laws of diffusion. The molecular flux, $J(x,t)$ (mol·s^{-1}·cm^{-2}), at membrane depth d_m (cm) and time t(s) can be calculated from:

$$J(x,t) = -D(c)\frac{\partial c(d_m,t)}{\partial d_m} \tag{21}$$

and the change of analyte concentration $c(d_m,t)$ at depth d_m and time t from:

$$\frac{\partial c(d_m,t)}{\partial t} = \frac{\partial}{\partial d_m}\left(D(c)\frac{\partial c(d_m,t)}{\partial d_m}\right) \tag{22}$$

where $D(c)$ is the concentration dependent diffusion coefficient (cm^2·s^{-1}) and c is the concentration (mol·L^{-1}). Diffusivity is related to the molecular properties of the analyte and membrane [164]. Diffusion is assumed to be the rate-limiting process while adsorption and desorption at the membrane surfaces are considered instantaneous [168]. The operating parameters have been reported to have a significant effect on the responses and responses times when analysing (see section 1.5.3).

1.5.2 Mass spectrometry - the core of the MIMS

Mass spectrometry (MS) is an analytical technique that measures the mass-to-charge ratio (m/z) of charged particles. The MS principle consists of ionizing chemical compounds to generate charged molecules or molecule fragments and measurement of their mass-to-charge ratios.

In MIMS case, analytes that have passed though the membrane are ionized by impacting them with an electron beam, which results in the formation of charged particles. The ions are accelerated and deflected by magnetic fields (Figure 6). The magnitude of the deflection of the moving ions trajectory depends on their mass-to-charge ratio. Lighter ions are more deflected than heavier ions. Then, the ions pass to the detector, which records the relative abundance of each ion type, and their signal is processed into mass spectra.

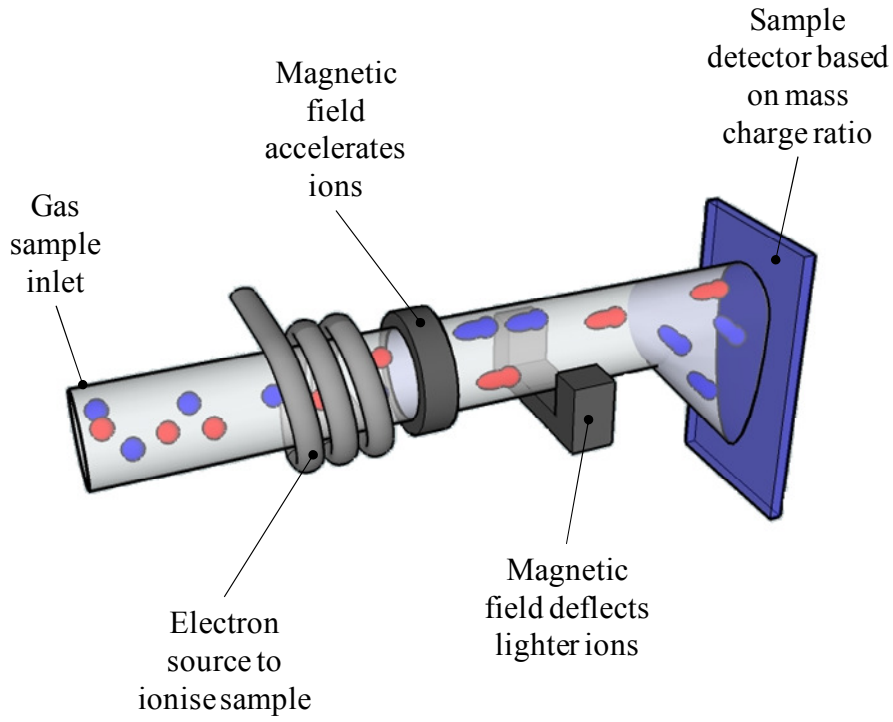

Figure 6: Mass spectrometer scheme. Heavy mass-to-charge ions are represented in red while light particles in blue.

1.5.3 Translation of MIMS signals

MIMS signal magnitude not only depends on the volatility of the analyte, but also on sample and experimental conditions, including membrane permeability, temperature, ionization, sample point hydraulics, and sample matrix composition [169]. These issues need to be addressed during calibration of the signal.

With good control of experimental equipment, the most variable of these is the chemical matrix. Chemical components can influence permeation rates and ionization efficiencies of analytes, cause long-term memory effects and change membrane properties [170,171]. There

is generally limited calibration information available, and early work using MIMS did not calibrate against an external reference, but instead presented relative kinetics [166,172].

Hillman *et al.* [173] and Radivojevic *et al.* [174] translated MIMS signals by estimating dissolved concentrations of gases in water using gas partial pressures and Henry law. Standard solutions [167,175-180] have been used, but this results in a different matrix from the sample. Heinzle and Lafferty [170] showed that three different liquid solutions (pure water, normal nutrient solution and sterilized fermentation broth) have an impact on calibration curves for dissolved H_2 and O_2. They also showed that presence of viable cells had an impact, and concluded that standard solution calibration was not suitable for biochemical experiments. Andersen *et al.* [181] attempted to address matrix issues by resuspending a known amount of viable cells into the calibration solutions. Yang *et al.* [182,183] used corrections in CO_2 MIMS signal for pH and ionic strength. Lloyd and James [184] used standard additions in fermentation experiments at constant pH and temperature. This approach was followed by other workers [185,186]. This is effective, but it has a chemical impact on the underlying processes. This approach also does not effectively address solution non-ideality. In addition, standard additions require a compound that is relatively easy to add, which is not the case for dissolved gases.

The best way to address variability in chemical matrix and other conditions is by off-line measurement against a matrix-independent method. This was done by Doerner *et al.* [187] and Tarkiainen *et al.* [171] who determined that calibration against standards was unsuccessful. They examined how different mixtures of gases and volatiles affect membrane transfer properties, and consequently MIMS signal magnitude. The conclusion was that MIMS signal calibration for fermentation processes has to be based on conventional off-line analysis such as gas chromatography.

Hence, calibration based on off-line analysis seems to be an effective method, but there is a lack of detailed information, particularly for measurement of dissolved gases in the liquid phase. This is critical for H_2 and CO_2 that are major products of acidogenic fermentation. The issues around H_2 are complicated by high diffusivity, low solubility, and a high degree of non-ideality in relation to the matrix, while dissolved CO_2 concentration is highly affected by liquid matrix pH. Hence, one of the objectives of this work is to assess MIMS calibration

methods for fermentation experiment systematically, and particularly with respect to dissolved gases.

2 MATERIALS AND METHODS

2.1 Fermentations Set-Up

Acidogenic cultures were carried out at the Advanced Water Management Centre, The University of Queensland, Australia, in a continuous stirred tank reactor (Figure 7), at constant temperature, hydraulic retention time (HRT) and stirring velocity as described in Table 3.

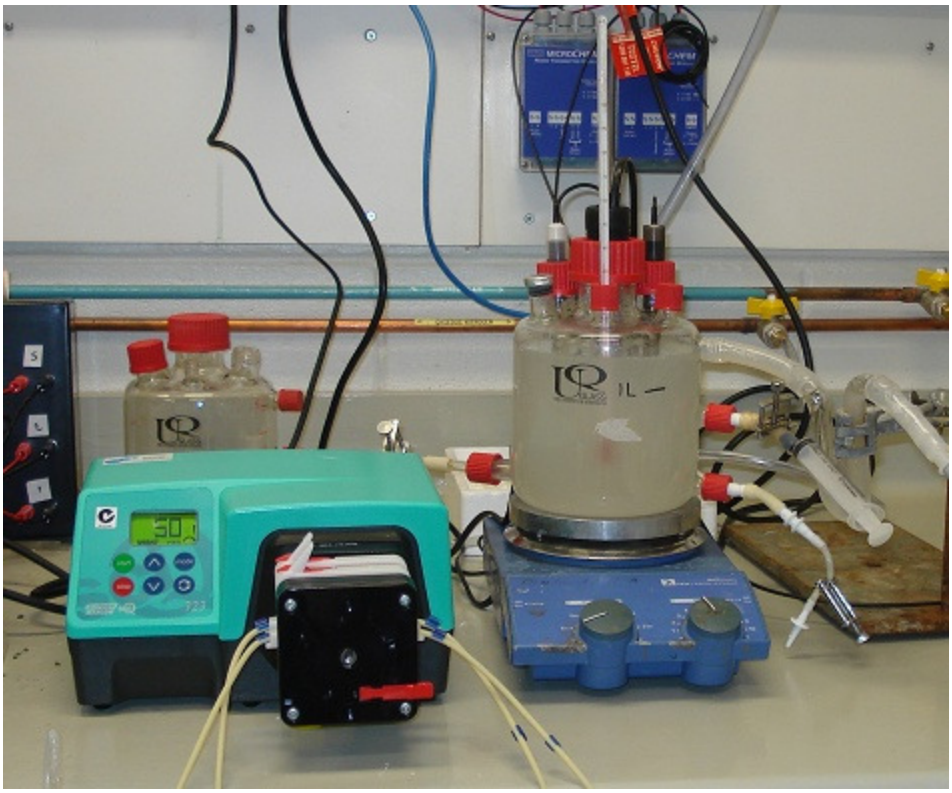

Figure 7: Picture of the acidogenic fermentation reactor system. From left to right: feeding pump, acidogenic reactor, magnetic stirrer.

The continuous culture ability to establish (quasi-) steady state conditions is a frequently stated advantage that allows environmental parameters to be manipulated without causing concomitant changes of the specific growth rate. Moreover, the use of continuous cultures also enables the critical study of specified transition states and chemical, physical or

biological perturbations. Such dynamic analyses enhance our understanding of microbial ecology and microbial pathways for example. They also can inform the optimisation of batch and fed-batch operations that are characterised by sequential transitions states [188].

Table 3: List of experimental conditions

Constant parameters	Temperature (°C)		37
	HRT (h)		6
	Stirring velocity (rpm)		600
	Glucose inlet concentration ($g \cdot L^{-1}$)		5

	experiment n°	pH	N_2 flushing ($L \cdot d^{-1}$)
N_2 flushing experiments	1	6.5	0
	2	6.5	2.5
	3	6.5	7.3
	4	6.5	58.4
	5	5.5	0
	6	5.5	7.3
	7	4.5	0
	8	4.5	2.5
	9	4.5	58.4
pH experiments	10	5.5	
	11	6	
	12	6.5	
	13	7	
	14	7.5	

A first set of experiments was set up to investigate the effect of head-space gas composition on the fermentation product spectrum. N_2 flushing, rather than sparging, was used to produce changes in the head-space gas composition. This avoids disturbing the liquid phase of the reactor. Head-space gas composition changes were set up at pH 4.5, 5.5 and 6.5. Selected N_2

flushing flow rates were sequentially stepped-up just after reaching steady state at each pH. Selected N_2 flushes (in $L \cdot d^{-1}$) were 2.5 and 58.4 at pH 4.5; 7.3 at pH 5.5; and 2.5, 7.3 and 58.4 at pH 6.5. Each N_2 flushing flow rate lasted for 6 HRT. Both 2.5 and 7.3 $L \cdot d^{-1}$ are common values found in literature [16,17,53] for gas sparged systems, while 58.4 $L \cdot d^{-1}$ allowed to reach very low H2 partial pressures in our experiments.

Furthermore, pH step changes were performed in order to determine their relationship with head-space composition changes due mainly to CO_2. pH was stepped up (from pH 5.5 to 7.5) by 0.5 pH units every 6 HRT. None of these experiments used N_2 flushing.

2.1.1 Reactor equipments

A diagram of the experimental equipment is shown in Figure 8. Liquid volume was 1.31 L and a headspace of 170 mL. Temperature was regulated at 37°C using an immersed glass heater (25W Aqua One^{TM}). A magnetic stirrer was used at approximately 600 rpm. For continuous experiments, the system was fed by a Watson Marlow peristaltic pump from split feed tanks containing basal media, and pure glucose solution. pH was controlled by automatic 1 M NaOH addition. Liquid lock was maintained by a glass u-tube. Gas flow was measured by a tipping-bucket type meter, with a bucket volume of 2 mL, and a constant pressure of approximately 1 cm water. Membrane inlet mass spectrometer (MIMS) probes were placed both in gas and liquid phases, respectively. All equipment was interfaced to computers via an Opto PLC used for data logging and set-point modification. N_2 flushing of the headspace was also available, with pure N_2 flow being regulated through parallel Cole Parker rotameters with limits of 0.5 $mL \cdot min^{-1}$ and 5 $mL \cdot min^{-1}$ (allowing full range of flow regulation). Anaerobic conditions were maintained connecting all feeding bottles, *i.e.* basal media, glucose solution and NaOH, to N_2 bags.

2.1.2 Media and inoculum

Media. Feed was held in two containers, in order to avoid microbial contamination, and fed simultaneously. Substrate solution consisted of 10 $g \cdot L^{-1}$ of glucose and silicone based antifoam (Dow Corning® antifoam RD emulsion) at 1 $mL \cdot L^{-1}$, autoclaved at 120°C for 45

min. The Basal Anaerobic (BA) media contained in $mg \cdot L^{-1}$: 2.4 $CaCl_2 \cdot 2H_2O$, 0.1 $(NH_4)_6Mo_7O_{24} \cdot 4H_2O$, 0.1 $CoCl_2 \cdot 6H_2O$, 4 $FeCl_2 \cdot 4H_2O$, 0.1 $MnCl_2 \cdot 4H_2O$, 0.184 $NiCl_2 \cdot 6H_2O$, 0.2 $Na_2SeO_3 \cdot 5H_2O$, 0.1 H_3BO_3, 0.076 $CuCl_2 \cdot 2H_2O$, 0.1 $ZnCl_2$, 0.1 $AlCl_3$, 1 EDTA, 0.01 aminobenzoic acid, 0.004 biotin, 0.004 folic acid, 0.01 nicotinic acid, 0.01 panthothenic acid, 0.02 pyridoxine, 0.01 riboflavin, 0.01 thiamine hydrochloride, 0.0002 cyanocobalamine, 0.01 lipoic acid; In $g \cdot L^{-1}$: 2 NH_4Cl, 0.2 NaCl, 0.2 $MgCl_2 \cdot 6H_2O$, 0.2 $K_2HPO_4 \cdot 3H_2O$, and 0.2 $Na_2S \cdot 9H_2O$; and HCl 2 ($\mu L \cdot L^{-1}$). BA media was based on Angelidaki and Sanders [189], modified to minimise calcium phosphate precipitation.

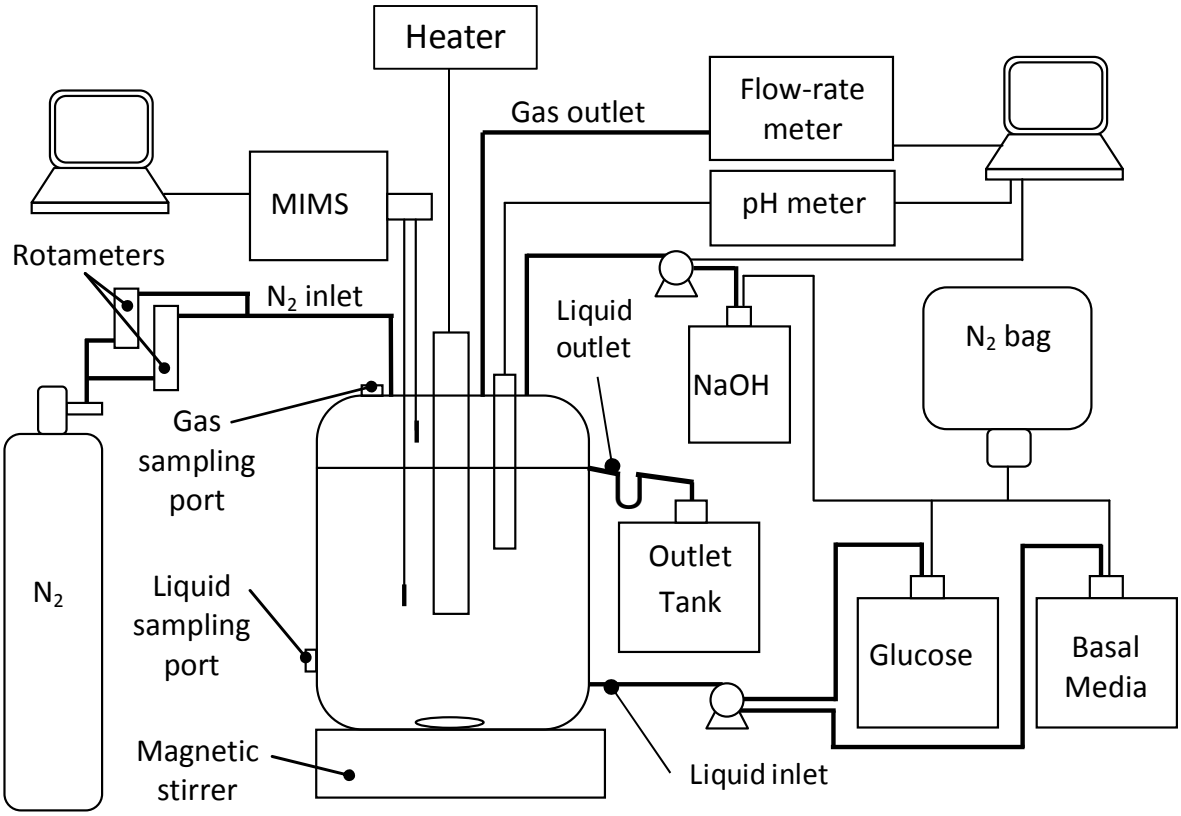

Figure 8: Reactor diagram equipment. From left to right: MIMS equipment for online liquid and gas phase kinetics monitoring; N_2 flushing system for head-space composition changes; submerged heater; magnetic stirrer; Gas outlet and gas flow-rate meter; automatic pH control; Liquid inlet and outlet.

Inoculum. Inoculum was anaerobic digestate from a primary sludge fed digester in Brisbane, Australia. The inoculum was conditioned by operation at 12 h hydraulic retention time (HRT) over 1 week without pH control (native pH of 5.5), until methane production stopped, giving as a result a standardized mixed culture fermentative community.

2.2 Analytical Methods

2.2.1 Gas phase

Gas samples of 0.5 mL were taken with a glass syringe, and analysed immediately by gas chromatography. H_2 was analysed using a GC-8A gas chromatograph (GC) equipped with a thermal conductivity detector (Shimadzu) with N_2 as a carrier gas at 100 kPa, 110°C for the injection and detector temperature and 40°C for the column temperature with a thermal conductivity detection (TCD) current of 80 mA. CO_2 was analysed using the same GC and conditions mentioned above, but using He as carrier gas and a current of 160 mA. Calibration was performed prior to each day's measurement using external gases provided by BOC Gases Australia Ltd. 5% CO_2 and 5% N_2 in methane, 20% CO_2 and 20% N_2 in methane, and 100% H_2, injected as 0.5 mL at 1 atm.

2.2.2 Liquid phase

Liquid samples were taken from the liquid sampling port (Figure 8). Each liquid sample consisted of 12 mL. Two samples of 4 mL each were injected via a sterile 0.22 μm cellulose acetate cartridge into 10 mL vacuum tubes (BD Vacutainer® serum tubes), while the remaining 4 mL was preserved with formic acid for ethanol analysis. The tubes for dissolved CO_2 measurement were previously injected with 0.5 mL of 2 M HCl.

Dissolved gas measurement was based on an equilibrium assumption. Tubes were equilibrated for 24 hours at 20°C. 0.5 mL gas sample from each tube was measured by gas chromatography. Dissolved H_2 was measured using a GC-8 equipped with a thermal conductivity detector (Shimadzu) and a 183 x 0.32 x 26 cm stainless steel molecular sieve (80/100 mesh, washed) column. The GC was fitted with a Clarity Lite Data analysis software package. A reference and a measurement channel were used simultaneously. Those channels worked a 300 and 400 kPa respectively using Ar as a carrier gas. Injection and detector temperatures were 80°C and 120°C for the column, with a TCD current of 70 mA. Calibration was performed prior to each day's measurement using external gas standards obtained from

BOC Gases Australia Ltd. with concentrations in % of 0.1, 1 and 3 H_2 in N_2. Dissolved CO_2 samples were analysed as for gas phase samples.

Liquid phase H_2 or CO_2 was estimated using the temperature corrected Henry's law coefficient, and the total H_2 or CO_2 concentration in the liquid sample calculated by a mass balance. Sample liquid and gas volumes were checked by weighing on a balance.

Reactor's dissolved CO_2 concentration was then calculated as a fraction of the total CO_2 measured by this method, function of the carbonates (HCO_3^- and CO_3^{2-}) equilibrium constants at 37°C (Ka_1: $5 \cdot 10^{-7}$, Ka_2: $5.8 \cdot 10^{-11}$) and reactor's pH as is expressed in the equation below.

$$CO_{2(dissolved)} = CO_{2(total)} \cdot \frac{[H^+]^2}{[H^+]^2 + Ka_1[H^+] + Ka_1 \cdot Ka_2} \quad (23)$$

Ethanol, acetic and butyric acids were measured on a GC equipped with a polar capillary column (Agilent technologies) and a flame ionization detector (FID). Samples were preserved with 1% of formic acid prior to analysis. Glucose, lactic and formic acids were measured by high-performance liquid chromatography (HPLC). Total and volatile solids were measured as indicated in Standard Methods [190]. 10 mL were filtered through a re-usable cartridge onto a 47mm diameter pre-dried glass fibre filter (Whatman GF/C).

2.3 MIMS Set-Up

On-line monitoring of fermentations was carried out by MIMS. Kinetics of H_2, CO_2 and ethanol were followed by a commercially available Hiden HPR-40 DSA dissolved species analyser bench top MIMS unit (Hiden Analytical Ltd., Cheshire, England), which contained a Hiden HAL 201 RC quadrupole mass spectrometer with dual faraday/electron multiplier detector and a mass range of 200 atomic mass units. MIMS unit inlets consist of a 4 way multistream selector for simultaneous sampling. Each MIMS probe had 0.5 m length, suited with silicon rubber membrane (Figure 9). A scheme and picture of this system is showed in Figure 10.

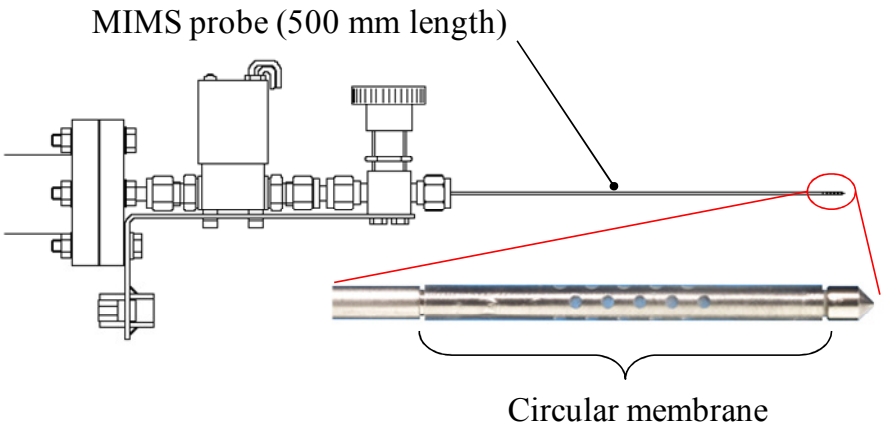

Figure 9: HPR-40 DSA MIMS probe (Hidden analytical Ltd.). The probe uses a circular silicone membrane (Zoom in).

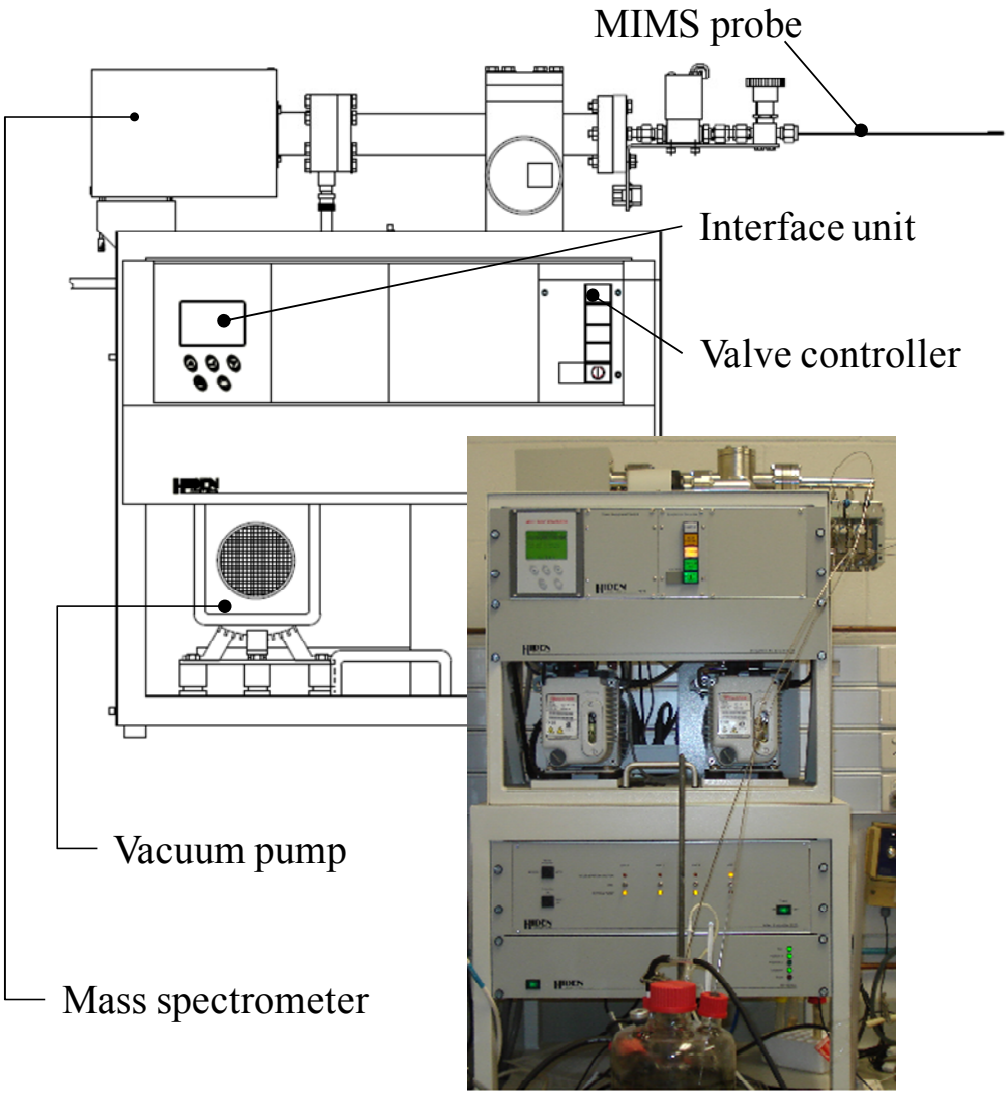

Figure 10: Hiden HPR-40 DSA membrane inlet mas spectrometer scheme and picture (bottom left).

Recorded mass to charge (m/z) ratio were 1, 31, and 44 (expressed as atomic molecular units) for H_2, ethanol and CO_2 respectively. These m/z ratios were selected after scanning these three pure compounds previous to the experiments.

Figure 11 illustrates relative intensities of typical acidogenic products. Figure 11A shows the relative intensities of the targeted analytes H_2, CO_2 and ethanol. Figure 11B shows the scan of H_2O, acetic and butyric acids that are present in acidogenic fermentation and could interfere with the targeted compounds

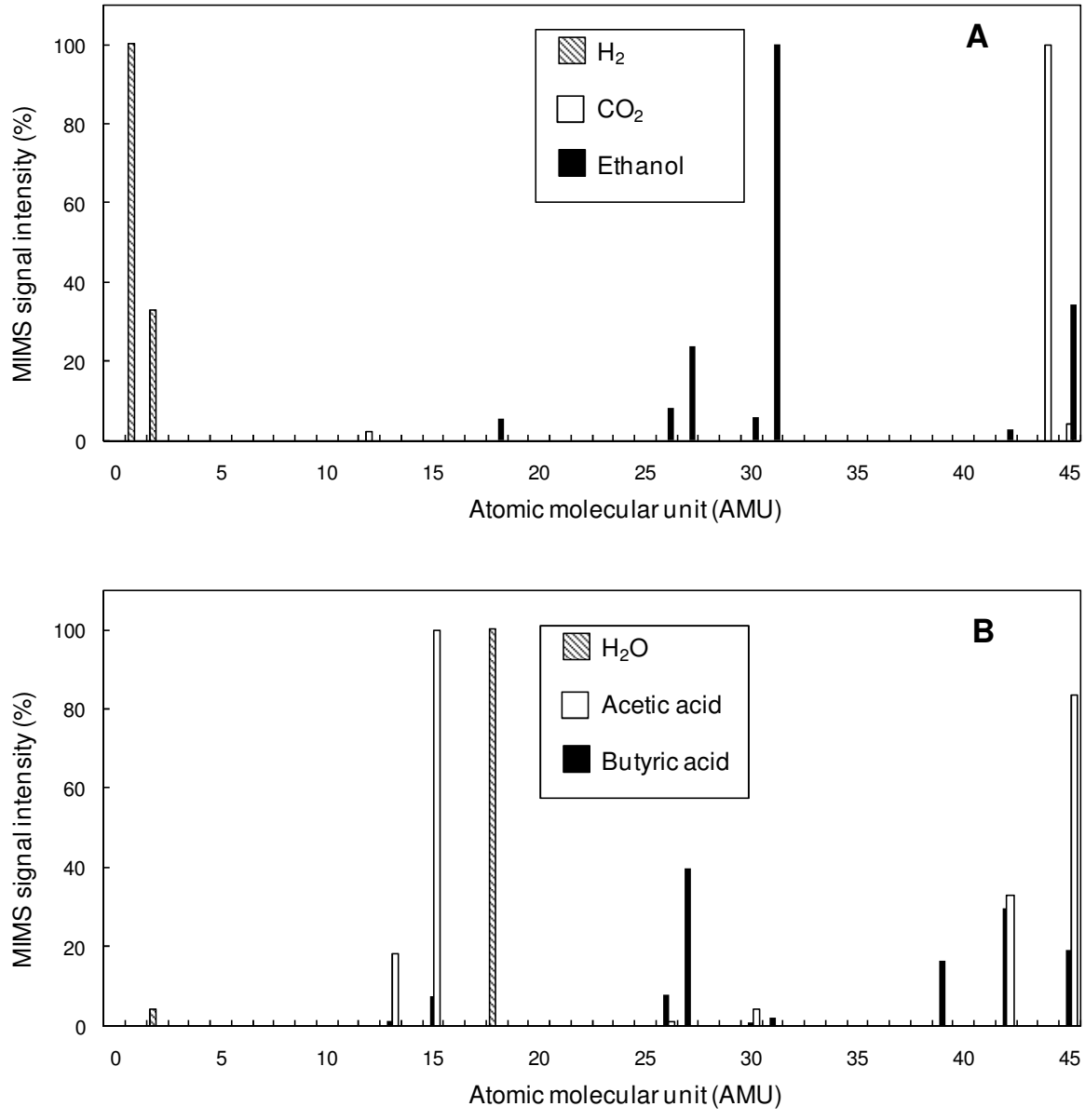

Figure 11: MIMS relative intensities scan for H_2, CO_2, and ethanol (A), and H_2O, acetic acid and butyric acid.

2.4 MIMS Calibration Procedures

Two calibration strategies, standard and in-process, were evaluated for on-line monitoring and quantification of H_2, CO_2 and ethanol in the previously listed set of fermentations (Table 3). Results for both standard and in-process calibrations are presented in section 3.1.

2.4.1 Standard calibration

In this procedure, pure compounds were added at different ratios to the bioreactor either in the gas and liquid phase with N_2 and reverse osmosis (RO) water in gas and liquid phases, in order to cover their expected concentration range in fermentations. Pure H_2 was injected into the head-space to give H_2 partial pressures: 0, 0.2, 0.35 and 0.65 bar, while CO_2 head-space partial pressures were: 0, 0.04, 0.3 and 0.5 bar. Both H_2 and CO_2 were monitored in the gas and liquid phases by MIMS. Gas samples were taken when both MIMS signals were stable. Liquid and gas phase concentrations were analysed as detailed in section 2.2. Pure ethanol was injected in the liquid phase reaching 0, 5, 10 and 30 mM. Ethanol was analysed, and compared to the MIMS signal only in the liquid phase.

2.4.2 In-process calibration

In-process calibration was performed alongside fermentations. Samples were taken from gas and liquid phases at different times and analysed (see section 2.2) to develop a correlation to their respective MIMS signal. Results of two fermentations operated in batch and continuous mode are presented in this work.

Batch experiment. Initial conditions were established by continuous mode fermentation over two days, with pH controlled at 6.5, and a HRT of 6 h. All fermentation conditions, media composition and inoculum are described in section 2.1. Prior to batch experiment, MIMS signal was stable for at least 12 h. Batch experiment consisted of a halt in feed, and injection of 2 mL autoclaved solution containing 325 $g \cdot L^{-1}$ glucose.

Continuous experiment. Continuous mode involved constant feed via a peristaltic pump. Experiments presented here corresponded to experiments 1 to 4 presented in Table 3, where pH set-point was 6.5 and changes in the gas phase composition were achieved by flushing the headspace with N_2. Flushes indirectly changed liquid partial pressures. Liquid partial

pressures were not changed by sparging, as this would also severely change mixing intensity over the MIMS probe.

2.5 Thermodynamic Calculations

Thermodynamic analysis was based on the standard Gibbs energy change of reactions, $\Delta G_j°$(kJ·mol^{-1}), that have been calculated from the free energy of formation data, $\Delta Gf_i°$ (kJ·mol^{-1}), listed in Table 4 [100,150,155] and the relationship with stoichiometric coefficients, v_{ij}, as follows:

$$\Delta G_j^\circ = \sum_i^n v_{ij} \cdot \Delta G f_i^\circ \tag{24}$$

The $\Delta G_j°$ standard conditions [191] for temperature and pressure are 298.15 K (25°C) and 101.325 kPa (1 atm). In aqueous solution, the standard condition of solutes is 1 M and that of water is the pure liquid. $\Delta Gf_i°$ refers to the standard free energy of formation of the substrates and the products from the elements. The subscripts "i" and "j" refer to compound i and reaction j respectively.

2.5.1 Temperature correction

The $\Delta G_j°$ has been defined at standard temperature, T°. The calculation of the Gibbs energy change at a different temperature, T, can be done using the Gibbs-Helmholz equation [192] as follows:

$$\Delta G_{jT}^\circ = \Delta G_j^\circ \frac{T}{T^\circ} + \Delta H_j^\circ \frac{T^\circ - T}{T^\circ} \tag{25}$$

where $\Delta H_j°$ (kJ·mol^{-1}) refers to the standard enthalpy of reaction. Analogous to $\Delta G_j°$, $\Delta H_j°$ is calculated from the enthalpy of formation, $\Delta Hf_i°$ (kJ·mol^{-1}), listed in Table 4 and the stoichiometric coefficients:

$$\Delta H_j^\circ = \sum_i^n \nu_{ij} \cdot \Delta H f_i^\circ \tag{26}$$

2.5.2 Correction for experimental concentrations

Under real conditions, the concentration of substrates and products are different than 1 M and 1 atm. This is considered in $\Delta G_j'$ (kJ·mol^{-1}), which is calculated as follow [157]:

$$\Delta G_j' = \Delta G_{jT}^\circ + \mathrm{R} \cdot T \sum_i^n \nu_{ij} \cdot \ln(c_i) \tag{27}$$

Where C_i is the actual concentration, in M for the aqueous phase and atm for the gas phase, of the "i" compounds participating in the reaction "j", R is the universal gas constant and T the actual temperature (K). The same applies for pH correction [193], where pH is the following proton concentration, [H^+], function:

$$pH = -\log [H^+] \tag{28}$$

Table 4: Gibbs free energy and entalphy formation data set for typical compounds found in acidogenic fermentation

COMPOUND	Abbr.	Phase	ΔG^{o}_{f} (kJ/mol)	ΔH^{o}_{f} (kJ/mol)
Acetate	**ACT**	aq.	-369.41	-486
Acetic acid	**ACTH**	aq.	-396.58	-522.59
Acetyl Coenzyme A	**ACOA**	aq.	-188.52	d.n.f.
Adenosin di-phosphate	**ADP**	aq.	-1906.1	d.n.f.
Adenosin tri-phosphate	**ATP**	aq.	-2768.1	d.n.f.
Butyrate	**BTR**	aq.	-352.63	-535
Butyric acid	**BTRH**	aq.	-380.14	d.n.f.
Carbon dioxide	**CO2**	gas	-394.4	0
Coenzyme A	**COA**	aq.	0	d.n.f.
Ethanol	**EOH**	aq.	-181.75	-288
Formate	**FRM**	aq.	-351	-425.6
Formic acid	**FRMH**	aq.	-372.37	d.n.f.
Glucose	**GLC**	aq.	-917.2	-1264
Hydrogen	**H2**	gas	0	0
Lactate	**LCT**	aq.	-517.2	-687
Lactic acid	**LCTH**	aq.	-539.21	d.n.f.
Nicotinamide adenine dinucleotide	**NAD**	aq.	0	d.n.f.
Nicotinamide adenine dinucleotide reduced	**NADH**	aq.	21.83	d.n.f.
Phosphate	**PI**	aq.	-1096.1	d.n.f.
Proton	**H**	aq.	0	0
Pyruvic acid	**PYR**	aq.	-474.6	-596
Water	**H2O**	liq.	-237.18	-285.8

aq.: aqueous
liq.: liquid
d.n.f.: data not found
Data obtained from literature [100,194,195]

3 RESULTS

This section presents the methodology developed to calibrate membrane inlet mass spectrometry signals in order to monitor acidogenic fermentations experiments; results for acidogenic fermentations experiments under environmental disturbances produced as gas-phase composition and pH; thermodynamic based metabolic network model; and finally the thermodynamic analysis of the acidogenic fermentation results.

3.1 MIMS Signal Translation

Results presented in this section were published in Talanta 83(2):482-492, entitled 'Development of membrane inlet mass spectrometry for examination of fermentation processes' [196]. See ANNEXES section 8.1.

As explained above in section 1.5.3, MIMS is useful for on-line monitoring of fermentation processes. However, readings are affected by the complex and dynamic matrix in which biological processes occur, making MIMS calibration a challenge. In this section, two calibration strategies, as described in section 2.4, were evaluated for measurement of typical products of acidogenic fermentation, *i.e.*, ethanol, H_2, and CO_2 in the liquid phase, and H_2 and CO_2 in the gas phase: 1) "standard calibration", which was performed independent of fermentation experiments with sterile standards in water with a N_2 headspace, and; 2) "in-process calibration" whereby fermentation was monitored concurrent with off-line analysis. Fermentation was operated in batch and continuous mode.

3.1.1 Correlation between MIMS signals and measurement

Figure 12 illustrates normalised slopes and intercepts for standard, batch and continuous linear correlation between MIMS signals and concentration of targeted compounds.

Normalisation was based on the maximum absolute slope and intercept values found among the standard, batch and continuous correlations of each compound at liquid or gas phase.

The calculated linear correlation parameters are summarised in Table 5, where slopes and intercepts are expressed in bar·faraday^{-1} and bar for the gas phase and in mM·faraday^{-1} and mM for the liquid phase.

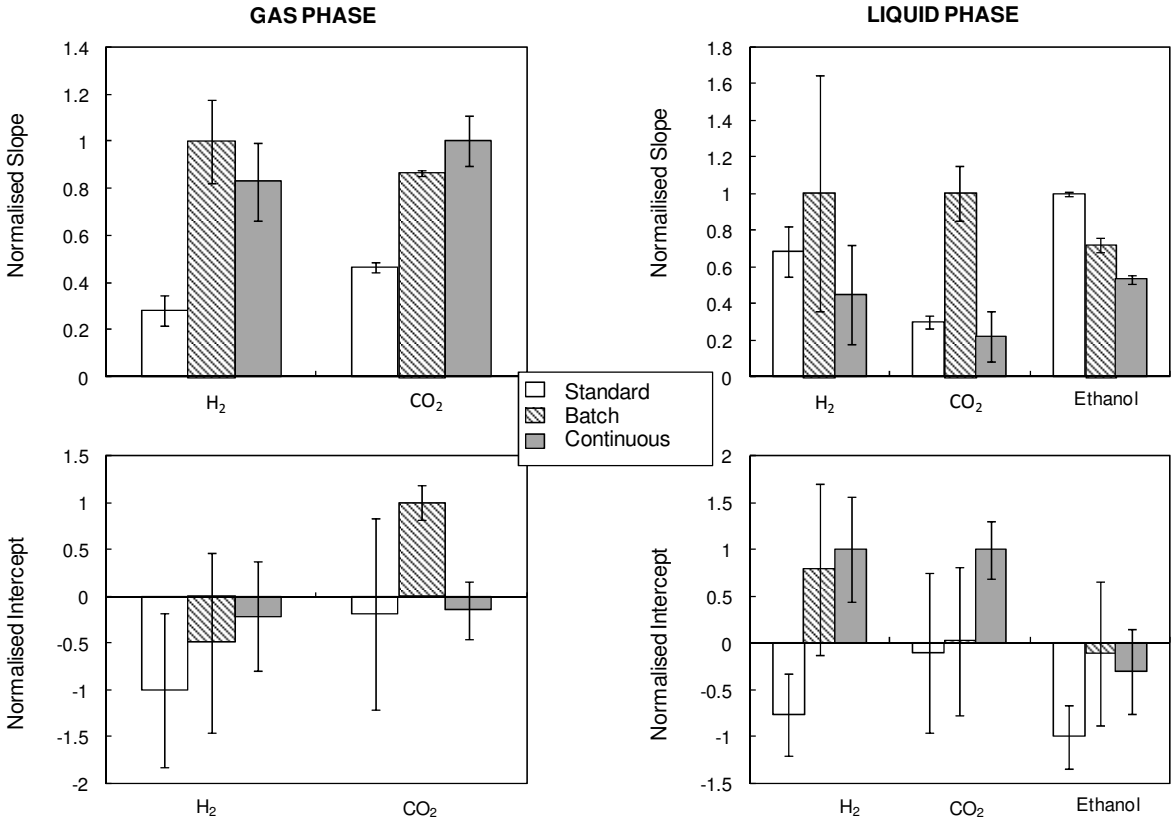

Figure 12: Correlation analysis between MIMS signals and H_2, CO_2, ethanol concentrations. Upper charts show normalised slopes for each targeted compound at standard, batch and continuous experiments, whilst lower charts depict normalised intercepts. Error bars are 95% confidence with appropriate t-values based on degrees of freedom.

Error is shown as 95% confidence in parameters, with appropriate t-values applied based on the number of degrees of freedom. High uncertainty in in-process correlation parameters are generally caused by a limited range in value variation as further addressed in the discussion (see section 4.1.5). Similarities and differences are summarised as follow.

In the gas phase (H_2, CO_2), standard correlation slopes were consistently lower than in-process correlation slopes, indicating high sensitivity for standard conditions (see section 4.1.1). As slopes are expressed in bar·faraday^{-1}, a given partial pressure change will produce larger MIMS signal changes in standard conditions compared to fermentation environments. Intercepts for both gases were statistically zero, except for batch CO_2 which was very low.

In the liquid phase, dissolved H_2 slopes were similar, with a mean of $9 \cdot 10^5$(mM·faraday^{-1}), due to the high errors. Intercept for standard correlation was the lowest, while batch and continuous intercepts were statistically the same.

Table 5: Calculated linear correlation parameters between MIMS signals and H_2, CO_2, ethanol concentrations for standard, batch and continuous experiments, with a confidence range of 95%.

	Gas phase slopes (bar·faraday^{-1})		Liquid phase slopes (mM·faraday^{-1})		
	$H_2 \cdot 10^{-6}$	$CO_2 \cdot 10^{-5}$	$H_2 \cdot 10^{-5}$	$CO_2 \cdot 10^{-7}$	Ethanol$\cdot 10^{-9}$
Standard	0.9 ± 0.2	3.2 ± 0.2	8 ± 2	1 ± 0.1	10 ± 1
Batch	3.2 ± 0.6	6 ± 0.07	12 ± 8	3.4 ± 0.5	7 ± 4
Continuous	2.8 ± 0.6	7 ± 0.7	6 ± 4	0.8 ± 0.5	5 ± 1.5
	Gas phase intercept (bar)		Liquid phase intercept (mM)		
	H_2	CO_2	H_2	CO_2	Ethanol
Standard	-0.13 ± 0.11	-0.002 ± 0.013	-0.14 ± 0.08	-0.1 ± 0.8	-7.7 ± 2.6
Batch	-0.06 ± 0.14	0.01 ± 0.002	0.14 ± 0.16	0.02 ± 0.8	-0.6 ± 6.3
Continuous	-0.07 ± 0.08	-0.002 ± 0.004	0.18 ± 0.11	0.9 ± 0.3	-2 ± 2

Dissolved CO_2 slope for batch correlation was the highest, while standard and continuous slopes were statistically the same. Intercepts were statistically zero for standard and batch correlations while for continuous was the highest.

For ethanol in the liquid phase, slopes and intercepts were statistically the same or very similar due to in-process correlation high errors, caused by limited variation in the ethanol concentration during experiments (see section 4.1.3).

As discussed in section 4.1.5, uncertainty in parameters, particularly slope, were strongly dependent on variation in the targeted compound. Where variation in value was low (*e.g.*, ethanol and dissolved H_2 in batch and continuous), estimates of slope were particularly poor, as would be expected.

3.1.2 Fermentation kinetics

Batch and continuous fermentations (see section 2.4.2) were set-up to investigate separately the effect of liquid and gas matrix dynamics on the translation of MIMS signal. Dynamics in the liquid matrix in batch fermentation were controlled by pH kinetics, while gas matrix dynamics in continuous fermentation were controlled by N_2 flushing. Both effects were analysed using off-line correlation of MIMS signals rather than calibration procedure (see section 4.1).

Figure 13 and Figure 14 illustrate the MIMS signal translation by in-process correlation parameters, solid line, and standard calibration, dashed line, applied for batch and continuous fermentations respectively. Experimental off-line correlation data set is shown as white squares. The dynamics of pH and gas flow rates are also presented in Figure 13F and Figure 14F.

Batch fermentation

Figure 13 illustrates the kinetics of the batch experiment where the estimation of H_2 and CO_2 was substantially improved by application of in-process correlation.

Dissolved CO_2 concentration is dependent of pH, as described in eq. (23) (see section 2.2.2). Measurement of pH dynamics, as is shown in Figure 13F, is crucial when the dissolved CO_2 MIMS calibration method relies on an off-line analytical method that measures total inorganic carbon.

A short period of oscillation on in-process calibrated signals is observed for all the compounds and phases. This issue is further discussed in section 4.1.4.

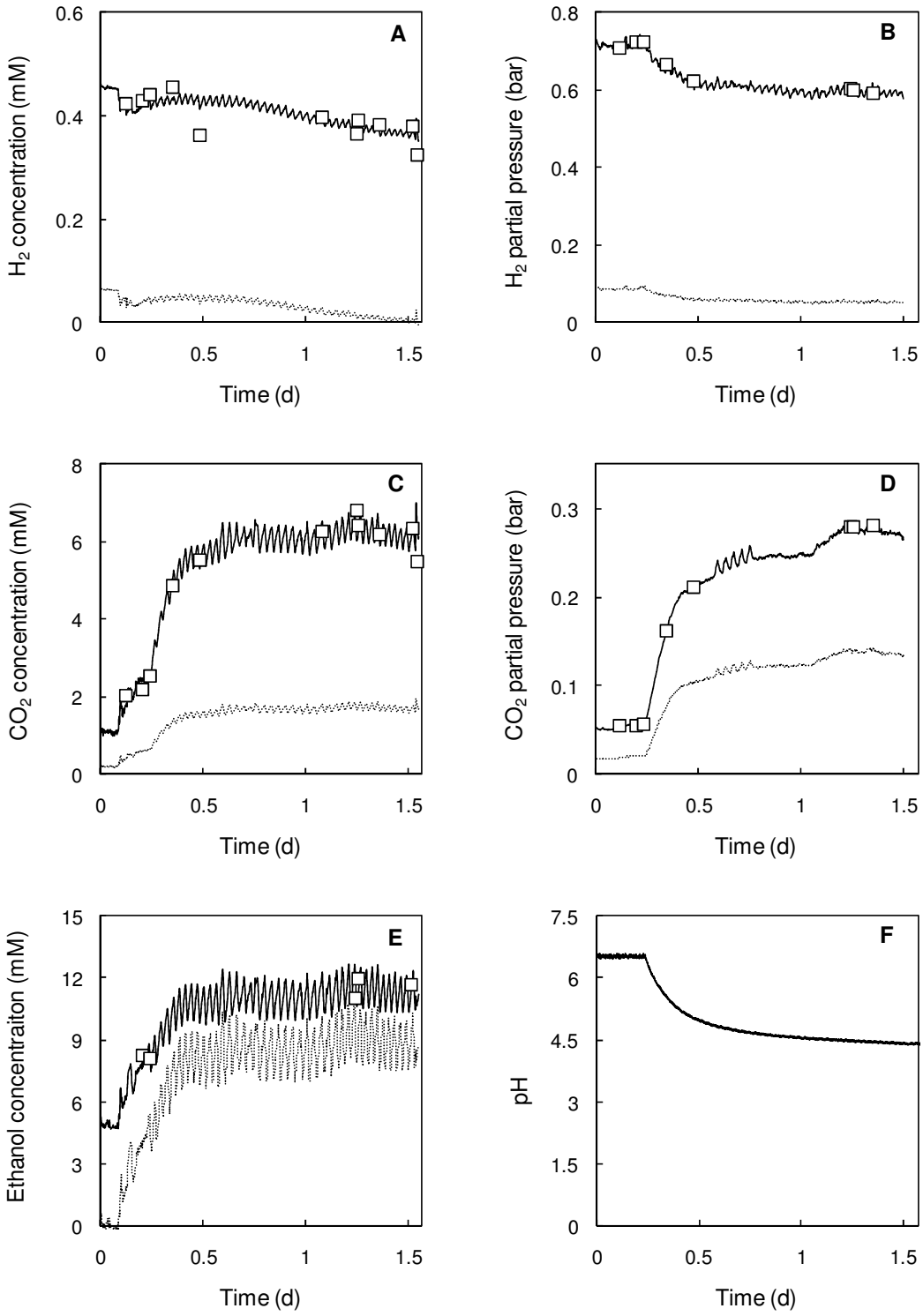

Figure 13: MIMS signal translation of batch fermentation kinetics using batch correlation parameters, solid line, and standard calibration, dashed line. Off-line experimental data set is depicted as white squares. A and B presents dissolved and gas phase H_2, C and D presents dissolved and gas phase CO_2, E shows ethanol while F presents pH kinetics.

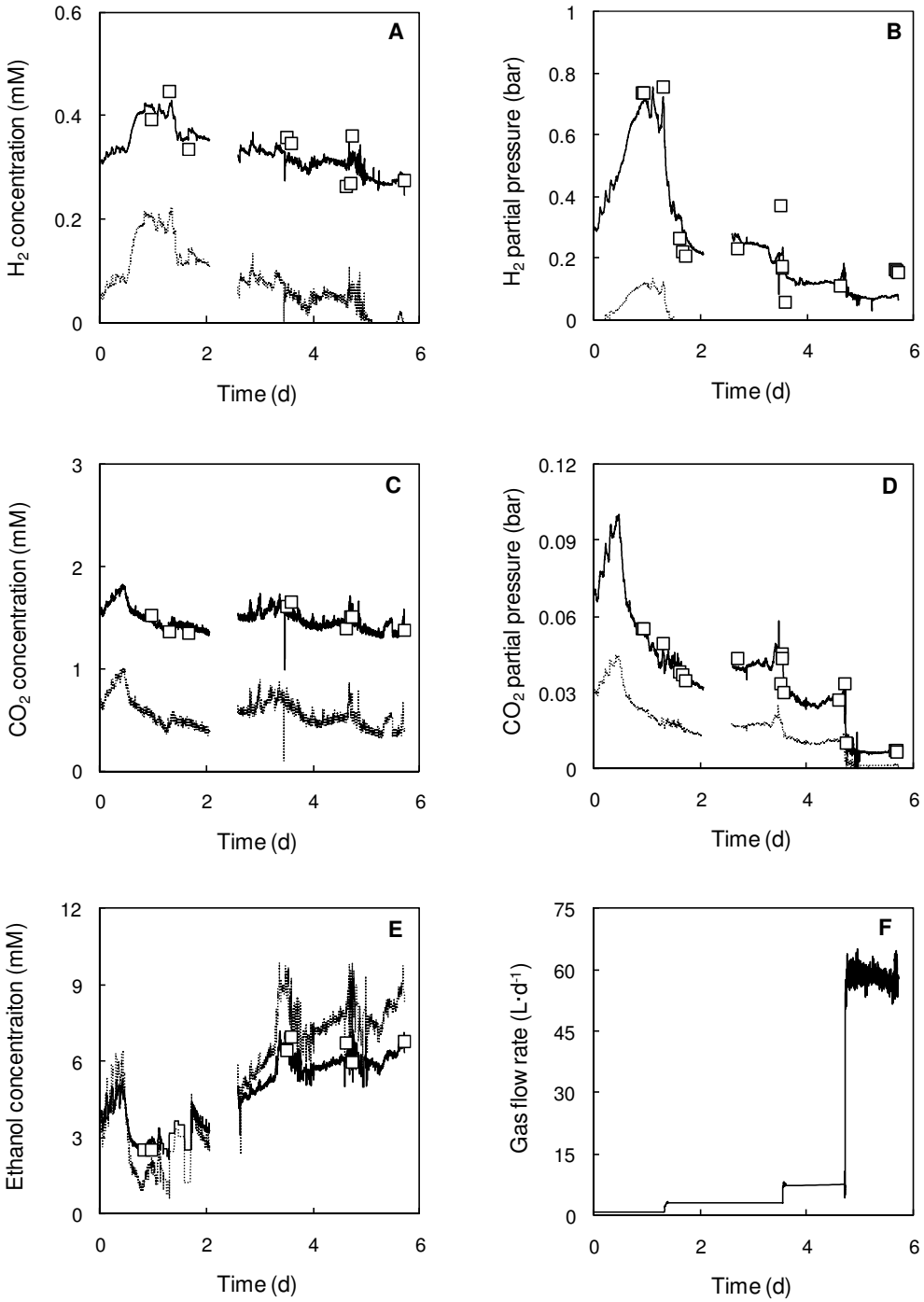

Figure 14: MIMS signal translation of continuous fermentation kinetics by in-process continuous correlation parameters, solid line, and standard calibration, dashed line. Off-line experimental data set is depicted as white squares. The dissolved and gas phase H_2 kinetics are presented in A and B, the same is presented for CO_2 in C and D, while ethanol is shown in E and gas flow rate is presented in F.

Continuous fermentation

Translated MIMS signals for the continuous experiment are shown in Figure 14. Dynamics were induced by flushing the headspace with N_2 at different flow rates. Changes in N_2 flushing rates were 0 L d^{-1}, 2.5 L.d^{-1}, 7 L.d^{-1}, and 50 L d^{-1} as is shown in Figure 14F.

As in the case of batch fermentation, H_2 and CO_2 estimations were also improved by the application of in-process correlation. Response of H_2 and CO_2 in the liquid was minimal, *i.e.* between 0.3 and 0.5 mM for H_2 and 1.2 and 1.7 mM for CO_2 (see Figure 14A and Figure 14C), while response of H_2 and CO_2 in the gas was substantial. There was also a continuous increase in ethanol concentration over the experimental period.

The solid line discontinuity in Figure 14 is due to an electric failiure experienced at day 2, which led to a stop of feeding and pH pumps, and consequently a decrease on pH. MIMS signal was lost from 2.4 to 2.6 days.

3.1.3 In-process MIMS signal calibration

The off-line data set shown in Figure 13 and Figure 14 were randomly divided into in-process MIMS calibration and validation data set for both batch and continuous fermentations. These data sets are shown in Figure 15 and Figure 16. The in-process calibrated curves are shown as solid lines, calibration data sets are shown as white squares and validation data sets as black circles.

3.1.4 Validation of calibration strategies

Table 6 illustrates the average validation errors between calibrated MIMS signals and their respective off-line experimental validation data sets for batch and continuous fermentation. The validation results of in-process and standard calibrations are presented for both fermentations. The last line of the table presents the errors for continuous fermentation with correlation parameters obtained using batch fermentation. See discussion in section 4.1.6.

In general, these results demonstrate that in-process calibration was the best calibration strategy. For both fermentations, in-process calibration average validation errors are in the range of 10%, whilst for standard calibration, they are around 100%.

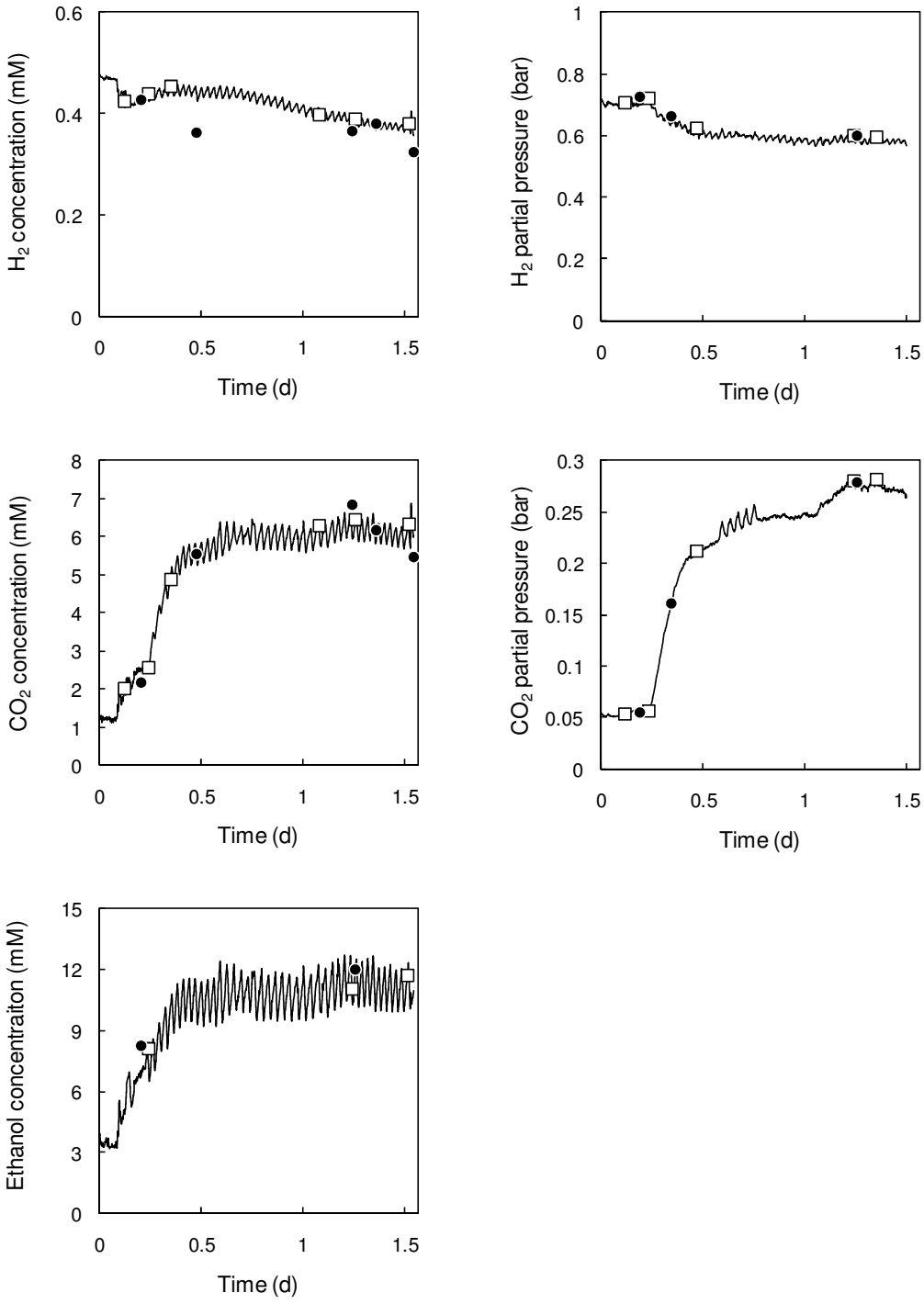

Figure 15: Batch fermentation kinetics showing MIMS signal translation by in-process calibration, solid line, which consists in dividing the off-line experimental data set into calibration points, white squares, and validation points, black circles.

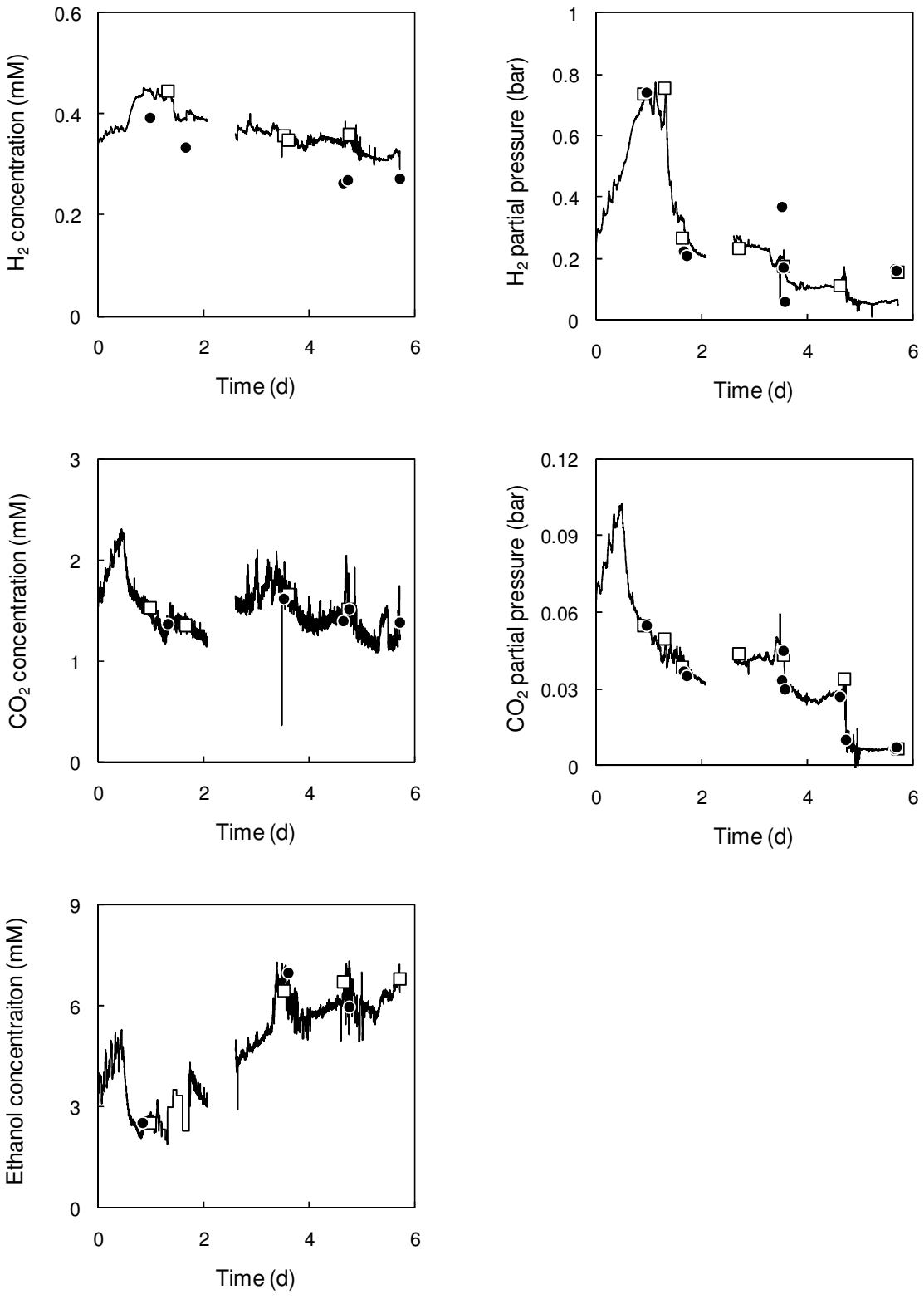

Figure 16: Continuous fermentation kinetics showing MIMS signal translation by in-process calibration, solid line. This consists in dividing the off-line experimental data set into calibration and validation points, white squares and black circles respectively. The lack of continuity in the solid lines was due to a shortcut.

Table 6: Average validation error and its standard deviation, calculated for in-process and prior-to-fermentation-run calibration strategies [(a)]. Validation errors are calculated as the difference between the calibrated MIMS signal and its respective off-line experimental validation point.

		Validation errors (%)				
		Gas phase		Liquid phase		
		H_2	CO_2	H_2	CO_2	Ethanol
Batch fermentation	In-process calibration	-3 ± 1.5	0.03 ± 3	-43 ± 35	1 ± 11	-11 ± 8
	Standard calibration	-90 ± 1.5	-55 ± 7	-91 ± 5	-72 ± 3	-30 ± 14
Continuous fermentation	In-process calibration	8 ± 70	7 ± 10	21 ± 10	3 ± 12	-3 ± 15
	Standard calibration	-130 ± 40	-62 ± 10	-70 ± 20	-62 ± 5	11 ± 40
	[(b)] Batch ferm. correlation	16 ± 60	64 ± 70	45 ± 20	50 ± 18	90 ± 35

[(a)] In this study, prior-to-fermentation-run calibration strategies correspond to standard calibration and continuous fermentation MIMS signal translation by batch fermentation correlation (see below).

[(b)] Continuous fermentation MIMS signal translation using the correlation parameters between targeted compound concentration and MIMS signal magnitudes of batch fermentation.

Special case was found for H_2 and ethanol. Validation error for H_2 gas phase at continuous fermentation was higher (8 ± 70 %) than at batch (-3±1.5%) due to the low H_2 partial pressure caused by the N_2 flushes, while dissolved H_2 errors for both fermentations are high (-43 ± 35 % for batch and 21 ± 10 % for continuous) due to low response in its concentration (between 0.3 and 0.5 mM). Ethanol errors are in the same order of magnitude, *i.e.* around -20% for batch and 10% for continuous fermentation (see section 4.1.5).

In-process calibration is necessary to calibrate fermentation MIMS signals for two reasons:
1) Each fermentation experiment is a unique and complex dynamic system that changes MIMS membrane transfer properties. Hence, it is advisable to not rely on calibrations conducted prior to the experimental run. This was demonstrated for the standard calibration and even when the calibration relied on a prior fermentation as illustrated in Figure 17, where batch correlation parameters were used to translate MIMS signals obtained during continuous

fermentation. Furthermore, this argument was demonstrated in terms of validation error as is presented in Table 6 where errors of this calibration strategy are largely higher than the in-process calibration.

2) In-process calibration is a relative easy and non-intrusive way to translate MIMS signals into quantifiable terms, allowing running experiments for long periods, as was the case for the continuous fermentation that lasted for 6 days.

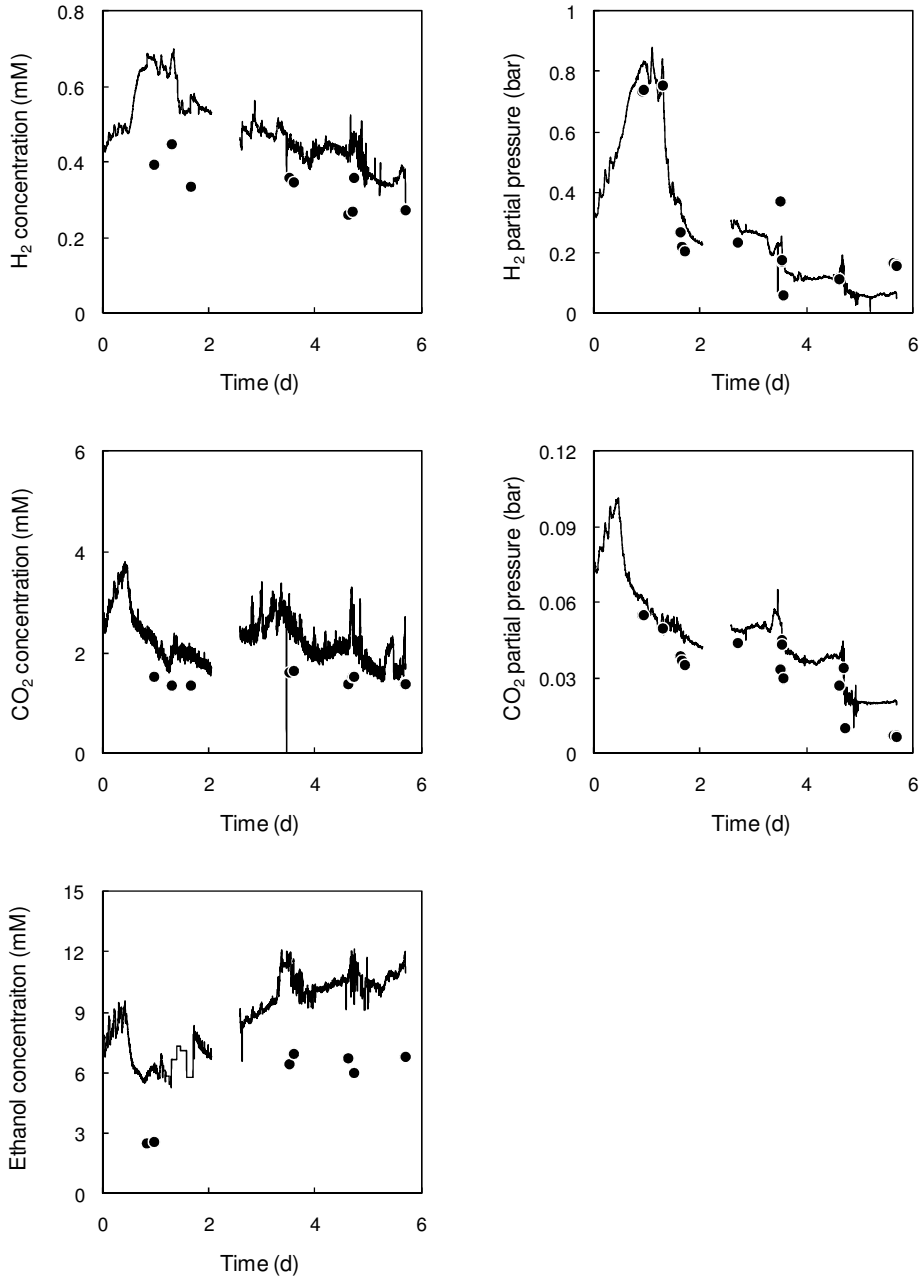

Figure 17: Kinetics of continuous fermentation showing in solid line their respective MIMS signals translation by batch correlation parameters. Off-line validation data set is presented in black circles.

3.2 Fermentation Results

The results presented in this section describe the effect of N_2-flushing and pH changes on the acidogenic product yield spectra and product composition kinetics under the studied operational condition.

Changes on product yield spectra have been based on steady state results for both N_2-flushing and pH experiments. Besides, H_2, CO_2 and ethanol kinetics parameters were calculated during transient states, which were produced after either N_2-flushing or pH changes.

For steady states, Table 7 presents a summary of carbon and chemical oxygen demand (COD) balances between the reactor's inlet and outlet. The balances consider the hydraulic retention time (HRT) and the outlet gas flow rate (see Table 16 in section 3.4) for liquid phase and gas phases respectively.

On average, carbon balances close at -5%, *i.e.* that a 5% of the substrate feed is missing. This was due to experimental errors and small quantities of products that could not be measured by the analytical methods used, as it was the case for propionic acid, i-butyric acid, valeric and i-valeric acid, whose measurements were below detection limits. Therefore, none of these compounds were further considered for mass and energy balance in this study.

Carbon balances close at -25%, in average, for experiments flushed at 58.4 $L \cdot d^{-1}$ N_2 flow rate. This is explained by unbalanced inorganic carbon and/or volatilisation of liquid products like ethanol (see discussion in section 4.2). For both N_2-flushing and pH experiments, COD balances close between 4.1±1 and -5.2±1.1. As for carbon balance, the COD value sign depends on the difference between the outlet and inlet COD, *i.e.* values are positive when the outlet is higher than the inlet, and negative in the opposite way.

The following section presents the effect of head-space composition on product yield spectra, together with pH effect and transient state kinetics results.

Table 7: Experimental carbon and COD balance.

	N_2 flushing ($L \cdot d^{-1}$)	pH	Carbon balance (%)	COD balance (%)
N_2 flushing experiments	**0**	**4.5**	-2.5±2.2	3.6±1.9
	2.5	**4.5**	-2.6±3.1	-0.1±1.8
	58.4	**4.5**	-29.6±2.3	-5.2±1.1
	0	**5.5**	-5.5±1.4	2.9±2.1
	7.3	**5.5**	-4.7±1.9	-3.2±1.8
	0	**6.5**	-4.4±1.6	-3.3±1.8
	2.5	**6.5**	-2.3±2.4	2.8±2
	7.3	**6.5**	-0.8±2.2	3±2.5
	58.4	**6.5**	-21.1±1.8	-2±1.8
pH experiments		**5.5**	-2.4±1.3	-4.3±1.5
		6.0	-8.6±1.5	1.7±2
		6.5	-5.9±1.4	-1.7±2
		7.0	-6.9±1.2	2.4±2
		7.5	-6.5±0.8	4.1±1

Yield results are presented as the total amount of the different compounds produced by glucose consumed, *i.e.* gas and dissolved hydrogen composition were considered to calculate hydrogen yield. For CO_2, gas composition was considered together with dissolved species concentration as CO_2 and bicarbonate. Organic acid yields considered both dissociated and undissociated acid forms.

3.2.1 Effect of head-space composition on product yield spectra

As expected, the changes on head-space composition, produced by N_2-flushing, affected the product yield spectra of acidogenic fermentations. Figure 18 illustrates the total product yield spectra, at steady state, under the applied operational conditions. This figure is divided into Figure 18A for hydrogen, carbon dioxide, ethanol, formic acid and Figure 18B for acetic acid, butyric acid, biomass and lactic acid.

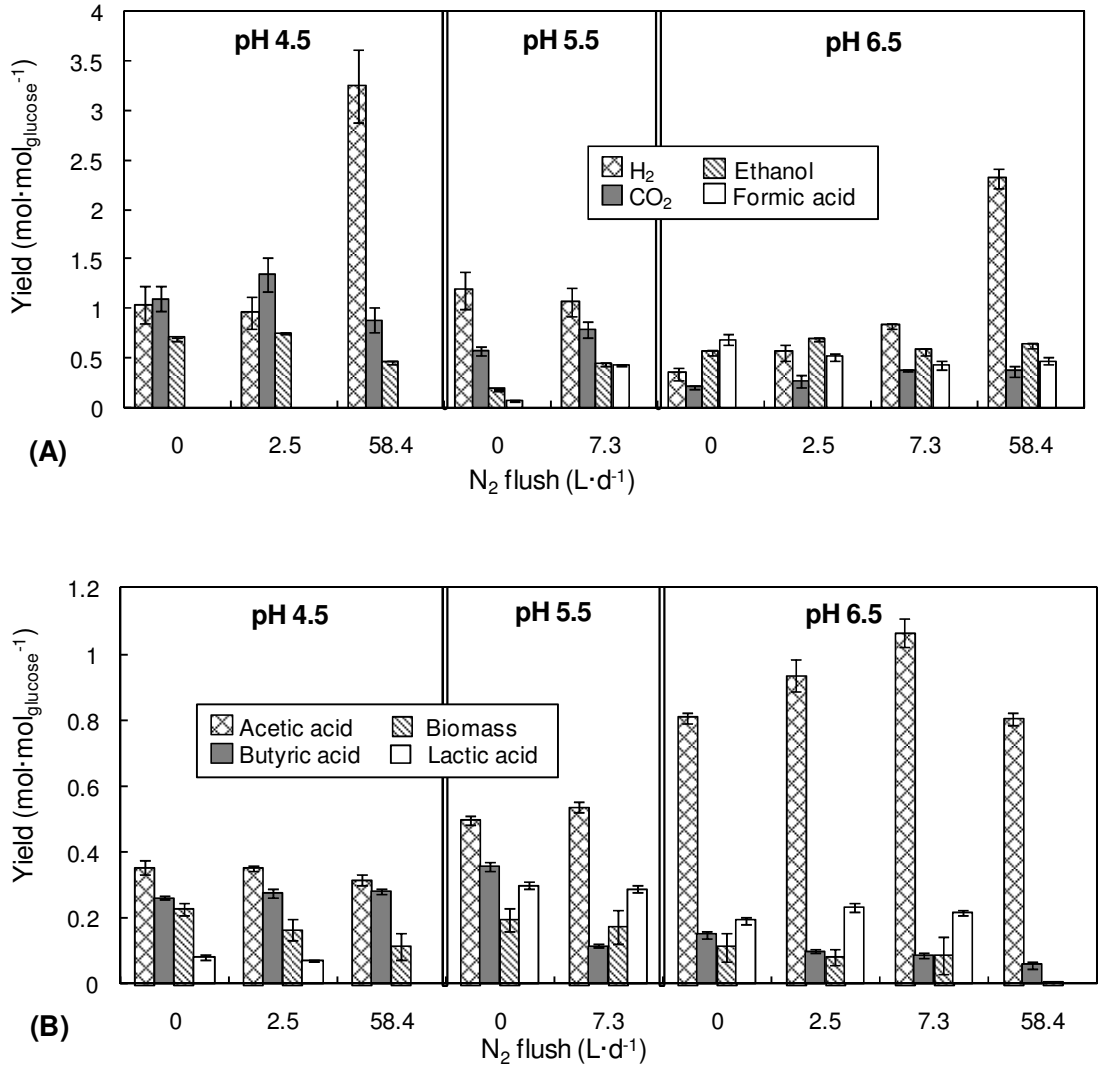

Figure 18: Influences of N_2-flushing on acidogenic product yields.

The most remarkable change was observed for hydrogen yield (Y_{H2}). At the highest N_2-flushing, *i.e.* 58.4 ($L \cdot d^{-1}$), Y_{H2} increased by 230±30% over the mean value (1±0.3 $mol_{H2} \cdot mol_{glucose}^{-1}$) at pH 4.5, while it increased by 300±20% over the 0.6±0.1 ($mol_{H2} \cdot mol_{glucose}^{-1}$) average yield at pH 6.5. The maximum Y_{H2}, 3.25±0.4 ($mol_{H2} \cdot mol_{glucose}^{-1}$), was found at pH 4.5. For the other N_2-flushing regimes (0, 2.5 and 7.3 $L \cdot d^{-1}$) the Y_{H2} results were statistically equal for pH 4.5 and 5.5, while at pH 6.5 a linear increase was found on Y_{H2} with N_2-flushing (see section 4.2.2)

Trends of CO_2 yield (Y_{CO2}) depended on pH, decreasing from 1.22±0.2 to 0.9±0.1 ($mol_{CO2} \cdot mol_{glucose}^{-1}$) at pH 4.5, while at pH 5.5 and 6.5 Y_{CO2} increased with N_2-flushing, from

0.58±0.4 to 0.79±0.1 (mol_{CO2}·$mol_{glucose}^{-1}$) at pH 5.5, and from 0.21±0.02 to 0.37±0.7 (mol_{CO2}·$mol_{glucose}^{-1}$) at pH 6.5.

Ethanol yield (Y_{EOH}) was affected differently by N_2-flushing. Y_{EOH} decreased (from 0.72±0.02 to 0.45±0.02 mol_{EOH}·$mol_{glucose}^{-1}$) with N_2-flushing at pH 4.5, increased from 0.18±0.01 to 0.44±0.02 (mol_{EOH}·$mol_{glucose}^{-1}$) at pH 5.5, and stayed constant (0.6±0.07 mol_{EOH}·$mol_{glucose}^{-1}$) at pH 6.5.

As expected, formic acid was not produced at pH 4.5. At pH 5.5, its yield (Y_{FRM}) increased from 0.08±0.01 to 0.43±0.01 (mol_{FRM}·$mol_{glucose}^{-1}$) when N_2-flushing was increased from 0 to 7.3 (L·d^{-1}). For the total of N_2-flushing regimes applied at pH 6.5, Y_{FRM} was close to its average (0.5±0.01 mol_{FRM}·$mol_{glucose}^{-1}$).

N_2-flushing did not affect acetic acid yield (Y_{ACT}) at pH 4.5 and 5.5. However, at pH 6.5, Y_{ACT} reached a maximum of 1±0.1 (mol_{ACT}·$mol_{glucose}^{-1}$) at 7.3 (L·d^{-1}) N_2-flushing. For butyric acid yield (Y_{BTR}) no N_2-flushing influence was observed at pH 4.5, but a decrease at pH 5.5 and 6.5. At pH 5.5 Y_{BTR} decreased drastically from 0.36±0.01 to 0.12±0.01 (mol_{ACT}·$mol_{glucose}^{-1}$), while at pH 6.5, it decreased from 0.15±0.01 to 0.06±0.01 (mol_{ACT}·$mol_{glucose}^{-1}$).

Biomass yield (Y_X) was negatively affected by increased of N_2-flushing rates. This trend was observed at the three studied pH values. The most critical was observed at pH 6.5 and 58.4 (L·d^{-1}) where Y_X decreased to a value of 0.01±0.002 (mol_X·$mol_{glucose}^{-1}$), which represented less than 10% of the average Y_X (0.15±0.1 mol_X·$mol_{glucose}^{-1}$) calculated for the rest of the experiments. Y_X was calculated considering a biomass molecular weight of 113 (g_X·mol_X^{-1}).

Another critical change was observed for lactic acid, which was not produced under 58.4 (L·d^{-1}) N_2-flushing, either for pH 4.5 or 6.5. For other experiments, lactic acid yield (Y_{LCT}) was not affected by N_2-flushing regimes. Y_{LCT} was 0.1±0.01 (mol_{LCT}·$mol_{glucose}^{-1}$) at pH 4.5, while at pH 5.5 and 6.5 it was 0.29±0.01 and 0.21±0.02 (mol_{LCT}·$mol_{glucose}^{-1}$), respectively.

3.2.2 Effect of pH on product yield spectra

Figure 19 illustrates the effects of pH on the product yield spectra. Figure 19A presents the yields of hydrogen, carbon dioxide, ethanol and formic acid, whilst Figure 19B the yields of acetic acid, butyric acid, biomass and lactic acid.

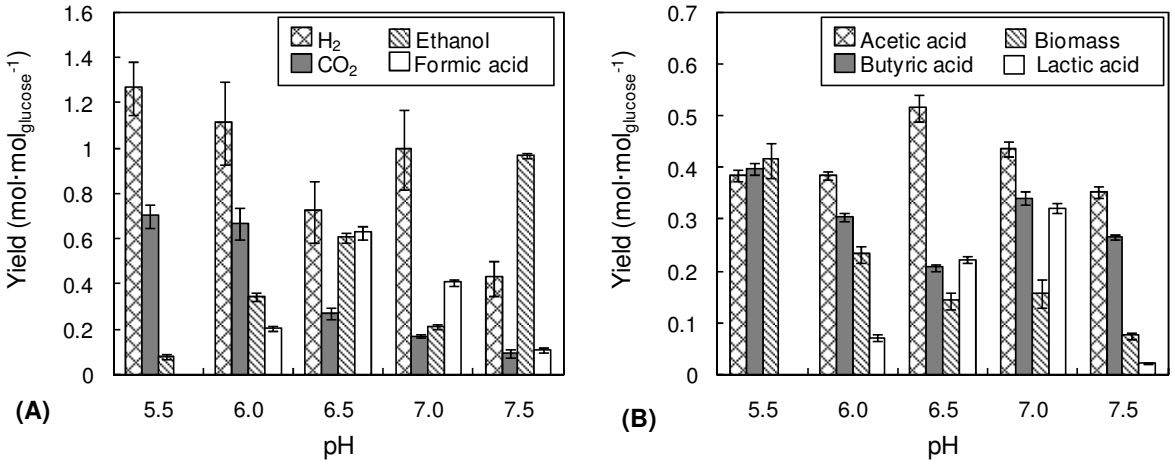

Figure 19: Influence of pH on acidogenic mixed culture glucose fermentation yields

Hydrogen yield was maintained around 1±0.1 (mol_{H2}·$mol_{glucose}^{-1}$) decreasing abruptly to 0.42±0.1 (mol_{H2}·$mol_{glucose}^{-1}$) at pH 7.5. This decrease was further observed at pH 8.0 and 8.5, where the Y_{H2} resulted on 0.05±0.007 mol_{H2}·$mol_{glucose}^{-1}$ (results not shown), nevertheless, steady states were never reached at these two pH.

Decrease of CO_2 yield with pH was a clear trend. This effect is not caused by bicarbonate formation since, as state above, the Y_{CO2} was calculated considering gas and total liquid-phase compositions, *i.e.* dissolved CO_2 and bicarbonate. This decrease is the combined effect of the catabolic stoichiometry.

As it will be described in section 3.3.3, the stoichiometry of catabolic reactions shows that CO_2 yield decrease with H_2 yield decreasing, since they are produced at the same rate, while yield increasing of the other products, *i.e.*, lactic acid, formic acid, acetic acid, butyric acid and ethanol, decrease the CO_2 yield, because the synthesis of these products does not imply

any CO_2 production. Another catabolic reaction that is involved on the CO_2 yield decrease is the homoacetogenesis that consumes 2 moles of CO_2 per mole of acetic acid produced.

Ethanol yield increased, reaching a maximum of 0.97±0.1 (mol_{EOH}·mol_{GLC}^{-1}) at pH 7.5, while at pH 6.5, yields of formic acid and acetic acid reached a maximum, 0.63±0.03 (mol_{FRM}·mol_{GLC}^{-1}) and 0.51±0.03 (mol_{ACT}·mol_{GLC}^{-1}) respectively. Also at pH 6.5 butyric acid yield reached its minimum value of 0.21±0.01 (mol_{BTR}·mol_{GLC}^{-1}).

As observed for N_2-flushing experiments, biomass yield also decreased with pH, from 0.41±0.03 (mol_X·$mol_{glucose}^{-1}$) at pH 5.5 to 0.07±0.01 (mol_X·$mol_{glucose}^{-1}$) at pH 7.5. Lactic acid yield reached a maximum of 0.32±0.01 (mol_{LCT}·$mol_{glucose}^{-1}$) at pH 7.0

3.2.3 Transient states

Transient states between steady states in fermentations were analysed using the kinetics data of H_2, CO_2 and ethanol obtained by MIMS. In-process calibration was used for the translation of MIMS signals as described in sections 2.4.2 and 3.1.

Transient states were induced by continuous environmental disturbances, *i.e.* by a new inlet flow rate of N_2-flushing or by a step change on fermentation pH. These two kinds of continuous environmental disturbances were grouped in N_2-flushing and pH experiments respectively, as described in section 2.1. The application of a continuous disturbance marked the beginning of a transient state, which ended when H_2, CO_2 and ethanol compositions reached a new steady state.

Table 8 presents the analysed transient states for both N_2-flushing and pH experiments. A total of 10 transient states were monitored. In N_2-flushing experiments, the analysed transitions were (in $L \cdot d^{-1}$ of N_2), 0 to 2.5, 2.5 to 7.3 and 7.3 to 58.4 at pH 6.5; 0 to 7.3 at pH 5.5; 0 to 2.5 and 2.5 to 58.4 at pH 4.5. Monitored transient states in pH experiments were (in pH units) 5.5 to 6.0, 6.0 to 6.5, 6.5 to 7.0 and 7.0 to 7.5.

The H_2, CO_2 and ethanol dynamic data, obtained by MIMS, were evaluated in a first order kinetic model, built on AQUASIM software. This model allowed the calculation of the

following kinetics parameters: first order rate constant, k (d^{-1}); concentration gain, CG (bar for gas phase and mM for liquid phase); and delay time, D (d).

Table 8: Transient states monitored by MIMS.

	Transient state n°		
		N_2 flow rate change ($L \cdot d^{-1}$)	pH
N_2 flushing Experiments	1	0-2.5	6.5
	2	2.5-7.3	6.5
	3	7.3-58.4	6.5
	4	0-7.3	5.5
	5	0-2.5	4.5
	6	2.5-58.4	4.5
		pH changes	
pH experiments	7	5.5-6.0	
	8	6.0-6.5	
	9	6.5-7.0	
	10	7.0-7.5	

The first order kinetic model consists of two equations, Eqs (29) and (30), describing the kinetics of decrease and increase in composition respectively, where the composition of the targeted compound, c_i, at time "t" is function of the initial concentration, c_0, *i.e.* , the concentration before the environmental disturbance was applied, and the kinetics parameters described above.

$$c_i = G \cdot e^{[-k(t-D)]} + (c_0 - CG) \tag{29}$$

$$c_i = (3c_0 - CG) - CG \cdot e^{[-k(t-D)]} \tag{30}$$

The first order rate constant, *k*, permits to compare different composition compounds kinetics that were exposed to a same environmental disturbance. High *k* values denote a rapid transition, on the targeted composition, between two steady states.

Table 9 presents the calculated first order rate constant, *k*, for the 10 transient states analysed. Comparison between *k* are summarised as follow. Kinetics results for gas phase H_2 show that *k* values were increased with N_2-flushing. In pH experiments, *k* values were consistently close to its average value, 290±19 (d^{-1}). They were also faster than N_2-flushing experiments, with an average *k* value of 24±1 (d^{-1}), *i.e.* one order of magnitude below those of pH experiments.

Increase on N_2-flushing also increased *k* values of gas phase CO_2, while in pH experiments all *k* values are statistically the same, 62±6 (d^{-1}), except for the first transition at pH change 5.5-6.0 where k was 127±20 (d^{-1}). Kinetics of gas phase is discussed in section 4.2.1.

Table 9: First order rate constant, *k*, on H_2, CO_2 and ethanol composition changes.

EXPERIMENT		*k* (d^{-1})				
N_2 flushing		Gas phase		Liquid phase		
pH	N_2 flow rate change ($L \cdot d^{-1}$)	H_2	CO_2	H_2	CO_2	Ethanol
4.5	0-2.5	15 ± 1	17 ± 2	n.c.	15 ± 1	27 ± 9
4.5	2.5-58.4	40 ± 2	107 ± 43	n.c.	11 ± 1	9 ± 1
5.5	0-7.3	40 ± 2	14 ± 1	n.c.	8 ± 1	10 ± 3
6.5	0-2.5	7 ± 0.3	n.c.	n.c.	n.c.	1 ± 0.2
6.5	2.5-7.3	21 ± 1	18 ± 1	n.c.	6 ± 1	n.c.
6.5	7.3-58.4	21 ± 4	95 ± 4	n.c.	10 ± 1	n.c.
pH step change		H_2	CO_2	H_2	CO_2	Ethanol
	5.5-6.0	255 ± 19	127 ± 20	n.c.	1023 ± 402	1 ± 0.1
	6.0-6.5	236 ± 18	59 ± 3	n.c.	1160 ± 307	3 ± 0.2
	6.5-7.0	345 ± 46	66 ± 4	n.c.	1597 ± 391	3 ± 0.2
	7.0-7.5	324 ± 56	62 ± 2	n.c.	1234 ± 410	7 ± 0.4

n.c. : No change in composition

In the liquid phase, dissolved H_2 concentration did not change between steady states (see discussion in section 4.2.1). In N_2-flushing experiments, *k* values for dissolved CO_2 were consistently close to its average, 9±2 (d^{-1}). The same trend was observed in pH experiments, where *k* values were statistically identical to its average, 1250±760 (d^{-1}). This value is 3 orders of magnitude higher than average *k* obtained in N_2-flushing experiments. Thus, dissolved CO_2 changes in pH experiments were faster than in N_2-flushing experiments (see section 4.2.1).

In N_2-flushing experiments, *k* values for gas phase CO_2 were higher than in liquid phase. This was expected since the environmental disturbance (N_2-flushing) was directly applied in the gas phase. While in pH experiments, where the disturbance was applied directly in the liquid phase, gas phase *k* values were lower than the liquid phase *k*. See discussion in section 4.2.1.

Ethanol *k* values obtained in N_2-flushing experiments were mixed. At pH 4.5, *k* decreased from 27±9 to 9±1 (d^{-1}) when N_2-flushing increased. At pH 5.0, *k* value was 10±3 (d^{-1}), while at pH 6.5, *k* decreased to 1±0.2 (d^{-1}) at N_2-flushing change from 0 to 2.5 ($L \cdot d^{-1}$), and not changed between the further steady states. For pH experiments, *k* increased from 1±0.1 to 7±0.4 (d^{-1}), with pH, see discussion in section 4.2.1.

In general, pH step changes experiments produce faster changes in gas phase CO_2 and H_2 than N_2-flushing. This could be explained by CO_2/HCO_3^- equilibria as explained in section 4.2.1.

Figure 20 and Figure 21 illustrate the kinetics of H_2, CO_2 and ethanol in transient states when increasing N_2-flushing from 0 to 7.3 ($L \cdot d^{-1}$) at pH 5.5 and pH step change from 7.0 to 7.5, respectively. Both figures are presented as examples of the observed transient periods.

In summary, neither N_2-flushing nor pH changes disturbed dissolved hydrogen concentration (Figure 20A and Figure 21A), which was close to its saturation for the whole set of experiments. Hydrogen partial pressure decreased with N_2-flushing (Figure 20B) and increased with pH (Figure 21B). Both CO_2 dissolved concentration and partial pressure decreased with N_2-flushing and pH.

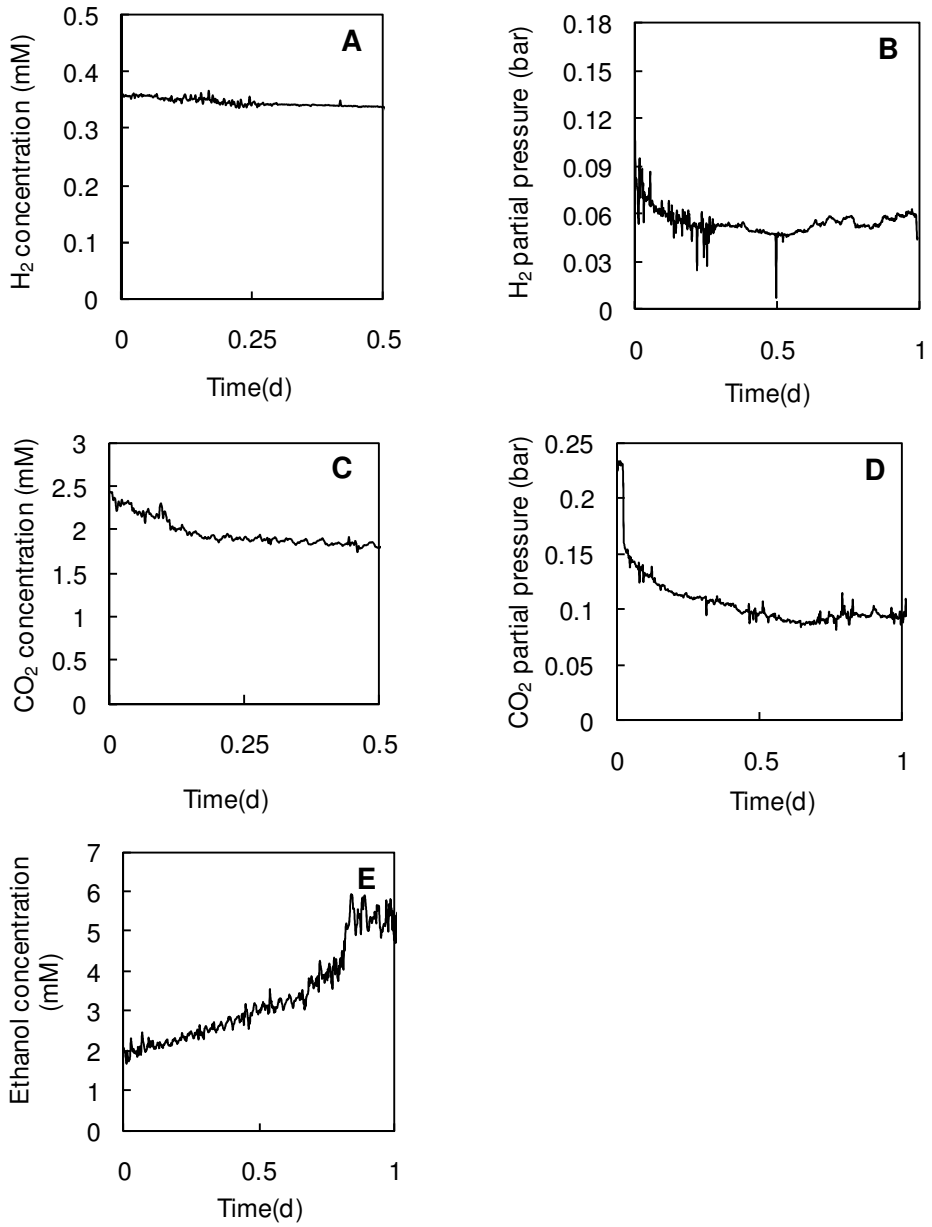

Figure 20: Online measurements of H_2, CO_2 and ethanol at N_2 flushing step increase from 0 to 7.3 ($L \cdot d^{-1}$) at pH 5.5.

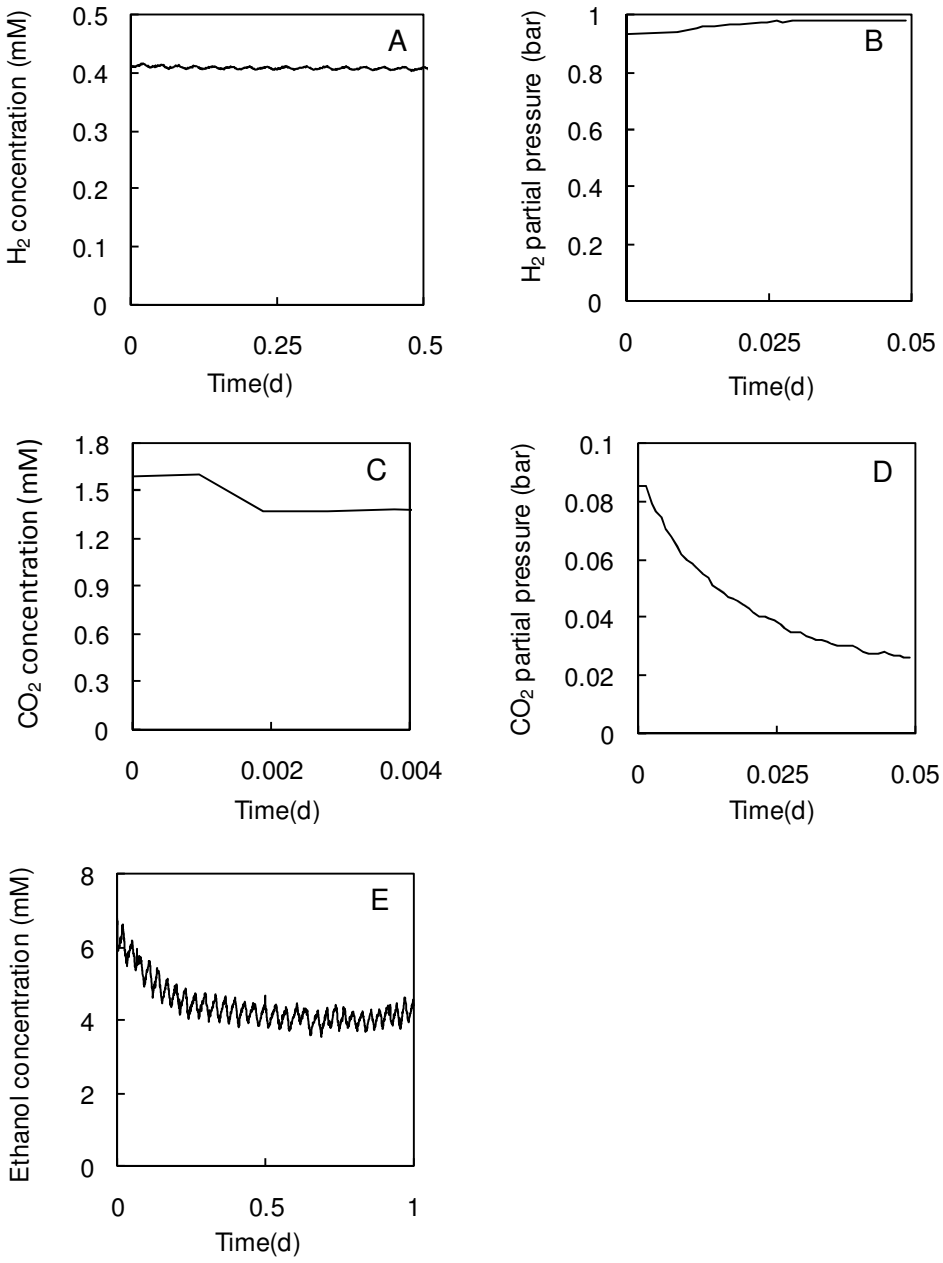

Figure 21: Online measurement of H_2, CO_2 and ethanol at pH change 7.0 to 7.5.

For ethanol, the results have more complex trends. Ethanol concentration increased with N_2-flushing at changes 0 to 2.5 ($L \cdot d^{-1}$), for both pH 4.5 and 6.5, and 0 to 7.3 ($L \cdot d^{-1}$) for pH 5.5, while it decreased at change 2.5 to 58.4 ($L \cdot d^{-1}$) for pH 4.5. Ethanol concentration remained constant for the rest of the N_2-flushing experiments, *i.e.* at changes 2.5 to 7.3 and 7.3 to 58.4 ($L \cdot d^{-1}$) for pH 6.5. For pH experiments, ethanol concentration increased with pH changes 5.5 to 6.0 and 6.0 to 6.5, decreasing with changes 6.5 to 7.0 and 7.0 to 7.5.

3.3 Thermodynamic Model

A thermodynamic model was developed to study the product yield spectra of acidogenic fermentation of glucose, Y [$mol_i \cdot mol_{GLC}^{-1}$], in steady state. The model is based on fundamental thermodynamic data, *i.e.* Gibbs energy, $\Delta G_f°$ [$kJ \cdot mol^{-1}$], and enthalpy, $\Delta H_f°$ [$kJ \cdot mol^{-1}$]; on mass, electrons and Gibbs energy balances; and on a simplified metabolic network, ν, of acidogenic glucose fermentation. The metabolic network can be modified by adding or removing metabolic reactions, and can be easily adapted to a different carbon source, which makes a flexible thermodynamic model.

Figure 22 illustrates a simplified structure of the model. The structure of the model was divided into a catabolic and an anabolic part. The catabolic part of the model allows the calculation of the Gibbs energy released from the energy source (glucose), ΔG_e [$kJ \cdot mol_{GLC}^{-1}$], and the Gibbs energy of catabolic reactions, ΔG_{intra} [$kJ \cdot mol_{GLC}^{-1}$] assuming that the concentration of the intracellular part is equal to the extracellular part. This hypothesis is discussed in section 4.3.

The anabolic part allows the calculation of the Gibbs energy for biomass synthesis, ΔG_S [$kJ \cdot mol_{GLC}^{-1}$], its related Gibbs energy dissipation, ΔG_o [$kJ \cdot mol_X^{-1}$] and energy transfer efficiency, ε.

The model is fed with experimental data, *i.e.* reaction temperature, T [K], pH, gas and liquid phase composition, c [bar, M], and in the case of continuous fermentation, hydraulic retention time, HRT [d], and produced gas flow rate, GFR [$L \cdot d^{-1}$].

However, this model was conceived for system analysis in steady state only, though it would be convenient to include modifications for its dynamic system application. Moreover, this model considers completely mixed reactor, thus it is not applicable to biofilms or aggregates systems.

The model variables and parameters nomenclature is described in Table 10.

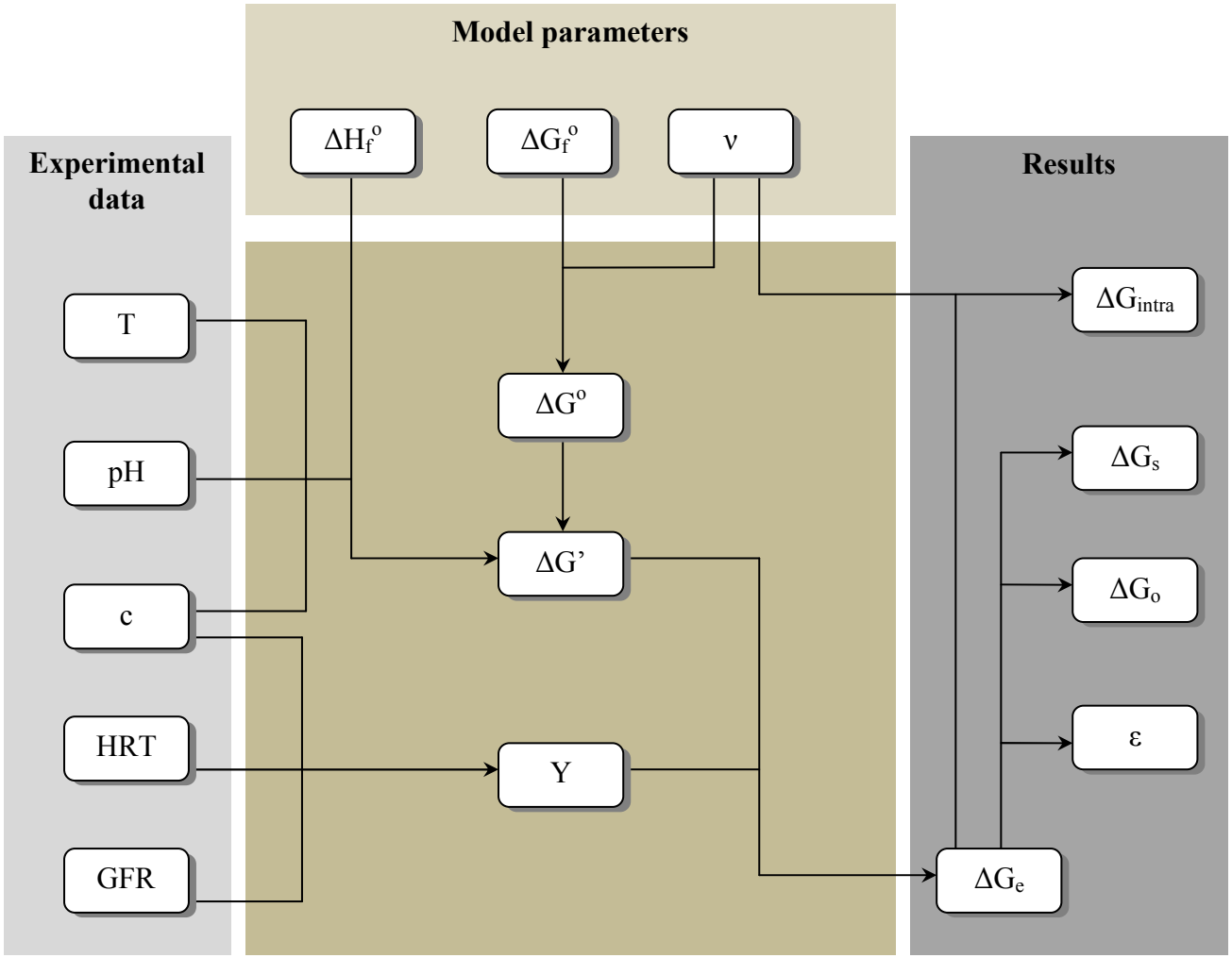

Figure 22: Simplified scheme of the thermodynamics based model.

Table 10: List of thermodynamic model variables and parameters

	Symbol	Description	Units
Parameters	$\Delta Gf°$	Standard Gibbs energy of compound formation	$[kJ \cdot mol^{-1}]$
	$\Delta Hf°$	Standard enthalpy of compound formation	$[kJ \cdot mol^{-1}]$
	v	Compound stoichiometric coefficient of reaction	
	γ	Reduction degree of compounds	$[eqq \cdot mol^{-1}]$
	ΔG_{pc}	Gibbs energy of the conversion of acetyl-CoA to biomass	$[kJ \cdot eeq^{-1}]$
	ΔG_{in}	Gibbs energy of acetyl-CoA reduction	$[kJ \cdot eeq^{-1}]$
	R	Ideal gas constant	$[m^3 \cdot Pa \cdot K^{-1} \cdot mol^{-1}]$
	T°	Standard temperature	[K]
State variables	c	Compound composition, *i.e.* concentration or partial pressure	[M] or [bar]
	GFR	Gas flow rate	$[L \cdot d^{-1}]$
	HRT	Hydraulic retention time	[d]
	T	Actual temperature of reaction	[K]
Variables	e	Electron exchanges in reaction	[eeq]
	fa	Fraction of dissociated acid	$[mol \cdot mol^{-1}]$
	fah	Fraction of undissociated acid	$[mol \cdot mol^{-1}]$
	f_e	Electron fraction used for energy released	
	f_s	Electron fraction used for biomass synthesis	
	$fGLC$	Fraction of catabolic glucose participating in reaction	$[mol_{catGLC} \cdot mol_{GLC}^{-1}]$
	Y	Yield of compounds on glucose	$[mol_i \cdot mol_{GLC}^{-1}]$
	$\Delta G°$	Standard Gibbs energy chage of reactions	$[kJ \cdot mol^{-1}]$
	$\Delta G'$	Actual Gibbs energy of reaction	$[kJ \cdot mol^{-1}]$
	$\Delta G'_{ab}$	Actual Gibbs energy of global acid-base reactions	$[kJ \cdot mol_{GLC}^{-1}]$
	$\Delta G'_{G}$	Global Gibbs energy	$[kJ \cdot mol_{GLC}^{-1}]$
	$\Delta G'_{Gp}$	Actual Gibbs energy of global reaction	$[kJ \cdot mol_{GLC}^{-1}]$
	$\Delta G'_{S}$	Actual Gibbs energy of the system	$[kJ \cdot mol_{GLC}^{-1}]$
	ΔG_a	Gibbs energy of the half electron acceptor	$[kJ \cdot mol_{GLC}^{-1}]$
	ΔG_d	Gibbs energy of the half electron donor	$[kJ \cdot mol_{GLC}^{-1}]$
	ΔG_e	Gibbs energy realeased from the energy source	$[kJ \cdot mol_{GLC}^{-1}]$
	ΔG_{ic}	Gibbs energy of the conversion of the electron donor to acetyl-CoA	$[kJ \cdot mol_{GLC}^{-1}]$
	ΔG_{intra}	Gibbs energy of metabolic reactions	$[kJ \cdot mol_{GLC}^{-1}]$
	ΔG_o	The Gibbs energy dissipation	$[kJ \cdot mol_X^{-1}]$
	ΔG_S	Gibbs energy for biomass synthesis	$[kJ \cdot mol_{GLC}^{-1}]$
	$\Delta G_T°$	Standard Gibbs energy chage of reaction at actual temperature	$[kJ \cdot mol^{-1}]$
	$\Delta H°$	Standard enthalpy of reaction	$[kJ \cdot mol^{-1}]$
	ε	Energy tranfer efficiency	

3.3.1 Mass and electron balances

Mass and electron balances were performed in this order: 1) reduction degree balance, 2) carbon balance, and 3) nitrogen balance [197]. An oxidation state reference for each element was arbitrarily defined to introduce the reduction degree, γ, of compounds. In this context, the oxidation state of hydrogen element, γ_H, was defined as the unit, *i.e.* γ_H=1. CO_2, NH_3 and H_2O were considered as carbon, nitrogen and oxygen references, respectively. With this set of reference compounds the oxidation states for the before mentioned elements are: γ_C=4, γ_N=-3, γ_O=-2. Then, the reduction degree of the compounds taking place in this analysis was calculated as the sum of the total reduction degree of each element in the compound as show in Eq. (31):

$$\gamma_i = \gamma_C C_i + \gamma_N N_i + \gamma_O O_i + \gamma_H Hc_i \tag{31}$$

where C_i, N_i O_i and Hc_i are the carbon, nitrogen, oxygen and hydrogen content of compound i, respectively. Following this, for each electron donor-acceptor half reaction j, the electron balance is expressed as:

$$\sum_i \gamma_i \cdot \nu_{ij} = -e_j \tag{32}$$

For each pair of electron donor-acceptor reaction, the electron balance must follow the relationship presented in Eq. (33):

$$e_{EA} = -e_{ED} \tag{33}$$

The mass balance for carbon, nitrogen, oxygen and hydrogen are presented in Eqs. (34) to (37) respectively.

$$\sum_i C_i \cdot \nu_{ij} = 0 \quad (34)$$

$$\sum_i N_i \cdot \nu_{ij} = 0 \quad (35)$$

$$\sum_i O_i \cdot \nu_{ij} = 0 \quad (36)$$

$$\sum_i Hc_i \cdot \nu_{ij} = 0 \quad (37)$$

The electron donor-acceptor half reaction are summarised in Table 11. This table also presents the biomass synthesis reaction, which was based on von Stockar *et al.* [151] work, using glucose and ammonia as carbon and nitrogen sources. Biomass synthesis reaction considered a biomass composition of $C_5H_7O_2N$ [150].

Table 11: Electron donor-acceptor and biomass synthesis reactions.

Electron donor	Acetate	$GLC + 2\ H_2O$	→	$2\ ACT + 10\ H^+ + 2\ CO_2 + 7\ e$
	Butyrate	GLC	→	$BTR + 5\ H^+ + 2\ CO_2 + 3.8\ e$
	Ethanol	$GLC + 3\ H_2O$	→	$EOH + 12\ H^+ + 4\ CO_2 + 12\ e$
	Formate	$GLC + 6\ H_2O$	→	$FRM + 23\ H^+ + 5\ CO_2 + 11\ e$
	Hydrogen	$GLC + 6\ H_2O$	→	$6\ H_2 + 12\ H^+ + 6\ CO_2 + 12\ e$
	Lactate	$GLC + 3\ H_2O$	→	$LCT + 13\ H^+ + 3\ CO_2 + 11\ e$
Electron acceptor	Acetate	$2\ CO_2 + 7\ H^+ + 7\ e$	→	$ACT + 2\ H_2O$
	Butyrate	$0.8\ CO_2 + 3.8\ H^+ + 3.8\ e$	→	$0.2\ BTR + 1.2\ H_2O$
	Ethanol	$2\ CO_2 + 12\ H^+ + 12\ e$	→	$EOH + 3\ H_2O$
	Formate	$11\ CO_2 + 11\ H^+ + 11\ e$	→	$11\ FRM$
	Hydrogen	$12\ H^+ + 12\ e$	→	$6\ H_2$
	Lactate	$3\ CO_2 + 11\ H^+ + 11\ e$	→	$LCT + 3\ H_2O$
Biomass synthesis		$GLC + 1.2\ NH_3$	→	$1.2\ C_5H_7O_2N + 3.6\ H_2O$

3.3.2 Extracellular thermodynamic model

A detailed extracellular thermodynamic model was published in Engineering in Life Science, 2008, 8(5): 487-498, entitled 'Thermodynamic analysis of energy transfer in acidogenic cultures' [197]. See ANNEXES section 8.2. An example of calculation is found in Box 1 at the end of this section.

Extracellular thermodynamic model is based on global stoichiometry, *i.e.* the substrate of the global reaction, glucose, is directly converted to the different final acidogenic products without metabolic intermediaries as is depicted in Figure 23.

As remarked in sections 3.2 and 3.2.2 acidogenic products observed in this study account for six global reactions listed as follow: rA: conversion of glucose to lactate; rB: conversion of glucose to formate; rC: conversion of glucose to H_2; rD: conversion of glucose to acetate; rE: conversion of glucose to butyrate; and rF: conversion of glucose to ethanol.

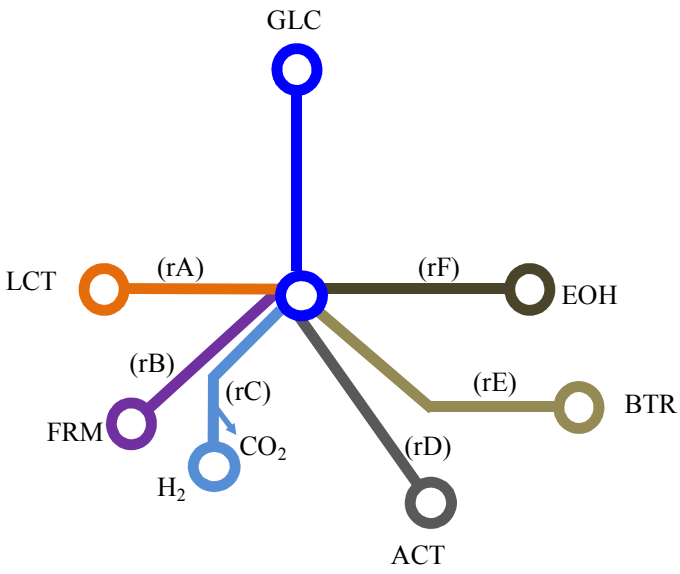

Figure 23: Simplified extracellular catabolic network of acidogenic fermentation of glucose. Conversion of glucose (GLC) to lactate (LCT) is notated by reaction rA; to formate (FRM) by rB; to H_2 by rC; to acetate (ACT) by rD; to butyrate (BTR) by rE and to ethanol (EOH) by rF.

Table 12 presents the stoichiometric coefficients of these six global reactions. In this extracellular model CO_2 is produced by reactions rC, rE and rF, and consumed by rB. Stoichiometric reactions were mass and electron balanced as described in section 3.3.1.

Table 12: Extracellular stoichiometric matrix

	Reactions					
	GLC→LCT	GLC→FRM	GLC→H2	GLC→ACT	GLC→BUT	GLC→EOH
Compounds	(rA)	(rB)	(rC)	(rD)	(rE)	(rF)
GLC	-1	-1	-1	-1	-1	-1
ACT	0	0	0	3	0	0
BTR	0	0	0	0	1.2	0
CO2	0	-6	6	0	1.2	2
EOH	0	0	0	0	0	2
FRM	0	12	0	0	0	0
H2	0	0	12	0	0	0
LCT	2	0	0	0	0	0
H	2	12	0	3	1.2	0
H2O	0	-6	-6	0	1.2	0

See abbreviations in Table 2

The Gibbs energy calculation of global reactions is based on the catabolic glucose fraction, *fGLC*, which is calculated as follow

$$fGLC_j = -Y_i \frac{\nu_{GLCj}}{\nu_{ij}} \tag{38}$$

where ν_{GLCj} and ν_{ij} are glucose and product "i" stoichiometric coefficient of reaction "j". The *fGLC* is related to the catabolic glucose yield, Y_{GLCcat} [$mol_{GLCcat} \cdot mol_{GLC}^{-1}$] by the next equation:

$$Y_{GLC_{cat}} = \sum_j fGLC_j \tag{39}$$

The Gibbs energy of reactions, $\Delta G'_{Gp}$, follows the next relationship:

$$\Delta G'_{Gpj} = fGLC_j \cdot \Delta G'_j \tag{40}$$

where $\Delta G'$ is the corrected Gibbs energy according to eqs. (25) and (27) (see section 2.5). Additionally terms for acid-base reactions were incorporated to the model as explain below.

The acid-base Gibbs energy of reaction, $\Delta G'_{ab}$, for the produced organic acids, was considered into the model. Table 13 presents the stoichiometric matrix of these reactions where dissociated acid is converted to undissociated acid by the consumption of protons.

$$A^- + H^+ \leftrightharpoons AH \tag{41}$$

Table 13: Acid-base stoichiometry of acidogenic organic acids.

	Acid-base reactions			
Compounds	LCT→LCTH	FRM→FRMH	ACT→ACTH	BUT→BUTH
ACT	0	0	-1	0
BTR	0	0	0	-1
FRM	0	-1	0	0
LCT	-1	0	0	0
H	-1	-1	-1	-1
ACTH	0	0	1	0
BTRH	0	0	0	1
FRMH	0	1	0	0
LCTH	1	0	0	0

Dissociated and undissociated species of organic acids in aqueous solution are in equilibrium. This equilibrium depends on pH. The fraction of dissociated acid, fa_i, as function of pH is expressed as:

$$fa_i = \frac{K_{ai}}{K_{ai} + [H^+]} \tag{42}$$

where acid base equilibrium constant, K_{ai}, is expressed as function of the temperature corrected Gibbs free energy at equilibrium:

$$K_{ai} = e^{\left(\frac{\Delta G^{\circ}_{Ti}}{RT}\right)} \tag{43}$$

The undissociated acid fraction, *fah*, was then calculated as:

$$fah_i = 1 - fa_i \tag{44}$$

Figure 24 illustrates the dissociated acid fraction of acetate, butyrate, formate and lactate versus pH. At pH 7.0, *fa* of these four organic acids become close to one.

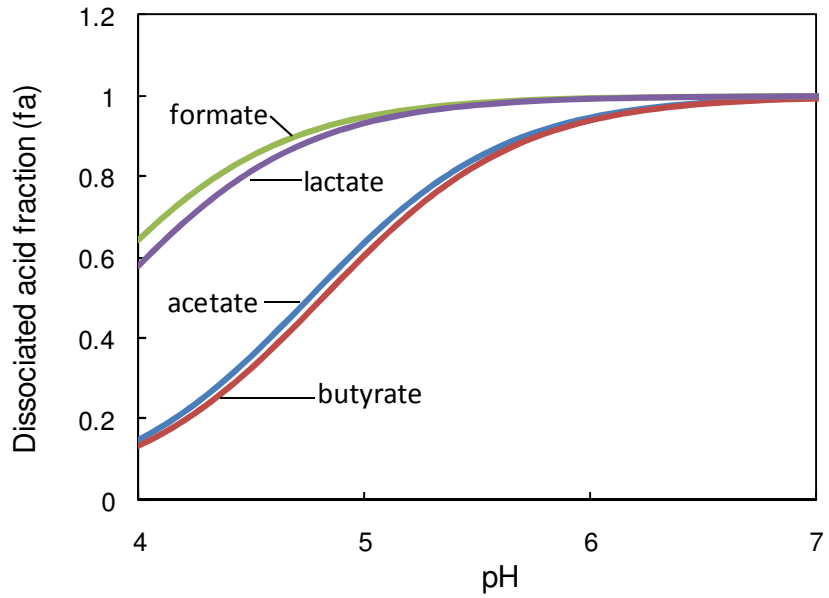

Figure 24: Dissociated organic acid fraction as pH function.

The calculation of $\Delta G'_{ab}$ used the same procedure employed for $\Delta G'_{Gp}$. Then, the Gibbs energy of reactions was corrected by acid-base reactions, giving global Gibbs free energy, ΔG_e, which was calculated using the following equation:

$$\Delta G_{ej} = \Delta G'_{Gpj} + \Delta G'_{abj} \tag{45}$$

Then, the Gibbs free energy of the system, $\Delta Gs'$ is calculated as:

$$\Delta G'_S = \sum_j \Delta G_{ej} \tag{46}$$

Box 1: calculation of extracellular ΔG'

This box exemplifies the calculation of extracellular ΔG' corrected for temperature and concentration.

For this aim, the procedure is divided into: 1) experimental data, 2) experimental yields, 3) glucose catabolic fractions, 4) $\Delta G'_{GP}$ calculations, 5) ΔG' acid-base, 6) ΔG'of the extracellular system.

1) Experimental data

A continuous acidogenic culture at a liquid phase hydraulic retention time (HRT) of 6 h, pH 4.5 and 37°C gave the following steady state results:

Liquid phase concentrations in mM. Inlet: glucose, 32. Outlet: glucose, 22.7; acetic acid, 3.3; butyric acid, 2.4; ethanol, 6.4; formic acid, 0; lactic acid, 0.7; biomass, 0.24 ($g \cdot L^{-1}$). Gas phase composition in bar, hydrogen 0.58 and CO_2 0.37. Outlet gas flow rate (GFR) in $L \cdot d^{-1}$, 2.

2) Experimental yields

The experimental yields are expressed in $mol_i \cdot mol_{glucose}^{-1}$, (referred to consumed glucose).

In the liquid phase, as substrates and products are under the same HRT regime, considering that inlet and outlet densities are very close, the products yield is calculated using the outlet concentration of products divided by the consumed glucose as is described in the following equation:

$$Y_i = \frac{[product_i]}{[inlet\_glucose] - [outlet\_glucose]}$$

Using acetic acid as an example we have:

$$Y_{ACT} = \frac{3.3}{32 - 22.7} = 0.35 \left(\frac{mol_{ACT}}{mol_{GLC}}\right)$$

For biomass, it was assumed a constant composition of $C_5H_7O_2N$, and a molecular weight of 113 $g \cdot mol^{-1}$, then its yield was calculated as:

$$Y_x = \frac{0.24}{32 - 22.7} \cdot \frac{1000}{113} = 0.23 \left(\frac{mol_x}{mol_{GLC}} \right)$$

In the gas phase, as the gas flow rate (GFR) and HRT are different, the yield is calculated considering the molar production rate of the gas product over the molar glucose consumption rate, as given in the following equation:

$$Y_i = \frac{P \cdot GFR}{R \cdot T} \cdot \left([inlet\_glucose] - [outlet\_glucose] \frac{V_L}{HRT} \cdot 24 \right)^{-1}$$

The molar gas production rate is on the first part of this equation, while the molar glucose consumption is inside the parenthesis. The molar gas rate is given by the product partial pressure, P (bar), the total gas flow rate (GFR, $L \cdot d^{-1}$), ideal gas constant R ($8.31 \cdot 10^{-5}$ $bar \cdot L \cdot (mmol \cdot K)^{-1}$) and experimental temperature (K). The molar glucose consumption rate is given by the difference between the inlet and outlet glucose concentrations (mM), the reactor liquid volume (1.3 L), and the HRT (h), the "24" is the factor to change h to days. The H_2 yield was used as example:

$$Y_{H2} = \frac{0.58 \cdot 2}{8.31 \cdot 10^{-5} \cdot 310.15} \left((32 - 22.7) \frac{1.3}{6} \cdot 24 \right)^{-1} = 1 \left(\frac{mol_{H2}}{mol_{GLC}} \right)$$

The yield summary in $mol_i \cdot mol_{GLC}^{-1}$ is as follow: acetic acid, 0.35; butyric acid, 0.26; ethanol, 0.7; formic acid, 0; hydrogen, 1; lactic acid, 0.08; biomass, 0.23.

3) Glucose catabolic fractions

They are calculated as in the following equation:

$$fGLC_j = -Y_i \frac{\nu_{GLCj}}{\nu_{ij}} \quad (38)$$

The stoichiometry coefficients (ν_{GLCj}, ν_{ij}) appear in Table 12. As an example, the glucose catabolic fraction for butyric acid production considers the 1.2 moles of butyrate produced per mol of glucose, and the experimental butyric acid yield (0.26 $mol_{BTR} \cdot mol_{GLC}^{-1}$).

$$fGLC_{but} = -0.26\frac{-1}{1.2} = 0.22\ \left(\frac{mol_{GLC}}{mol_{GLC}}\right)$$

The summary of glucose catabolic fraction is as follow: lactic acid, 0.04; formic acid, 0; hydrogen, 0.09; acetic acid, 0.12; butyric acid, 0.22; ethanol, 0.35.

4) Gibbs energy of reaction

In this part we explain the calculation of $\Delta G'_{Gp}$ ($kJ \cdot mol_{GLC}^{-1}$), which considers for experimental temperature and concentrations, but does not consider acid-base correction for organic acids. The calculation is as follow:

$$\Delta G'_{Gpj} = fGLC_j \cdot \Delta G'_j \qquad (40)$$

In this equation, $\Delta G'_j$ ($kJ \cdot mol_{GLC}^{-1}$) is the corrected temperature and concentration Gibbs energy as described in section 2.5. We use butyric acid as an example. The global butyrate ($C_4H_7O_2^-$) synthesis reaction from glucose ($C_6H_{12}O_6$), as is presented in Table 12, is:

$$C_6H_{12}O_6 \rightarrow 1.2\ C_4H_7O_2^- + 1.2\ CO_2 + 1.2\ H^+ + 1.2\ H_2O$$

The standard Gibbs energy of formation (ΔGf_i^o $kJ \cdot mol^{-1}$) is listed, according to Table 4, as: glucose, -917.2; butyrate, -352.63; CO_2, -394.4; H^+, 0; H_2O, -237.18. The standard enthalpy of formation (ΔHf_i^o $kJ \cdot mol^{-1}$) is also listed in Table 4. For glucose, -1264; butyrate, -535; CO_2, 0; H^+, 0; H_2O, -285.8.

The Gibbs energy (ΔG_j^o $kJ \cdot mol^{-1}$) and enthalpy (ΔH_j^o $kJ \cdot mol^{-1}$) of reaction at standard conditions are calculated as in Eq. (24) and (26):

$$\Delta G_j^o = \sum_i^n \nu_{ij} \cdot \Delta Gf_i^o \qquad (24)\ , \qquad \Delta H_j^o = \sum_i^n \nu_{ij} \cdot \Delta Gf_i^o \qquad (26)$$

In the case of substrates, their stoichiometric coefficient is always negative. For global butyrate synthesis we have:

$$\Delta G^o_{BTR} = -1 \cdot (-917.2) + 1.2 \cdot (-352.63) + 1.2 \cdot (-394.4) + 1.2 \cdot (0) + 1.2 \cdot (-237.18)$$

$$\Delta G^o_{BTR} = -263.85 \left(\frac{kJ}{mol_{GLC}}\right)$$

And

$$\Delta H^o_{BTR} = -1 \cdot (-1264) + 1.2 \cdot (-535) + 1.2 \cdot (-0) + 1.2 \cdot (0) + 1.2 \cdot (-285.8)$$

$$\Delta H^o_{BTR} = 279 \left(\frac{kJ}{mol_{GLC}}\right)$$

The temperature corrected Gibbs energy (ΔG_{jT}^{o} kJ·mol^{-1}) consider ΔG_{BTR}^{o}, ΔH_{BTR}^{o}, standard temperature (298.15 K) and experimental temperature (310.15 K), according to Eq. 25:

$$\Delta G^o_{jT} = \Delta G^o_j \frac{T}{T^o} + \Delta H^o_j \frac{T^o - T}{T^0} \quad (25)$$

Following the butyric acid example we have:

$$\Delta G^o_{BTR\_T} = -263.85 \frac{310.15}{298.15} + 279 \frac{298.15 - 310.15}{298.15} = -285.7 \left(\frac{kJ}{mol_{GLC}}\right)$$

Summarising the ΔG_{jT}^{o} of global synthesis reactions, in kJ·mol$_{GLC}^{-1}$ for lactic acid, -117.4; formic acid, 600.3; hydrogen, -147; acetic acid, -191; butyric acid, -285.7; ethanol, -272.2. Note that theses value does not depend on actual pH or concentrations. The concentration correction is made according to Eq. (27). In the case of pH, this is considered as H^+ concentration according to the Eq. (28).

$$\Delta G'_j = \Delta G^o_{jT} + R \cdot T \sum_i^n \nu_{ij} \cdot ln(c_i) \quad (27), \qquad pH = -log[H^+] \quad (28)$$

It should be noted that the concentration term (c_i) in Eq. (27) is indeed the actual concentration of compound "i" divided by its standard concentration (c_i^o), *i.e.*: $ln\left(\frac{c_i}{c_i^o}\right)$.

For compounds in aqueous solutions, as is the case of glucose, acetic acid, butyric acid,

ethanol, formic acid and lactic acid, their c_i^o corresponds to 1M. For gases, as H_2 and CO_2, their respective c_i^o corresponds to 1.01 bar (1 atm). Particular case is found for water. While considering for ΔG_j^o, is influence in neglected when working with aqueous solutions, since we assumed that the liquid phase was enough diluted to consider the water concentrations as a constant equal to 55·M, which is also its c_i^o. Then the ratio $\frac{c_i}{c_i^o} = 1$.

In Eq. (27), the composition is given in M for liquids and in bar for gases. The ideal gas constant is equal to $8.31 \cdot 10^{-3}$ kJ·(K·mol)$^{-1}$. The temperature (T) corresponds to the actual temperature (310.15 K).

For calculations we considered the outlet concentrations, assuming that these concentrations are the
same at the bioreactor. For H^+ concentration we used $3.16 \cdot 10^{-5}$ M (pH 4.5). The calculation of $\Delta G_j^{'}$ for butyric acid is as follow:

$$\Delta G'_{BTR} = -285.7 + 8.31 \cdot 310.15 \cdot [ln(0.0227^{-1} \cdot 0.0024^{1.2} \cdot 0.37^{1.2} \cdot 3.16^{1.2-5})]$$

$$\Delta G'_{BTR} = -329.76 \left(\frac{kJ}{mol_{GLC}}\right)$$

This expression gives the Gibbs energy released by the butyric synthesis reaction per one mole of glucose consumed, *i.e.* it assumes that one mole of glucose is completely consume for butyric acid production. As already said above, this mole of catabolic glucose is divided into different fractions producing not only butyric acid but the other catabolic products (acetic acid, ethanol, formic acid, H_2 and lactic acid). Then ΔG_j' is corrected for catabolic glucose fraction as described in Eq. (40). Then for butyric acid this is solved as follow:

$$\Delta G'_{GpBTR} = 0.22 \cdot -329.79 = -71.2 \left(\frac{\text{kJ}}{\text{mol}_{\text{GLC}}}\right)$$

In summary, the $\Delta G'_{Gpj}$, in kJ·mol_{GLC}^{-1} for the total of reaction is: lactic acid, -8; formic acid, 0; H_2, -14.6; acetic acid, -36; butyric acid, -71.2; ethanol, -102.1. In the next part it is explained the effect of pH on organic acids $\Delta G'_{Gpj}$.

5) ΔG acid-base reactions

Organic acids have been treated as dissociated forms for the calculation of the previous $\Delta G'_{Gpj}$. As presented in Figure 24 (page 96), the ratio of undissociated/dissociated organic acids is affected by pH. The Gibbs energy related to these acid-base equilibrium reaction is denoted as $\Delta G'_{abj}$. The calculation of this variable is analogous to $\Delta G'_{Gpj}$, *i.e.*, it is corrected for temperature and concentration. Following the example of butyric acid, the $\Delta G'_{GpBTR}$ gives the Gibbs energy of butyrate synthesis (assuming that the total butyric acid is in the dissociated form). At the experimental pH this butyrate is also present in the undissociated form ($C_4H_8O_2$). The stoichiometric matrix of these reactions is presented in Table 13 (page 95). The reaction for butyrate/butyric acid is as follow:

$$C_4H_7O_2^- + H^+ \leftrightarrow C_4H_8O_2$$

The ΔGf^o for undissociated butyric acid is -380.14 kJ·mol^{-1}. The calculated ΔG^o and $\Delta G_T{}^o$ for this reaction are -27.5 and -50.2 kJ·mol^{-1}, respectively. At pH 4.5 the undissociated acid fraction, *fah* is equal to 0.68. This is calculated according to Eqs. (42) and (44) (page 95). The $\Delta G'_{ab}$ for butyric acid is calculated as follow:

$$\Delta G'_{abBTR} = Y_{BTR} \cdot fah_{BTR} \cdot \left(\Delta G_T^0 + R \cdot T \cdot ln\left(\frac{[BTRH]}{[BTR][H^+]} \right) \right)$$

According to the experimental data

$$\Delta G'_{abBTR} = 0.26 \cdot 0.68 \cdot \left(-50.2 + R \cdot T \cdot ln\left(\frac{1.62 \cdot 10^{-3}}{7.7 \cdot 10^{-4} \cdot 3.16 \cdot 10^{-5}} \right) \right)$$

$$\Delta G'_{abBTR} = -3.77 \left(\frac{kJ}{mol_{GLC}} \right)$$

The summary of $\Delta G'_{ab}$, in kJ·mol$_{GLC}^{-1}$, is: lactic acid, -0.42; formic acid, 0; acetic acid, 0.34; butyric acid, -3.77.

Then the Gibbs energy of reactions is corrected by acid-base reactions according to Eq. (45) giving ΔG_{ej}:

$$\Delta G_{ej} = \Delta G'_{Gpj} + \Delta G'_{abj} \quad (45)$$

For butyric acid synthesis we have:

$$\Delta G_{eBTR} = -71.2 - 3.77 = -74.97 \left(\frac{kJ}{mol_{GLC}}\right)$$

The summary of ΔG_e, in $kJ \cdot mol_{GLC}^{-1}$, is as follow: lactic acid, -8.45, formic acid, 0; H_2,-14.65; acetic acid, -35.58; butyric acid, -74.93; ethanol,, -102.

6) ΔG of the extracellular system

The total Gibbs energy of the system (ΔG_S') is obtained from the sum of ΔG_{ej}, according to Eq. (46). In this example ΔG_S' is equal to -235.67 $kJ \cdot mol_{GLC}^{-1}$.

3.3.3 Catabolic thermodynamic model

This catabolic model was thought as an "intracellular thermodynamic" model, based on the stoichiometry of acidogenic glucose metabolism. The catabolic reactions that were incorporated in this model correspond to those pathways responsible for the synthesis of the products detected in this work, *i.e.* H_2, CO_2, acetic acid, butyric acid, ethanol, formic acid, and lactic acid. Metabolic pathways can be added or removed in order to simulate other metabolic products such as propionic acid, hexanoic acid, which could be present in acidogenic cultures, or even adapt the stoichiometric matrix to a different carbon source.

Table 14 presents the catabolic stoichiometric matrix used for this model. All the stoichiometric reactions were mass and electron balanced as described in section 3.3.1. As stated previously, negative stoichiometric coefficients stand for substrates of reactions, whilst positive coefficients for products. This stoichiometric matrix considers 20 components and 9 reactions. The components are 8 intracellular compounds (pyruvate, acetil-CoA, CoA, NAD^+, NADH, ATP, ADP and inorganic phosphorous) and 12 compound that can be transported out of the cytoplasm, which are the compounds that can be measured by the analytical methods used in the experimental work.

The 9 reactions considered in this model were simplified. This simplification consists in lumping together reactions between two metabolic nodes as described in section 1.2.3. Figure

25 illustrates the simplified metabolic network. In this work, we opted to represent stoichiometric matrix as subway networks, instead of the classical representation of metabolic networks, in order to facilitate the understanding of readers that would not be familiarised with this topic.

In this model, glucose is consumed to produce pyruvate by the reaction (r1), in which 2 moles of NADH and 2 moles of ATP are produced per mole of glucose consumed. Pyruvate serves as a node, which can produce lactate, by reaction (r2), or acetyl-CoA, which fuels the production of H_2, acetic acid, butyric acid and ethanol, by reaction (r3).

Table 14: Intracellular stoichiometric matrix

	Reactions								
Compounds	GLC→PYR (r1)	PYR→LCT (r2)	PYR→ACOA (r3)	FRM→H2 (r4)	ACOA→ACT (r5)	ACOA→BTR (r6)	ACOA→EOH (r7)	H2→NADH (r8)	H2+CO2→ACT (r9)
GLC	-1	0	0	0	0	0	0	0	0
ACT	0	0	0	0	1	-1	0	0	1
BTR	0	0	0	0	0	1	0	0	0
CO2	0	0	0	1	0	0	0	0	-2
EOH	0	0	0	0	0	0	1	0	0
FRM	0	0	1	-1	0	0	0	0	0
H2	0	0	0	1	0	0	0	-1	-4
LCT	0	1	0	0	0	0	0	0	0
H	4	-1	0	-1	1	-2	-2	1	1
H2O	2	0	0	0	0	2	0	0	2
NAD	-2	1	0	0	0	2	2	-1	0
NADH	2	-1	0	0	0	-2	-2	1	0
ADP	-2	0	0	0	-1	-1	0	0	0
ATP	2	0	0	0	1	1	0	0	0
PI	-2	0	0	0	-1	-1	0	0	0
ACOA	0	0	1	0	-1	-1	-1	0	0
COA	0	0	-1	0	1	1	1	0	0
PYR	2	-1	-1	0	0	0	0	0	0

The production of lactate consumes one mole of NADH per mol of pyruvate consumed. Acetyl-CoA synthesis produces one mole of formic acid per mol of pyruvate consumed.

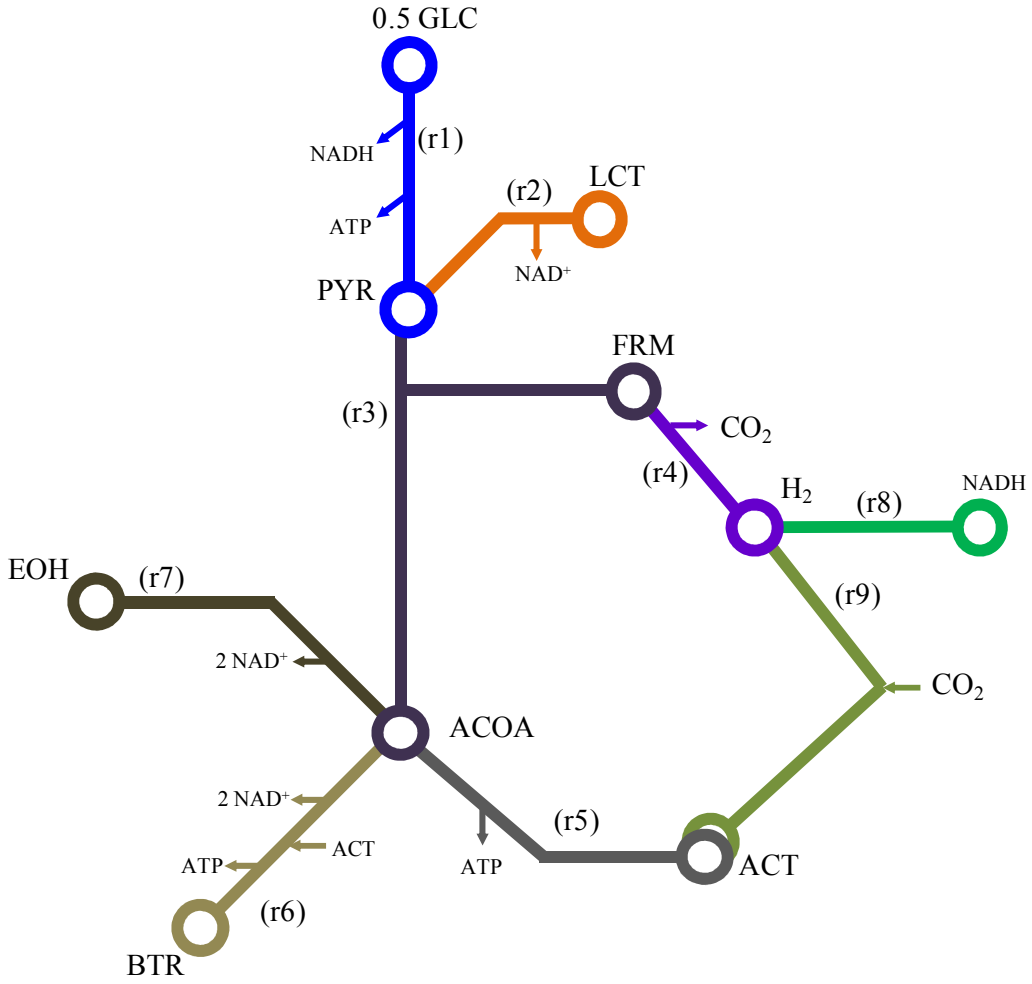

Figure 25: Simplified catabolic network of acidogenic glucose fermentation.

Then, formic acid can be transported out of the cytoplasm or serve as a precursor of H_2, by reaction (r4). The acetyl-CoA is the precursor of acetic acid, butyric acid and ethanol, reactions (r5), (r6) and (r7) respectively. The synthesis of acetic acid produces one mole of ATP per mole of acetyl-CoA consumed, while the synthesis of butyric acid, together with the production of ATP, consumes 2 moles of NADH per mol of acetyl-CoA. Also, the production of butyric acid considers the consumption of one mole of acetic acid. Ethanol synthesis consumes two moles of NADH.

It was considered, as well, that hydrogen can be consumed or produced by H_2/NAD^+ redox reaction, reaction (r8), or by homoacetogenesis, reaction (r9). Both reactions were considered as reversible.

As it was not possible to measure intracellular concentrations with the used analytical materials and methodology, the thermodynamic treatment of the data was based in two hypotheses: 1) no difference between intracellular and extracellular concentrations; and 2) constant intracellular pH of 7.0.

Then, only intracellular compound concentrations, *i.e.* NAD^+/NADH, ATP/ADP and ACOA/COA, are unknown variables, which were calculated by linear algebra based on the stoichiometric model and the Gibbs energy balance. As intracellular pH was assumed to be 7.0, the organic acids are present in the dissociated form (more than 95%), as previously shown in Figure 24. Thus, no organic acid-base Gibbs energy correction was performed in the catabolic thermodynamic model

3.3.4 Thermodynamics of Anabolism

In anaerobic digestion, as in any living system, following the concepts of von Stockar *et al.* [151] and McCarty [150], the energy balance can be obtained, as shown in Eq. (47):

$$\Delta G_o = \frac{1}{Y_X}\left(\Delta G_e \frac{f_e}{f_s} + \Delta G_s\right) \tag{47}$$

Given that the driving force for the growth, the Gibbs energy dissipation, ΔG_o ($kJ \cdot mol_X^{-1}$) must be equal to the energy released from the energy source consumed, ΔG_e ($kJ \cdot mol_{glucose}^{-1}$) and the energy of the biomass synthesis, ΔG_s ($kJ \cdot mol_{glucose}^{-1}$). However, by following the model presented by McCarty [150], it can be reformulated as:

$$\varepsilon \cdot f_e \cdot \Delta G_e = -f_s \cdot \Delta G_s \tag{48}$$

This equation shows that the energy of biomass synthesis is equal to the energy released from the energy source multiplied by an energy transfer efficiency term, ε, which is described as the efficiency at which organisms capture energy [150,156]. In literature, this parameter is indeed considered (or fitted) as a constant [150,156,198]. However, as it will be demonstrate further below, the analysis of experimental data showed that ε is affected by environmental variables as pH.

3.3.5 Equation for the calculation of ε

Global ΔG_e, as proposed by McCarty [150], is determined from the Gibbs energy change of the half electron donor, ΔG_d, and acceptor, ΔG_a, reactions as in the following equation:

$$\Delta G_e = \Delta G_d + \Delta G_a \tag{49}$$

ΔG_s consist of two energy terms, *i.e.*, one for the conversion of the electron donor to an intermediate compound, ΔG_{ic}, and another one for the conversion of the intermediate to cells, ΔG_{pc}, as in the following equation:

$$\Delta G_s = \frac{\Delta G_{ic}}{\varepsilon^n} + \frac{\Delta G_{\mathrm{pc}}}{\varepsilon} \tag{50}$$

Energy may be required to convert the cell carbon source to the intermediate compound, *i.e.* $\Delta G_{ic} > 0$, in which case $n = 1$, or it may be obtained from the conversion itself when $\Delta G_{ic} < 0$, in which case $n = -1$. The intermediate compound was taken to be acetyl-CoA with a half-reaction reduction potential, ΔG_{in}, of 30.9 kJ·eeq^{-1}:

$$\Delta G_{ic} = \Delta \mathrm{G_{in}} + \Delta G_d \tag{51}$$

The value of ΔG_{pc} is estimated from literature ATP required for cell synthesis, and assuming a constant cell composition of $C_5H_7O_2N$. This set its value to 18.8 kJ·eeq^{-1} when ammonia is the nitrogen source for cell synthesis [150]. It is then possible to calculate ε, *i.e.* if $\Delta G_{ic} < 0$ then $n = -1$, and

$$\varepsilon = \left(\frac{\Delta \mathrm{G_{pc}}}{\Delta G_e \left[1 - \frac{\gamma_d}{\gamma_\mathrm{X} \cdot Y_X} \right] - \Delta G_{ic}} \right)^{0.5} \tag{52}$$

However, if $\Delta G_{ic} > 1$, then $n = 1$, and:

$$\varepsilon = \left(\frac{\Delta \mathrm{G_{pc}} + \Delta G_{ic}}{\Delta G_e \left[1 - \frac{\gamma_d}{\gamma_\mathrm{X} \cdot Y_X} \right]} \right)^{0.5} \tag{53}$$

3.4 Thermodynamic Analysis of Product Yield Spectra

Liquid and gas phase experimental steady state data obtained from the 14 experiments is presented in Table 15 and Table 16 respectively. Liquid and gas compositions correspond to the concentration in the bioreactor. It was assumed that both phases were perfectly mixed (stirring velocity was 600 rpm in a liquid volume of 1.3 L).

The results presented in Table 15 show that glucose was not limiting the fermentations. The average glucose concentration in the reactor was 15 mM. In N_2-flushing experiments, biomass concentration decreased when N_2-flushing was increased. A similar trend was observed in pH experiments where biomass decreased with pH increases. The concentration of organic acids

presented in Table 15 corresponds to total organic acid, *i.e.* undissociated/dissociated total concentration of the acids.

Results corresponding to pH experiment presented in Table 16 show that hydrogen head-space composition increased with pH while gas flow rate decreased. The decrease of head-space CO_2 whit pH was due to effect of pH on CO_2/bicarbonate equilibrium.

Experimental results on Table 15 and Table 16 were then used to calculate the experimental yield of acidogenic products on glucose, Y_i, as is presented in Table 17. Yield results were already described in section 3.2.

Table 18 presents the fraction of catabolic glucose participation in each reaction, *fGLC*, which is calculated according to Eq. (38), using the Y_i data on Table 17 and the extracellular stoichiometric matrix presented in Table 12 (section 3.3.2).

Table 15: Liquid phase experimental composition.

	N_2 flushing ($L \cdot d^{-1}$)	pH	GLC	ACT	BTR	EOH	FRM	LCT	Biomass ($g \cdot L^{-1}$)
			(mM)						
N_2 flushing experiments	**0**	**4.5**	22.7±0.12	3.3±0.14	2.4±0.04	6.4±0.06	0	0.7±0.06	0.24±0.006
	2.5	**4.5**	20.8±0.26	3.8±0.05	3±0.08	8.1±0.15	0	0.8±0.05	0.2±0.01
	58.4	**4.5**	12.6±0.09	4.3±0.22	3.8±0.13	6.1±0.23	0	0	0.18±0.01
	0	**5.5**	17.9±0.1	4.9±0.18	3.5±0.1	1.8±0.12	0.8±0.08	3±0.09	0.22±0.01
	7.3	**5.5**	19.1±0.1	6.1±0.18	1.3±0.09	5±0.19	4.9±0.16	3.3±0.12	0.22±0.01
	0	**6.5**	19.1±0.06	7±0.19	1.3±0.08	4.8±0.21	6±0.41	1.7±0.07	0.11±0.01
	2.5	**6.5**	11.2±0.09	8.7±0.37	0.9±0.06	6.4±0.14	4.8±0.38	2.2±0.13	0.08±0.006
	7.3	**6.5**	14.6±0.05	8.4±0.34	0.7±0.06	4.5±0.3	3.4±0.3	1.7±0.07	0.08±0.01
	58.4	**6.5**	19.9±0.07	8.6±0.26	0.6±0.13	6.7±0.22	5±0.35	0	0.01±0.001
pH experiments		**5.5**	19.3±0.02	5.4±0.04	5.6±0.03	1.1±0.04	0	0	0.66±0.01
		6.0	11±0.02	7±0.003	5.5±0.002	6.2±0.005	3.7±0.004	1.3±0.002	0.48±0.008
		6.5	10.8±0.03	10.7±0.008	4.3±0.002	12.6±0.007	13.1±0.01	4.6±0.002	0.34±0.01
		7.0	16±0.03	7.2±0.005	5.6±0.004	3.5±0.003	6.7±0.004	5.3±0.003	0.29±0.01
		7.5	12.6±0.03	6.1±0.003	4.6±0.001	16.7±0.002	1.9±0.003	0.4±0.0006	0.14±0.003

Table 16: Gas phase experimental composition.

	N_2 flushing ($L \cdot d^{-1}$)	pH	H_2 (bar)	CO_2 (bar)	Outlet Gas flow rate ($L \cdot d^{-1}$)
N_2 flushing experiments	**0**	**4.5**	0.58±0.03	0.37±0.02	2±0.26
	2.5	**4.5**	0.26±0.02	0.26±0.02	4.7±0.7
	58.4	**4.5**	0.09±0.01	0.02±0.01	60±3
	0	**5.5**	0.75±0.04	0.23±0.02	1.9±0.2
	7.3	**5.5**	0.16±0.03	0.1±0.02	9±1.5
	0	**6.5**	0.7±0.03	0.05±0.003	0.46±0.06
	2.5	**6.5**	0.24±0.04	0.05±0.04	2.6±0.4
	7.3	**6.5**	0.11±0.013	0.03±0.004	7.31±0.34
	58.4	**6.5**	0.05±0.01	0.01±0.002	57±5
pH experiments		**5.5**	0.68±0.01	0.29±0.006	3.2±0.23
		6.0	0.68±0.01	0.33±0.01	3.6±0.3
		6.5	0.76±0.02	0.19±0.01	2.4±0.3
		7.0	0.94±0.02	0.08±0.004	2.1±0.2
		7.5	0.89±0.007	0.02±0.002	0.98±0.1

Table 19 presents both temperature and concentration corrected Gibbs free energy of the global reactions. Both corrections were done according to section 2.5, *i.e.*, Eqs. (25), (27) using the thermodynamic data presented on Table 4, together with the developed extracellular stoichiometric matrix (Table 12) and the liquid and gas composition presented in Table 15 and Table 16. This correction is also presented for acid-base reactions in Table 20 where it was done as explained for Table 19, but using the acid-base stoichiometric matrix presented in Table 13. Table 21 presents the calculated Gibbs energy of reactions, ΔG_e, and system, ΔG_S', calculated according to Eqs. (45) and (46).

Table 17: Experimental yields.

	N_2 flushing ($L \cdot d^{-1}$)	pH	Experimental yields Y ($mol_i \cdot mol_{GLC}^{-1}$)								
			Products							Substrate	
			ACT	BUT	EOH	FRM	H2	LCT	Biomass	GLC_{tot}	GLC_{cat}
N_2 flushing experiments	**0**	**4.5**	0.35±0.02	0.26±0.01	0.70±0.02	0	1.03±0.19	0.08±0.01	0.23±0.02	1±0.19	0.77±0.2
	2.5	**4.5**	0.35±0.01	0.27±0.01	0.75±0.01	0	0.95±0.16	0.07±0.00	0.16±0.03	1±0.16	0.84±0.17
	58.4	**4.5**	0.32±0.01	0.28±0.01	0.45±0.02	0	3.25±0.37	0	0.11±0.04	1±0.37	0.89±0.37
	0	**5.5**	0.49±0.01	0.36±0.01	0.18±0.01	0.08±0.01	1.19±0.19	0.30±0.01	0.20±0.04	1±0.19	0.80±0.2
	7.3	**5.5**	0.54±0.02	0.12±0.01	0.44±0.02	0.43±0.01	1.07±0.15	0.29±0.01	0.17±0.05	1±0.16	0.83±0.17
	0	**6.5**	0.81±0.02	0.15±0.01	0.55±0.03	0.69±0.05	0.34±0.06	0.19±0.01	0.11±0.04	1±0.09	0.89±0.1
	2.5	**6.5**	0.93±0.05	0.10±0.01	0.69±0.02	0.51±0.04	0.56±0.08	0.23±0.01	0.08±0.02	1±0.10	0.92±0.11
	7.3	**6.5**	1.06±0.04	0.09±0.01	0.57±0.04	0.43±0.04	0.82±0.03	0.21±0.01	0.09±0.06	1±0.09	0.91±0.11
	58.4	**6.5**	0.81±0.02	0.06±0.01	0.63±0.02	0.47±0.04	2.31±0.09	0	0.01±0.00	1±0.11	0.99±0.11
pH experiments		**5.5**	0.38±0.01	0.40±0.01	0.08±0.01	0	1.27±0.12	0	0.41±0.03	1±0.12	0.59±0.13
		6.0	0.38±0.01	0.30±0.01	0.34±0.02	0.20±0.01	1.11±0.18	0.07±0.01	0.23±0.02	1±0.18	0.77±0.18
		6.5	0.51±0.03	0.21±0.01	0.61±0.02	0.63±0.03	0.72±0.14	0.22±0.01	0.14±0.01	1±0.14	0.86±0.14
		7.0	0.44±0.02	0.34±0.01	0.21±0.01	0.41±0.01	0.99±0.18	0.32±0.01	0.16±0.03	1±0.18	0.84±0.18
		7.5	0.35±0.01	0.27±0.01	0.97±0.01	0.11±0.01	0.43±0.08	0.02±0.00	0.07±0.01	1±0.08	0.93±0.1

Table 18: Calculated catabolic glucose fraction, fGLC, participating on global reactions.

	N_2 flushing ($L \cdot d^{-1}$)	pH	fGLC ($mol_{GLCcat} \cdot mol_{GlC}^{-1}$) GLC→LCT (rA)	GLC→FRM (rB)	GLC→H2 (rC)	GLC→ACT (rD)	GLC→BUT (rE)	GLC→EOH (rF)	GLC_{cat}
N_2 flushing experiments	**0**	**4.5**	0.04±0.01	0	0.09±0.19	0.12±0.02	0.22±0.01	0.35±0.02	0.81±0.2
	2.5	**4.5**	0.03±0.00	0	0.08±0.16	0.12±0.01	0.23±0.01	0.37±0.01	0.83±0.17
	58.4	**4.5**	0	0	0.27±0.37	0.11±0.01	0.23±0.01	0.22±0.02	0.83±0.37
	0	**5.5**	0.15±0.01	0.01±0.01	0.1±0.19	0.16±0.01	0.3±0.01	0.09±0.01	0.8±0.2
	7.3	**5.5**	0.14±0.01	0.04±0.01	0.09±0.15	0.18±0.02	0.1±0.01	0.22±0.02	0.76±0.17
	0	**6.5**	0.1±0.01	0.06±0.05	0.03±0.06	0.27±0.02	0.12±0.01	0.28±0.03	0.85±0.1
	2.5	**6.5**	0.12±0.01	0.04±0.04	0.05±0.08	0.31±0.05	0.08±0.01	0.34±0.02	0.94±0.11
	7.3	**6.5**	0.11±0.01	0.04±0.04	0.07±0.03	0.35±0.04	0.07±0.01	0.28±0.04	0.92±0.11
	58.4	**6.5**	0	0.04	0.19±0.09	0.27±0.02	0.05±0.01	0.32±0.02	0.86±0.11
pH experiments		**5.5**	0	0	0.11±0.12	0.13±0.01	0.33±0.01	0.04±0.01	0.6±0.13
		6.0	0.04±0.01	0.02±0.01	0.09±0.18	0.13±0.01	0.25±0.01	0.17±0.02	0.7±0.18
		6.5	0.11±0.01	0.05±0.03	0.06±0.14	0.17±0.03	0.17±0.01	0.3±0.02	0.87±0.14
		7.0	0.16±0.01	0.03±0.01	0.08±0.18	0.15±0.02	0.28±0.01	0.11±0.01	0.81±0.18
		7.5	0.01±0.00	0.01±0.01	0.04±0.08	0.12±0.01	0.22±0.01	0.48±0.01	0.88±0.08

Table 19: Temperature and concentration corrected Gibbs free energy, ΔG'.

			Temperature corrected ΔG ($kJ \cdot mol_{GLC}^{-1}$)					
			GLC→LCT (rA)	GLC→FRM (rB)	GLC→H2 (rC)	GLC→ACT (rD)	GLC→BUT (rE)	GLC→EOH (rF)
			-117.4	600.3	-147	-191	-285.7	-272.2
	N_2 flushing ($L \cdot d^{-1}$)	pH	Concentration corrected Gibbs free energy, $\Delta G'_{Gp}$ ($kJ \cdot mol_{GLC}^{-1}$)					
N_2 flushing experiments	0	4.5	-8	0	-14.6	-36	-71.2	-102.1
	2.5	4.5	-6.9	0	-15.8	-35.5	-75.5	-109.8
	58.4	4.5	0	0	-73.5	-31.8	-78.2	-69.1
	0	5.5	-30.3	0.1	-16.7	-52.7	-99.6	-26.8
	7.3	5.5	-29.1	3.2	-20.3	-56.8	-32.9	-65.5
	0	6.5	-20.9	2	-5.4	-90.1	-43.6	-84.5
	2.5	6.5	-24.9	1.3	-10.6	-103.4	-29.2	-103.7
	7.3	6.5	-23.2	1	-18	-118	-25.4	-87.6
	58.4	6.5	0	2.5	-59.4	-89.5	-17.2	-99.4
pH experiments		5.5	0	0	-17.7	-40.9	-111.2	-11.8
		6	-7.5	0.5	-15.2	-41.6	-85.2	-50
		6.5	-23.4	2.1	-10.2	-56.6	-58.9	-88.3
		7	-34.9	-0.09	-14.7	-49.9	-99	-32.2
		7.5	-2.6	-0.5	-7.1	-41.4	-79.1	-146.3

Table 20: Temperature and concentration corrected Gibbs free energy for acid-base reactions, ΔG_a'.

			Temperature corrected delta G ($kJ \cdot mol_{GLC}^{-1}$)			
			LCT→LCTH	FRM→FRMH	ACT→ACTH	BUT→BUTH
			-50.57	-39.361	-26.791	-50.153
	N_2 flushing ($L \cdot d^{-1}$)	pH	Concentration corrected Gibbs free energy, ΔG_a' ($kJ \cdot mol_{GLC}^{-1}$)			
N_2 flushing experiments	0	4.5	-0.42	0	0.34	-3.77
	2.5	4.5	-0.36	0	0.33	-4
	58.4	4.5	0	0	0.30	-4.1
	0	5.5	-0.19	-0.02	0.11	-1.32
	7.3	5.5	-0.18	-0.13	0.12	-0.43
	0	6.5	-0.01	-0.02	0.02	-0.07
	2.5	6.5	-0.01	-0.02	0.02	-0.04
	7.3	6.5	-0.01	-0.01	0.03	-0.04
	58.4	6.5	0	-0.01	0.02	-0.03
pH experiments		5.5	0	0	0.09	-1.48
		6	-0.01	-0.02	0.03	-0.41
		6.5	-0.01	-0.02	0.01	-0.09
		7	-0.01	0	0	-0.05
		7.5	0	0	0	-0.01

Table 21: Calculated global Gibbs free energy, ΔG_e, at the experimental condition applied.

	N_2 flushing ($L \cdot d^{-1}$)	pH	Global Gibbs free energy ΔG_e GLC→LCT (rA) ($kJ \cdot mol_{GLC}^{-1}$)	GLC→FRM (rB)	GLC→H2 (rC)	GLC→ACT (rD)	GLC→BUT (rE)	GLC→EOH (rF)	Total ΔG_S'
N_2 flushing experiments	0	4.5	-8.45	0	-14.65	-35.58	-74.93	-102.06	-235.67
	2.5	4.5	-7.27	0	-15.82	-35.19	-79.51	-109.85	-247.65
	58.4	4.5	0	0	-73.46	-31.46	-82.21	-69.09	-256.23
	0	5.5	-30.46	0.10	-16.67	-52.59	-100.93	-26.80	-227.35
	7.3	5.5	-29.31	3.07	-20.27	-56.7	-33.35	-65.54	-202.12
	0	6.5	-20.91	1.93	-5.45	-90.03	-43.66	-84.49	-242.61
	2.5	6.5	-24.95	1.27	-10.57	-103.37	-29.26	-103.67	-270.54
	7.3	6.5	-23.25	0.99	-18.01	-117.97	-25.48	-87.64	-271.34
	58.4	6.5	0	2.49	-59.38	-89.44	-17.24	-99.45	-263.02
pH experiments		5.5	0	0	-17.74	-40.86	-112.71	-11.75	-183.06
		6	-7.51	0.45	-15.23	-41.6	-85.62	-50.03	-199.53
		6.5	-23.42	2.10	-10.21	-56.6	-59.03	-88.33	-235.48
		7	-34.88	-0.09	-14.74	-49.9	-99.05	-32.19	-230.86
		7.5	-2.61	-0.51	-7.12	-41.4	-79.12	-146.31	-277.08

The results presented in Table 21 are summarised as follows. For N_2-flushing experiments, lactate ΔG_e synthesis, reaction (rA), was constant for pH 4.5 (-8 kJ·mol$_{GLC}^{-1}$), pH 5.5 (-30 kJ·mol$_{GLC}^{-1}$) and pH 6.5 (-23 kJ·mol$_{GLC}^{-1}$), with the exemption of experiments at 58.4 (L·d^{-1}) N_2-flushing, where lactate synthesis was stopped. For pH experiments, lactate ΔG_e achieved a maximum of -35 (kJ·mol$_{GLC}^{-1}$) at pH 7.0.

Formic acid was not produced at N_2-flushing experiment at pH 4.5, for the rest of the N_2-flushing experiments, its ΔG_e was always positive, which means that the production of formate was endergonic. At pH 5.5, its energy consumption increased from 0.1 to 3 (kJ·mol$_{GLC}^{-1}$), while at pH 6.5, its energy consumption was constant (1.4 kJ·mol$_{GLC}^{-1}$), increasing to 2.5 (kJ·mol$_{GLC}^{-1}$) at 58.4 (L·d^{-1}) N_2-flushing. For pH experiments, formic ΔG_e was endergonic at pH 6.0 and 6.5, and exergonic at pH 7.0 and 7.5. However, in all cases the absolute values of formic acid ΔG_e are very low and always smaller than 3 (kJ·mol$_{GLC}^{-1}$).

Hydrogen ΔG_e decreased with N_2-flushing, *i.e.* becomes more favourable. At pH 4.5 it decreased from -15 to -73 (kJ·mol$_{GLC}^{-1}$), at pH 5.5 from -17 to -20 (kJ·mol$_{GLC}^{-1}$), and at pH 6.5 from -5.5 to -60 (kJ·mol$_{GLC}^{-1}$). On the other hand, hydrogen ΔG_e increased with pH (being less favourable), it increased from -18 to -7 (kJ·mol$_{GLC}^{-1}$) from pH 5.5 to 7.5.

The energy related to Acetate synthesis was constant. For N_2-flushing experiments acetate ΔG_e was -34, -55 and -100 (kJ·mol$_{GLC}^{-1}$) at pH 4.5, 5.5 and 6.5 respectively. For pH experiments it was -46 (kJ·mol$_{GLC}^{-1}$).

Butyrate ΔG_e was constant (-80 kJ·mol$_{GLC}^{-1}$) at pH 4.5 N_2-flushing experiment, while it increased from -100 to -33 (kJ·mol$_{GLC}^{-1}$) at pH 5.5 and from -44 to -17 (kJ·mol$_{GLC}^{-1}$) at pH 6.5. Similar trend was observed at pH experiments where butyrate ΔG_e increased from -113 to -79 (kJ·mol$_{GLC}^{-1}$) from pH 5.5 to 7.5.

Ethanol related energy increased with N_2-flushing at pH 4.5, from -102 to -69 (kJ·mol$_{GLC}^{-1}$), while decreased with N_2-flushing at pH 5.5, from -27 to -66 (kJ·mol$_{GLC}^{-1}$), staying constant at pH 6.5 (-94 kJ·mol$_{GLC}^{-1}$). The observed effect of pH is favourable, since ethanol ΔG_e decreases from -12 to -146 (94 kJ·mol$_{GLC}^{-1}$) from pH 5.5 to 7.5.

Energy system was rather constant for N_2-flushing experiments, -247 ($kJ \cdot mol_{GLC}^{-1}$) at pH 4.5, and, -215 and -260 ($kJ \cdot mol_{GLC}^{-1}$) for pH 5.5 and 6.5 respectively. For pH experiments, ΔG_S' decreased from -183 to -277 ($kJ \cdot mol_{GLC}^{-1}$), *i.e.* the energy released by catabolic processes is favoured by pH increase.

3.4.1 Thermodynamic analysis of metabolism

The thermodynamic analysis of the acidogenic metabolism was based on the thermodynamics of hydrogen synthesis and consumption. An example of calculation is given in Box 2 at the end of this section. Figure 26 illustrates the acetyl-CoA node, where extracellular products are highlighted with its respective catabolic glucose fraction (*fGLC*). The fraction *fb* ($mol_{catGLC} \cdot mol_{GLC}^{-1}$) represents the catabolic glucose fraction deviated from H_2 (*fH2*) or acetate (*fACT*) for the non acetyl-CoA related synthesis/consumption of H_2 by reaction (r8) and/or (r9).This fraction *fb* was calculated considering the stoichiometry of the acetyl-CoA node as follow:

$$f_b = \frac{Y_{ACT} + 2 \cdot Y_{BTR} + Y_{EOH} - Y_{FRM} - Y_{H2}}{12} \quad (54)$$

In this equation, if no extra reactions, *i.e.* (r8) and (r9), consume or produce hydrogen, the moles of acetate, butyrate and ethanol produced should be equal to the formate and hydrogen moles produced. When $fb < 0$ extra hydrogen is produced by these reactions, and is consumed when $fb > 0$.

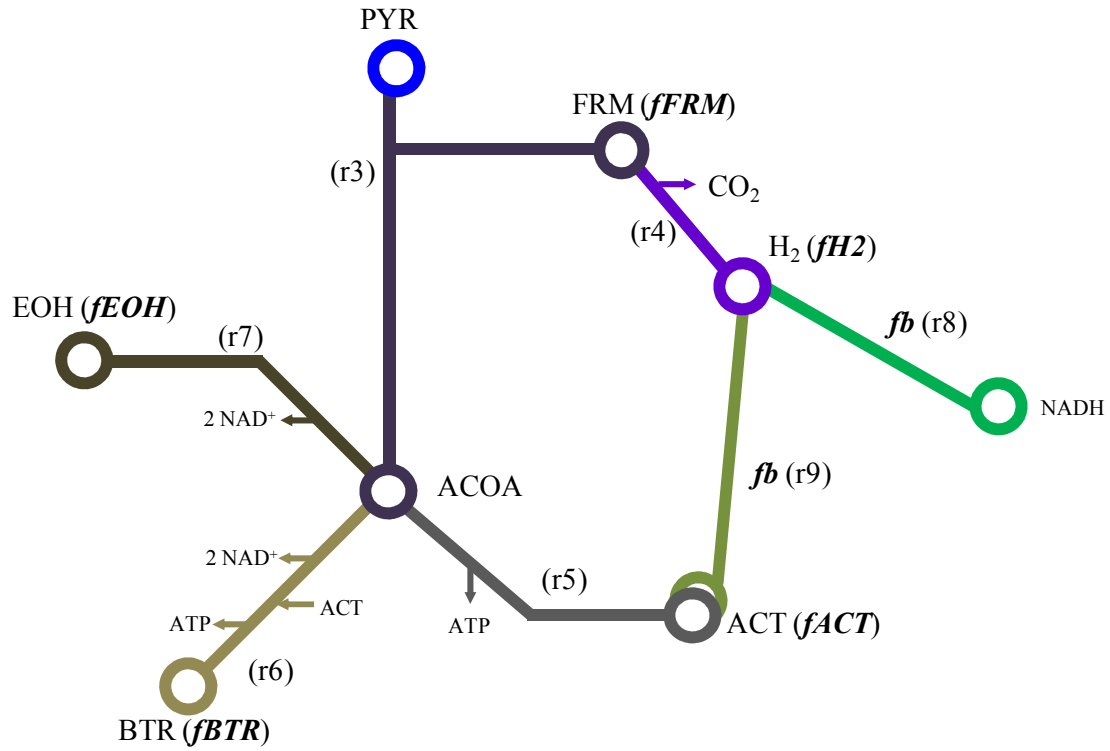

Figure 26: Simplified diagram of acetyl-CoA node.

The calculation of intracellular Gibbs energy considered the energy balance between ΔG_e and ΔG_{intra}, and, catabolic glucose fractions, $fGLC_i$, and fb. Gibbs energy balance was grouped into $fb > 1$ and $fb < 1$. Two independent calculation where done to test reaction (r8) and (r9).

The following matrices illustrates the Gibbs energy balance for (r8) when $fb > 1$ (Table 22) and $fb < 1$ (Table 23). Table 24 and Table 25 present the Gibbs energy balance matrices for homoacetogenesis for $fb > 1$ and $fb < 1$ respectively.

Intracellular catabolic Gibbs energies are presented as subindex numbered $\Delta G'$, numbers correspond to its intracellular reaction. The intracellular Gibbs energy of reaction (r4) and homoacetogenesis (r9) were directly calculated according to the stoichiometry and experimental composition. A particular case, when formic acid was not produced, allowed to lump reactions (r3) and (r4), and then the Gibbs energy of (r4) cannot be directly calculated.

Table 22: Gibbs energy balance matrix for hydrogen consumtion by H_2/NAD^+ redox reaction.

$$\begin{bmatrix} \frac{fFRM}{fACOA} & 0 & 0 & 0 & 0 \\ \frac{fH2+fb}{fACOA} & 0 & 0 & 0 & 0 \\ \frac{fACT}{fACOA} & 1 & 0 & 0 & 0 \\ \frac{fBTR}{fACOA} & 0 & 1 & 0 & 0 \\ \frac{fEOH}{fACOA} & 0 & 0 & 1 & 0 \\ 1 & 1 & 1 & 1 & 1 \end{bmatrix} X \begin{bmatrix} \Delta G_3 \\ \Delta G_5' \\ \Delta G_6' \\ \Delta G_7' \\ \Delta G_8' \end{bmatrix} = \begin{bmatrix} \Delta G_B \\ \Delta G_c - \Delta G_4' \\ \Delta G_D \\ \Delta G_E \\ \Delta G_F \\ \Delta G_S' - \Delta G_4' - \Delta G_A \end{bmatrix}$$

Table 23: Gibbs energy balance matrix for hydrogen synthesis by H_2/NAD^+ redox reaction.

$$\begin{bmatrix} \frac{fFRM}{fACOA} & 0 & 0 & 0 & 0 \\ \frac{fH2+fb}{fACOA} & 0 & 0 & 0 & 1 \\ \frac{fACT}{fACOA} & 1 & 0 & 0 & 0 \\ \frac{fBTR}{fACOA} & 0 & 1 & 0 & 0 \\ \frac{fEOH}{fACOA} & 0 & 0 & 1 & 0 \\ 1 & 1 & 1 & 1 & 1 \end{bmatrix} X \begin{bmatrix} \Delta G_3 \\ \Delta G_5' \\ \Delta G_6' \\ \Delta G_7' \\ \Delta G_8' \end{bmatrix} = \begin{bmatrix} \Delta G_B \\ \Delta G_c - \Delta G_4' \\ \Delta G_D \\ \Delta G_E \\ \Delta G_F \\ \Delta G_S' - \Delta G_4' - \Delta G_A \end{bmatrix}$$

Table 24: Gibbs energy balance matrix for hydrogen consumption by homoacetogenesis.

$$\begin{bmatrix} \frac{fFRM}{fACOA-fb} & 0 & 0 & 0 \\ \frac{fH2+fb}{fACOA-fb} & 0 & 0 & 0 \\ \frac{fACT-fb}{fACOA-fb} & 1 & 0 & 0 \\ \frac{fBTR}{fACOA-fb} & 0 & 1 & 0 \\ \frac{fEOH}{fACOA-fb} & 0 & 0 & 1 \\ 1 & 1 & 1 & 1 \end{bmatrix} X \begin{bmatrix} \Delta G_3 \\ \Delta G_5' \\ \Delta G_6' \\ \Delta G_7' \end{bmatrix} = \begin{bmatrix} \Delta G_B \\ \Delta G_c - \Delta G_4' \\ \Delta G_D - \Delta G_9' \\ \Delta G_E \\ \Delta G_F \\ \Delta G_S' - \Delta G_A - \Delta G_4' - \Delta G_9' \end{bmatrix}$$

Table 25: Gibbs energy balance matrix for hydrogen synthesis by homoacetogenesis.

$$\begin{bmatrix} \frac{fFRM}{fACOA-fb} & 0 & 0 & 0 \\ \frac{fH2+fb}{fACOA-fb} & 0 & 0 & 0 \\ \frac{fACT-fb}{fACOA-fb} & 1 & 0 & 0 \\ \frac{fBTR}{fACOA-fb} & 0 & 1 & 0 \\ \frac{fEOH}{fACOA-fb} & 0 & 0 & 1 \\ 1 & 1 & 1 & 1 \end{bmatrix} X \begin{bmatrix} \Delta G_3 \\ \Delta G_5' \\ \Delta G_6' \\ \Delta G_7' \end{bmatrix} = \begin{bmatrix} \Delta G_B \\ \Delta G_c - \Delta G_4' - \Delta G_9' \\ \Delta G_D \\ \Delta G_E \\ \Delta G_F \\ \Delta G_S' - \Delta G_A - \Delta G_4' - \Delta G_9' \end{bmatrix}$$

The variable *fACOA*, *i.e.* catabolic glucose fraction on acetyl-CoA node, was calculated as follows:

$$fACOA = fH2 + fFRM + fACT + fBTR + fEOH + fb \quad (55)$$

Figure 27 illustrates the catabolic Gibbs energy flow when H_2/NAD^+ redox reaction (r8) is active.

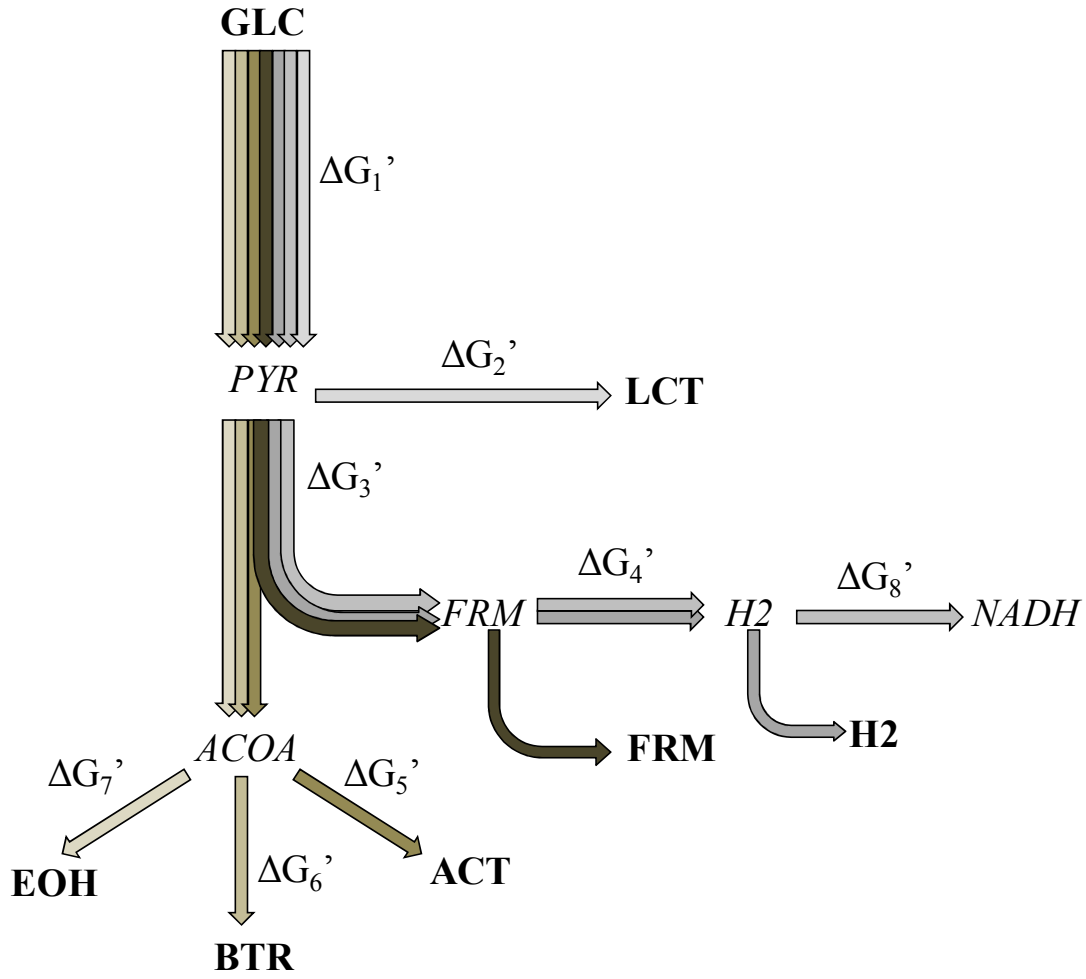

Figure 27: Catabolic Gibbs energy flow when considering H_2/NAD^+ redox reaction.

The thermodynamic analysis also considered that both H_2/NAD^+ redox reaction (r8) and homoacetogenesis are reversible (r9). Thus the analysis considered separately the

consumption and synthesis of H_2 by these two reactions. As stated above, the consumption of H_2 was identified by $fb > 0$, and their synthesis, *i.e.* by reversed (r8) and/or (r9), by $fb < 0$.

Table 26 presents the calculations of intracellular $\Delta G'$ when considering H_2/NAD^+ redox reaction (r8). This table also presents the calculated values of *fb*. The used of this reaction describes the metabolism of the experiments at 58.4 ($L \cdot d^{-1}$) N_2-flushing (pH 4.5 and 6.5), and the pH experiments at pH 7.0 and 7.5. For the rest of experiments, reaction (r8) resulted endergonic.

The intracellular Gibbs energy calculation for homoacetogenesis is presented in

Table 27. This reaction is capable to explain the metabolism of all the experiments, excepting experiment "N_2-flushing 58.4 ($L \cdot d^{-1}$) pH 6.5" where it resulted on endergonic synthesis of acetate, butyrate and ethanol.

Table 28 presents the summary of intracellular Gibbs energies for both (r8) and (r9) reactions. In general, homoacetogenesis explained metabolic thermodynamics when *fb* confirmed H_2 consumption, *i.e.* $fb > 0$. A particular case was observed at experiment pH 7.5 where H_2/NAD^+ redox reaction can also explain the metabolism at this operational condition, both reactions yields similar results, but as expected, acetate synthesis reaction was affected by homoacetogenesis, *i.e.* the use of (r8) resulted in a acetate ΔG' of -39 ($kJ \cdot mol_{GLC}^{-1}$), while using (r9) resulted in -31 ($kJ \cdot mol_{GLC}^{-1}$). This difference agreed with the value of homoacetogenesis Gibbs energy (-10 $kJ \cdot mol_{GLC}^{-1}$).

Reversed homoacetogenesis, *i.e.* synthesis of H_2 from acetate, explained the metabolism for *fb* values above -0.03, as seen in experiments '7.3 ($L \cdot d^{-1}$) N_2-flushing pH 5.5', 'pH 5.5' and 'pH 7.0'. Another particular case was observed at this pH, where the metabolism could be also explained using the reversed H_2/NAD^+ redox reaction. In this case both reversed reaction yielded very different results. Gibbs energy of (r3) was -1.7 and -80 ($kJ \cdot mol_{GLC}^{-1}$) for (r8) and (r9) respectively, whilst the use of reversed (r8) decreased the Gibbs energies of acetate, butyrate and ethanol synthesis reactions.

Reversed H_2/NAD^+ redox reaction explained the metabolism of N_2-flushing experiments at 58.4 ($L \cdot d^{-1}$). At this condition, *fb* was lower than -0.1, the lowest values observed in the total set of experiments. Reversed (r8) Gibbs energy calculated was -60 ($kJ \cdot mol_{GLC}^{-1}$). At N_2-flushing experiment pH 6.5 the Gibbs energy of reaction (r3) is endergonic.

Gibbs energy of (r3) decreased, becoming more exergonic, for N_2-flushing experiments at pH 4.5 (from -86 to -137 $kJ \cdot mol_{GLC}^{-1}$) and 5.5 (-90 to -98 $kJ \cdot mol_{GLC}^{-1}$). At pH 6.5 it achieved a minimum value (-78 $kJ \cdot mol_{GLC}^{-1}$) at 7.3 ($L \cdot d^{-1}$) N_2-flushing. For pH experiments, this Gibbs energy increased (from -102 to -41 $kJ \cdot mol_{GLC}^{-1}$) in the range of pH 5.5 to 6.5.

Gibbs energy of (r4) could not be calculated when formate was absent of the fermentations, *i.e.* N_2-flushing experiments at pH 4.5 and pH experiment 5.5. This Gibbs energy becomes more exergonic with both N_2-flushing and pH increase.

Acetate, butyrate and ethanol Gibbs energies became more endergonic in N_2-flushing experiment at pH 4.5. The trend changed at pH 5.5 where ethanol synthesis became more exergonic with N_2-flushing. At pH 6.5, N_2-flushing produced a more exergonic acetate and ethanol synthesis, an endergonic butyrate synthesis. pH affected positively these three reactions, *i.e.* they became exergonic with pH.

Table 29 reports the intracellular ratio of NAD^+/NADH, ATP/ADP and ACOA/COA. They were calculated using the Gibbs energy results of acetate, butyric and ethanol reactions, their respective *fGLC* and stoichiometry (Table 14). For N_2-flushing experiments, the ratio NAD^+/NADH results are mixed, at pH 4.5 it increased from 0.003 to 0.007 when increasing N_2-flushing from 0 to 2.5 ($L \cdot d^{-1}$), then it decreased to 0.001 at 58.4 ($L \cdot d^{-1}$) N_2-flushing.

Table 26: Intracellular Gibbs energy considering H_2/NADH redox reaction.

	N_2 flushing ($L \cdot d^{-1}$)	pH	$fb \cdot 10^2$	Intracellular ΔG ($kJ \cdot mol_{GLC}^{-1}$)						
				$\Delta G_3'$	$\Delta G_4'$	$\Delta G_5'$	$\Delta G_6'$	$\Delta G_7'$	$\Delta G_8'$	$\Delta G_8'$rev
N_2 flushing experiments	0	4.5	4.4	-91.1	—	-22.4	-50.7	-63	0	—
	2.5	4.5	5.8	-98.7	—	-21.7	-53.1	-66.8	0	—
	58.4	4.5	-16	-137.4	—	-10	-34.7	-23.2	—	-50.9
	0	5.5	1	-92.5	-1.5	-29.6	-59.7	-14.5	0.9	—
	7.3	5.5	-2.4	51.1	-2.3	-72.1	-41.6	-84.3	—	-23.6
	0	6.5	5.3	-10	-2.6	-86.7	-42.1	-81.1	0.8	—
	2.5	6.5	6.3	-42.7	-4	-88.4	-25.3	-87.2	2	—
	7.3	6.5	4.6	-87.8	-4.9	-81.8	-18.2	-58.6	3.2	—
	58.4	6.5	-10.3	48.3	-5	-106.5	-20.3	-119.5	—	-60
pH experiments		5.5	-0.1	151	—	-72.9	-195.8	-21.4	—	-44
		6	0.2	-90.2	-1.9	-24.2	-51.2	-26.8	2.2	—
		6.5	1.5	-45.4	-2.2	-46.6	-48.9	-70.6	1.6	—
		7	-0.6	-1.7	-2.2	-49.5	-98.3	-31.9	—	-12.3
		7.5	11.0	-18.7	-4.4	-39.2	-74.9	-137	-0.3	—

Table 27: Intracellular Gibbs energy considering homoacetogenesis reaction.

	N_2 flushing ($L \cdot d^{-1}$)	pH	$fb \cdot 10^2$	Intracellular ΔG ($kJ \cdot mol_{GLC}^{-1}$)						
				$\Delta G_3'$	$\Delta G_4'$	$\Delta G_5'$	$\Delta G_6'$	$\Delta G_7'$	$\Delta G_9'$	$\Delta G_9'$rev
N_2 flushing experiments	0	4.5	4.4	-86.1	—	-22	-50.7	-63	-5.3	—
	2.5	4.5	5.8	-92.1	—	-22.6	-53.1	-66.8	-5.8	—
	58.4	4.5	-16	-494.6	—	126.2	55.9	64.2	—	-8
	0	5.5	1	-90	-1.5	-29.9	-60.1	-14.4	-1.2	—
	7.3	5.5	-2.4	-98	-2.3	-23.9	-17.4	-30.4	—	-1.9
	0	6.5	5.3	-8	-2.6	-82.3	-42.2	-81.4	-5.3	—
	2.5	6.5	6.3	-36.4	-4	-87.3	-25.2	-88.2	-4.7	—
	7.3	6.5	4.6	-78.3	-4.9	-85.3	-18	-59.7	-2.4	—
	58.4	6.5	-10.3	-386.4	-5.1	78.6	6.2	43.9	—	-2.4
pH experiments		5.5	-0.1	-101.8	—	-19.2	-56.8	-5.2	—	-0.1
		6	0.2	-86.6	-1.9	-24.4	-52.1	-27.2	-0.2	—
		6.5	1.5	-41.4	-2.2	-46.1	-49.4	-71.6	-1.7	—
		7	-0.6	-80	-2.2	-30.9	-63.8	-18.8	—	-0.7
		7.5	11	-17	-4.4	-30.8	-74.8	-136.9	-10.5	—

Table 28: Resulting catabolic analysis based on thermodynamics.

	N_2 flushing ($L \cdot d^{-1}$)	pH	$fb \cdot 10^2$	Intracellular ΔG ($kJ \cdot mol_{GLC}^{-1}$)								
				$\Delta G_3'$	$\Delta G_4'$	$\Delta G_5'$	$\Delta G_6'$	$\Delta G_7'$	$\Delta G_8'$	$\Delta G_8'$rev	$\Delta G_9'$	$\Delta G_9'$rev
N_2 flushing experiments	0	4.5	4.4	-86.1	—	-22	-50.7	-63	—	—	-5.3	—
	2.5	4.5	5.8	-92.1	—	-22.6	-53.1	-66.8	—	—	-5.8	—
	58.4	4.5	-16	-137.4	—	-10	-34.7	-23.2	—	-50.9	—	—
	0	5.5	1	-90	-1.5	-29.9	-60.1	-14.4	—	—	-1.2	—
	7.3	5.5	-2.4	-98	-2.3	-23.9	-17.4	-30.4	—	—	—	-1.9
	0	6.5	5.3	-8	-2.6	-82.3	-42.2	-81.4	—	—	-5.3	—
	2.5	6.5	6.3	-36.4	-4	-87.3	-25.2	-88.2	—	—	-4.7	—
	7.3	6.5	4.6	-78.3	-4.9	-85.3	-18	-59.7	—	—	-2.4	—
	58.4	6.5	-10.3	48.3	-5	-106.5	-20.3	-119.5	—	-60	—	—
pH experiments		5.5	-0.1	-101.8	—	-19.2	-56.8	-5.2	—	—	—	-0.1
		6	0.2	-86.6	-1.9	-24.4	-52.1	-27.2	—	—	-0.2	—
		6.5	1.5	-41.4	-2.2	-46.1	-49.4	-71.6	—	—	-1.7	—
		7	-0.6	-1.7	-2.2	-49.5	-98.3	-31.9	—	-12.3	—	—
				-80	-2.2	-30.9	-63.8	-18.8	—	—	—	-0.7
		7.5	11	-18.7	-4.4	-39.2	-74.9	-137	-0.3	—	—	—
				-17	-4.4	-30.8	-74.8	-136.9	—	—	-10.5	—

Table 29: Intracellular ratios of NAD^+/NADH, ATP/ADP and ACOA/COA.

	N_2 flushing ($L \cdot d^{-1}$)	pH	NAD+/NADH $\cdot 10^4$	ATP/ADP	ACOA/COA
N_2 flushing experiments	0	4.5	30	0.03	$2 \cdot 10^{17}$
	2.5	4.5	70	0.04	$1 \cdot 10^{18}$
	58.4	4.5	10	0.11	$2 \cdot 10^{10}$
	0	5.5	400	0.11	$4 \cdot 10^{17}$
	7.3	5.5	70	0.85	$4 \cdot 10^{14}$
	0	6.5	280	0.34	$6 \cdot 10^{28}$
	2.5	6.5	1150	0.85	$1 \cdot 10^{27}$
	7.3	6.5	4410	2.00	$1 \cdot 10^{24}$
	58.4	6.5	890	1.25	$1 \cdot 10^{37}$
pH experiments		5.5	350	0.12	$1 \cdot 10^{15}$
		6	850	0.11	$4 \cdot 10^{18}$
		6.5	1100	0.2	$4 \cdot 10^{25}$
		7	2090	0.08	$1 \cdot 10^{31}$
			1120	0.05	$1 \cdot 10^{20}$
		7.5	2360	0.07	$2 \cdot 10^{30}$
			2	0.06	$2 \cdot 10^{24}$

A similar trend was observed at pH 6.5. The NAD^+/NADH ratio increased from 0.028 to 0.441 (N_2-flushingig 0 to 7.5 $L \cdot d^{-1}$), then it decreased to 0.089 at 58.4 ($L \cdot d^{-1}$) N_2-flushing. At pH 5.5, this ratio decreased with N_2-flushing. For pH experiments, this ratio increased when considering that reaction (r8) was active at pH 7.0 and 7.5.

The ATP/ADP ratio increased with N_2-flushing. This trend was observed at the three pH studied. This ratio increased from 0.03 to 0.11, from 0.11 to 0.85 and 0.34 to 1.25 at pH 4.5, 5.5 and 6.5 respectively. For pH experiments, this ratio showed a maximum (0.2) at pH 6.5.

For N_2-flushing experiments, at pH 4.5 the ACOA/COA ratio achieved a maximum (10^{18}) at 2.5 ($L \cdot d^{-1}$) N_2-flushing. This ratio decreased at pH 5.5 and achieved a minimum (10^{24}) at pH 6.5 and 7.5 ($L \cdot d^{-1}$) N_2-flushing. For pH experiments, and considering that reaction (r8) was

active at pH 7.0 and 7.5, the ACOA/COA ratio increased from 10^{15} to $2 \cdot 10^{30}$ at the pH range 5.5 to 7.5.

Although intracellular ratios were calculated, the calculation of intracellular pyruvate concentration is not possible, neither algebraically nor numerically. The next section presents the results obtained for the anabolic thermodynamic analysis of the fermentations.

Box 2: thermodynamic analysis of acidogenic metabolism

This box gives an example of how the thermodynamic analysis of the metabolic pathways was done. This example is structured as: 1) fb calculation, 2) metabolic Gibbs energy

1) Calculation of fb

Here it is explained how fb was obtained for the fermentations at pH 4.5-N_2-flushing 58.4 ($L \cdot d^{-1}$) and pH 6.5-N_2-flushing 0 ($L \cdot d^{-1}$), these two examples are referred from here as example I and II respectively. The parameter fb is calculated according to the Eq. (54).

$$f_b = \frac{Y_{ACT} + 2Y_{BTR} + Y_{EOH} - Y_{FRM} - Y_{H2}}{12} \quad (54)$$

In this equation the numerator is a mass balance that relates the acetyl-CoA products (acetic acid, butyric acid and ethanol) with the products of the pyruvate/acetyl-CoA reaction (formic acid and hydrogen). The denominator (12) is a coefficient to transform the result of the mass balance into a catabolic glucose fraction in terms of hydrogen equivalents.

For example I, the yield, in $mol \cdot mol_{GLC}^{-1}$, are: Y_{ACT}, 0.32; Y_{BTR}, 0.28; Y_{EOH}, 0.45; Y_{FRM}, 0; Y_{H2}, 3.25. Yields for example II are: Y_{ACT}, 0.81; Y_{BTR}, 0.15; Y_{EOH}, 0.55; Y_{FRM}, 0.69; Y_{H2}, 0.34. The fb for example I is:

$$f_b = \frac{0.32 + 2 \cdot 0.28 + 0.45 - 0 - 3.25}{12} = -0.16 \left(\frac{mol_{GLC}}{mol_{GLC}}\right)$$

Analogously for example II fb = 0.053 ($mol_{GLC} \cdot mol_{GLC}^{-1}$). These results are interpreted as

follow. In example I, hydrogen is been further synthetised by another reaction different from those of pyruvate/acetyl-CoA, while in example II hydrogen is been consumed.

2) Metabolic Gibbs energy calculation

Intracellular calculation of Gibbs energy was done under the assumption that the intracellular Gibbs energy (ΔG_{intra}) and the extracellular Gibbs energy of the system (ΔG_S') are equal.

$$\Delta G_{intra} = \Delta G'_S$$

According to fb, there are two possibilities, fb<1 and fb>1. We have proposed two alternative reactions for each possibility. These alternatives are H_2/NAD^+ redox reaction (r8) and homoacetogenesis (r9).

The combination of them were presented in Tables 22 to 25 (pages 114 and 115).

We used reversed reaction r8 (matrix on Table 23) to solve example I, and r9 (matrix on Table 24) for example II. According to the intracellular Gibbs energy assumption we have that:

Example I $$\Delta G'_S = \Delta G'_1 + \Delta G'_2 + \Delta G'_3 + \Delta G'_4 + \Delta G'_5 + \Delta G'_6 + \Delta G'_7 + \Delta G'_{8rev}$$

Example II $$\Delta G'_S = \Delta G'_1 + \Delta G'_2 + \Delta G'_3 + \Delta G'_4 + \Delta G'_5 + \Delta G'_6 + \Delta G'_7 + \Delta G'_9$$

Metabolic reactions are represented by its respective under numbered Gibbs energy. Because the incapacity of solving ΔG_1' due the unknown pyruvate concentration, ΔG_1' is combined to ΔG_2'and ΔG_3' as explain below:

$$\Delta G'_1 + \Delta G'_2 + \Delta G'_3 = (x \cdot \Delta G'_1 + \Delta G'_2) + \left((1-x)\Delta G'_1 + \Delta G'_3\right)$$

$$x = \frac{f_{GLC\_LCT}}{\sum f_{GLC\_i}}$$

$$\Delta G_A = x \cdot \Delta G'_1 + \Delta G'_2$$

$$\Delta G_3 = (1-x)\Delta G'_1 + \Delta G'_3$$

Where *x* represents the ratio between the catabolic glucose used for lactic acid synthesis over the total catabolic glucose. ΔG_A corresponds to the lactic acid ΔG_e (extracellular Gibbs energy), while ΔG_3 is the combined intracellular Gibbs energy of ΔG_1' and ΔG_3'.

From experimental results we know that in example I neither lactic acid nor formic acid is produced, *i.e.* ΔG_A and ΔG_B (extracellular Gibbs energy for formic acid synthesis) are zero. When formic acid is not produced, reactions r3 and r4 are lapped together, as follow:

$$PYR + COA + H^+ \rightarrow H_2 + CO_2 + ACOA$$

For this special case, ΔG_3 takes the following form:

$$\Delta G_3 = (1 - x)\Delta G_1' + \Delta G_3' + \Delta G_4'$$

The overall Gibbs energy balance for examples I and II becomes:

Example I $$\Delta G_S' = \Delta G_3 + \Delta G_5' + \Delta G_6' + \Delta G_7' + \Delta G_{8rev}'$$

Example II $$\Delta G_S' = \Delta G_A + \Delta G_3 + \Delta G_4' + \Delta G_5' + \Delta G_6' + \Delta G_7' + \Delta G_9'$$

In order to solve these two equations, we used the Tables 23 and 24 for examples I and II respectively. The matrixes on these two tables represent the energy balance over the acetyl-CoA node. For example, the extracellular energy for hydrogen synthesis (ΔG_C) in example I is equal to a fraction of ΔG_3 represented by the ratio between the fraction of catabolic glucose for hydrogen plus fb (which is negative in this case) over the f_{ACOA} fraction defined in Eq. (55), and $\Delta G_{8rev}'$ as described below:

$$\Delta G_C = \frac{f_{H2} + f_b}{f_{ACOA}} \Delta G_3 + \Delta G_{8rev}'$$

In example II this relationship becomes:

$$\Delta G_C = \frac{f_{H2} + f_b}{f_{ACOA}} \Delta G_3 + \Delta G_4' + \Delta G_9'$$

Analogously, the extracellular Gibbs energy for acetic acid, butyric acid and ethanol are described in terms of intracellular Gibbs energies. Also, ΔG_4' and ΔG_9' can be calculated from experimental data as describe below:

$$\Delta G_4' = 2(f_{H2} + f_b)\left(\Delta G_{4T}^o + R \cdot T \sum \nu_i \cdot ln(C_i)\right)$$

$$\Delta G_9' = 2f_b\left(\Delta G_{9T}^o + R \cdot T \sum \nu_i \cdot ln(C_i)\right)$$

The factor 2 that appears in both equations transforms the temperature and concentration corrected Gibbs energies that are based in terms of hydrogen and acetic acid (for r4 and r9 respectively) in terms of moles of glucose. In box 1 is presented an example for the calculation of ΔG_T^o and $\nu_i \cdot \ln(C_i)$.

Reorganising these expressions into matrix we obtained Table 23 and 24. The equation system formed can be then solved by linear algebra.

3.4.2 Thermodynamic analysis of anabolism

The results presented in this section were calculated following the instructions given in section 3.3.4. Table 30 presents the calculate energy transfer efficiency, ε, from the energy source, glucose, to biomass; the biomass synthesis ΔG_S ($kJ \cdot mol_{GLC}^{-1}$); and the microbial energy dissipation of the systems, ΔG_o ($kJ \cdot mol_X^{-1}$). This three variables, ε, ΔG_S and ΔG_o were calculated according to Eqs (52),(50) and (47) respectively.

Efficiency has decreased with N_2-flushing at pH 4.5 (from 0.12 to 0.08) and pH 6.5 (from 0.08 to 0.02), excepting for pH 5.5 where efficiency remained constant (0.11). Efficiency also decreased with pH, from 0.17 to 0.06 in the pH range 5.5 to 7.5.

Biomass synthesis Gibbs energy becomes more endergonic with efficiency decrease. For N_2-flushing experiments this energy increased from 117 to 203 ($kJ \cdot mol_{GLC}^{-1}$) at pH 4.5, and from 193 to 760 ($kJ \cdot mol_{GLC}^{-1}$) at pH 6.5. At pH 5.5, it remained relatively constant (130 $kJ \cdot mol_{GLC}^{-1}$). pH experiments also affected negatively this variable, which became more endergonic, it increased from 62 to 273 ($kJ \cdot mol_{GLC}^{-1}$) at the pH range studied.

For N_2-flushing experiments, microbial energy dissipation decreased from -3800 to -9700 ($kJ \cdot mol_X^{-1}$) at pH 4.5, and from -10900 to 91000 ($kJ \cdot mol_X^{-1}$) at pH 6.5, whilst increased from -4000 to -3000 ($kJ \cdot mol_X^{-1}$) at pH 5.5. For pH experiments, ΔG_o decreased from -500 to -24800 ($kJ \cdot mol_X^{-1}$) at the pH range studied.

Table 30: Thermodynamic analysis of anabolism results.

	N_2 flushing ($L \cdot d^{-1}$)	pH	Efficiency ε	Biomass synthesis ΔGs ($kJ \cdot mol_{GLC}^{-1}$)	Microbial energy dissipation ΔG_o ($kJ \cdot mol_X^{-1}$)
N_2 flushing experiments	0	4.5	0.12	117.00	-3791
	2.5	4.5	0.10	156.53	-6782
	58.4	4.5	0.08	203.20	-9741
	0	5.5	0.11	126.26	-4050
	7.3	5.5	0.11	131.31	-3012
	0	6.5	0.08	192.64	-10976
	2.5	6.5	0.07	248.33	-52770
	7.3	6.5	0.07	231.77	-33317
	58.4	6.5	0.02	760.25	-91155
pH experiments		5.5	0.17	61.59	-534
		6	0.13	105.44	-1541
		6.5	0.09	161.09	-10091
		7	0.10	146.20	-5344
		7.5	0.06	272.74	-24799

4 DISCUSSION

4.1 MIMS Signal Translation

The three options for calibration were standard calibration (in a water/N_2 system), calibration by standard additions, and in-process calibration. For fermentation experiments, spiking with compounds such as H_2, CO_2, bicarbonate or ethanol can have a strong influence on the biochemical process, and it is difficult to add gases for the purposes of standard additions. Therefore, we opted for standard calibration and in-process calibration. The results, particularly those in Figure 13 and Figure 14, demonstrate that standard calibration, even when using exactly the same equipment is ineffective for H_2 and CO_2, and may be sub-optimal for ethanol. The process itself has a strong impact on both measurement threshold, represented by correlation intercept, and sensitivity, represented by correlation slope. Our results confirmed that in-process calibration is necessary in fermentations to follow the evolution of analytes such as ethanol, H_2 and CO_2. In the following sections, we go on to discuss how measurement of specific compounds was impacted upon by transfer issues. Compounds were divided into three classes based on liquid solubility (low/high) and volatility.

4.1.1 Measurement in the gas phase

As illustrated in Figure 12 and Table 5, slope is higher for in-process calibrations, than for standard calibrations. This indicates a loss of sensitivity in the fermentation environment. As an explanation, with standard calibrations, the headspace remains relatively dry (gas is not bubbled through the liquid). In contrast, under fermentation reactions, gas is continuously produced, which both volatilises and aspirates water. In our experiments, we noted that a liquid film formed on the surface of the MIMS probe, presenting a barrier to gas transfer. As both H_2 and CO_2 are relatively insoluble gases [199], the resistance to gas-liquid transfer is mainly in the liquid film. Such a film at the surface of the MIMS probe in a gas phase may control mass transfer, and completely changes the characteristics in comparison to dry experiments, as well as makes the MIMS signal strongly dependent on the thickness of the liquid film. In contrast, low variability in H_2 and CO_2 correlation intercepts (Table 5) suggests that measurement thresholds are not

influenced by gas composition changes or gas turbulence caused by N_2 flushing in the continuous fermentation (Figure 14F).

4.1.2 Detection of low solubility volatiles in the liquid phase - H_2 & CO_2

The three slopes for H_2 results presented in Figure 12 and Table 5 appear to be similar, indicating sensitivity in the liquid phase is not particularly influenced by the matrix. Because H_2 has high diffusivity ($4.65 \cdot 10^{-5}$ $cm^2 \cdot s^{-1}$) [199] in pure water, we expected no change in MIMS sensitivity. In contrast, intercept results suggest that a complex fermentation matrix increases the dissolved H_2 concentration threshold in fermentations compared to standard calibration (making it harder to detect). Both batch and continuous in-process calibrations correlations are similar in terms of intercept. This can be explained according to Engel *et al.* [200] model. The average fermentation sodium bicarbonate concentration (21.5 mM) may decrease H_2 solubility by 4%, a very minor change, but possibly responsible for the change in intercept.

In the case of CO_2, the high slope in batch condition, *i.e.* 3.4±0.5 ($mM \cdot faraday^{-1}$) compared to approximately 1 ($mM \cdot faraday^{-1}$) for both standard and continuous slopes, indicates a gain in sensitivity in batch fermentations. A mixed model from Schumpe *et al.* [201] and Gros *et al.* [202] indicates that non-biochemical fermentation media composition decreases CO_2 solubility by 1%, *i.e.* Henry constant at 36ºC (39.7 $bar \cdot L \cdot mol^{-1}$) increases to 40.2 $bar \cdot L \cdot mol^{-1}$. An alternative explanation is non-ideal solution behaviour, which would decrease the activity of the bicarbonate ion, and hence that of CO_2. This is quite likely, since at the solution ionic strength of approximately 0.2M, the impact of ion activity is significant. However, the results show low variability in CO_2 intercept (concentration threshold), *i.e.* between -0.1± 0.8 and 0.9±0.3 mM, suggesting that changes in matrix composition, (the presence and changes in fermentation substrate, nutrients and products concentrations) do not affect the CO_2 concentration threshold.

4.1.3 Detection of high solubility volatiles in the liquid phase - ethanol

Standard and in-process correlations for ethanol in both batch and continuous fermentations are qualitatively (Figure 12, Figure 13E and Figure 14E) and statistically (Table 5) similar, but with some significant differences. Correlations between MIMS signals and ethanol concentration indicate an increase of MIMS sensitivity and concentration threshold in the fermentation matrix. Tarkiainen *et al.* [171] showed that sugars, salts, and CO_2 affect the MIMS response of ethanol. Glucose and sodium chloride has a positive effect, due to salting out, increasing ethanol MIMS

sensitivity, while dissolved CO_2 has the opposite effect. Salts and glucose, therefore, have a higher impact in our case, even if salts were only added as necessary for biological growth. This is likely different in higher concentration waste conversion systems, where salts and ammonia have far higher concentrations. In any case, differences are low among the three correlations for ethanol H_2 and CO_2 correlations either in gas or liquid phase, as can be seen in Figure 13 and Figure 14.

4.1.4 MIMS signal oscillation and noise

Some oscillations and noise were observed in signal. Oscillations showed in Figure 13 are due to the temperature controller (3ºC range). This temperature oscillation causes changes on diffusivity and solubility of the volatile analytes [203], which changes their flow rates through MIMS membrane and consequently their MIMS signals. These signal oscillations could be minimised using better temperature regulation, and highlights the need for good temperature control. Random noise (Figure 14) is due to electrical issues occurring in the MIMS device, and can be addressed by using signal filters.

4.1.5 Limitations of in-process calibration

As stated above, in-process calibration is required as compared to standard or prior experiment run calibration to provide correlation between MIMS signals and actual concentrations. The main issue that we have observed is occasional low variability, which makes it very difficult to determine slope. This is especially evident in the continuous experiments (Figure 14A, C, and E). Proper determination of the calibration slope depends heavily on wide variation in concentration of the target compounds during sampling. That is, it is not useful if all samples have the same concentration. An increase of concentration variability will improve calibration, but will have an impact on the biological process. We suggest that targeted analytes be introduced at the end of the fermentation, so that concentration variability can be artificially induced increasing calibration accuracy without invalidating the experiment itself.

4.1.6 Applications of MIMS to fermentation experiments

Our results indicate that while standard calibration is recommended for quantifying the analyte range concentration, in-process calibration is necessary to translate signals of fermentation, which would otherwise be missed.

In fermentation processes, where dynamics play a very important role, it is very important to have a chemical analytical method with a short sample period. This is especially true for organic chemicals. Off-line analysers such as GC-FID offer non-matrix-dependant quantification, but are relatively expensive and time-consuming. With in-process calibration using MIMS, only a few off-line experimental samples are necessary to obtain an accurate view of the dynamics of the process.

An advantage of MIMS over other on-line methods is that calibration frequency is relatively low, with, in the example of Figure 14, six days of operation without recalibration. Other alternatives such as titrimetric off-gas analysis [204] require recalibration every 2-3 hours.

The main challenge to increase the usefulness of MIMS for fermentation experiments is detection of other organic compounds such as lactic, acetic, propionic, and butyric acids. While we attempted this, detection of organic acids was not possible due to: (a) overlap in spectrum peaks, and (b) because most of these compounds have pK_a values of <5.0, and are therefore mainly present as charged (non-volatile) compounds at a pH of >5.0. The first of those 2 obstacles could be overcome by either an increase in MS accuracy (allowing for differentiation of compounds with the same MW, but different atomic formula), and/or advanced regression techniques. The second requires accounting for both solution non-ideality, and pH, as well as possibly, off-line titration. Addressing these issues would make MIMS a requisite instrument for analysing fermentation and other mixed-culture biotechnological processes.

4.2 Acidogenic Product Spectra Under Environmental Changes

A total of fourteen steady states were achieved, where nine corresponded to N_2-flushing disturbances and 5 to pH changes. Also, 10 transient states kinetics where followed, divided into 6 N_2-flushing and 4 pH changes.

At steady state, carbon and COD balance was satisfactory, with the exception of two N_2-flushing experiments, where the carbon balance closed at -25%. These two experiment were performed at

pH 4.5 and 6.5, both of them at 58.4 ($L \cdot d^{-1}$) N_2-flushing. This difference in carbon is justified by the volatilisation of acidogenic products, *e.g.* ethanol and undissociated organic acids. However, if this -25% difference is considered as for example volatilised ethanol, then the COD balance would be closed at -245% and not at -5% or -2% as was observed for both experiments. This suggests an unbalanced inorganic carbon which was not detected by the analytical methodology applied. However, as no direct COD measurements were performed, this issue could not be proved. Despite this fact, in the next sections is discussed the effect of N_2-flushing and pH over the products that were detected and analysed in this work.

As a general effect, pH changes produced fast changes on gas composition, *i.e.* H_2 and CO_2 partial pressures. This confirmed the hypothesis that gas composition (at pH constant) plays a crucial role on the control of the product yield spectra of acidogenic fermentation, as was demonstrated with N_2-flushing experiments.

Also, the developed thermodynamic model and analysis of acidogenic fermentation catabolism, have yield on the parameter *fb*, which accounts for the catabolic glucose fraction deviated for either H_2 consumption or synthesis by metabolic pathways different to those of the acetyl-CoA. In this context the thermodynamic analysis of two reactions, H_2/NAD^+ redox and homoacetogenesis, allowed evaluating their metabolic feasibility in order to explain the variation on *fb*.

4.2.1 Transient states kinetics under environmental changes

Literature shows that metabolic shift in acidogenic fermentation is directly affected by pH changes [24,51,108,109], *i.e.* by changes that occurs in the liquid phase. However, pH change generates fast responses in the head-space composition that are also responsible for the metabolic shift as is observed in this work.

Our results showed that gas products, H_2 and CO_2, kinetics were faster than the liquid ethanol. The fast response on gas products is justified by CO_2/HCO_3^- equilibria. Dissolved CO_2 and HCO_3^- equilibrium is function of pH. In our experiments this equilibrium was reached instantaneously. The kinetic constant of CO_2 concentration under pH changes is 1200 d^{-1},

reaching a new head-space steady state in an average of 6h. In contrast, liquid steady state was reached after 18h on average.

The rapid kinetic of dissolved CO_2 was the responsible of changes inn the gas phase, where the main products are CO_2 and H_2. On the other hand, liquid ethanol response depends on biochemical metabolic kinetics, which is thought slower than purely chemical equilibria, as in the case of CO_2.

In this context, gas phase perturbations (N_2-flushing) produced faster response on H_2 and CO_2 partial pressures than in the liquid, while liquid perturbation (pH changes) produces faster responses on dissolved CO_2. However, the ethanol response to any of these two perturbations was slower since its kinetics are related to metabolic changes rather than chemical equilibria, as discussed above.

Dissolved H_2 concentration was close to its saturation for all the experiments. This is due to the low solubility and high diffusivity of H_2, and due to the high stirring velocity, *i.e.* 600 rpm, applied to the fermentations.

4.2.2 Metabolic shift effects on hydrogen yield

The effect of gas phase composition on H_2 yield was discussed previously by other authors [16,17,53]. They argue that H_2 partial pressure affects thermodynamically the biologically mediated reactions responsible of H_2 synthesis. In addition, we argue that the H_2 consuming reactions are also affected by this partial pressure.

The present work analysed in detail the acidogenic glucose fermentation metabolic pathways, including those that either consume or produce H_2. This analysis resulted on valuable information. The variability of H_2 yield is a consequence of two metabolic processes, lactate synthesis (r2) and H_2 electron transfer to NADH (r8) and acetate (r9).

4.2.3 The role of lactate synthesis

Lactate synthesis deviates electrons from pyruvate node decreasing formate and/or hydrogen yields. Tanisho *et al.* [52] studies on acidogenic hydrogen production showed that the H_2 yield increase was due to a decrease of succinic acid yield, another product that deviates carbon and electrons from pyruvate node as lactic acid synthesis does. Lactic acid synthesis is directly influenced by intracellular pyruvate concentration and NAD^+/NADH ratio, as is describe in the equation below.

$$\Delta G'_{LCT} = RT\left[\ln\left(\frac{1}{[PYR]}\right) + \ln\left(\frac{[NAD^+]}{[NADH]}\right) + \ln\left(\frac{[LCT]}{[H^+]}\right)\right] + \Delta G^{\circ}_{LCT} \quad (56)$$

Figure 28 illustrates the effect of pyruvate concentration on lactate synthesis Gibbs energy reaction. This reaction becomes thermodynamically not feasible when pyruvate concentration approaches zero and/or the NAD^+/NADH ratio increases. For NAD^+/NADH ratios of 1 and 10^{-8}, Gibbs energy becomes zero at a pyruvate concentration of 10^{-20} and 10^{-28} (M) respectively.

The work done by Pianosi *et al.* [205], on blood pyruvate and lactate concentrations, concluded that both compound concentrations increase significantly when substrate metabolic oxidation capacity is exceeded. Therefore, the presence of lactate on acidogenic glucose fermentation is explain by the surpassed glucose oxidation capacity and consequently by pyruvate accumulation. Decreasing head-space hydrogen partial pressure by N_2-flushing or other means, like gas sparging, allows to unlocking the glucose oxidation capacity, decreasing pyruvate concentration, then making lactate synthesis thermodynamically unfeasible.

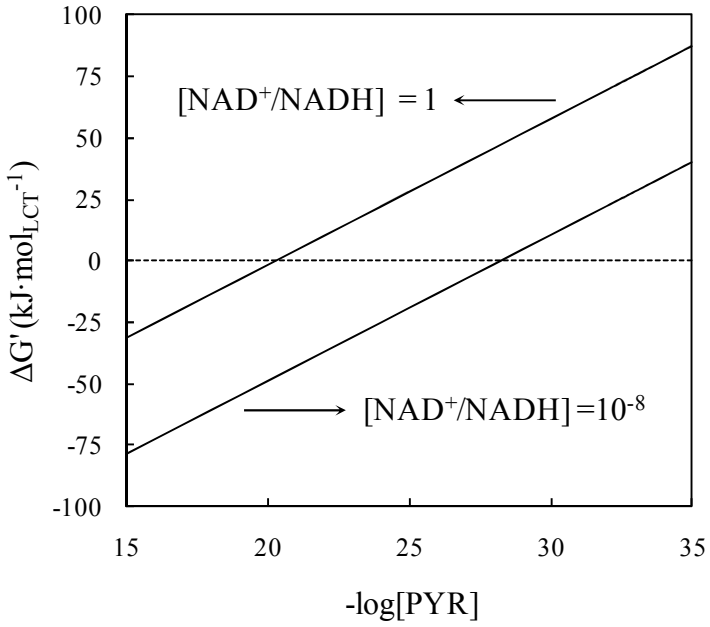

Figure 28: Pyruvate concentration effect on Gibbs energy of intracellular lactic acid synthesis reaction at NAD^+/NADH ratio of 1 and 10^{-8}. Both curves used a lactate concentration of 2.5 mM, intracellular pH of 7.0 and reaction temperature of 37°C.

When lactate is not produced, extra carbon and electrons from pyruvate increase H_2 yield. Stoichiometrically, H_2 yield increases by one mole of hydrogen per mole of glucose consumed every lactate mole not produced. In our experiments, only 3±1% and 14±1% of the total H_2 yield increase was accounted by the stopped producing lactate when N_2 flushing was increased to 58.4 $L \cdot d^{-1}$ at pH 4.5 and 6.5 respectively. Therefore, another metabolic route is thus needed to explain the observed high increase of H_2 yield that cannot be explained by a shift of the lactate production.

4.2.4 The Acetyl-CoA node

The work performed by Zeng *et al.* [206] revealed that pyruvate metabolism is significantly affected under transient states. This is in accordance with the hypothesis that states the presence of more than one pyruvate decarboxilation enzyme system in acidogenic fermentation. These enzymes systems would give flexibility to the metabolism. This in turn, could lead to a regulation of the acidogenic products.

As discussed by Temudo *et al.* [108], H_2 and formic acid produced are linearly related to the number of acetyl-CoA derived products, *i.e.* acetic acid, butyric acid and ethanol. Our results have shown that this happens only when the *fb* fraction is equal to zero (see section 3.4.1). Previously, we have defined *fb* in Eq. (54) as the catabolic glucose fraction deviated from H_2 (*fH2*) or acetate (*fACT*) for the non acetyl-CoA related synthesis/consumption of H_2. Values of *fb* higher than zero represents a consumption of hydrogen, while negative *fb* an extra synthesis.

For N_2-flushing experiments, *fb* ratio was in the range of 0.01 to 0.06 for experiments not performed at 58.4 ($L \cdot d^{-1}$) N_2-flushing. When this high N_2 flow rate was applied, *fb* strongly decreased to -0.16 and -0.1 at pH 4.5 and 6.5 respectively. This extra H_2 is expected to come from H_2 electron transfer reactions. H_2 electron transfer involves two reactions, H_2/NAD^+ redox reaction (r8) and homoacetogenesis (r9).

4.2.5 H_2/NAD^+ redox reaction

In H_2/NAD^+ redox reaction, H_2 donates electrons reducing NAD^+ to NADH as described below.

$$H_2 + NAD^+ \rightleftarrows NADH + H^+ \tag{57}$$

Figure 29 illustrates the effect of hydrogen partial pressure on H_2/NAD^+ redox reaction Gibbs energy. Decreasing H_2 partial pressure increases the Gibbs energy of reaction, making the reverse reaction thermodynamically feasible, *i.e.* H_2 synthesis by NADH oxidation. This is also possible when the NAD^+/NADH ratio decreases. However, our results predict this reverse reaction only at 58.4 ($L \cdot d^{-1}$) N_2-flushing experiments.

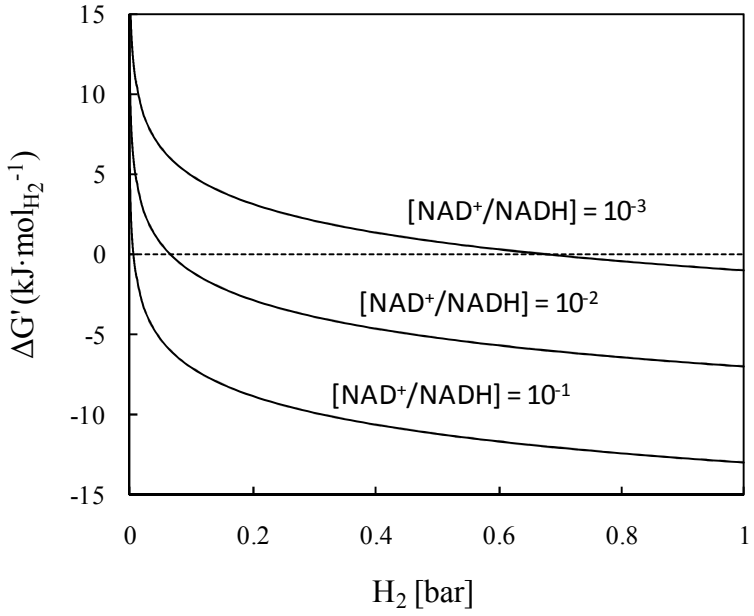

Figure 29: Effect of H_2 partial pressure on Gibbs energy of H_2 oxidation at NAD^+/NADH ratio of 10^{-3}, 10^{-2} and 10^{-1}.

4.2.6 Homoacetogenesis

Homoacetogenesis produces acetic acid from H_2 and CO_2 as described in the following equation

$$4H_2 + 2CO_2 \rightleftarrows ACT + H^+ + 2H_2O \quad (58)$$

Figure 30 illustrates the effect of hydrogen partial pressure on Gibbs energy of homoacetogenesis reaction at pH 7.0, CO_2 partial pressure of 0.2 (bar), 37°C, and acetate concentrations of 0.1, 1 and 10 mM. Homoacetogenesis is thermodynamically feasible at experimental conditions normally found in conventional acidogenic fermentations, *i.e.* H_2 partial pressures higher than 0.4 (bar) and acetic acid concentration of 10 (mM).

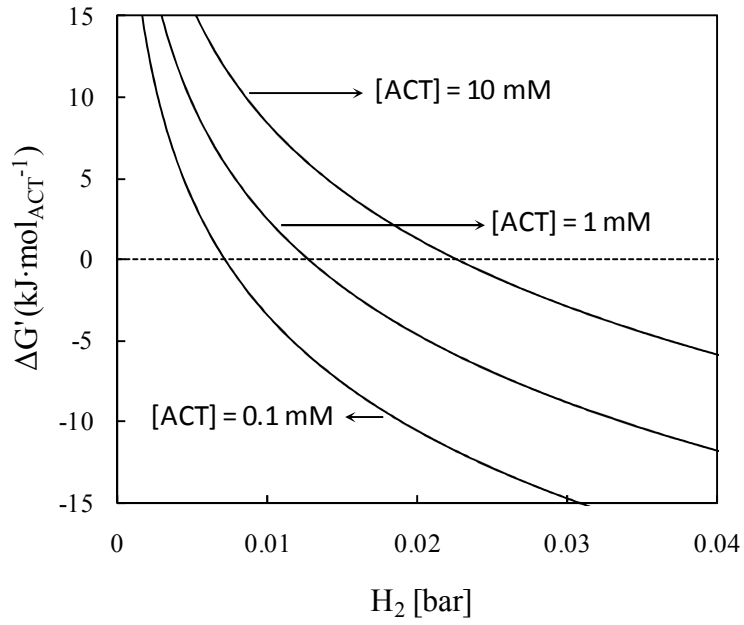

Figure 30: Effect of H_2 partial pressure on Gibbs energy of homoacetogenesis reaction at acetate concentration of 0.1, 1 and 10 mM, CO_2 partial pressure of 0.2 (bar), intracellular pH of 7.0, and 37ºC.

Homoacetogenesis reversibility, *i.e.* anaerobic acetate oxidation producing H_2, is thermodynamically feasible at H_2 partial pressure lower than 0.02 atm for acetate concentration around 10 mM. This agrees with the fact that N_2-flushing decreased both H_2 and CO_2 partial pressures, allowing anaerobic acetate oxidation to occur, thus increasing H_2 yield.

4.2.7 Acetate, butyrate and ethanol shifts

Shift from acetate-ethanol to butyrate have been explained by Temudo *et al.* [108]. They suggested two hypotheses, the first states that the intracellular pH is regulated by acetic and butyric acid synthesis (reactions r5 and r6 respectively). When extracellular pH is high, acetic acid production would help maintaining the intracellular pH more acidic than the extracellular, and *vice versa*. The second hypothesis associates ethanol and formic acid yields, but the exact mechanism is not clear.

Although we suggest that metabolic shifts in acidogenic fermentation are controlled by the intracellular energetic and redox states, our results are still far to clarify the mechanisms that govern the shift of these three compounds.

4.3 The Thermodynamic Model

The thermodynamic model relates extracellular product composition with acidogenic metabolism. In this sake two hypothesis were formulated: 1) no gradient between intra and extracellular concentration, and 2) constant intracellular pH of 7.0.

4.3.1 Intra-extracellular concentration

There are several physiological mechanisms that produce gradients between the intra and extracellular concentration of fermentation products. Although the measurement of intracellular concentration leads to valuable information, the assumption of equal intra and extracellular concentration serves as a reference point for the thermodynamic analysis. We strongly suggest future research on measuring intracellular concentration of acidogenic products.

4.3.2 Constant intracellular pH

Intracellular pH affects all biochemical processes, including enzyme activity, protein folding, and metabolic thermodynamics. Although pH variations have been reported in the literature [207], a constant intracellular pH of 7.0 is considered as standard [144,195] for biochemical thermodynamics calculations, thus this assumption can be considered as relevant.

4.3.3 Limitations of this thermodynamic model

The thermodynamic model predicts the presence of reversible reactions that synthesise or consume hydrogen, *i.e.* H_2/NAD^+ redox and homoacetogenesis. However, the presence of these reactions can be only validated by enzymatic assays capable to measure the activity of the enzyme systems responsible to catalyse these two reactions.

Although this model is based on acidogenic catabolism, considering the principal routes of acidogenic glucose fermentation, it is not capable to explain the metabolic shifts on acetate, butyrate and ethanol. We suggest the design of new experiments that would clarify the metabolic mechanism controlling the shift of these three compounds.

This model lacks of dynamic formulations, thus cannot be applied for kinetic process simulation. The addition of dynamic equations into this model is thought as a crucial step. Moreover, this model assumes that the liquid phase is perfectly mixed, therefore it is not applicable for biofilms systems.

5 CONCLUSIONS

The conclusions achieved in this work address relevant issues related to hydrogen metabolism on acidogenic glucose fermentation by mixed cultures. The experimental design, the MIMS methodology for kinetic monitoring of acidogenic fermentation and the developed thermodynamic model allowed to explain the metabolic mechanisms responsible of the hydrogen yield shifts. The main conclusions are detailed below:

1) The designed experiments based on N_2-flushing of the reactor head-space (gas phase composition changes) and pH step changes (liquid phase changes), have allowed achieving several metabolic states, represented by changes on acidogenic yield product spectra. The main experimental result was the increase of hydrogen yield to 3.2 ($mol_{H2} \cdot mol_{GLC}^{-1}$), which is very close to the theoretical value (4 $mol_{H2} \cdot mol_{GLC}^{-1}$) for acidogenic fermentation.

2) The simultaneous and quantitative monitoring of H_2 and CO_2 in both gas and liquid phase, together with ethanol in liquid phase by membrane inlet mass spectrometry (MIMS), allowed analysing the kinetic of these three compounds during transient states of acidogenic fermentation, and have demonstrated that gas phase composition changes produce changes on acidogenic product spectra. Gas composition is thus an environmental parameter that allows controlling acidogenic fermentation.

3) The developed metabolic network described the experimental results obtained in this work. This metabolic network includes 9 reactions: 1) glycolysis, 2) lactate synthesis, 3) pyruvate formate lyase reaction, 4) formate hydrogenase reaction, 5) acetic fermentation, 6) butyric fermentation, 7) ethanol fermentation, 8) H_2/NAD^+ redox reaction and 9) homoacetogenesis.

4) This developed metabolic network can be modified by adding or removing metabolic reactions, and also can be adapted to a different carbon source, which makes a flexible model

5) The thermodynamic model based on the simplified acidogenic metabolic network, was developed under two hypotheses: 1) no gradient between intra and extracellular concentration, and 2) constant intracellular pH of 7.0.

6) The thermodynamic model was used to analyse the acidogenic fermentation results. This analysis allowed explaining the mechanisms that govern lactate metabolic shifts, which respond to glucose oxidation capacity and pyruvate intracellular concentration.

7) This analysis also explained the shifts on hydrogen metabolism, defining the catabolic glucose fraction deviation, *fb* ($mol_{catGLC} \cdot mol_{GLC}^{-1}$), from H_2 (*fH2*) or acetate (*fACT*) for the non acetyl-CoA related synthesis/consumption. This *fb* variable allows accounting for hydrogen consumption or extra synthesis, using the experimental results of acetate, butyrate, ethanol, formate and hydrogen.

8) The thermodynamic analysis showed that hydrogen consumption was due to homoacetogenesis action, while the extra synthesis of hydrogen was due either by the reverse homoacetogenesis or reverse H_2/NAD^+ redox reaction, which are thermodynamically feasible at low hydrogen partial pressures (*e.g.* 0.02 bar).

9) However, the model was not capable to explain the metabolic shifts of acetate, butyric and ethanol on acidogenic glucose fermentation.

6 PERSPECTIVES

The decreased of hydrogen partial pressure by N_2-flushing the bioreactor head-space, resulted in an increase of its hydrogen yield up to 3.2 mol_{H2}·mol^{-1}_{GLC} (which is close to the theoretical yield 4 mol_{H2}·mol^{-1}_{GLC}). The decrease of hydrogen partial pressure by other means, *e.g.* gas sparging will also increase hydrogen yield. Moreover, gas sparging will promote the gas stripping of volatile fermentation products. This technology can be also coupled to acidogenic biofilms in order to increase the capacity of organic removal. Finally we present a general scheme of a gas controlled acidogenic fermentation system. These four perspectives are discussed bellow.

6.1 Gas Sparging

Different studies on acidogenic gas sparging have concluded that the hydrogen yield production is improved by this mean [16,17,53]. Mizuno *et al.* [53] results shown an increase on H_2 yield production from 0.85 mol_{H2}·mol_{GLC}^{-1}, with no N_2 sparging, to 1.43 mol_{H2}·mol_{GLC}^{-1} with a N_2 rate of 15 mL·(min·L-liquid)$^{-1}$.

Similar results were obtained by Kraemer and Bagley [17]. They reported a H_2 yield increase from 1 mol_{H2}·mol_{GLC}^{-1}, with no N_2 sparging, to 2 mol_{H2}·mol_{GLC}^{-1} with a N_2 sparging rate of 12 mL·(min·L-liquid)$^{-1}$. The authors concluded that this N_2 rate also maximised the H_2 yield, since they have observed no significant increase in H_2 yield at sparging rates higher than 12 mL·(min·L-liquid)$^{-1}$, the range of N_2 rate used was up to 80 mL·(min·L-liquid)$^{-1}$. The N_2-flush rates used in this thesis expressed in these units results on 32, 93 and 748 mL·(min·L-liquid)$^{-1}$ for 2.5, 7.3 and 58.4 L·d^{-1}, respectively.

Other exciting results were obtained by Kim *et al.* [16]. They have found that CO_2 sparging was more effective for H_2 production than N_2. In their experiments, they obtained the highest H_2 yield of 1.68 mol_{H2}·mol_{hexose}^{-1} at a CO_2 sparging rate of 60 mL·(min·L-liquid)$^{-1}$. Moreover, the authors observed the presence of only H_2 producing bacteria at CO_2 sparging conditions, and they concluded that the dissolved CO_2 increase by the CO_2 sparging, would have little effect on H_2 producing bacteria but inhibitory effect on other microorganisms such as acetogens and lactic

acid bacteria. After this result, we advised the use of CO_2 sparging as a selection parameter for acidogenic bacteria.

In any case, *i.e.* sparging CO_2, N_2 or other gas, high sparging rates, *e.g.* 748 mL·(min·L-liquid)$^{-1}$, will create biomass stress issues. Thus we recommend the combined used of gas flushing and sparging. As presented in this study, gas flushing allows decreasing H_2 partial pressure, without directly affecting liquid phase, which increases H_2 yield close to its theoretical value, while gas sparging will facilitate the stripping of volatile compounds like ethanol. This volatilisation would produce metabolic changes that we expect will increase volatile product yields as well.

6.2 Volatilisation of Fermentation Products by Gas Stripping

The volatilisation of fermentation products by gas stripping is a known technology. In 1986, Ennis *et al.* [208] used this principle on *Clostridium acetobutylicum* fermentations for separation and recovery of butanol. Further research, based on this principle, has been performed for the separation (from the fermentation broth) and recovery of acetone, butanol and ethanol [209-212]. This gas stripping fermentation product recovery has been reviewed by Vane [213] in 2005, and it was also applied to separate ethanol from winery waste water [214]. Though, product volatilisation by gas stripping, applied to acidogenic fermentation, is an attractive technology with an obvious application on biorefinery.

This technology could be applied in both bioreactor and liquid outlet stream. As stated before, gas stripping directly applied in the bioreactor could increase the product yield of ethanol and organic acids, while stripping the outlet stream would allow recover the remaining volatile products.

Organic acids are volatile in the undissociated form, thus their volatilisation depends on pH. The undissociated form of an organic acid increases with pH decrease, *e.g.* at pH 5.0 and 4.0, the undissociated form of both formic and lactic acids is 10% and 40%, respectively, while for both acetic and butyric acids is 40% and 80%. Thus low pH will improve the volatilisation and consequently, the product yield on acidogenic fermentation. The pH of a liquid solution

decreases as a consequence of CO_2 sparging. Then CO_2 sparging is also attractive since it will allow organic acid volatilisation.

However, literature shows that suspended biomass acidogenic fermentation is hardly accomplished at pH lowers than 4.5 [108]. Suspended biomass fermentation is a crucial system that allows the metabolic study of either pure or mixed cultures. Nevertheless, the acidogenic pH issue could be bypassed by the development of acidogenic biofilms in the reactor. Biofilms are aimed to be a technological system rather than an analysis system as suspended biomass fermentation.

6.3 Acidogenic Biofilm

The increase of acidogenic product yields by gas stripping can be also coupled to other technologies, in particular biofilms. Hafez *et al.* [57] research demonstrates that decoupling solid retention time (SRT) from hydraulic retention time (HRT) increases H_2 yield. The STR can be decoupled by biofilm formation. The biofilm formation also allows to increasing the capacity of organic waste treatment.

6.4 Gas Controlled Acidogenic Biofilm Reactor

The combination of these three perspectives resulted in a new conception for acidogenic bioreactor configuration. This new conception could be called “Gas Controlled Acidogenic Biofilm Reactor”.

Figure 31 illustrates this new concept, which contains the following parts: 1) the acidogenic biofilm, which accomplish the biological transformation of organic wastes into valuable products; 2) the sparging port; 3) the flushing port; 4) the gas outlet; 5) the separation unit, which allows the selective recovery of volatile products as ethanol and organic acids; 6) the CO_2 recirculation; 7) the inert gas inlet; 8) the CO_2 purge; 9) the feeding inlet port; and 10) the liquid outlet.

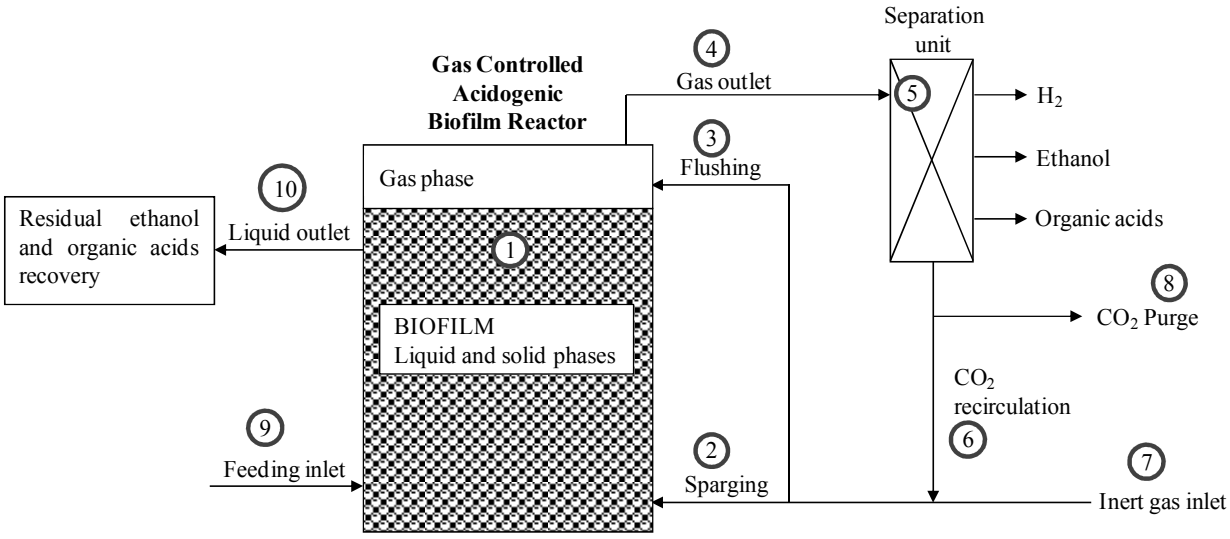

Figure 31: General scheme of gas controlled acidogenic biofilm reactor. 1) Biofilm reactor, 2) sparging port, 3) flushing port, 4) reactor gas outlet, 5) gas separation unit, 6) CO_2 recirculation, 7) inert gas inlet, 8) CO_2 purge, 9) reactor feeding inlet, and 10) reactor liquid outlet.

As a general concept, the biofilm could be any of the different existing technologies of immobilised biomass. As stated above, we recommended the combined use of flushing and sparging, the recirculation of CO_2, for the sparging and flushing, that will allow to decrease the biofilm pH, while increasing the volatility of organic acids. The use of inert gas in combination with CO_2 is an alternative.

We have also considered the gas sparging of the liquid outlet stream, in order to recover the residual volatile products. Anyhow, different technologies can be used at the separation unit, *i.e.* membranes for H_2 and CO_2 separation, together with fractional condensation for recovery of liquid products.

The reactor could operate in batch, fed batch or continuous mode, and also be fed by liquid and/or solid organic waste. Stirring could be accomplished by a combination of mechanical stirring and gas sparging. In order to maintain the simplicity of this scheme, pH and temperature control were not depicted.

7 REFERENCES LIST

[1] Kamm B, Kamm M. Biorefinery - systems. Chem. Biochem. Eng. Q. 2004;18:1-6.

[2] Kamm B, Kamm M. Principles of biorefineries. Appl. Microbiol. Biotechnol. 2004;64:137-145.

[3] Rodriguez J, Kleerebezem R, Lema JM, van Loosdrecht MCM. Modeling product formation in anaerobic mixed culture fermentations. Biotechnol. Bioeng. 2006;93:592-606.

[4] Rodriguez J, Lema JM, Kleerebezem R. Energy-based models for environmental biotechnology. Trends Biotechnol. 2008;26:366-374.

[5] Martindale W, Trewavas A. Fuelling the 9 billion. Nature Biotechnology 2008;26:1068-1070.

[6] Lee HS, Vermaas VFJ, Rittman B. Biological hydrogen production: prospects and challenges. Trends Biotechnol. 2010;28:262-271.

[7] Hahn-Hagerdal B, Galbe M, Gorwa-Grauslund MF, Liden G, Zacchi G. Bio-ethanol - the fuel of tomorrow from the residues of today. Trends Biotechnol. 2006;24:549-556.

[8] Rittman BE. Opportunities for renewable bioenergy using microorganisms. Biotechnol. Bioeng. 2008;100:203-212.

[9] Kleerebezem R, van Loosdrecht MCM. Mixed culture biotechnology for bioenergy production. Curr. Opin. Biotechnol. 2007;18:207-212.

[10] Hawkes FR, Hussy I, Kyazze G, Dinsdale R, Hawkes DL. Continuous dark fermentative hydrogen production by mesophilic microflora: principles and progress. Int. J. Hydrogen Energy. 2007;32:172-184.

[11] Angenent LT, Karim K, Al-Dahhan MH, Wrenn BA, Dominguez-Espinosa R. Production of bioenergy and biochemicals from industrial and agricultural wastewater. Trends Biotechnol. 2004;22:477-485.

[12] Li C, Fang HHP. Fermentative hydrogen production from wastewater and solid wastes by mixed cultures. Crit. Rev. Env. Sci. Tec. 2007;37:1-39.

[13] Chong ML, Sabaratnam V, Shirai Y, Hassan MA. Biohydrogen production from biomass and industrial wastes by dark fermentation. Int. J. Hydrogen Energy. 2009;34:3277-3287.

[14] Guo XM, Trably E, Latrille E, Carrere H, Steyer JP. Hydrogen production from agricultural waste by dark fermentation: a review. Int. J. Hydrogen Energy. 2010;35:10660-10673.

[15] Karlsson A, Vallin L, Ejlertsson J. Effects of temperature, hydraulic retention time and hydrogen extraction rate on hydrogen production from the fermentation of food industry residues and manure. Int. J. Hydrogen Energy. 2008;33:953-962.

[16] Kim DH, Han SK, Kim SH, Shin HS. Effect of gas sparging on continuous fermentative hydrogen production. Int. J. Hydrogen Energy. 2006;31:2158-2169.

[17] Kraemer JT, Bagley DM. Optimisation and design of nitrogen-sparged fermentative hydrogen production bioreactors. Int. J. Hydrogen Energy. 2008;33:6558-6565.

[18] Hawkes FR, Dinsdale R, Hawkes DL, Hussy I. Sustainable fermentative hydrogen production: challenges for process optimisation. Int. J. Hydrogen Energy. 2002;27:1339-1347.

[19] Hussy I, Hawkes FR, Dinsdale R, Hawkes DL. Continuous fermentative hydrogen production from a wheat starch co-product by mixed microflora. Biotechnol. Bioeng. 2003;84:619-626.

[20] Liang TM, Cheng SS, Wu KL. Behavioral study on hydrogen fermentation reactor installed with silicone rubber membrane. Int. J. Hydrogen Energy. 2001;27:1157-1165.

[21] Teplyakov VV, Gassanova LG, Sostina EG, Slepova EV, Modigell M, Netrusov AI. Lab-scale bioreactor integrated with active membrane system for hydrogen production: experience and prospects. Int. J. Hydrogen Energy. 2002;27:1149-1155.

[22] Kataoka N, Miya A, Kirimaya K. Studies on hydrogen production by continuous culture system of hydrogen-producing anaerobic bacteria. Water Sci. Technol. 1997;36:41-47.

[23] Hwang MH, Jang NJ, Hyun SH, Kim IS. Anaerobic bio-hydrogen producion from ethanol fermentation: the role of pH. J. Biotechnol. 2004;111:297-309.

[24] Ruggeri B., Tommasi T., Sassi G. Experimental kinetics and dynamics of hydrogen production on glucose by hydrogen forming bacteria (HFB) culture. Int. J. Hydrogen Energy. 2009;34:753-763.

[25] Gavala HN, Skiadas IV, Ahring BK. Biological hydrogen production in suspended and attached growth anaerobic reactor systems. Int. J. Hydrogen Energy. 2006;31:1164-1175.

[26] Chen WH, Chen SY, Khanal SK, Sung S. Kinetic study of biological hydrogen production by anaerobic fermentation. Int. J. Hydrogen Energy. 2006;31:2170-2178.

[27] van Ginkel SW, Logan SW. Increased biological hydrogen production with reduced organic loading. Water Res. 2005;39:3819-3826.

[28] Lin CY, Chang RC. Fermentative hydrogen production at ambient temperature. Int. J. Hydrogen Energy. 2004;29:715-720.

[29] Lin CY, Chang RC. Hydrogen production during the anerobic acidogenic conversion of glucose. J. Chem. Technol. Biot. 1999;74:498-500.

[30] Chen CC, Lin CY. Start-up of anaerobic hydrogen producing reactors seeded with sewage sludge. Acta Biotechnol. 2001;21:371-379.

[31] Zheng XJ, Yu HQ. Inhibitory effect of butyrate on biological hydrogen production with mixed anaerobic cultures. J. Environ. Manage. 2005;74:65-70.

[32] Chen CC, Lin CY. Using sucrose as a substrate in an anaerobic hydrogen producing reactor. Adv. Environ. Res. 2003;7:695-699.

[33] Lee YJ, Miyahara T, Noike T. Effect of pH on microbial hydrogen fermentation. J. Chem. Technol. Biot. 2002;77:694-698.

[34] Lin CY, Lay CH. Effects of carbonate and phosphate concentrations on hydrogen production using anaerobic sewage sludge microflora. Int. J. Hydrogen Energy. 2004;29:275-281.

[35] Lin CY, Lay CH. Carbon/nitrogen-ratio effect on fermentative hydrogen production by mixed microflora. Int. J. Hydrogen Energy. 2004;29:41-45.

[36] Hussy I, Hawkes FR, Dinsdale R, Hawkes DL. Continuous fermentative hydrogen production from sucrose and sugarbeet. Int. J. Hydrogen Energy. 2005;30:471-483.

[37] Lin CY, Lay CH. A nutrient formulation for fermentative hydrogen production using anaerobic sewage sludge microflora. Int. J. Hydrogen Energy. 2005;30:285-292.

[38] Ueno Y, Kawai T, Sato S, Otsuka S, Morimoto M. Biological production of hydrogen from cellulose by natural anaerobic microflora. J. Ferment. Bioeng. 1995;79:395-397.

[39] Lay JJ. Biohydrogen generation by mesophilic anaerobic fermentation of microcrystalline cellulose. Biotechnol. Bioeng. 2001;74:280-287.

[40] Guwy AJ, Hawkes FR, Hawkes DL, Rozzi AG. Hydrogen production in a high rate fluidised bed anaerobic digester. Water Res. 1997;31:1291-1298.

[41] Yu H, Zhu Z, Hu W, Zhang H. Hydrogen production from rice winery wastewater in an upflow anaerobic reactor by using mixed anaerobic cultures. Int. J. Hydrogen Energy. 2002;27:1359-1365.

[42] Han SK, Shin HS. Biohydrogen production by anaerobic fermentation of food waste. Int. J. Hydrogen Energy. 2004;29:567-577.

[43] Shin HS, Younb JH, Kim SH. Hydrogen production from food waste in anaerobic mesophilic and thermophilic acidogenesis. Int. J. Hydrogen Energy. 2004;29:1355-1363.

[44] Lay JJ, Lee YJ, Noike T. Feasibility of biological hydrogen production from organic fraction of municipal solid waste. Water Res. 1999;33:2579-2586.

[45] Nielsen AT, Amandusson H, Bjorklund R, Dannentun H, Ejlertsson J, Ekedahl LG, Lundstrom I, Svensson BH. Hydrogen production from organic waste. Int. J. Hydrogen Energy. 2001;26:547-550.

[46] Tanisho S, Ishiwata Y. Continuous hydrogen production from molasses by fermentation using urethane foam as a support of flocks. Int. J. Hydrogen Energy. 1995;20:541-545.

[47] Ueno Y, Otsuka S, Morimoto M. Hydrogen production from industrial wastewater by anaerobic microflora in chemostat culture. J. Ferment. Bioeng. 1996;82:194-197.

[48] Ruzicka M. The effect of hydrogen on acidogenic glucose cleavage. Water Res. 1996;30:2447-2451.

[49] Kraemer JT. Effects of methanogenic effluent recycle on fermentative hydrogen production. University of Toronto, 2004.

[50] Kraemer JT, Bagley DM. Supersaturation of dissolved H_2 and CO_2 during fermentative hydrogen production with N_2 sparging. Biotechnol. Lett. 2006;28:1485-1491.

[51] Fang HHP, Liu H. Effect of pH on hydrogen production from glucose by a mixed culture. Bioresour. Technol. 2002;82:87-93.

[52] Tanisho S, Kuromoto M, Kadokura N. Effect of co2 removal on hydrogen production by fermentation. Int. J. Hydrogen Energy. 1998;23:559-563.

[53] Mizuno O, Dinsdale R, Hawkes FR, Hawkes DL, Noike T. Enhancement of hydrogen production from glucose by nitrogen gas sparging. Bioresour. Technol. 2000;73:59-65.

[54] Mu Y, Zheng XJ, Yu HQ, Zhu RF. Biological hydrogen production by anaerobic sludge at various temperatures. Int. J. Hydrogen Energy. 2006;31:780-785.

[55] Rodriguez J, Lema JM, van Loosdrecht MCM, Kleerebezem R. Variable stoichiometry with thermodynamic control in ADM1. Water Sci. Technol. 2006;54:101-110.

[56] Mu Y, Yu HQ, Wang G. A kinetic approach to anaerobic hydrogen-producing process. Water Res. 2007;41:1152-1160.

[57] Hafez H, Naggar MHE, Nakhla G. Steady-state and dynamic modeling of biohydrogen production in an integrated biohydrogen reactor clarifier system. Int. J. Hydrogen Energy. 2010;35:6634-6645.

[58] Lin PY, Whang LM, Wu YR, Ren WJ, Hsiao CJ, Li SL, Chang JS. Biological hydrogen production of the genus *Clostridium*: metabolic study and mathematical model simulation. Int. J. Hydrogen Energy. 2007;32:1728-1735.

[59] Whang LM, Hsiao CJ, Cheng SS. A dual-substrate steady-state model for biological hydrogen production in anaerobic hydrogen fermentation process. Biotechnol. Bioeng. 2006;95:492-500.

[60] Peiris BRH, Rathnasiri PG, Johansen JE, Kuhn A, Bakke R. ADM1 with modifications for bio-hydrogen simulations. Oral Pres. Proceedings, 1st int. workshop on Anaerobic Digestion Model No. 1. Copenhagen, Denmark. 2005. p. 105-112.

[61] Oh ST, Martin AD. Thermodynamic equilibrium model in anaerobic digestion process. Biochem. Eng. J. 2007;34:256-266.

[62] Gadhamshetty V, Arudchelvam Y, Nirmalakhandan N, Johnson DC. Modeling dark fermentation for biohydrogen production: ADM1-based model vs. gompertz model. Int. J. Hydrogen Energy. 2010;35:479-490.

[63] Jianlong W, Wei W. Kinetic models for fermentative hydrogen production: a review. Int. J. Hydrogen Energy. 2009;34:3313-3323.

[64] Chen X, Sun Y, Xiu Z, Li X, Zhang D. Stoichiometric analysis of biological hydrogen production by fermentative bacteria. Int. J. Hydrogen Energy. 2006;31:539-549.

[65] Aceves-Lara CA, Latrille E, Bernet N, Buffiere P, Steyer JP. A pseudo-stoichiometric dynamic model of anaerobic hydrogen production from molasses. Water Res. 2008;42:2539-2550.

[66] Penumathsa BKV, Premier GC, Kyazze G, Dinsdale R, Guwy AJ, Esteves S, Rodriguez J. ADM1 can be applied to continuous bio-hydrogen production using a variable stoichiometry approach. Water Res. 2008;42:4379-4385.

[67] Nikhil, Koshinen PEP, Visa A, Kaksonen AH, Puhakka JA, Yli-Harja O. Clustering hybrid regression: a novel computational approach to study and model biohydrogen production through dark fermentation. Bioprocess Biosyst. Eng. 2008;31:631-640.

[68] Nikhil, Visa A, Yli-Harja O, Lin CY, Puhakka JA. Application of CHR approach to model xylose-based fermentative hydrogen production. Energ. Fuel. 2008;22:128-133.

[69] Zehnder A, Svensson B. Life without oxygen: what can and what cannot? Experientia. 1986;42:1197-1205.

[70] Energy after rio: prospects and challenges. United Nations Development Programme (UNDP), 1997.

[71] Energy poverty, how to make modern energy access universal? United Nations Development Programme (UNDP), 2010.

[72] Kamm B, Gruber PR, Kamm M. Biorefineries - industrial processes and products. Wiley-VCH, 2006.

[73] Hoffmann P. Tomorrow's energy, hydrogen, fuel cells, and the prospects for a cleaner planet. Cambridge, Massachusetts, United States of America: The MIT Press, 2001.

[74] Boucher S. La revolution de l'hydrogene, vers une energie propre et performante? Paris, France: Editions du Felin, 2006.

[75] Berry GD, Aceves SM. The case of hydrogen in a carbon constrained world. J. Energ. Resour. – ASME. 2005;127:189-194.

[76] Peighambardoust SJ, Rowshanzamir S, Amjadi M. Review of the proton exchange membranes for fuelcell applications. Int. J. Hydrogen Energy. 2010;35:9349-9384.

[77] Agreda VH, Zoeller JR. Acetic acid and its derivatives, vol. 49. New York, United States of America: Marcel Dekker, Inc., 1993.

[78] Lindblad MS, Liu Y, Albertsson AC, Ranucci E, Karlsson S. Polymers from renwable resources. In: Degradable aliphatic polyesters, vol. 157. 2002. p. 139-161.

[79] Weissermel K, Arpe HJ. Industrial organic chemistry. New York, United States of America: VCH Publishers, 1997.

[80] Freudenberger R. A guide to small-scale ethanol, alcohol fuel, making and using ethanol as a renewable fuel. Gabriola Island, Canada: New Society Publishers, 2009.

[81] Roehr M. The biotechnology of ethanol, classical and future applications. Weinheim, Germany: Wiley-VCH verlag GmbH, 2001.

[82] Joo F. Breakthroughs in hydrogen storage - formic acid as a sustainable storage material for hydrogen. ChemSusChem. 2008;1:805-808.

[83] Rice C, Ha S, Masel RI, Waszczuk P, Wieckowski A, Barnard T. Direct formic acid fuel cells. J. Power Sources. 2002;111:83-89.

[84] Uhm S, Chung ST, Lee J. Characterization of direct formic acid fuel cells by impedance studies: in comparison of direct methanol fuel cells. J. Power Sources. 2008;178:34-43.

[85] Moletta R. La méthanisation. Paris: Lavoisier, 2008.

[86] Fergusson T, Mah R. Methanogenic bacteria. In: Anaerobic digestion of biomass. Essex, England: Elsevier Applied Science Publishers LTD, 1987.

[87] Meynell PJ. Methane: planning a digester. New York: Schocken Books, 1976.

[88] McCabe J, Eckenfelder W. Biological treatment of sewage and industrial wastes. New York: Reinhold Publishing, 1957.

[89] Nishio N, Nakashimada Y. Recent development of anaerobic digestion processes for energy recovery from wastes. J. Biosci. Bioeng. 2007;103:105-112.

[90] Gerardi MH. The microbiology of anaerobic digesters. Hoboken, New Jersey, United States of America: John Wiley & Sons, Inc., 2003.

[91] Hanaki K, Nagase M. Mechanism of inhibition caused by long-chain fatty acids in anaerobic digestion process. Biotechnol. Bioeng. 1981;23:1591-1610.

[92] Gujer W, Zehnder AJB. Conversion processes in anaerobic digestion. Water Sci. Technol. 1983;15:127-167.

[93] Mitchell R, Gu JD. Environmental microbiology. Hoboken, New Jersey, United States of America: Wiley-Blackwell, 2010.

[94] Pavlostathis SG, Gossett JM. Preliminary conversion mechanisms in anaerobic digestion of biological sludges. J. Environ. Eng. 1988;114:575-592.

[95] Insam H, Franke-Whittle I, Goberna M. Microbes at work, from wastes to resources. Berlin Heidelberg, Germany: Springer, 2010.

[96] McCarty P, Smith D. Anaerobic wastewater treatment. Environ. Sci. Technol. 1986;20:1200-1206.

[97] Yu HQ, Mu Y, Fang HHP. Thermodynamic analysis of product formation in mesophilic acidogenesis of lactose. Biotechnol. Bioeng. 2004;87:813-822.

[98] Sparling R, Islam R, Cicek N, Carere C, Chow H, Levin DB. Formate synthesis by clostridium thermocellum during anaerobic fermentation. Can. J. Microbiol. 2006;52:681-688.

[99] Louis P, Flint HJ. Diversity, metabolism and microbial ecology of butyrate-producing bacteria from the human large intestine. FEMS Microbiology Letters. 2009;294:1-8.

[100] Thauer RK, Jungermann K, Decker K. Energy conservation in chemotrophic anaerobic bacteria. Bacteriol. Rev. 1977;41:100-180.

[101] Kurzynski M. The thermodynamic machinery of life. Leipzig, Germany: Springer, 2006.

[102] Romano AH, Conway T. Evolution of carbohydrate metabolic pathways. Res. Microbiol. 1996;147:448-455.

[103] Tholozan JL, Touzel JP, Samain E, Grivet JP, Prensier G, Albagnac G. *Clostridium neopropionicum* sp-nov a strict anaerobic bacterium fermenting ethanol to propionate through acrylate pathway. Arch. Microbiol. 1992;157:249-257.

[104] Schink B, Kremer DR, Hansen TA. Pathway of propionate formation from ethanol in *Pelobacter propionicus*. Arch. Microbiol. 1987;147:321-327.

[105] Collet C, Girbal L, Peringer P, Schwitzguebel JP, Soucaille P. Metabolism of lactose by *Clostridium thermolacticum* growing in continuous culture. Arch. Microbiol. 2006;185:331-339.

[106] Hillman K, Williams AG, Lloyd D. The influence of headspace gas composition on the production of VFA by rumen ciliate protozoa. Lett. Appl. Microbiol. 1991;13:11-15.

[107] Hallenbeck PC. Fundamentals of the fermentative production of hydrogen. Water Sci. Technol. 2005;52:21-29.

[108] Temudo MF, Kleerebezem R, van Loosdrecht MCM. Influence of the pH on (open) mixed culture fermentation of glucose: a chemostat study. Biotechnol. Bioeng. 2007;98:69-79.

[109] Horiuchi JI, Shimizu T, Tada K, Kanno T, Kobayashi M. Selective production of organic acids in anaerobic acid reactor by pH control. Bioresour. Technol. 2002;82:209-213.

[110] Bernard O, Hadj-Sadok Z, Dochain D, Genovesi A, Steyer JP. Dynamical model development and parameter identification for an anaerobic wastewater treatment process. Biotechnol. Bioeng. 2001;75:424-438.

[111] Batstone DJ, Keller J, Angelidaki I, Kalyuzhnyi SV, Pavlostathis SG, Rozzi A, Sanders WTM, Siegrist HD, Vavilin VA. The IWA anaerobic digestion model no 1 (ADM1). Water Sci. Technol. 2002;45:65-73.

[112] Gavala HN, Skiadas IV, Bozinis NA, Lyberatos G. Anaerobic codigestion of agricultural industries' wastewaters. Water Sci. Technol. 1996;34:67-75.

[113] Graef S, Andrews J. Stability and control of anaerobic digestion. J. Water Pollut. Control Fed. 1974;46:666-683.

[114] Hill DT, Barth CL. Dynamic model for simulation of animal waste digestion. J. Water Pollut. Control Fed. 1977;49:2129-2143.

[115] Kleinstreuer C, Poweigha T. Dynamic simulator for anaerobic digestion processes. Biotechnol. Bioeng. 1982;24:1941-1951.

[116] Moletta R, Verrier D, Albagnac G. Dynamic modelling of anaerobic digestion. Water Res. 1986;20:427-434.

[117] Lyberatos G, Skiadas IV. Modelling of anaerobic digestion - a review. Global Nest: The Int. J. 1999;1:63-76.

[118] Kalyuzhnyi SV, Davlyastshina MA. Batch anaerobic digestion of glucose and its mathematical modeling. i. kinetic investigations. Bioresour. Technol. 1997;59:73-80.

[119] Kalyuzhnyi SV. Batch anaerobic digestion of glucose and its mathematical modeling. ii. description, verification and application of model. Bioresour. Technol. 1997;59:249-258.

[120] Angelidaki I, Ellegaard L, Ahring BK. A mathematical model for dynamic simulation of anaerobic digestion of complex substrates: focusing on ammonia inhibition. Biotechnol. Bioeng. 1993;42:159-166.

[121] Siegrist HD, Renggli D, Gujer W. Mathematical modelling of anaerobic mesophilic sewage sludge treatment. Water Sci. Technol. 1993;27:25-36.

[122] Mosey FE. Mathematical modelling of the anaerobic digestion process: regulatory mechanisms for the formation of short-chain volatile acids from glucose. Water Sci. Technol. 1983;15:209-232.

[123] Costello DJ, Greenfield PF, Lee PL. Dynamic modelling of a single-stage high-rate anaerobic reactor -i. model derivation. Water Res. 1991;25:847-858.

[124] Costello DJ, Greenfield PF, Lee PL. Dynamic modelling of a single-stage high-rate anaerobic reactor -ii. model verification. Water Res. 1991;25:859-871.

[125] Gavala HN, Angelidaki I, Ahring BK. Kinetics and modelling of anaerobic digestion process. In: Biomethanation, vol. 81. Heidelberg: 2003. p. 57-93.

[126] Romli M, Keller J, Lee PL, Greenfield PF. The influence of pH on the performance of a two-stage anaerobic treatment system: model prediction and validation. Water Sci. Technol. 1994;30:35-44.

[127] Batstone DJ, Keller J, Newel RB, Newland M. Modelling anaerobic degradation of complex wastewater. i: model development. Bioresour. Technol. 2000;75:67-74.

[128] Batstone DJ, Keller J, Newel RB, Newland M. Modelling anaerobic degradation of complex wastewater. ii: parameter estimation and validation using slaughterhouse effluent. Bioresour. Technol. 2000;75:75-85.

[129] Blumensaat F, Keller J. Modelling of two-stage anaerobic digestion using the IWA anaerobic digestion model no 1 (ADM1). Water Res. 2005;39:171-183.

[130] Batstone DJ, Keller J, Blackhall LL. The influence of substrate kinetics on the microbial community structure in granular anaerobic biomass. Water Res. 2004;38:1390-1404.

[131] Batstone DJ, Picioreanu C, van Loosdrecht MCM. Multidimensional modelling to investigate interspecies hydrogen transfer in anaerobic biofilms. Water Res. 2006;40:3099-3108.

[132] Kohonen T. Self-organizing maps, vol. 30. Berlin, Germany: Springer, 1995.

[133] Arudchelvam Y, Perinpanayagam M, Nirmalakhandan N. Predicting VFA formation by dark fermentation of particulate substrates. Bioresour. Technol. 2010;101:7492-7499.

[134] Vital-Lopez FG, Armaou A, Nikolaev EV, Maranas CD. A computational procedure for optimal engineering interventions using kinetic models of metabolism. Biotechnol. Prog. 2006;22:1507-1517.

[135] Kleerebezem R, Stams AJM. Kinetics of syntrophic cultures: a theoretical treatise on butyrate fermentation. Biotechnol. Bioeng. 2000;67:529-543.

[136] Liu Y. Overview of some theoretical approaches for derivation of the monod equation. Appl. Microbiol. Biotechnol. 2007;73:1241-1250.

[137] Monod J. The growth of bacterial cultures. Annu. Rev. Microbiol. 1949;3:371-394.

[138] Jin Q, Bethke CM. The thermodynamics and kinetics of microbial metabolism. Am. J. Sci. 2007;307:643-677.

[139] Vlyssides A, Barampouti EM, Mai S. An alternative approach of UASB dynamic modeling. AIChE J. 2007;53:3269-3276.

[140] Hoh CY, Cord-Ruwisch R. A practical kinetic model that considers endproduct inhibition in anaerobic digestion processes by including the equilibrium constant. Biotechnol. Bioeng. 1996;51:597-604.

[141] Schopf JW. Cradle of life. the discovery of earth's earliest fossils. Princeton, New Jersey, United States of America: Princeton University Press, 1999.

[142] Francis KA. Charles darwin and the origin of species. Westport, Connecticut, United States of America: Greenwood Press, 2007.

[143] Cann RL, Stoneking M, Wilson AC. Mitochondrial DNA and human evolution. Nature 1987;325:31-36.

[144] Haynie DT. Biological thermodynamics. Cambridge, United Kingdom: Cambridge University Press, 2001.

[145] Pattabhi V, Gautham N. Biophysics. Hingham, United States of America: Kluwer Academic Publishers, 2002.

[146] Organisation Intergouvernementale de la Convention du Metre. The international system of units (SI). Bureau International des Pois et Mesures, 2006.

[147] Martyushev LM, Seleznev VD. Maximum entropy production principle in physics, chemistry and biology. Phys. Rep. 2006;426:1-45.

[148] Wolfe J. Cellular thermodynamics. Encyclopedia of Life Sciences, Macmillan Publishers Ltd, Nature Publishing Group 2002.

[149] McCarty PL. Thermodynamics of biological synthesis and growth. Int. J. Air Water Pollut. 1965;9:621-639.

[150] McCarty PL. Thermodynamic electron equivalents model for bacterial yield prediction: modifications and comparative evaluations. Biotechnol. Bioeng. 2007;97:377-388.

[151] von Stockar U, Vojinovic V, Maskow T, Liu J. Can microbial growth yield be estimated using simple thermodynamic analogies to technical processes? Chem. Eng. Process. 2008;47:980-990.

[152] Heijnen JJ, Roels JA. A macroscopic model describing yield and maintenance relationships in aerobic fermentation processes. Biotechnol. Bioeng. 1981;23:739-763.

[153] Heijnen JJ, vanDijken JP. In search of a thermodynamic description of biomass yields for the chemotrophic growth of microorganisms. Biotechnology and Bioengineering 1992;39:833-858.

[154] Heijnen JJ, van Loosdrecht MCM, Tijhuis L. A black box mathematical model to calculate auto- and heterotrophic biomass yields based on Gibbs energy dissipation. Biotechnol. Bioeng. 1992;40:11391154.

[155] van Briesen JM. Evaluation of methods to predict bacterial yield using thermodynamics. Biodegradation. 2002;13:171-190.

[156] Xiao J, VanBriesen JM. Expanded thermodynamic model for microbial true yield prediction. Biotechnol. Bioeng. 2006;93:110-121.

[157] Mavrovouniotis ML. Duality theory for thermodynamic bottlenecks in bioreaction pathways. Chem. Eng. Sci. 1996;51:1495-1507.

[158] Qian H, Beard D. Thermodynamics of stoichiometryc biochemical networks in living systems far from equilibrium. Biophys. Chem. 2005;114:213-220.

[159] Beard DA, Babson E, Curtis E, Qian H. Thermodynamic constraints for biochemical networks. J. Theor. Biol. 2004;228:327-333.

[160] Kuypers MMM, Sliekers AO, Lavik G, Schmid M, Jorgensen BB, Kuenen JG, Damste JSS, Strous M, Jetten MSM. Anaerobic ammonium oxidation by anammox bacteria in the black sea. Nature. 2003;422:608-611.

[161] Hinrichs KU, Hayes JM, Sylva SP, Brewer PG, DeLong EF. Methane-consuming archaebacteria in marine sediments. Nature. 1999;398:802-805.

[162] Raghoebarsing AA, Pol A, van de Pas-Schoonen KT, Smolders AJP, Ettwig KF, Rijpstra WIC, Schouten S, Damste JSS, Op de Camp HJM, Jetten MSM, Strous M. A microbial consortium couples anaerobic methane oxidation to denitrification. Nature. 2006;440:918-921.

[163] Lloyd D, Scott RI. Direct measurements of dissolved gases in microbial systems using membrane inlet mass spectrometry. J. Microbiol. Methods. 1983;1:313-328.

[164] Johnson RC, Cooks RG, Allen TM, Cisper ME, Hemberger PH. Membrane introduction mass spectrometry: trends and applications. Mass Spectrom. Rev. 2000;19:1-37.

[165] Hoch GK, Kok B. A mass spectrometer inlet system for sampling gases dissolved in liquid phases. Arch. Biochem. Biophys. 1963;101:160-170.

[166] Reuss M, Piehl H, Wagner F. Application of mass spectrometry to the measurement of dissolved gases and volatile substances in fermentation. Eur. J. Appl. Microbiol. 1975;1:323-325.

[167] Bell RJ, Short RT, van Amerom FHW, Byrne RH. Calibration of an in situ membrane inlet mass spectrometer for measurements of dissolved gases and volatile organics in seawater. Environ. Sci. Technol. 2007;41:8123-8128.

[168] LaPack MA, Tou JC, Enke CG. Membrane mass spectrometry for the direct trace analysis of volatile organic compounds in air and water. Anal. Chem. 1990;62:1265-1271.

[169] Ferreira BS, van Keulen F, da Fonseca MMR. A microporous membrane interface for the monitoring of dissolved gaseous and volatile compounds by on-line mass spectrometry. J. Membr. Sci. 2002;208:49-56.

[170] Heinzle E, Lafferty RM. Continuous mass spectrometric measurement of dissolved H_2, O_2, and CO_2 during chemolithoautotrophic growth of *Alcaligenes eutrophus* strain H 16. Eur. J. Appl. Microbiol. Biotechnol. 1980;11:17-22.

[171] Tarkiainen V, Kotiaho T, Mattila I, Virkajarvi I, Aristidou A, Ketola RA. On-line monitoring of continuous beer fermentation process using automatic membrane inlet mass spectrometric system. Talanta. 2005;65:1254-1263.

[172] Poulsen AK, Lauritsen FR, Olsen LF. Sustained glycolytic oscillations – no need for cyanide. FEMS Microbiol. Lett. 2004;236:261-266.

[173] Hillman K, Lloyd D, Williams AG. Interactions between the methanogen *Methanosarcina barkeri* and rumen holotrich ciliate protozoa. Lett. Appl. Microbiol. 1988;7:49-53.

[174] Radivojevic D, Ruitenbeek M, Seshan K, Lefferts L. Development of a transient response technique for heterogeneous catalysis in liquid phase, Part 2: Applying membrane inlet mass spectrometry (MIMS) for detection of dissolved gasses. J. Catal. 2008;257:255-261.

[175] Baumgardner JE, Quinn JA, Neufeld GR. Micropore membrane inlet mass spectrometer probes suitable for measurement of tissue surface gas tensions. J. Mass Spectrom. 1995;30:563-571.

[176] Hernandez MRS. Membrane introduction mass spectrometry for the on-line analysis of volatile organic compounds in aqueous solutions. The Ohio state University, 2005.

[177] Pungor E, Perley CR, Cooney CL, Weaver JC. Continuous monitoring of fermentation outlet gas using a computer coupled MS. Biotechnol. Lett. 1980;2:409-414.

[178] Sheppard SK, Lloyd D. Direct mass spectrometric measurement of gases in soil monoliths. J. Microbiol. Methods. 2002;50:175-188.

[179] Tu C, Swenson E, Silverman D. Membrane inlet for mass spectrometric measurement of nitric oxide. Free Radical Biol. Med. 2007;43:1453-1457.

[180] Teeter BK, Dejarme LE, Choudhury TK, Cooks RG, Kaiser RE. Determination of ammonia, ethanol and acetic acid in solution using membrane introduction mass spectrometry. Talanta. 1994;41:1237-1245.

[181] Andersen AZ, Lauritsen FR, Olsen LF. On-line monitoring of CO_2 production in *Lactococcus lactis* during physiological pH decrease using membrane inlet mass spectrometry with dynamic pH calibration. Biotechnol. Bioeng. 2005;92:740-747.

[182] Yang TH, Wittman C, Heinzle E. Respirometric ^{13}C flux analysis, Part I: Desing, construction and validation of a novel multiple reactor system using on-line membrane inlet mass spectrometry. Metab. Eng. 2006;8:417-431.

[183] Yang TH, Wittman C, Heinzle E. Dynamic calibration and dissolved gas analysis using membrane inlet mass spectrometry for the quantification of cell respiration. Rapid Commun. Mass Spectrom. 2003;17:2721-2731.

[184] Lloyd D, James CJ. The Pasteur effect in yeast: mass spectrometric monitoring of oxygen uptake, and carbon dioxide and ethanol production. FEMS Microbiol. Lett. 1987;42:27-31.

[185] de Vos Petersen C, Beck HC, Lauritsen FR. On-line monitoring of important organoleptic methyl-branched aldehydes during batch fermentation of starter culture *Staphylococcus xylosus* reveal new insight into their production in a model fermentation. Biotechnol. Bioeng. 2004;85:298-305.

[186] Guegen C, Tortell PD. High-resolution measurement of southern ocean CO_2 and O_2/Ar by membrane inlet mass spectrometry. Mar. Chem. 2008;108:184-194.

[187] Doerner P, Lehmann J, Piehl H, Megnet R. Process analysis of the acetone-btanol fermentation by quadrupole mass spectrometry. Biotechnol. Lett. 1982;4:557-562.

[188] Bull AT. The renaissance of continuous culture in the post-genomics age. J. Ind. Microbiol. Biotechnol. 2010;37:993-1021.

[189] Angelidaki I, Sanders W. Assessment of the anaerobic biodegradability of macropollutants. Rev. Environ. Sci. Biotechnol. 2004;3:117-129.

[190] APHA. Standard methods for the examination of water and wastewater. New York. USA: American Public Health Association, 1995.

[191] Standards of performance for new sources. In: 40 CFR protection of the environment. United States Environmental Protection Agency (EPA), 1990.

[192] Kleerebezem R, van Loosdrecht MCM. Thermodynamic state analysis of environmental systems. Crit. Rev. Env. Sci. Tec. 2010;40:1-54.

[193] Alberty RA. Thermodynamics of systems of biological reactions. J. Theor. Biol. 2002;215:491-501.

[194] Kleerebezem R, van Loosdrecht MCM. A generalized method for thermodynamic state analysis of environmental systems. Crit. Rev. Environ. Sci. Technol. 2010;40:1-54.

[195] Alberty RA. Biochemical thermodynamics, applications of mathematica ®. Hoboken, New Jersey, United States of America: John Wiley & Sons, Inc., 2006.

[196] Bastidas-Oyanedel JR, Mohd-Zaki Z, Pratt S, Steyer JP, Batstone DJ. Development of membrane inlet mass spectrometry for examination of fermentation processes. Talanta. 2010;83:482-492.

[197] Bastidas-Oyanedel JR, Aceves-Lara CA, Ruiz-Filippi G, Steyer JP. Thermodynamic analysis of energy transfer in acidogenic cultures. Eng. Life Sci. 2008;8:487-498.

[198] von Stockar U, Maskow T, Liu J, Marison I, Patino R. Thermodynamics of microbial growth and metabolism: an analysis of the current situation. J. Biotechnol. 2006;121:517-533.

[199] Pauss A., Andre G., Perrier M., Guiot S. Liquid-to-mass transfer in anaerobic processes: inevitable transfer limitations of methane and hydrogen in the biomethanation process. Appl. Environ. Microbiol. 1990;56:1636-1644.

[200] Engel DC, Versteeg GF, van Swaaij WPM. Solubility of hydrogen in aqueous solutions of sodium and potassium bicarbonate from 293 to 333 K. J. Chem. Eng. Data. 1996;41:546-550.

[201] Schumpe A, Quicker G, Deckwer WD. Gas solubilities in microbial culture media. Adv. Biochem. Eng./Biotechnol. 1982;24:1-38.

[202] Gros JB, Dussap CG, Catte M. Estimation of O_2 and CO_2 solubility in microbial culture media. Biotechnol. Prog. 1999;15:923-927.

[203] Lloyd D, Thomas KL, Cowie G, Tammam JD, Williams AG. Direct interface of chemistry to microbial systems: membrane inlet mass spectrometry. J. Microbiol. Methods. 2002;48:289-302.

[204] Pratt S, Yuan Z, Gapes D, Dorigo M, Zeng RJ, Keller J. Development of a novel tritation and off-gas analysis (TOGA) sensor for the study of biological processes in wastewater treatment systems. Biotechnol. Bioeng. 2003;81:482-495.

[205] Pianosi P, Seargeant L, Haworth J. Blood lactate and pyruvate concentrations, and their ratio during exercise in healthy children: developmental perspective. Eur. J. Appl. Physiol. O. 1995;71:518-522.

[206] Zeng AP, Menzel K, Deckwer WD. Kinetic, dynamic, and pathway studies of glycerol metabolism by *Klebsiella pneumoniae* in anaerobic continuous culture: ii. analysis of metabolic rates and pathways under oscillation and steady-state conditions. Biotechnol. Bioeng. 1996;52:561-571.

[207] Orij R, Postmus J, Ter Beek A, Brul S, Smits GJ. In vivo measurement of cytosolic and mitochondrial pH using a pH-sensitive GFP derivative in *Saccharomyces cerevisiae* reveals a relation between intracellular pH and growth. Microbiology-SGM. 2009;155:268-278.

[208] Ennis BM, Marshall CT, Maddox IS, Paterson AHJ. Continuous product recovery by in-situ gas stripping/condensation during solvent production from whey permeate using *Clostridium acetobutylicum*. Biotechnol. Lett. 1986;8:725-730.

[209] Ezeji TC, Qureshi N, Blaschek HP. Production of acetone, butanol and ethanol by *Clostridium beijerinckii* ba101 and in situ recovery by gas stripping. World J. Microb. Biot. 2003;19:595-603.

[210] Groot WJ, van der Lans RGJM, Luyben KCAM. Batch and continuous butanol fermentations with free cells: integration with product recovery by gas-stripping. Appl. Microbiol. Biotechnol. 1989;32:305-308.

[211] Maddox IS, Qureshi N, Roberts-Thomson K. Production of acetone-butanol-ethanol from concentrated susbtrates using *Clostridium acetobutylicum* in an integrated fermentation-product removal process. Process Biochem. 1995;30:209-215.

[212] Ezeji TC, Karcher PM. Improving performance of a gas stripping-based recovery system to remove butanol from *Clostridium beijerinckii* fermentation. Bioprocess Biosyst. Eng. 2005;27:207-214.

[213] Vane LM. A review of pervaporation for product recovery from biomass fermentation processes. J. Chem. Technol. Biot. 2005;80:603-629.

[214] Colin T, Bories A, Sire Y, Perrin R. Treatment and valorisation of winery wastewater by a new biophysical process (ECCF®). Water Sci. Technol. 2005;51:99-106.

8 APPENDIX

8.1 Development of membrane inlet mass spectrometry for examination of fermentation processes

This present publication consists on the final draft post-refereeing, in order to respect the Talanta -Elsevier restrictions concerning author archiving.

Reference: Bastidas-Oyanedel JR, Mohd-Zaki Z, Pratt S, Steyer JP, Batstone DJ. Development of membrane inlet mass spectrometry for examination of fermentation processes. Talanta. 2010;83:482-492. DOI: 10.1016/j.talanta.2010.09.034

Title: Development of membrane inlet mass spectrometry for examination of fermentation processes

Authors: Juan-Rodrigo Bastidas-Oyanedel[a], Zuhaida Mohd-Zaki[b], Steven Pratt[b], Jean-Philippe Steyer[a], Damien J. Batstone[b,*]

Authors affiliations:

[a] INRA, UR0050, Laboratoire de Biotechnologie de l'Environnement, Narbonne, F-11100, France.

[b] AWMC, Advanced Water Management Centre, Environmental Biotechnology CRC, The University of Queensland, St Lucia, Brisbane, QLD 4072, Australia.

* Corresponding author. fax: +61 7 3365 4726

Authors e-mail address list:

oyanede@supagro.inra.fr (J.R. Bastidas-Oyanedel)

z.zaki@uq.edu.au (Z. Mohd-Zaki)

s.pratt@awmc.uq.edu.au (S. Pratt)

steyer@supagro.inra.fr (J.P. Steyer)

damienb@awmc.uq.edu.au (D.J. Batstone)

Abstract: Membrane inlet mass spectrometry (MIMS) is useful for on-line monitoring of fermentation processes. However, readings are affected by the complex and dynamic matrix in which biological processes occur, making MIMS calibration a challenge. In this work, two

calibration strategies were evaluated for measurement of typical products of acidogenic fermentation, i.e., ethanol, H_2, and CO_2 in the liquid phase, and H_2 and CO_2 in the gas phase: 1) "standard calibration", which was performed independent of fermentation experiments with sterile standards in water with a N_2 headspace, and; 2) "in-process calibration" whereby fermentation was monitored concurrent with off-line analysis. Fermentation was operated in batch and continuous mode. In-process calibration was shown to be most effective for measurements of H_2 and CO_2 in both gas and liquid phases; standard calibration gave erroneous results. In the gas phase, this was due to a lower sensitivity during experiments compared to the independent standard calibration, believed to be caused by formation of a liquid film on the surface of the probe. In the liquid phase, moving from the standard calibration environment to the fermentation caused the linear relationship between the H_2 concentration and MIMS signal to change in intercept, and the relationship for CO_2 to change in slope, possibly due to dissolved ions, and related non-ideality. For ethanol, standard calibration results were fairly consistent with in-process calibration results. The main limitation with in-process calibration is the potential for a lack of variability in target concentration. This could be addressed by spiking the targeted compound at the end of the experiment. Regardless, MIMS is an ideal instrument for analysing fermentation experiments, due to its ability to measure targeted compounds semi-continuously, and due to a lack of drift over long periods.

Keywords: Membrane inlet mass spectrometry; Calibration; Anaerobic fermentation; Hydrogen; Carbon dioxide; Ethanol

INTRODUCTION

Membrane inlet mass spectrometry (or membrane introduction mass spectrometry, MIMS) is a method of introducing analytes into a mass spectrometer's vacuum chamber via a semipermeable membrane [1]. MIMS is most useful for the measurement of small, non-polar molecules, since they have a high affinity to the membrane. After samples have been extracted via the membrane, they are analysed by a mass spectrometer. A more detailed description is given elsewhere [2]. Membrane inlet mass spectrometry has the following advantages over other on-line analytical methods: (1) Minimally invasive technique, (2) rapid response of seconds to minutes, (3) measures volatile compounds up to 200 molecular weight, (4) high sample frequency, (5) high sensitivity (e.g. 0.25 μM O_2), (6) measurements can be made in gas and/or liquid phase, (7) and

low analytical costs [3]. Disadvantages include preferential retention of some compounds (e.g., H_2S) causing memory effects [4], however, the major issue is that the MIMS signal is not a direct measure of target concentration, but rather a measure of the ionization of compounds that pass through the membrane [5]. Calibration is therefore crucial in order to have an absolute measure of the analyte.

MIMS signal magnitude not only depends on the volatility of the analyte, but also on sample and experimental conditions, including membrane permeability, temperature, ionization, sample point hydraulics, and sample matrix composition [5]. These issues need to be addressed during calibration of the signal. With good control of experimental equipment, the most variable of these is chemical matrix. Chemical components can influence permeation rates and ionization efficiencies of analytes, cause long-term memory effects and change membrane properties [6,7]. There is generally limited calibration information available, and early work using MIMS did not calibrate against an external reference, but instead presented relative kinetics [8,9]. Hillman et al. [10] and Radivojevic et al. [11] translated MIMS signals by estimating dissolved concentrations of gases in water using gas partial pressures and Henry law. Standard solutions [3,12-17] have been used, but this results in a different matrix from the sample. Heinzle and Lafferty [6] showed that three different liquid solutions (pure water, normal nutrient solution and sterilized fermentation broth) have an impact on calibration curves for dissolved H_2 and O_2. They also showed that presence of viable cells had an impact, and concluded that standard solution calibration was not suitable for biochemical experiments. Andersen et al. [18] attempted to address matrix issues by resuspending a known amount of viable cells into the calibration solutions. Yang et al. [4,19] used corrections in CO_2 MIMS signal for pH and ionic strength. Lloyd and James [20] used standard additions in fermentation experiments at constant pH and temperature. This approach was followed by other workers [21,22]. This is effective and is one approach to in-process calibration, but it has a chemical impact on the underlying processes. This approach also does not effectively address solution non-ideality. In addition, standard additions require a compound that is relatively easy to add, which is not the case for dissolved gases.

The best way to address variability in chemical matrix and other conditions is by off-line measurement against a matrix-independent method. This was done by Doerner et al. [23] and Tarkiainen et al. [7] who determined that calibration against standards was unsuccessful. They examined how different mixtures of gases and volatiles affect membrane transfer properties, and

consequently MIMS signal magnitude. The conclusion was that MIMS signal calibration for fermentation processes has to be based on conventional off-line analysis such as gas chromatography.

Hence, calibration based on off-line analysis seems to be an effective method, but there is a lack of detailed information, particularly for measurement of dissolved gases in the liquid phase. This is critical for H_2 and CO_2 that are major products of acidogenic fermentation. H_2 is increasingly being investigated as a renewable fuel. The issues around H_2 are complicated by high diffusivity, low solubility, and a high degree of non-ideality in relation to the matrix. While dissolved CO_2 concentration is highly affected by liquid matrix pH. The purpose of this study is thus to assess MIMS calibration methods for fermentation experiment systematically, and particularly with respect to dissolved gases.

MATERIALS AND METHODS

Fermentation experiments

Fermentation and calibration procedures were performed in a mixed culture fermentation system, using a glass reactor, with constant temperature, headspace pressure (regulated through a gas flow-rate meter), liquid stirring velocity, gas and liquid volumes. Feed was glucose in basal anaerobic (BA) media. Two different fermentation modes were performed; continuous and batch. During continuous experiments, the system was operated at a constant feed rate, with optional flushing of the headspace with N_2 to change gas partial pressures. During batch experiments, dynamics were assessed by introducing a glucose pulse at time 0.1 days. MIMS probes were used in gas and liquid phases simultaneously.

Reactor equipment. A diagram of the experimental equipment is shown in Figure 1. Liquid volume was 1.31 L and a headspace of 170 mL. Temperature was regulated at 37°C using an immersed glass heater (25W Aqua One^{TM}). A magnetic stirrer was used at approximately 600 rpm. For continuous experiments, the system was fed by a Watson Marlow peristaltic pump from split feed tanks containing basal media, and pure glucose solution. pH was controlled by a pH probe and peristaltic pump feeding 1M NaOH. Liquid lock was maintained by a glass u-tube. Gas flow was measured by a tipping-bucket type meter, with a bucket volume of 2 mL, and a

constant pressure of approximately 1 cm water. MIMS probes were placed both in gas and liquid phases, respectively. All equipment was interfaced to computers via an Opto PLC used for data logging and set-point modification. N_2 flushing of the headspace was also available, with pure N_2 flow being regulated through parallel Cole Parker rotameters with limits of 0.5 $mL \cdot min^{-1}$ and 5 $mL \cdot min^{-1}$ (allowing full range of flow regulation).

Media. Feed was held in two containers (in order to avoid microbial contamination), fed simultaneously. Substrate solution consisted of 10 $g \cdot L^{-1}$ of glucose and silicone based antifoam (Dow Corning ® antifoam RD emulsion) at 1 $mL \cdot L^{-1}$, autoclaved at 120°C for 45 min. The Basal Anaerobic (BA) media contained in $mg \cdot L^{-1}$: 2.4 $CaCl_2 \cdot 2H_2O$, 0.1 $(NH_4)_6Mo_7O_{24} \cdot 4H_2O$, 0.1 $CoCl_2 \cdot 6H_2O$, 4 $FeCl_2 \cdot 4H_2O$, 0.1 $MnCl_2 \cdot 4H_2O$, 0.184 $NiCl_2 \cdot 6H_2O$, 0.2 $Na_2SeO_3 \cdot 5H_2O$, 0.1 H_3BO_3, 0.076 $CuCl_2 \cdot 2H_2O$, 0.1 $ZnCl_2$, 0.1 $AlCl_3$, 1 EDTA, 0.01 aminobenzoic acid, 0.004 biotin, 0.004 folic acid, 0.01 nicotinic acid, 0.01 panthothenic acid, 0.02 pyridoxine, 0.01 riboflavin, 0.01 thiamine hydrochloride, 0.0002 cyanocobalamine, 0.01 lipoic acid; In $g \cdot L^{-1}$: 2 NH_4Cl, 0.2 NaCl, 0.2 $MgCl_2 \cdot 6H_2O$, 0.2 $K_2HPO_4 \cdot 3H_2O$, and 0.2 $Na_2S \cdot 9H_2O$; and HCl 2 ($\mu L \cdot L^{-1}$). BA media was based on Angelidaki and Sanders [24], modified to minimize calcium phosphate precipitation.

Inoculum. Inoculum was anaerobic digestate from a primary sludge fed digester in Brisbane, Australia. The inoculum was conditioned by operation at 12 h hydraulic retention time (HRT) over 1 week without pH control (native pH of 5.5), until methane production stopped, giving as a result a standardized mixed culture fermentative community.

Batch experiments. Initial conditions were established by continuous mode fermentation over two days, with pH controlled at 6.5, and a HRT of 6 h. Prior to batch experiments, MIMS signal was stable for at least 12 h. Batch experiments consisted of a halt in feed, and injection of 2 mL autoclaved solution containing 325 $g \cdot L^{-1}$ glucose. After 24 hours, a new glucose pulse was added to the bioreactor.

Continuous experiments. Continuous mode involved constant feed via a peristaltic pump. In experiments presented here, a pH set-point of 6.5 was used, with a HRT of 6h. Changes in the gas phase composition were achieved by flushing the headspace with N_2 at 0, 2.5, 7, and 50 $L \cdot d^{-1}$ over a period of 6 days. Flushes indirectly changed liquid partial pressures. Liquid partial

pressures were not changed by sparging, as this would also severely change mixing intensity over the MIMS probe.

MIMS set-up and operation

A commercially available Hiden HPR-40 DSA dissolved species analyser bench top MIMS unit (Hiden Analytical Ltd., Cheshire, England) was used, which contained a Hiden HAL 201 RC quadrupole mass spectrometer with dual faraday/electron multiplier detector and a mass range of 200 atomic mass units. MIMS unit inlets consist of a 4 way multistream selector for simultaneous sampling. Each MIMS probe had 0.5 m length, suited with silicon rubber membrane. Recorded mass to charge (m/z) ratio were 1, 31, and 44 for H_2, ethanol and CO_2 respectively. The m/z ratios were selected after scanning these three pure compounds during previous experiments.

MIMS signal translation

The different experiments were used to identify the different impacts of experimental equipment (including hydraulics), and sample chemical matrix on MIMS signal translation into quantitative information, i.e. composition of targeted compounds in gas and/or liquid phase.

Standard calibration. In this procedure, standard matrix consisted on reversed osmosis (RO) water liquid phase and N_2 gas phase. Temperature and agitation was the same as in both batch and continuous fermentations. Pure compounds were added at different ratios into the reactor in order to cover their expected concentration range during fermentation. Pure H_2 was injected into the headspace reactor to give the following H_2 partial pressures: 0, 0.2, 0.35 and 0.65 bar, while CO_2 headspace partial pressures were: 0, 0.04, 0.3 and 0.5 bar. Both H_2 and CO_2 were monitored in the gas and liquid phases by MIMS. Gas samples were taken when both MIMS signals were stable. Liquid and gas phase concentrations were analysed as detailed below. Pure ethanol was injected in the liquid phase reaching 0, 5, 10 and 30 mM. Ethanol was analysed only in the liquid phase. The data was analysed to develop a correlation with their respective MIMS signal.

In-process off-line data acquisition. Off-line data acquisition was performed concurrent to both batch and continuous fermentations. Samples were taken from gas and liquid phases at different times, resulting in off-line data sets, and analysed to develop a correlation with their respective MIMS signal.

Correlation analysis. It consisted in a linear correlation of targeted compound composition (bar or mM) versus its respective MIMS signal magnitude (faraday).

In-process calibration. It consisted in splitting randomly each fermentation off-line data set into calibration and validation sets. Calibration was performed, as a linear correlation explained above, for the calibration data set.

Validation of MIMS calibration. It was calculated as the difference between the standard or in-process calibrated MIMS signal and its respective validation off-line data set. This difference was expressed as percentage.

Analytical Methods

Gas phase. Gas samples of 0.5 mL were taken with a glass syringe, and analyzed immediately by gas chromatography. H_2 was analyzed using a GC-8A gas chromatograph (GC) equipped with a thermal conductivity detector (Shimadzu) with N_2 as a carrier gas at 100 kPa, 110°C for the injection and detector temperature and 40°C for the column temperature with a thermal conductivity detection (TCD) current of 80 mA. CO_2 was analysed using the same GC and conditions mentioned above, but using He as carrier gas and a current of 160 mA. Calibration was performed prior to each day's measurement using external gases provided by BOC Gases Australia Ltd. 5% CO_2 and 5% N_2 in methane, 20% CO_2 and 20% N_2 in methane, and 100% H_2, injected as 0.5 mL at 1 atm.

Liquid phase. Liquid samples were taken from the liquid sampling port (Figure 1). Each liquid sample consisted of 12 mL. Two samples of 4 mL each were injected via a sterile 0.22 μm cellulose acetate cartridge into 10 mL vacuum tubes (BD Vacutainer ® serum tubes), while the remaining 4 mL was preserved with formic acid for ethanol analysis. The tubes for dissolved CO_2 measurement were previously injected with 0.5 mL of 2 M HCl.

Dissolved gas measurement was based on an equilibrium assumption. Tubes were equilibrated for 24 hours at 20°C. 0.5 mL gas sample from each tube was measured by gas chromatography. Dissolved H_2 was measured using a GC-8 equipped with a thermal conductivity detector (Shimadzu) and a 183 x 0.32 x 26 cm stainless steel molecular sieve (80/100 mesh, washed)

column. The GC was fitted with a Clarity Lite Data analysis software package. A reference and a measurement channel were used simultaneously. Those channels worked a 300 and 400 kPa respectively using Ar as a carrier gas. Injection and detector temperatures were 80°C and 120°C for the column, with a TCD current of 70 mA. Calibration was performed prior to each day's measurement using external gas standards obtained from BOC Gases Australia Ltd. with concentrations in % of 0.1, 1 and 3 H_2 in N_2. Dissolved CO_2 samples were analysed as for gas phase samples.

Liquid phase H_2 or CO_2 was estimated using the temperature corrected Henry's law coefficient, and the total H_2 or CO_2 concentration in the liquid sample calculated by a mass balance. Sample liquid and gas volumes were checked by weighing on a balance.

Reactor's dissolved CO_2 concentration was then calculated as a fraction of the total CO_2 measured by this method, function of the carbonates (HCO_3^- and CO_3^{2-}) equilibrium constants and reactor's pH as is expressed in the equation below.

$$CO_{2(dissolved)} = CO_{2(total)} \cdot \frac{[H^+]^2}{[H^+]^2 + Ka_1[H^+] + Ka_1 \cdot Ka_2}$$

Ethanol samples were preserved in 1% formic acid, and measured on a GC equipped with a polar capillary column (Agilent technologies) and a flame ionization detector (FID).

RESULTS

Correlation between MIMS signals and measurement

Figure 2 illustrates normalised slopes and intercepts for standard, batch and continuous linear correlation between MIMS signals and concentration of targeted compounds. Normalisation was based on the maximum absolute slope and intercept values found among the standard, batch and continuous correlations of each compound at liquid or gas phase.

The calculated linear correlation parameters are summarised in Table 1, where slopes and intercepts are expressed in bar·faraday^{-1} and bar for the gas phase and in mM·faraday^{-1} and mM for the liquid phase.

Errors are shown as 95% confidence in parameters, with appropriate t-values applied based on the number of degrees of freedom. High uncertainty in in-process correlation parameters are generally caused by a limited range in value variation as further addressed in the discussion. Similarities and differences are summarized as follow.

In the gas phase (H_2, CO_2), standard correlation slopes were consistently lower than in-process correlation slopes, indicating high sensitivity for standard conditions (see discussion). As slopes are expressed in bar·faraday^{-1}, a given partial pressure change will produce larger MIMS signal changes in standard conditions compared to fermentation environments. Intercepts for both gases were statistically zero, except for batch CO_2 which was very low.

In the liquid phase, dissolved H_2 slopes were similar, with a mean of $9 \cdot 10^5$(mM·faraday^{-1}), due to the high errors. Intercept for standard correlation was the lowest, while batch and continuous intercepts were statistically the same.

Dissolved CO_2 slope for batch correlation was the highest, while standard and continuous slopes were statistically the same. Intercepts were statistically zero for standard and batch correlations while for continuous was the highest.

For ethanol in the liquid phase, slopes and intercepts were statistically the same or very similar due to in-process correlation high errors, caused by limited variation in the ethanol concentration during experiments (see discussions).

As discussed further below, uncertainty in parameters, particularly slope, were strongly dependent on variation in the targeted compound. Where variation in value was low (e.g., ethanol and dissolved H_2 in batch and continuous), estimates of slope were particularly poor, as would be expected.

Fermentation kinetics

Batch and continuous fermentations were set-up to investigate separately the effect of liquid and gas matrix dynamics on the translation of MIMS signal. Dynamics in the liquid matrix in batch fermentation were controlled by pH kinetics, while gas matrix dynamics in continuous fermentation were controlled by N_2 flushing. Both effects were analysed using off-line correlation of MIMS signals rather than calibration procedure (see discussion).

Figures 3 and 4 illustrate the MIMS signal translation by in-process correlation parameters, solid line, and standard calibration, dashed line, applied for batch and continuous fermentations respectively. Experimental off-line correlation data set is shown as white squares. The dynamics of pH and gas flow rates are also presented in Figures 3F and 4F.

Batch fermentation. Figure 3 illustrates the kinetics of the batch experiment where the estimation of H_2 and CO_2 was substantially improved by application of in-process correlation.

Dissolved CO_2 concentration is dependent of pH. Measurement of pH dynamics, as is shown in Figure 3F, is crucial when the dissolved CO_2 MIMS calibration method relies on an off-line analytical method that measures total inorganic carbon.

A short period of oscillation on in-process calibrated signals is observed for all the compounds and phases (see discussion).

Continuous fermentation. Translated MIMS signals for the continuous experiment are shown in Figure 4. Dynamics were induced by flushing of the headspace, and consisted of changes in N_2 flushing rates from 0 L d^{-1}, 2.5 L.d^{-1}, 7 L.d^{-1}, and 50 L d^{-1} as is shown in Figure 4F.

As in the case of batch fermentation, H_2 and CO_2 estimations were also improved by the application of in-process correlation. Response of H_2 and CO_2 in the liquid was minimal, i.e. between 0.3 and 0.5 mM for H_2 and 1.2 and 1.7 mM for CO_2 (see Figures 4A and 4C), while response of H_2 and CO_2 in the gas was substantial. There was also a continuous increase in ethanol concentration over the experimental period.

The solid line discontinuity in Figure 4 is owned to an electric shortcut experienced at day 2, which led to a stop of feeding and pH pumps, and consequently a decrease on pH. MIMS signal was lost from 2.4 to 2.6 days.

In-process MIMS signal calibration

The off-line data set shown in Figures 3 and 4 were randomly divided into in-process MIMS calibration and validation data set for both batch and continuous fermentations. These data sets are shown in Figures 5 and 6. The in-process calibrated curves are shown as solid lines, calibration data sets are shown as white squares and validation data sets as black circles.

Validation of calibration strategies

Table 2 illustrates the average validation errors between calibrated MIMS signals and their respective off-line experimental validation data sets for batch and continuous fermentation. The validation results of in-process and standard calibrations are presented for both fermentations. The last line of the table presents the errors for continuous fermentation with correlation parameters obtained using batch fermentation (see discussion).

In general, these results demonstrate that in-process calibration was the best calibration strategy. For both fermentations, in-process calibration average validation errors are in the range of 10%, whilst for standard calibration, they are around 100%.

Special case was found for H_2 and ethanol. Validation error for H_2 gas phase was high (8 ± 70 %) at continuous fermentation due to the low H_2 partial pressure caused by the N_2 flushes, while dissolved H_2 errors for both fermentations are high (-43 ± 35 % for batch and 21 ± 10 % for continuous) due to low response in its concentration(between 0.3 and 0.5 mM).

Ethanol errors are in the same order of magnitude, i.e. around -20% for batch and 10% for continuous fermentation (see discussion).

DISCUSSION

Standard vs. in-process calibration

The three options for calibration were standard calibration (in a water/N_2 system), calibration by standard additions, and in-process calibration. For fermentation experiments, spiking with compounds such as H_2, CO_2, bicarbonate or ethanol can have a strong influence on the biochemical process, and it is difficult to add gases for the purposes of standard additions. Therefore, we opted for standard calibration and in-process calibration. The results, particularly those in Figures 3 and 4 demonstrate that standard calibration, even when using exactly the same equipment is ineffective for H_2 and CO_2, and may be sub-optimal for ethanol. The process itself has a strong impact on both measurement threshold, represented by correlation intercept, and sensitivity, represented by correlation slope. Our results confirmed that in-process calibration is necessary in fermentations to follow the evolution of analytes such as ethanol, H_2 and CO_2. In the following sections we go on to discuss how measurement of specific compounds was impacted upon by transfer issues. Compounds were divided into three classes based on liquid solubility (low/high) and volatility.

Measurement in the gas phase. As is illustrated in Figure 2 and Table 1 slope is higher for in-process calibrations, than for standard calibrations. This indicates a loss of sensitivity in the fermentation environment. By way of explanation, with standard calibrations, the headspace remains relatively dry (gas is not bubbled through the liquid). In contrast, under fermentation reactions, gas is continuously produced, which both volatilises and aspirates water. In our experiments, we noted that a liquid film formed on the surface of the MIMS probe, presenting a barrier to gas transfer. As both H_2 and CO_2 are relatively insoluble gases [25], the resistance to gas-liquid transfer is mainly in the liquid film. Such a film on the surface of the MIMS probe in a gas phase may control mass transfer, and change the characteristics completely in comparison to dry experiments, as well as make the MIMS signal strongly dependent on the thickness of the liquid film. In contrast, low variability in H_2 and CO_2 correlation intercepts (Table 1) suggests that measurement thresholds are not influenced by gas composition changes or gas turbulence caused by N_2 flushing in the continuous fermentation (Figure 4F).

Detection of low solubility volatiles in the liquid phase (e.g., H_2, CO_2). The three slopes for H_2 results presented in Figure 2 and Table 1 appear to be similar, indicating sensitivity in the liquid phase is not particularly influenced by the matrix. Because H_2 has high diffusivity ($4.65 \cdot 10^{-5}$ $cm^2 \cdot s^{-1}$) [25] in pure water we expected no change in MIMS sensitivity. In contrast, intercept results suggest that a complex fermentation matrix increases the dissolved H_2

concentration threshold in fermentations compared to standard calibration (making it harder to detect). Both batch and continuous in-process calibrations correlations to be similar in terms of intercept. This can be explained according to Engel et al. [26] model. The average fermentation sodium bicarbonate concentration (21.5 mM) may decrease H_2 solubility by 4%, a very minor change, but possibly responsible for the change in intercept.

In the case of CO_2 the high slope at batch condition, i.e. 3.4±0.5 ($mM \cdot faraday^{-1}$) compared to approximately 1 ($mM \cdot faraday^{-1}$) for both standard and continuous slopes, indicates a gain in sensitivity in batch fermentations. A mixed model from Schumpe et al. [27] and Gros et al. [28] indicates that non-biochemical fermentation media composition decreases CO_2 solubility by 1%, i.e. Henry constant at 36ºC (39.7 $bar \cdot L \cdot mol^{-1}$) increases to 40.2 $bar \cdot L \cdot mol^{-1}$. An alternative explanation is non-ideal solution behaviour, which would decrease the activity of the bicarbonate ion, and hence that of CO_2. This is quite likely, since at the solution ionic strength of approximately 0.2M, the impact of ion activity is significant. However, the results show low variability in CO_2 intercept (concentration threshold), i.e. between -0.1± 0.8 and 0.9±0.3 mM, suggesting that changes in matrix composition, (the presence and changes in fermentation substrate, nutrients and products concentrations) do not affect the CO_2 concentration threshold.

Detection of high solubility volatiles in the liquid phase. Standard and in-process correlations for ethanol in both batch and continuous fermentations are qualitatively (Figures 2, 3E and 4E), and statistically (Table 1) similar, but with some significant differences. Correlations between MIMS signals and ethanol concentration indicate an increase of MIMS sensitivity and concentration threshold in the fermentation matrix. Tarkiainen et al. [7] showed that sugars, salts, and CO_2 affect the MIMS response of ethanol. Glucose and sodium chloride has a positive effect, due to salting out, increasing ethanol MIMS sensitivity, while dissolved CO_2 has the opposite effect. Salts and glucose, therefore, have a higher impact in our case, even if salts were only added as necessary for biological growth. This is likely different in higher concentration waste conversion systems, where salts and ammonia have far higher concentrations. In any case, differences are low among the three correlations for ethanol H_2 and CO_2 correlations either in gas or liquid phase, as can be seen in Figures 3 and 4.

In-process calibration

In-process calibration is necessary to calibrate fermentation MIMS signals for two reasons:

1) Each fermentation experiment is a unique and complex dynamic system that changes MIMS membrane transfer properties. Hence it is advisable to not rely on calibrations conducted prior to the experimental run. This was demonstrated for the standard calibration and even when the calibration relied on a prior fermentation as illustrated in Figure 7. The last was also compared in terms of validation error as is presented in Table 2 where errors of this calibration strategy are largely higher than the in-process calibration.

2) In-process calibration is a relative easy and non-intrusive way to translate MIMS signals into quantifiable terms, allowing running experiments for long periods, as was the case for the continuous fermentation that lasted for 6 days.

MIMS signal oscillation and noise

Some oscillations and noise were observed in signal. Oscillations showed in Figure 3 are due to the temperature controller (3ºC range). This temperature oscillation causes changes on diffusivity and solubility of the volatile analytes [29], which changes their flow rates through MIMS membrane and consequently their MIMS signals. These signal oscillations could be minimised using better temperature regulation, and highlights the need for good temperature control. Random noise (Figure 4) is due to electrical issues occurring in the MIMS device, and can be addressed by using signal filters.

Limitations of in-process calibration

As stated above, in-process calibration is required as compared to standard or prior experiment run calibration to provide correlation between MIMS signals and actual concentrations. The main issue that we have observed is occasional low variability, which makes it very difficult to determine slope. This is especially evident in the continuous experiments (Figure 4A, C, and E, as well as Figure 2E). Proper determination of the calibration slope depends heavily on wide variation in concentration of the target compounds during sampling. That is, it is not useful if all samples have the same concentration. An increase of concentration variability will improve calibration, but will have an impact on the biological process. We suggest that targeted analytes be introduced at the end of the fermentation, so that concentration variability can be artificially induced increasing calibration accuracy without invalidating the experiment itself.

Applications of MIMS to fermentation experiments

Our results indicate that while standard calibration is recommended for quantifying the analyte range concentration, in-process calibration is necessary to translate signals of fermentation, which would otherwise be missed.

In fermentation processes, where dynamics play a very important role, it is very important to have a chemical analytical method with a short sample period. This is especially true for organic chemicals. Off-line analysers such as GC-FID offer non-matrix-dependant quantification, but are relatively expensive and time-consuming. With in-process calibration using MIMS, only a few off-line experimental samples are necessary to obtain an accurate view of the dynamics of the process.

An advantage of MIMS over other on-line methods is that calibration frequency is relatively long, with, in the example of Figure 4, six days of operation without recalibration. Other alternatives such as titrimetric off-gas analysis [30] require recalibration every 2-3 hours.

The main challenge to increase the usefulness of MIMS for fermentation experiments is detection of other organic compounds such as lactic, acetic, propionic, and butyric acids. While we attempted this, detection of organic acids was not possible due to: (a) overlap in spectrum peaks, and (b) because most of these compounds have pK_a values of <5.0, and are therefore mainly present as charged (non-volatile) compounds at a pH of >5.0. The first of those 2 obstacles could be overcome by either an increase in MS accuracy (allowing for differentiation of compounds with the same MW, but different atomic formula), and/or advanced regression techniques. The second requires accounting for both solution non-ideality, and pH, as well as possibly, off-line titration. Addressing these issues would make MIMS a requisite instrument for analysing fermentation and other mixed-culture biotechnological processes.

ACKNOWLEDGEMENTS

This research was supported under Australian Research Council's *Linkage Projects* funding scheme (project number LP0669527). J.R. Bastidas-Oyanedel acknowledges the support received by the PhD scholarship from the Chilean Commission for Science and Technology

(CONICYT). Travel support was provided by the Anamix IRSES EU Project Contract Grant No. GA-2008-230829.

Authors would like to thanks PhD candidate Hang Zheng (BioMass BioEnergy Group, School of Engineering, The University of Queensland) for the help measuring dissolved H_2 analysis; Dr Oriol Gutierrez (Advance Water Management Centre, The University of Queensland) and Dr Raymond Zeng for their pertinent commentaries and discussions.

REFERENCES

[1] R. Johnson, R. Cooks, T. Allen, M. Cisper, P. Hemberger, Mass Spectrom. Rev. 19 (2000) 1-37.

[2] D. Lloyd, R. Scott, J. Microbiol. Methods. 1 (1983) 313-328.

[3] R. Bell, R. Short, F. van Amerom, R. Byrne, Environ. Sci. Technol. 41 (2007) 8123-8128.

[4] T. Yang, C. Wittman, E. Heinzle, Rapid Commun. Mass Spectrom. 17 (2003) 2721-2731.

[5] B. Ferreira, F. van Keulen, M. da Fonseca, J. Membr. Sci. 208 (2002) 49-56.

[6] E. Heinzle, R. Lafferty, Eur. J. Appl. Microbiol. Biotechnol. 11 (1980) 17-22.

[7] V. Tarkiainen, T. Kotiaho, I. Mattila, I. Virkajarvi, A. Aristidou, R. Ketola, Talanta. 65 (2005) 1254-1263.

[8] M. Reuss, H. Piehl, F. Wagner, Eur. J. Appl. Microbiol. 1 (1975) 323-325.

[9] A. Poulsen, F. Lauritsen, L. Olsen, FEMS Microbiol. Lett. 236 (2004) 261-266.

[10] K. Hillman, D. Lloyd, A. Williams, Lett. Appl. Microbiol. 7 (1988) 49-53.

[11] D. Radivojevic, M. Ruitenbeek, K. Seshan, L. Lefferts, J. Catal. 257 (2008) 255-261.

[12] J. Baumgardner, J. Quinn, and G. Neufeld, J. Mass Spectrom.30 (1995) 563-571.

[13] M. Hernandez, "Membrane introduction mass spectrometry for the on-line analysis of volatile organic compounds in aqueous solutions." The Ohio state University, 2005.

[14] E. Pungor, C. Perley, C. Cooney, and J. Weaver, Biotechnol. Lett. 2 (1980) 409-414.

[15] S. Sheppard and D. Lloyd, J. Microbiol. Methods. 50 (2002) 175-188.

[16] C. Tu, E. Swenson, and D. Silverman, Free Radical Biol. Med. 43 (2007) 1453-1457.

[17] B. Teeter, L. Dejarme, T. Choudhury, R. Cooks, and R. Kaiser, Talanta. 41 (1994) 1237-1245.

[18] A. Andersen, F. Lauritsen, L. Olsen, Biotechnol. Bioeng. 92 (2005) 740-747.

[19] T. Yang, C. Wittman, and E. Heinzle, Metab. Eng. 8 (2006) 417-431.

[20] D. Lloyd, C. James, FEMS Microbiol. Lett. 42 (1987) 27-31.

[21] C. de Vos Petersen, H. Beck, and F. Lauritsen, Biotechnol. Bioeng. 85 (2004) 298-305.

[22] C. Guegen and P. Tortell, Mar. Chem. 108 (2008) 184-194.

[23] P. Doerner, J. Lehmann, H. Piehl, R. Megnet, Biotechnol. Lett. 4 (1982) 557-562.

[24] I. Angelidaki, W. Sanders, Rev. Environ. Sci. Biotechnol. 3 (2004) 117-129.

[25] A. Pauss, G. Andre, M. Perrier, S. Guiot, Appl. Environ. Microbiol. 56 (1990) 1636-1644.

[26] D. Engel, G. Versteeg, and W. van Swaaij, J. Chem. Eng. Data. 41 (1996) 546-550.

[27] A. Schumpe, G. Quicker, and W. Deckwer, Adv. Biochem. Eng./Biotechnol. 24 (1982) 1-38.

[28] J. Gros, C. Dussap, and M. Catte, Biotechnol. Prog. 15 (1999) 923-927.

[29] D. Lloyd, K. Thomas, G. Cowie, J. Tammam, A. Williams, J. Microbiol. Methods. 48 (2002) 289-302.

[30] S. Pratt, Z. Yuan, D. Gapes, M. Dorigo, R. Zeng, and J. Keller, Biotechnol. Bioeng. 81 (2003) 482-495.

FIGURES AND TABLES

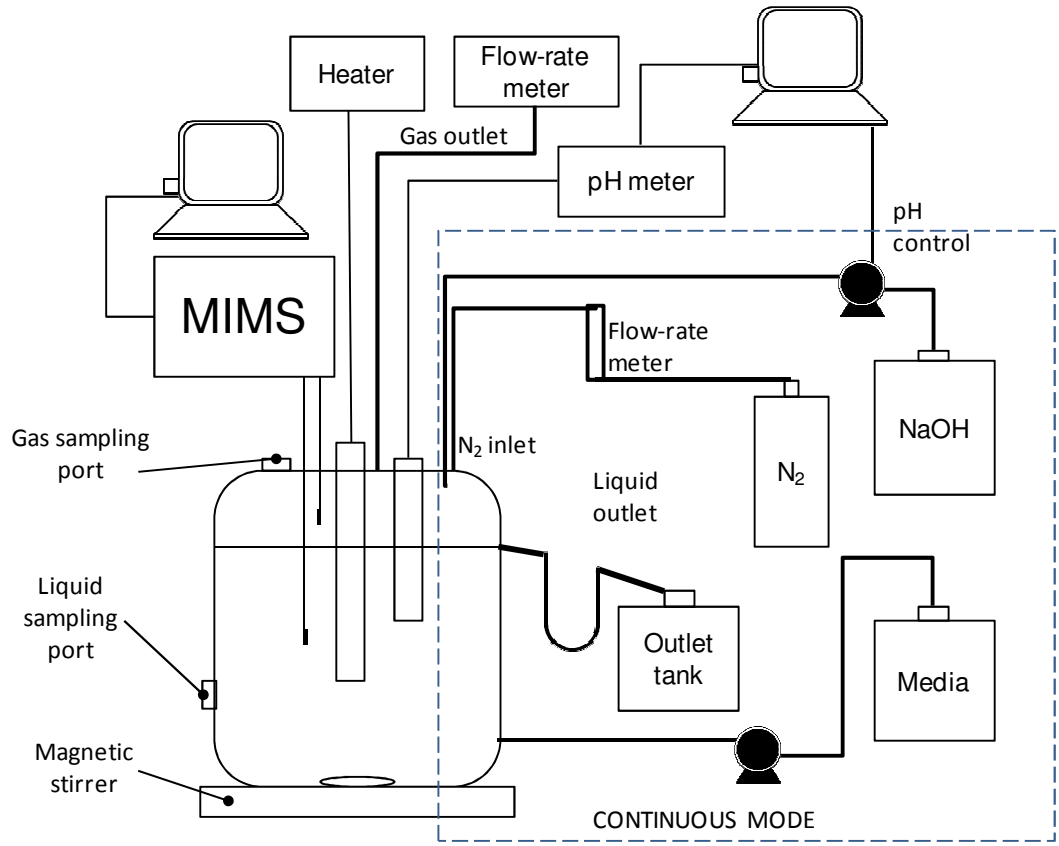

Figure 1: Reactor diagram. Modules surrounded by the dashed square were added to the rest of the equipments at the continuous fermentation mode.

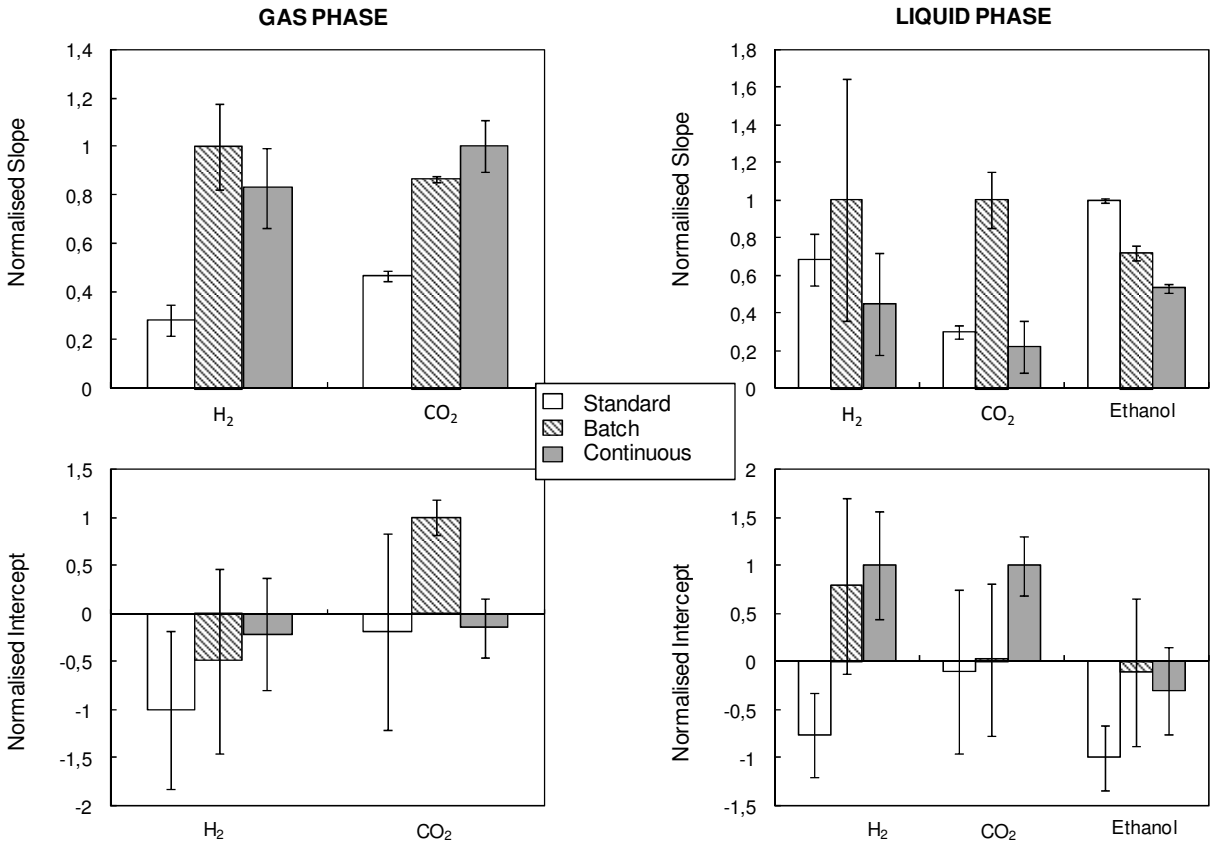

Figure 2: Correlation analysis between MIMS signals and H_2, CO_2, ethanol concentrations. Upper charts show normalised slopes for each targeted compound at standard, batch and continuous experiments, whilst lower charts depict normalised intercepts. Error bars are 95% confidence with appropriate t-values based on degrees of freedom.

Table 1: Calculated linear correlation parameters between MIMS signals and H_2, CO_2, ethanol, for standard, batch and continuous experiments, with a confidence range of 95%.

	Gas phase slopes (bar·faraday^{-1})		Liquid phase slopes (mM·faraday^{-1})		
	$H_2 \cdot 10^{-6}$	$CO_2 \cdot 10^{-5}$	$H_2 \cdot 10^{-5}$	$CO_2 \cdot 10^{-7}$	Ethanol$\cdot 10^{-9}$
Standard	0.9 ± 0.2	3.2 ± 0.2	8 ± 2	1 ± 0.1	10 ± 1
Batch	3.2 ± 0.6	6 ± 0.07	12 ± 8	3.4 ± 0.5	7 ± 4
Continuous	2.8 ± 0.6	7 ± 0.7	6 ± 4	0.8 ± 0.5	5 ± 1.5

	Gas phase intercept (bar)		Liquid phase intercept (mM)		
	H_2	CO_2	H_2	CO_2	Ethanol
Standard	-0.13 ± 0.11	-0.002 ± 0.013	-0.14 ± 0.08	-0.1 ± 0.8	-7.7 ± 2.6
Batch	-0.06 ± 0.14	0.01 ± 0.002	0.14 ± 0.16	0.02 ± 0.8	-0.6 ± 6.3
Continuous	-0.07 ± 0.08	-0.002 ± 0.004	0.18 ± 0.11	0.9 ± 0.3	-2 ± 2

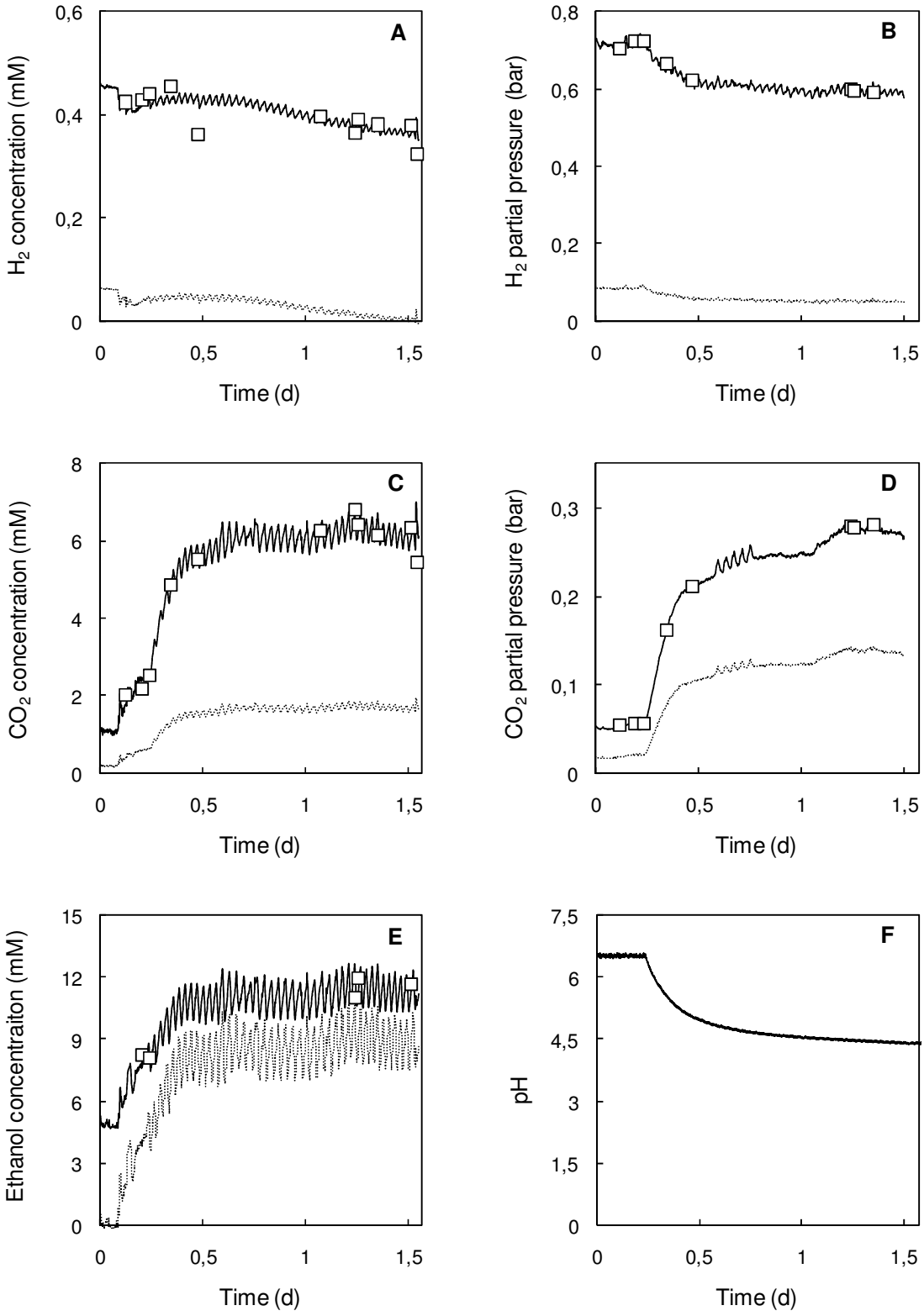

Figure 3: MIMS signal translation of batch fermentation kinetics using batch correlation parameters, solid line, and standard calibration, dashed line. Off-line experimental data set is depicted as white squares. A and B presents dissolved and gas phase H_2, C and D presents dissolved and gas phase CO_2, E shows ethanol while F presents pH kinetics.

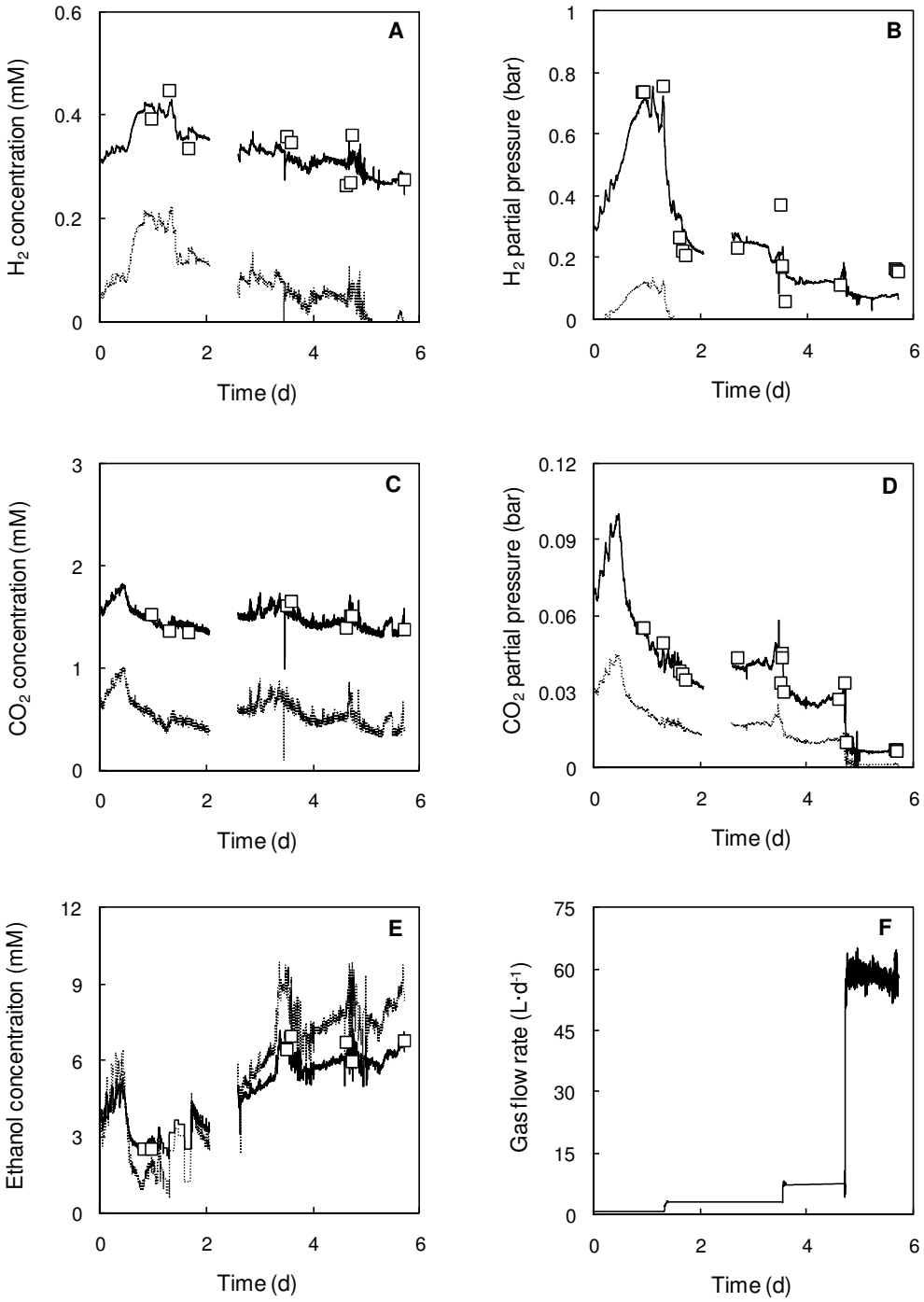

Figure 4: MIMS signal translation of continuous fermentation kinetics by in-process continuous correlation parameters, solid line, and standard calibration, dashed line. Off-line experimental data set is depicted as white squares. The dissolved and gas phase H_2 kinetics are presented in A and B, the same is presented for CO_2 in C and D, while ethanol is shown in E and gas flow rate is presented in F.

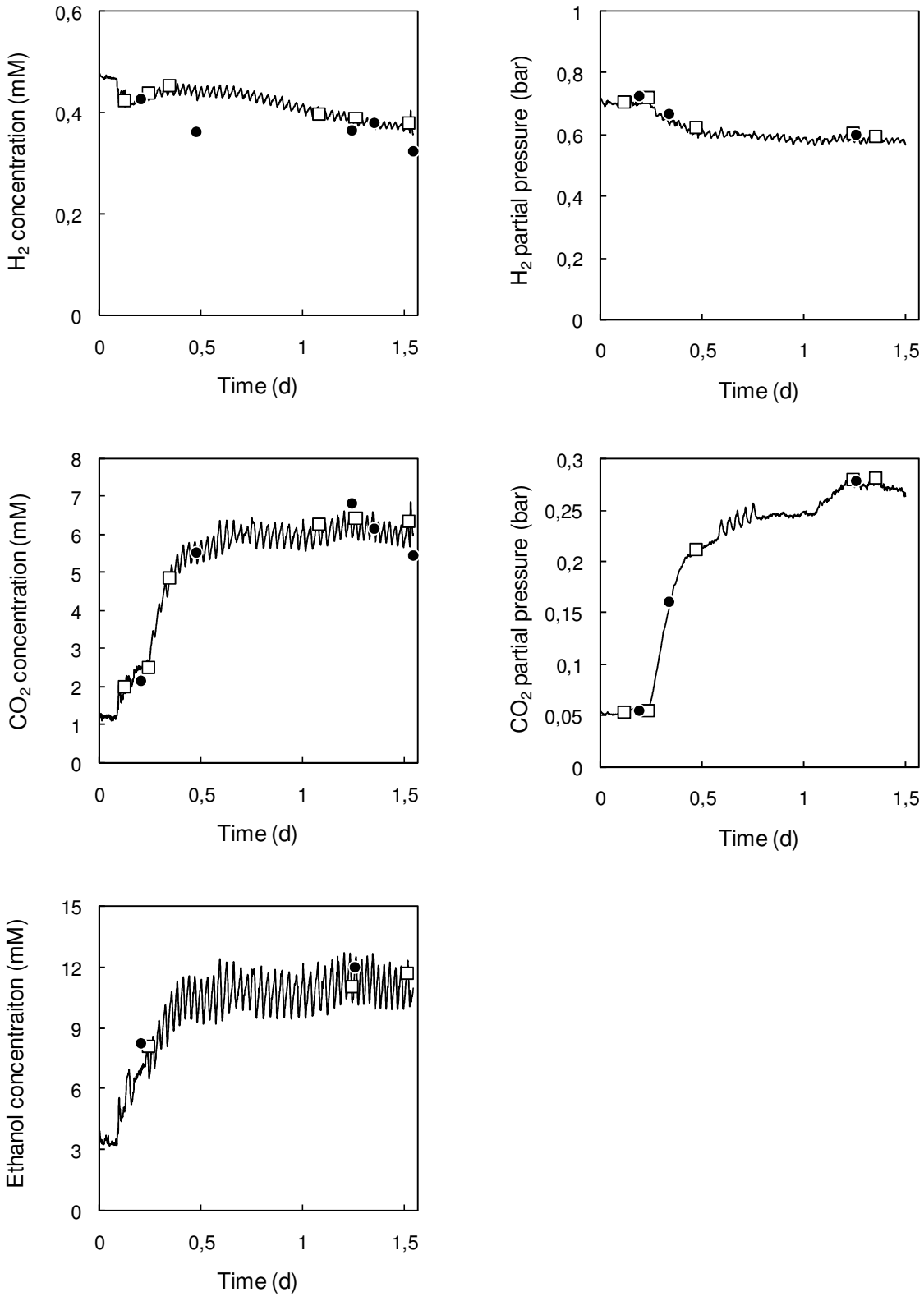

Figure 5: Batch fermentation kinetics showing MIMS signal translation by in-process calibration, solid line, which consists in dividing the off-line experimental data set into calibration points, white squares, and validation points, black circles.

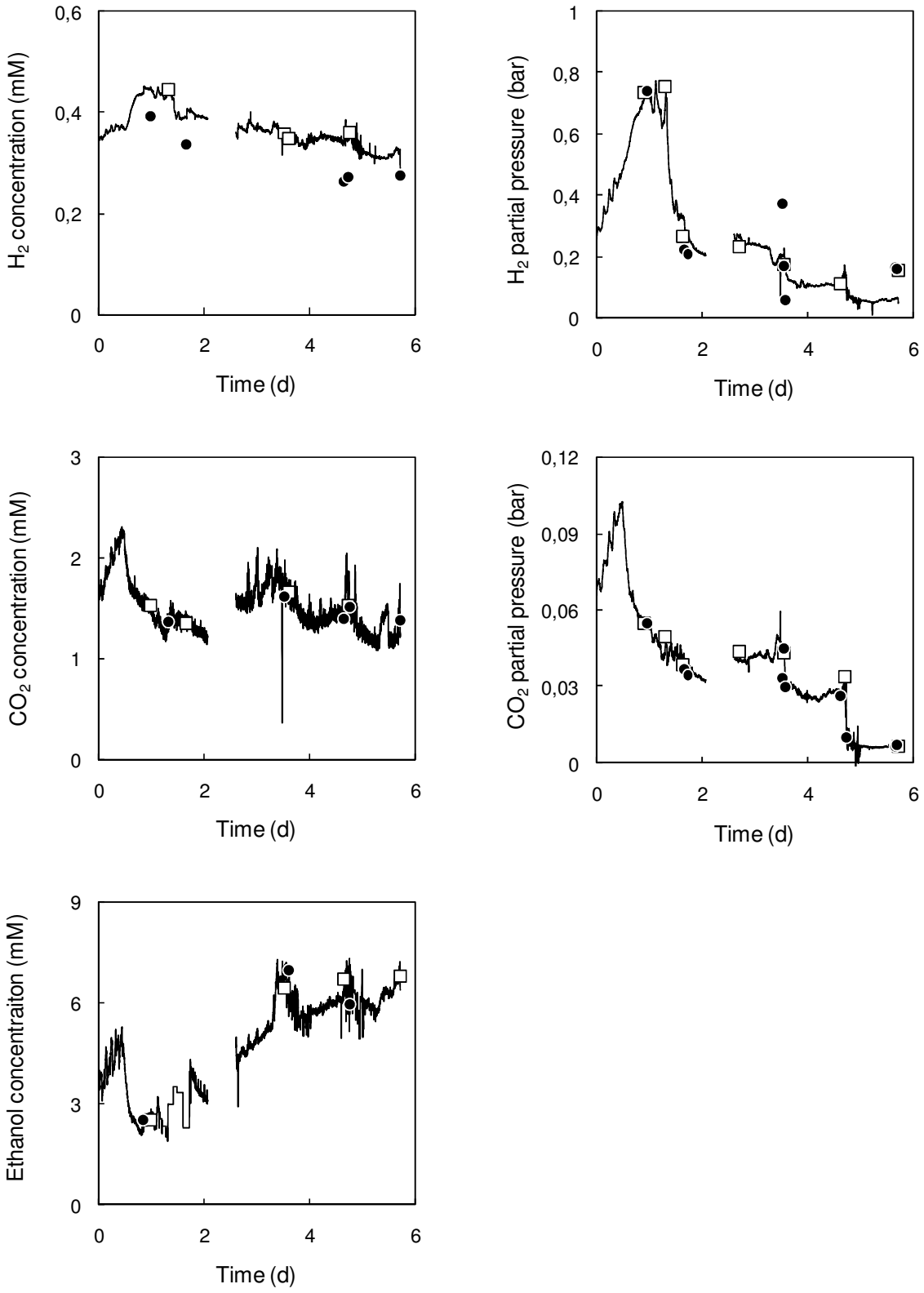

Figure 6: Continuous fermentation kinetics showing MIMS signal translation by in-process calibration, solid line. This consists in dividing the off-line experimental data set into calibration and validation points, white squares and black circles respectively. The lack of continuity in the solid lines was due to a shortcut.

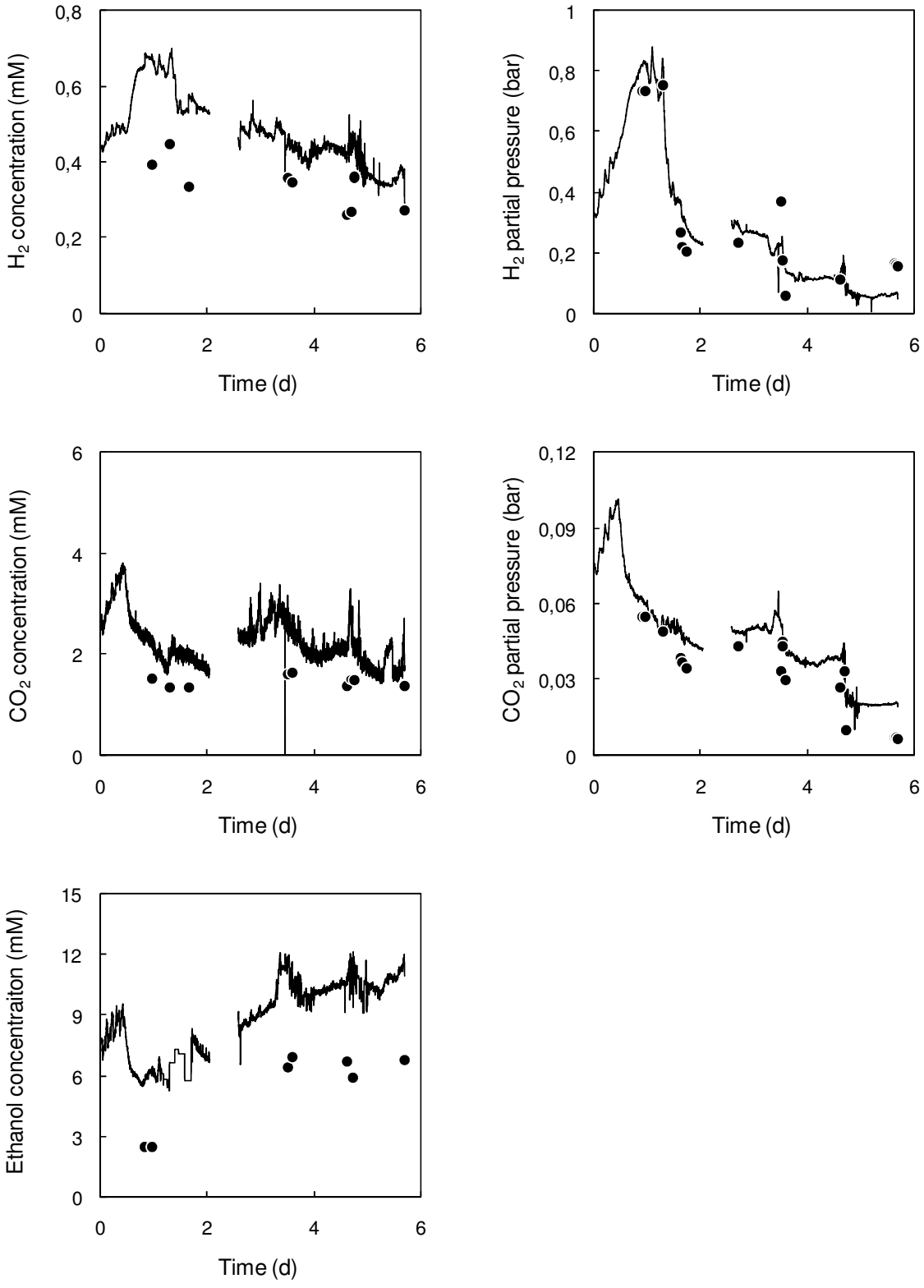

Figure 7: Kinetics of continuous fermentation showing in solid line their respective MIMS signals translation by batch correlation parameters. Off-line validation data set is presented in black circles.

Table 2: Average validation error and its standard deviation, calculated for in-process and prior-to-fermentation-run calibration strategies [(a)]. Validation errors are calculated as the difference between the calibrated MIMS signal and its respective off-line experimental validation point.

		Validation errors (%)				
		Gas phase		Liquid phase		
		H_2	CO_2	H_2	CO_2	Ethanol
Batch fermentation	In-process calibration	-3 ± 1.5	0.03 ± 3	-43 ± 35	1 ± 11	-11 ± 8
	Standard calibration	-90 ± 1.5	-55 ± 7	-91 ± 5	-72 ± 3	-30 ± 14
Continuous fermentation	In-process calibration	8 ± 70	7 ± 10	21 ± 10	3 ± 12	-3 ± 15
	Standard calibration	-130 ± 40	-62 ± 10	-70 ± 20	-62 ± 5	11 ± 40
	[(b)] Batch ferm. correlation	16 ± 60	64 ± 70	45 ± 20	50 ± 18	90 ± 35

[(a)] In this study it corresponds to standard calibration and continuous fermentation MIMS signal translation by batch fermentation correlation (see below).

[(b)] Continuous fermentation MIMS signal translation using the correlation parameters between targeted compound concentration and MIMS signal magnitudes of batch fermentation.

8.2 Thermodynamic analysis of energy transfer in acidogenic cultures

This present publication consists on the pre-refereeing document, in order to respect the Engineering in life sciences – Wiley-Blackwell restrictions concerning author archiving.

Reference: Bastidas-Oyanedel JR, Aceves-Lara CA, Ruiz-Filippi G, Steyer JP. Thermodynamic analysis of energy transfer in acidogenic cultures. Eng. Life Sci. 2008;8:487-498. DOI: 10.1002/elsc.200800044.

Thermodynamic Analysis of Energy Transfer in Acidogenic Cultures

Juan-Rodrigo BASTIDAS-OYANEDEL[1]*, César-Arturo Aceves-Lara[1], Gonzalo RUIZ[2], Jean-Philippe STEYER[1]

[1] INRA, UR50, Laboratoire de Biotechnologie de l'Environnement, Avenue des Etangs, Narbonne, F-11100, France.
[2] Escuela de Ingeniería Bioquímica, Pontificia Universidad Católica de Valparaiso, General Cruz, Valparaíso, Chile.

* oyanede@supagro.inra.fr
Tel: +33 4 68 42 51 51
Fax: +33 4 68 45 51 60

Running Title: Thermodynamic Analysis.
Keywords: Anaerobic digestion, biothermodynamics, energy transfer efficiency, Gibbs free energy dissipation.

Abstract

A global thermodynamic analysis has been done for steady state data sets from acidogenic cultures. This analysis has taken into account the energy transfer efficiency (ε) and the Gibbs free energy dissipation (ΔG_o) analysis of the different data as well. The thermodynamic analysis was done utilizing global mass and

electron balances, and standard Gibbs free energy of formation of the different chemical compounds presents in the studied cultures. In most of the studied cases, both ε and ΔG_o analysis show that chemotrophic anaerobic systems (as acidogenic cultures) are energetically efficient. These also show that both ε and ΔG_o are dependent of the environmental conditions as pH, stirring velocity or hydraulic retention time. A relationship between ε and ΔG_o was obtained too.

1 Introduction

Under anaerobic conditions, hydrogen is produced during conversion of organic wastes into organic acids which are then used for methane generation [1].

The anaerobic digestion processes are important for the treatment of urban and/or industrial organic waste. Together with its environmental friendship character and given the increasing interest in the effective use of natural resources, anaerobic digestion processes nowadays become an important source for the recovery-production of bioenergy and/or chemical building blocks [1-3]. The bioenergy can be recovered as methane or hydrogen, and among the chemical products acetate, propionate, butyrate, formate, lactate and ethanol are produced. This products range gives to this processes a flexible character, being possible to maximize the productivity of any of the products. The anaerobic digestion (for waste treatment) is a mixed culture fermentation, where the factors that determine product formation distribution in different environmental conditions are still unclear despite extensive research efforts. In order to obtain more insight of these processes a global analysis of the energy transfer, based on thermodynamics, from the substrates to products in acidogenic cultures (producing hydrogen and a mixture of chemicals) was done, work that will help to begin the study of the optimization of product formation.

As in any biotechnological process involving microbial cultures biomass yield is one of the key parameters, since it determines the final biomass concentration reached after substrate consumption, i.e. it allows one to understand the behavior of microorganism in the environment [4,5]. Mathematical models of biological systems are based in this quantitative parameter which allows to quantify substrate utilization, product formation and biomass generation [6], which must imperatively be optimized in order to obtain reasonable productivities [5]. Prediction of biomass yield allows optimization of biological processes using estimation methods, and this prediction

requires a fundamental understanding of the phenomena controlling bacterial systems [4,6]. Equilibrium thermodynamics plays an important role in chemistry, chemical engineering and in chemical process development. In biotechnology, thermodynamic analysis is hardly ever applied. Based on such analyses, it ought to be possible to roughly estimate key parameters of biotechnological cultures and thus to address the economic viability of the process before even performing experiments [5]. Equilibrium thermodynamic methods to predict true yield and stoichiometry of bacterial reactions have been widely used in biotechnology [7], however they are sometimes far from experimental results where many factors as experimental errors, maintenance energy estimates, and simplifying assumptions are present [4].

Microbial growth occurs spontaneously and is a highly irreversible phenomenon. It must therefore be coupled with the production of entropy. Entropy may be exchange with the environment due to heat transfer to or from the cell, and exchanging products of higher entropy than substrates [4,5]. The relationship between the driving force for microbial growth ΔG_o (or dissipation energy) and the biomass yield $Y_{x/s}$ is best understood by splitting the macrochemical reaction into a catabolic and an anabolic part. Formation of biomass clearly produces matter with high Gibbs energy due to its low entropy content and therefore increases the Gibbs energy in the bioreactor. Anabolic reactions taken by themselves are thus subjected to a driving force in the opposite sense of growth and are endergonic. In order to pull the anabolic reactions against this driving force up-hill, they are coupled to catabolism, which is characterized by a large negative ΔG and thus is highly exergonic. The net driving force ΔG_o remaining for the whole process clearly depends on the stoichiometric load anabolism places on catabolism, i.e. in the biomass yield [5]. Thus, the Gibbs energy lost due the generation of entropy in the irreversible growth process is represented as a decrease in energy available for synthesis [6]. In other terms, this decrease would be treated as an efficiency of energy transfer ε from the substrates to the biomass. It has been widely hypothesized that energy transfer efficiency is not a constant, but rather is controlled by environmental conditions. If this is true, the thermodynamic method for bacterial yield prediction will remain limited to cases when optimal conditions ensure predictable, high energy capture efficiencies. The next great challenge for bacterial yield prediction with thermodynamics is to understand how environmental conditions affect energy efficiency [4,5].

The objective of this study is to analyze and compare the behavior of ε and ΔG_o in different environmental conditions of acidogenic fermentations. In the scientific literature ε is indeed considered (or fitted) as constant [4,5,8]. However, the analysis of experimental data obtained in our laboratory [9] and in another study [10] shows that ε should be better considered as a function of environmental variables such as stirring velocity, hydraulic retention time or pH.

2 Materials and Methods

2.1 Materials

Two different acidogenic (anaerobic) chemostat mixed culture reactor data sets were analyzed. The first are from our laboratory [9] and the second from Temudo *et al.* (2007) [10].

2.1.1 Reactor design and analytical methods

The Aceves-Lara *et al.* (2008) [9] data were performed using a continuous stirred reactor of 2 *l* with a working volume of 1.125 *l*, equipped with a mechanical stirring system and a revolution counter to access to the measurement on the stirring velocity. The gas flow rate was measured with an electronic gas volumeter. The reactor was also equipped with two sensors for measuring the redox potential and pH. The pH-meter and the transmitter for redox potential were connected to a computer for on-line data acquisition. The pH was controlled by automatic addition of NaOH (2M). The temperature was controlled by a heating electric resistance, and maintained constant at 37±0.08°C.

Gas composition (H_2 and CO_2) was analyzed by manual sampling using a gas chromatograph. In the liquid phase, acetic acid, propionic acid, butyric and iso-butyric acids, valeric and iso-valeric acids were determined by liquid injection into a gas chromatograph. The presence of sugar, lactic acid, ethanol and acetone was confirmed by an High Performance Liquid Chromatography analysis.

Biomass was determined through the volatile suspended solid concentration measured according to the standard method of the APHA (1995) [9].

A complex cultivation media including molasses resulting from the sugar beet production were used as carbon and energy source, diluted to a concentration of 9.4g/l equivalent in glucose by adding a nutritional medium rich in minerals [9].
The inoculum was prepared with 1 *l* of sludge taken from an anaerobic methane digester fixed bed reactor of $1m^3$ used for several years for the treatment of wine distillery wastewater. The sludge was centrifuged before inoculating. The reactor was stripped with nitrogen for 15 min before continuous feeding was applied.
The data from Temudo *et al.* (2007) [10] were performed in a continuous stirred reactor of 3*l* with a working volume of 2*l* . Temperature was maintained constant at 30±1℃ using a water jacket. The reactor was sparged with nitrogen gas at a flow rate of 120 ml/min, to maintain anaerobic conditions. The pH was controlled (pH±0.1) by automatic titration with 4 M NaOH and HCl solutions.

The inoculum consisted of a mixture of two sludges obtained from two different sources. The first inoculum was from a distillery wastewater treatment plant. The second inoculum was a sludge solution from a potato starch processing acidification tank. Before each experiment the reactor was freshly inoculated with approximately 20g of each inoculum, and operated in batch conditions until biomass growth was observed.

A well defined cultivation medium contained as a carbon and energy source glucose at final concentration of 4.0 g/l and a solution of mineral described in [10].
Glucose, acetate, propionate, butyrate, iso-butyrate, valerate, iso-valerate, caproate, lactate, succinic acid, formic acid were determined by HPLC. Ethanol, propanol, and butanol were determined by gas chromatography. Measurements of H_2 and CO_2 were performed on-line with a infrared gas detection system coupled to the bioreactor outlet. Total dissolved and suspended chemical oxygen demand (COD) were measured in the influent and in the reactor liquid with the Dr Lange kit for the range 1,000–10,000 mgCOD/l. Total organic carbon (TOC) and total inorganic carbon (TIC) were measured using a Shimadzu TOC 5050A analyzer. For total TOC and COD in samples with suspended solids, the samples were first homogenized through cell disruption during 15 s in an ultrasound bath. The inorganic carbon was also estimated from the off-gas concentration of CO_2 based on the mass transfer

coefficient (k_La) of the system and the acid-base equilibrium constants for inorganic carbon dissociation. The k_La was measured for oxygen and corrected for molecular hydrogen and carbon dioxide based on the relative diffusivity coefficients. The diffusion coefficient for oxygen, molecular hydrogen and carbon dioxide used were 2.1, 5.0, and $1.92 \cdot 10^{-9}$ m^2 s^{-1} and corrected for temperature according to the Stokes–Einstein relation [10].

The biomass dry weight was determined after filtration according to the standard methods (Greenberg et al., 1992) [10]. The yields of the fermentation products were calculated per glucose consumed, corrected for the dilution factor of the base added to control pH.

2.1.2 Experimental design

In the work of Aceves-Lara *et al.* (2008) [9], in order to determine the influences of pH, HRT, stirring velocity and their interactions on the hydrogen production, a factorial experimental design of three factors duplicated and two levels with a central point was defined. In the present analysis this central point was not utilized, whereas the central point was conducted with an HRT of 10 h, pH of 5.75 and stirring velocity of 225 rpm. Overall, nine different operating conditions were applied, carrying out a total of 18 experiments. The retention times were 6 and 14 h, pH 5.5 and 6 and the stirring velocity 150 and 300 rpm for the factorial points Each operating condition was maintained for a duration ranging from 5 to 8 HRT in order to reach a steady state.

Measurements of the different concentrations in liquid and gas phases were performed after reaching each steady state.

Reynolds number for these stirring velocities were calculated, they were 6250, 9375 and 12,500, respectively, for 150, 225 and 300 rpm. These Reynolds number show that the stirring velocity is turbulent, then it is possible to assume well stirred conditions.

In Temudo *et al.* (2007) [10], to evaluate the impact of the pH on the product distribution during glucose fermentation by an undefined mixed microbial culture, 9 experiments were performed at pH values ranging from 4 to 8.5. The experiments at pH 4, 4.75, 5 and 5.5 were performed at a HRT of 20 h given the difficulties of

reaching a steady state at these pH-values. While the experiments at pH 5.5, 6.25, 7, 7.75 and 8.5 were performed at a HRT of 8 h.

To characterize the product spectrum at each pH, the reactor was run in continuous mode until a stable product composition and a biomass concentration was established. It took always approximately 3 weeks to reach stable operation, which means more than 25 generation times at low pH, and more than 60 generation times at pH higher than 5.5. The gas productivities (H_2 and CO_2) and the base added for pH control are monitored on-line, allowing for direct analysis of the system stability. When these three rate measurements were stable or varied within a limited range (±10%), not tending to increase or decrease, a set of samples was taken during the following week. Concentrations of soluble organic fermentation products and biomass concentration in the reactor volume were determined.

2.2 Methods

In order to analyze both experimental data sets thermodynamically, we differentiate three parts, **inputs**, **mathematical models** and **outputs** as is depicted in Figure 1. Our inputs correspond to the experimental data concentrations (C_i); electron donor acceptor half reactions stoichiometry (v_{ij}) and standard free energy of formation ($\Delta Gf_i°$). The inputs are combined into mathematical models to calculated global yield coefficients ($Y_{i/s}$), standard free energy of reaction ($\Delta G_j°$), free energy of reaction at the actual compounds concentrations ($\Delta G_j'$) and free energy of global catabolic (ΔG_e) and biosynthesis (ΔG_s) reactions. To these ends, two mathematical models are utilized: Liu *et al.* (2007) [11] and McCarty (2007) [8], and they are briefly explained in part 2.2.2. Finally the outputs are the energy transfer efficiency (ε) and the free energy of dissipation (ΔG_o).

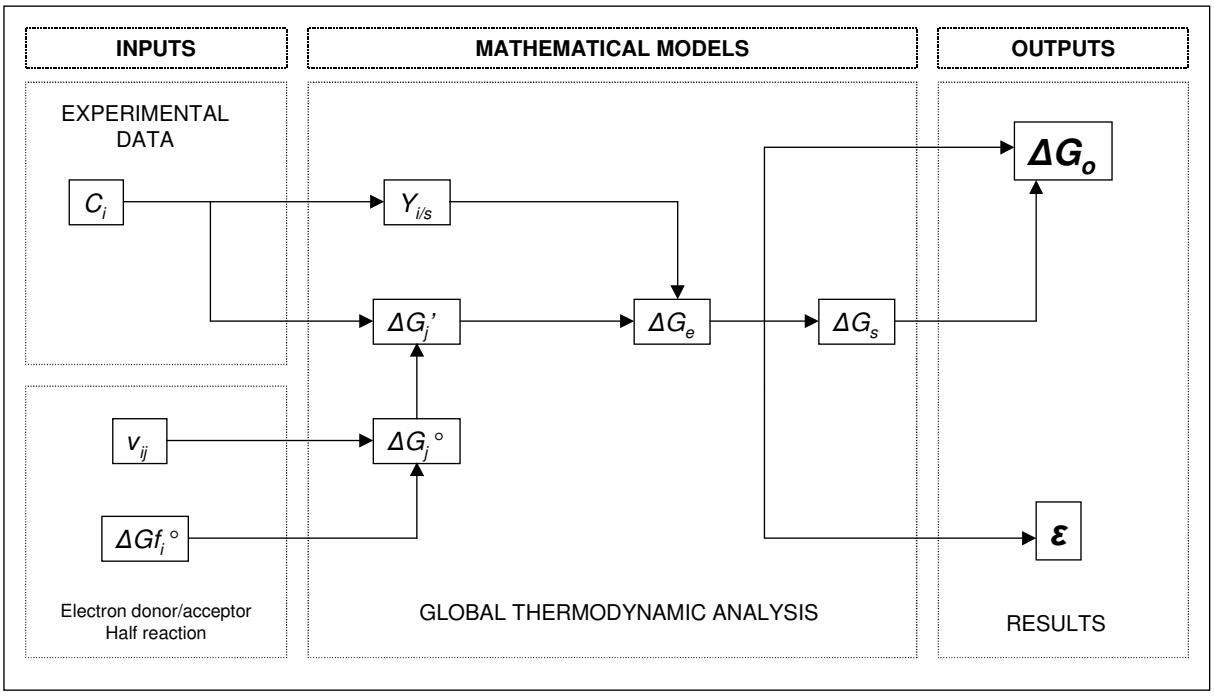

Figure 1: Simplified thermodynamic Analysis Diagram.

A further explanation of the construction of electron donor/acceptor half reaction and its stoichiometry is given in section 2.2.1. Together with, the reactions utilized for both data sets are given. In section 2.2.2 the calculation of $\Delta G_j°$, $\Delta G_j'$, ΔG_e, ΔG_s, ε and ΔG_o it is explained.

2.2.1 Global stoichiometry

Microbial heterotrophic metabolism can be simplified and represented as a global reaction which is the result of the combination of two processes: the energy releasing catabolism and the energy consuming anabolism. In the catabolism a substrate (an electron donor substrate) is converted to a product and metabolic energy is generated. In anabolism, the numerous biomass components are constructed from nutrients (carbon and nitrogen sources), electrons to send to the electron acceptor to generate Gibbs energy to drive synthesis reactions, under consumption of energy. Clearly, the electron and energy balances are inter-related [6,12]. Uncoupling between the catabolism and anabolism can be established by consumption of energy for non-growth related maintenance process [12]. Neglecting energy consumption for maintenance purposes, the catabolic and anabolic fluxes would be coupled by a stoichiometric relationship.

Catabolism

Catabolism, i.e. the energy and electrons supplier for biomass synthesis can be divided into electron donor and acceptor reactions. Half reactions for an electron donor and an electron acceptor can be combined to produce an energy reaction with its associated Gibbs free energy (ΔG_e). Half reactions for electron donor and cell synthesis can be combined to produce the synthesis reaction, from which the Gibbs free energy for synthesis is derived (ΔG_s). A Global reaction for cell growth is obtained by combining in proper proportion the energy reaction and synthesis reaction (**Anabolism**). This proportion depends upon the energy transfer efficiency ε as is explained by [8], and is represented by the experimental yield coefficients ($Y_{i/s}$). These relationships are depicted in a simplified way in Figure 2:

Electron donor/acceptor half reactions and energy catabolism reaction			
$S \rightarrow EA + (\gamma_d - \gamma_{EA})e$		ΔG_d	Electron donor reaction
$\alpha \cdot \gamma_{EA} \cdot e \rightarrow \alpha\, EA$		ΔG_a	Electron acceptor reaction
$S \rightarrow \frac{\gamma_d}{\gamma_{EA}} EA$		ΔG_e	Energy catabolism reaction

Synthesis and energy reactions and global reaction			
$S \cdot \left(Y_{x/s} \frac{\gamma_x}{\gamma_d}\right) \rightarrow \frac{\gamma_d}{\gamma_x} X \cdot \left(Y_{x/s} \frac{\gamma_x}{\gamma_d}\right)$		ΔG_s	Synthesis reaction
$S \cdot \left(1 - Y_{x/s} \frac{\gamma_x}{\gamma_d}\right) \rightarrow \frac{\gamma_d}{\gamma_{EA}} EA \cdot \left(1 - Y_{x/s} \frac{\gamma_x}{\gamma_d}\right)$		ΔG_e	Energy reaction
$S \rightarrow Y_{x/s} X + Y_{EA/S} EA$		ΔG_o	Global reaction

Figure 2: Simplified schema of global reaction.

Electron donor/acceptor half reactions

In order to balance these two equations, we follow the electron balance (reduction degree (γ) balance), carbon balance and nitrogen balance, in this order.

To introduce the reduction degree of a compound, γ, a redox neutral compound for each element of interest it is define arbitrary. In our case, CO_2 for Carbon, NH_3 for

Nitrogen and H_2O for Oxygen. With this set of neutral compounds and with the unit of redox defined as $\gamma_H = 1$, one obtains the following redox levels of the three listed elements [13]:

$$\gamma_C = 4 \qquad \gamma_N = -3 \qquad \gamma_O = -2$$

Now the degree of reduction of any compound taking place in this work (analysis) can be calculated as the sum of the total reduction degree of each element in the compound as is shown in the Equation 1:

Equation 1

$$\gamma_i = Cc_i \cdot \gamma_C + Nc_i \cdot \gamma_N + Oc_i \cdot \gamma_O + Hc_i \cdot \gamma_H$$

where Cc_i, Nc_i, Oc_i and Hc_i are the carbon, nitrogen, oxygen and hydrogen composition of the i compound respectively.

Then for each half electron donor/acceptor j reaction, the electron balance is expressed as in Equation 2:

Equation 2

$$\sum_i \nu_{ij} \gamma_i = 0$$

The equation which relates electron donor and acceptor reactions represents the proportion of the electron donor acceptor reaction in order to balance the electrons donated and accepted as is shown in Equation 3:

Equation 3

$$\gamma_{EA}(1+\alpha) = \gamma_d$$

Carbon and nitrogen balances follow the Equations 4 and 5:
Carbon balance:

Equation 4

$$\sum_i \nu_{ij} Cc_i = 0$$

Nitrogen balance:

Equation 5

$$\sum_i \nu_{ij} Nc_i = 0$$

In Table 1 and 2 are summarized the electron donor half reaction for both data sets utilized in these study. For Aceves-Lara *et al.* (2008) [9] the electron acceptor compounds were acetic acid, propionic acid, butyric acid and hydrogen. And for Temudo *et al.* (2008) [10] the electron acceptors were acetic acid, propionic acid, butyric acid, formic acid, ethanol, lactic acid, succinic acid, glycerol and hydrogen.

	Aceves-Lara *et al.* (2008)			
Electron donor	Acetic acid	$Glc + 2H_2O$	$\rightarrow$	$2\,Act + 8H^+ + 2CO_2 + 8e$
	Propionic acid	$Glc + 2H_2O$	$\rightarrow$	$Prn + 10H^+ + 3CO_2 + 10e$
	Butyric acid	Glc	$\rightarrow$	$Btr + 4H^+ + 2CO_2 + 4e$
	Hydrogen	$Glc + 6H_2O$	$\rightarrow$	$6H2 + 12H^+ + 6CO_2 + 12e$
Electron acceptor	Acetic acid	$2CO_2 + 8H^+ + 8e$	$\rightarrow$	$Act + 2H_2O$
	Propionic acid	$10H^+ + 2.14CO_2 + 10e$	$\rightarrow$	$0.71Prn + 2.86H_2O$
	Butyric acid	$4\,H^+ + 0.8CO_2 + 4e$	$\rightarrow$	$0.2Btr + 1.2\,H_2O$
	Hydrogen	$12H^+ + 12e$	$\rightarrow$	$6H_2$

Table 1: Half electron donor acceptor reactions for Aceves-Lara et al. 2008 [9].

	Temudo *et al.* (2007)			
Electron donor	Acetic acid	$Glc + 2H_2O$	→	$2Act + 8H^+ + 2CO_2 + 8e$
	Propionic acid	$Glc + 2H_2O$	→	$Prn + 10H^+ + 3CO_2 + 10e$
	Butyric acid	Glc	→	$Btr + 4H^+ + 2CO_2 + 4e$
	Formic acid	$Glc + 6H_2O$	→	$Frm + 22H^+ 5CO_2 + 22e$
	Ethanol	$Glc + 3H_2O$	→	$EOH + 12H^+ + 4CO_2 + 12e$
	Lactic acid	$Glc + 3H_2O$	→	$Lct + 12H^+ + 3CO_2 + 12e$
	Succinic acid	$Glc + 2H_2O$	→	$Scn + 10H^+ 2CO_2 + 10e$
	Glycerol	$Glc + 3H_2O$	→	$GOH + 10H^+ + 3CO_2 + 10e$
	Hydrogen	$Glc + 6H_2O$	→	$12H^+ + 6H_2 + 6CO_2 + 12e$
Electron acceptor	Acetic acid	$8H^+ + 2CO_2 + 8e$	→	$Act + 2H_2O$
	Propionic acid	$10H^+ + 2.14CO_2 + 10e$	→	$0.71Prn + 2.85H_2O$
	Butyric acid	$4H^+ + 0.8CO_2 + 4e$	→	$0.2Btr + 1.2H_2O$
	Formic acid	$22H^+ + 11CO_2 + 22e$	→	$11Frm$
	Ethanol	$12H^+ + 2CO_2 + 12e$	→	$EOH + 3H_2O$
	Lactic acid	$12H^+ + 3CO_2 + 12e$	→	$Lct + 3H_2O$
	Succinic acid	$10H^+ + 2.86CO_2 + 10e$	→	$0.71Scn + 2.86H_2O$
	Glycerol	$10H^+ + 2.14CO_2 + 10e$	→	$0.71GOH + 2.14H_2O$
	Hydrogen	$12H^+ + 12e$	→	$6H_2$

Table 2: Half electron donor/acceptor for Temudo et al. 2007 [10].

Biosynthesis reaction

Utilizing a biomass composition of $C_5H_7O_2N$ [8], the biomass synthesis reaction was constructed, as shown in Table 3. This reaction was applied for both data set analysis.

Biomass synthesis	$Glc + 1.2NH3$	→	$1.2X + 3.6H_2O$

Table 3: Biomass synthesis reaction.

2.2.2 Thermodynamic analysis

Basis

The standard free energy changes $\Delta G°$ associated with the partial reactions of energy metabolism have been calculated from free energy of formation data $\Delta Gf_i°$ form ([6,8,14]) and the relationship with the stoichiometric coefficients v_{ij} as is shown in Equation 6:

Equation 6

$$\Delta G_j^o = \sum_i^n \nu_{ij} \cdot \Delta Gf_i^o$$

ΔG° is the increment of free energy for the reaction under standard conditions, which are 298.15 K (25°C) and a pressure of 1 atm. In aqueous solution, the standard condition of all solutes is 1 M, that of water is the pure liquid. $\Delta Gf_i°$ refers to the standard free energy of formation from the elements of the substrates and the products [14].

But under real conditions, the concentrations of substrates and products are different than 1M and 1 atm. This is considered in ΔG', which are calculated using Equation 7:

Equation 7

$$\Delta G_j^{'} = \Delta G_j^o + R \cdot T^o \sum_i^n \nu_{ij} \ln(C_i)$$

where C_i are the actual concentrations (in M for aqueous phase, and in atm for gas phase) of all compounds participating in the reaction, R universal gas constant and T° the standard temperature (298.15 K) [14].

Relationship between thermodynamics and biomass yield

In anaerobic digestion, as in any living-systems, the energy balance can be done, as is shown in Equation 8:

Equation 8

$$\frac{\Delta G_e}{Y_{x/s}} = \Delta G_o - \Delta G_s$$

knowing that the energy released from the energy source consumed (left hand of Equation 8) is equal to the energy consumed for biomass synthesis (second term to the right hand of Equation 8) and the dissipation energy (i.e. net entropy production due to the irreversible processes of cell growth increases the cost of cell synthesis (first terms to the right hand of Equation 8) [5]. However, reformulating as is shown in the Equation 9:

Equation 9

$$\left(\left[1-Y_{x/s}\cdot\frac{\gamma_x}{\gamma_d}\right]\Delta G_e^{eeq}\right)\cdot\varepsilon=-\left(Y_{x/s}\cdot\frac{\gamma_x}{\gamma_d}\right)\Delta G_s^{eeq}$$

the energy consumed for biomass synthesis (right hand of Equation 9) is equal to the energy released from the energy source consumed (first terms to the left hand of Equation 9) multiplied by an energy transfer efficiency (i.e., efficiency of energy captured by the organisms), called "ε" ([4,8]). In the scientific literature, this parameter is indeed considered (or fitted) as constant [4,5,8]. However, the analysis of experimental data obtained in our laboratory [9] and in Temudo *et al.* (2007) [10] study shows that ε should be better considered as a function of environmental variables such as stirring velocity, hydraulic retention time or pH.

Equation for ε calculation

ΔG_e is determined from the free energy change of the half electron donor (ΔG_d) and acceptor (ΔG_a) reactions, as in Equation 10:

Equation 10

$$\Delta G_e=\Delta G_d+\Delta G_a$$

ΔG_s consists of two energy terms, one for the conversion of the electron donor to an intermediate compound, ΔG_{ic}, and another for conversion of the intermediate to cells, ΔG_{pc}, as in Equation 11:

Equation 11

$$\Delta G_s=\frac{\Delta G_{ic}}{\varepsilon^n}+\frac{\Delta G_{pc}}{\varepsilon}$$

Energy may be required to convert the cell carbon source to the intermediate compound (ΔG_{ic} >0), in which case n = 1, or it may be obtained from the conversion itself when ΔG_{ic} <0, in which case n=-1. The intermediate compound was taken to be acetyl-CoA with a half-reaction reduction potential of 30.9kJ/eeq (ΔG_{in}) [8], thus as in Equation 12:

Equation 12

$$\Delta G_{ic}=\Delta G_{in}+\Delta G_d$$

Delta ΔG_{pc} was estimated from reported values of ATP in moles required for cell synthesis, and with an assumed cell relative composition of $C_5H_7O_2N$ was set equal to 18.8 kJ/eeq when ammonia serves as the source for cell synthesis [8].

Then it is possible to calculate epsilon:

If $\Delta G_{ic} < 0$ then n =-1, and

Equation 13

$$\varepsilon = \left(\frac{\Delta G_{pc}}{\Delta G_e \left[1 - \frac{\gamma_d}{\gamma_x \cdot Y_{x/s}} \right] - \Delta G_{ic}} \right)^{0.5}$$

If $\Delta G_{ic} > 1$, then n=1, and

Equation 14

$$\varepsilon = \left(\frac{\Delta G_{pc} + \Delta G_{ic}}{\Delta G_e \left[1 - \frac{\gamma_d}{\gamma_x \cdot Y_{x/s}} \right]} \right)^{0.5}$$

Equation for Gibbs energy dissipation

Where ΔG_e, ΔG_s and $Y_{x/s}$ are calculated from experimental data, ΔG_o is calculated as in Equation 15.

Equation 15

$$\Delta G_o = \frac{\Delta G_e}{Y_{x/s}} + \Delta G_s$$

3 Results and Discussions

The results present in Figure 3 were obtained as is shown in the diagram of Figure 1 (section 2.2), utilizing the equation presented in sections 2.2.1 and 2.2.2. The present analysis suggests a dependence of ε and ΔG_o with operational (environmental) conditions such as the stirring velocity (rpm), Hydraulic Retention Time (HRT) and pH.

In Figure 3A, at pH 5.5, the increase of the stirring velocity leads to an increase of ε. At HRT = 14h, it increases by 2.9% from 150 to 300 rpm and, at HRT = 6h, it increases by 11.4%. In contrast, at pH 6.0, ε decreases with increase of stirring velocity: at HRT = 14h, it decreases by 11.1% and, at HRT = 6h, it decreases by 8.1%. The reason of this influence is not clear.

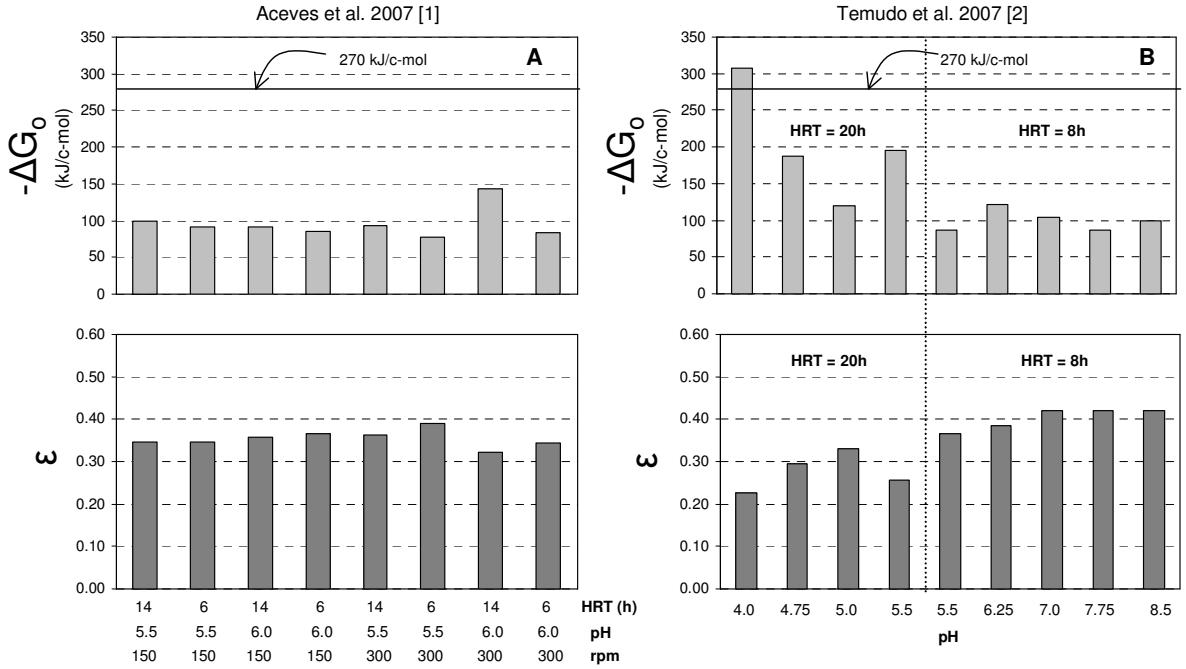

Figure 3 : ε (bottom) and energy dissipation $-\Delta G_o$ (top) versus operational conditions. A data ser from Aceves *et al.* (2008) [9]; B data from Temudo *et al.* (2007) [10].

The HRT influence on ε is clearer. A decrease of HRT increases ε: in Figure 3A, the range of increment is 0.16% - 7.3% for decreasing HRT from 14h to 6h; in Figure 3B, the most dramatic increase of ε occurs (42.35%) when the HRT decreases from 20h

to 8h (at pH 5.5). This can be compared with Figure 2A: at 300 rpm, pH 5.5 and a HRT decreasing from 14h to 6h, ε increases only by 7.3%. The reason of this influence seems to be related with maintenance energy consumption.

The pH influence is not clear when combining it with other operational variables: in Figure 3A, the increase of pH from 5.5 to 6.0 at a stirring velocity of 150 rpm increases ε by 2.9% and by 5.71% for HRT 14h and 6h respectively. But the same pH increase at a stirring velocity of 300 rpm decreases ε by 11.1% and 12.8% for HRT 14h and 6h respectively.

In Figure 3B, at HRT 20h, ε has a maximum value of 0.33 at pH 5.0 in the pH range 4.0 - 5.5 and, for HRT of 8h, ε reaches a maximum value of 0.42 in the pH range 7.0 - 8.5. The minimum value of ε (0.23) for pH 4.0 can be explained by a pH inhibition, and the decrease at pH 5.5 is due to a change in metabolism shifting the product distribution from butyrate, acetate and hydrogen (H_2) into acetate, ethanol and formate [10].

At the top of Figure 3, $-\Delta G_o$ are plotted for each data set. The line represents the estimation of $-\Delta G_o$ as in [11] for aerobic cultures. The only operating condition which reaches this estimated value is at pH 4 (see Figure 2B) where ε is also close to the range for aerobic cultures as in [8]. The rest of data are below this value confirming the fact that anaerobic cultures are more efficient in energy utilization [8].

This analysis shows a relationship between ε and $-\Delta G_o$. This relationship is depicted in Figure 4 using both data set values. Notice that both data set are from mixed culture fermentations, where the ecosystem composition are unknown, and these variable would be responsible of the R^2 0.6705. Another remark is that for these systems ε have a maximum value corresponding to 0.48 as $-\Delta G_o$ = 434.31 (kJ/c-mol).

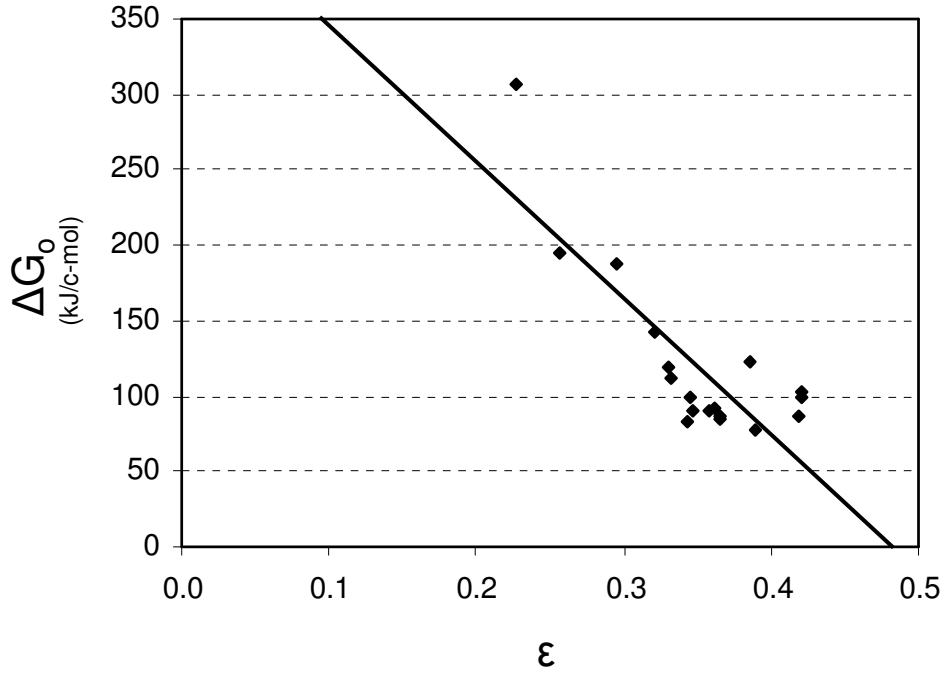

Figure 4 : Relationship between energy dissipation ($-\Delta G_o$) and energy transfer efficiency (ε).

5 Conclusion

From this analysis of experimental data sets, the energy transfer efficiency for acidogenic cultures is not constant but seems to be controlled by operational conditions. Further work will focus onto mathematical modeling of ε and ΔG_o.

Additional studies with acidogenic pure cultures will help to compare it with ecological diversity found in the considered experiments and to determine if the ecological diversity is another factor that should be accounted for.

A final approach would be the analysis of the metabolic pathways since this study has been done considering biomass only as a black box.

It is critical to note that equilibrium thermodynamics applies only to reversible processes since by definition irreversible processes, as microbial growth cannot reach equilibrium. However a non-equilibrium thermodynamic approach is necessary.

Abbreviation list

ΔG_a	Free energy change of the half electron acceptor reaction (kJ/mol).
$\Delta G_j°$	Standard free energy of reaction (kJ/mol).
$\Delta G_j'$	Free energy of reaction at the actual compound concentrations (kJ/mol).
ΔG_d	Free energy change of the half electron donor reaction (kJ/mol).
ΔG_e	Gibbs free energy of catabolic reaction (kJ/mol)
ΔG_e^{eeq}	Gibbs energy of catabolic reaction (kJ/eeq)
ΔGf_i^o	Standard free energy of formation (kJ/mol)
ΔG_{ic}	Free energy of the conversion of the electron donor to acetyl-CoA (kJ/eeq).
ΔG_{in}	Free energy of acetil-CoA reduction (kJ/eeq).
ΔG_o	Gibbs free energy of overall growth reaction per mol of dry biomass grown (kJ/mol).
ΔG_{pc}	Free energy of the conversion of acetyl-CoA to biomass (kJ/eeq).
ΔG_S	Gibbs free energy of anabolic reaction (kJ/mol).
ΔG_s^{eeq}	Gibbs energy of anabolic reaction (kJ/eeq)
α	Fraction of electron acceptor reduction over electron donor reduction.
γ	Degree of reduction (eeq/mol).
γ_d	Degree of reduction of electron donor (eeq/mol).
γ_{EA}	Degree of reduction of electron acceptor (eeq/mol).
γ_x	Degree of reduction of biomass (eeq/mol)
ε	Energy transfer efficiency

ν	stoichiometric coefficient.
Act	acetic acid
Btr	butyric acid
C_i	Concentration of the i compound (mol/l)
Cc_i	Carbon content of the i compound (mol-C/mol).
CO_2	carbon dioxide
EA	Electron acceptor.
EOH	Ethanol
Frm	formic acid
Glc	Glucose
GOH	Glycerol
H^+	Proton
H_2	Hydrogen
H_2O	Water
Hc_i	Hydrogen content of the i compound (mol-H/mol).
Lct	lactic acid
Nc_i	Nitrogen content of the i compound (mol-N/mol).
Oc_i	Oxygen content of the i compound (mol-O/mol).
Prn	propionic acid
S	Electron donor.
Scn	succinic acid
X	Biomass
$Y_{x/s}$	Yield of biomass from electron donor substrate (molbiomass/molsubstrate).
$Y_{i/s}$	Yield of i compound from electron donor substrate (molbiomass/molsubstrate).
e	electron

Acknowledgements

This work is co-supported by the Chilean commission for science and technology CONICYT and the French Embassy in Chile.

References

[1] I. K. Kapdan and F. Kargi, Bio-hydrogen production from waste materials. *Enzyme and microbial technology*, **2006**, *38*, 569-582.

[2] R. Kleerebezem and M. C. M. van Loosdrecht, Mixed culture biotechnology for bioenergy production. *Curr. Opin. Biotechnol.*, **2007**, *18 (3)*, 207-212. DOI: 10.1016/j.copbio.2007.05.001.

[3] Y. Ueno, M. Tatara, H. Fukui, T. Makiuchi, M. Goto, and K. Sode, Production of hydrogen and methane from organic solid wastes by phase-separation of anaerobic process. *Bioresource Technology*, **2007**, *98*, 1861-1865.

[4] J. Xiao and J. M. VanBriesen, Expanded thermodynamic true yield prediction model: adjustments and limitations. *Biodegradation*, **2008**, *19*, 99-127.

[5] U. von Stockar, T. Maskow, J. Liu, I. W. Marison, and R. Patiño, Thermodynamic of microbial growth and metabolism: an analysis of the current situation. *J. Biotechnol.*, **2006**, *121*, 517-533.

[6] J. M. van Briesen, Evaluation of methods to predict bacterial yield using thermodynamics. *Biodegradation*, **2002**, *13*, 171-190.

[7] J. Xiao and J. M. VanBriesen, Expanded thermodynamic model for microbial true yield prediction. *Biotechnology and Bioengineering*, **2005**, *93*, 110-121.

[8] P. L. McCarty, Thermodynamic electron equivalents model for bacterial yield prediction: modifications and comparative evaluations. *Biotechnol. Bioeng.*, **2007**, *97 (2)*, 377-388.

[9] C. A. Aceves-Lara, E. Latrille, P. Buffiere, N. Bernet, and J. P. Steyer, Experimental determination by principal component analysis of a reaction pathway of biohydrogen production by anaerobic fermentation. *Chem. Eng. Process.*, **2008**, *DOI:10.1016/j.cep.2007.12.007*.

[10] M. F. Temudo, R. Kleerebezem, and M. van Loosdrecht, Influence of the pH on (open) mixed culture fermentation of glucose: A chemostat study. *Biotechnol. Bioeng.*, **2007**, *98 (1)*, 69-79.

[11] J. S. Liu, V. Vojinovic, R. Patiño, T. Maskow, and U. von Stockar, A comparison of various Gibbs energy dissipation correlations for predicting microbial growth yields. *Thermochim. Acta*, **2007**, *458*, 38-46.

[12] S. J. Pirt, Energy and carbon source requirements. in *Principles of microbe and cell cultivation*, S. J. Pirt, Ed. London, Blackwell Scientific Publications, **1975**, 63-80.

[13] J. Nielsen, J. Villadsen, and G. Lidén, Chapter 3. Biochemical reactions - a first look. in *Bioreaction engineering principles*, J. Nielsen, J. Villadsen, and G. Lidén, Eds., 2nd ed. New York, Kluwer Academic / Plenum, **2003**, 47-94.

[14] R. K. Thauer, K. Jungermann, and K. Decker, Energy conservation in chemotrophic anaerobic bacteria. *Bacteriol. Rev.*, **1977**, *41 (1)*, 100-180.